The Impact of Nutrient Restriction and Metformin Treatment on Genome Structure and Function in Hutchinson-Gilford Progeria Syndrome (HGPS) Fibroblasts

A Thesis Submitted to the College of
Graduate and Postdoctoral Studies
in Partial Fulfilment of the Requirements for the
Degree of Doctor of Philosophy in the Department of
Biochemistry, Microbiology, and Immunology
University of Saskatchewan
Saskatoon, Saskatchewan, Canada

By

Zoe Elizabeth Gillespie

PERMISSION TO USE

In presenting this thesis/dissertation in partial fulfilment of the requirements for a Postgraduate degree from the University of Saskatchewan, I agree that the Libraries of this University may make it freely available for inspection. I further agree that permission for copying of this thesis/dissertation in any manner, in whole or in part, for scholarly purposes may be granted by the professor or professors who supervised my thesis/dissertation work or, in their absence, by the Head of the Department or the Dean of the College in which my thesis work was done. It is understood that any copying or publication or use of this thesis/dissertation or parts thereof for financial gain shall not be allowed without my written permission. It is also understood that due recognition shall be given to me and to the University of Saskatchewan in any scholarly use which may be made of any material in my thesis/dissertation.

Requests for permission to copy or to make other uses of materials in this thesis/dissertation in whole or part should be addressed to:

Head of the Department of Biochemistry, Microbiology and Immunology
University of Saskatchewan
107 Wiggins Road
Saskatoon, Saskatchewan S7N 5E5 Canada

OR

Dean
College of Graduate and Postdoctoral Studies
University of Saskatchewan
116 Thorvaldson Building, 110 Science Place
Saskatoon, Saskatchewan S7N 5C9 Canada

ABSTRACT

Hutchinson-Gilford Progeria Syndrome (HGPS) is a rare disease in which children age at an accelerated rate. Patients suffering from HGPS have a shortened lifespan and succumb to cardiac events at ~14 years of age. At the cellular level, HGPS patient fibroblasts exhibit numerous hallmarks of the disease, including irregular nuclear morphology, hindered DNA damage repair pathways, global loss of gene repression, and mislocalization of chromosomes within the nuclear volume. Combined, these defects increase the rates at which HGPS fibroblasts become old (senescent). These defects are attributed to accumulation of the mutant protein, progerin, resulting from of a single point mutation in the *laminA/C* gene. Previously, inhibition of the mammalian target of rapamycin (mTOR) pathway via rapamycin induced progerin degradation and improved cellular phenotypes of HGPS; however, this compound has potentially severe side effects. Therefore, other methods of inhibiting mTOR, such as restriction of amino acids, or treatment with the antidiabetic drug metformin, could decrease progerin levels and restore normal genome organization and function in HGPS patient cells.

Using HGPS primary fibroblasts grown in cell culture, this data demonstrates that restriction of amino acids (specifically arginine and leucine) or treatment with the nutrient restriction mimetic metformin decrease progerin levels across patient cell lines. Furthermore, these HGPS fibroblasts also exhibited improved nuclear morphology, increased rates of DNA damage repair and re-localization of chromosome territories. These same conditions also significantly increased survival time of HGPS fibroblasts and non-diseased fibroblasts in culture. Importantly, no changes in nuclear morphology or decreases in cell viability were observed in non-diseased primary fibroblasts. On examining HGPS fibroblasts at 5 weeks of arginine and leucine restriction or metformin treatment, molecular pathways associated with HGPS disease progression (including (class A/1 (rhodopsin-like receptors) viral protein interaction with cytokine and cytokine receptor, and transforming growth factor (TGF)-β signalling) were down-regulated. Analyses also identified pathways, such as PLK1 signalling events, that may be associated with the health and lifespan extending properties of these treatments independent of ameliorating HGPS phenotypes. These findings indicate that amino acid restriction or treatments with nutrient restriction mimetics such as metformin, could supply potential therapeutic options for HGPS patients.

ACKNOWLEDGEMENTS

I would like to first thank my supervisor, Dr. Christopher Eskiw, not only for giving me the opportunity to conduct my MSc research in Canada with his lab, but then continuing to support my scientific ambitions through this PhD thesis. I am particularly grateful for his enthusiasm for research, willingness to always talk science, creating a welcoming, supportive, and entertaining lab environment, and finally, for the numerous coffees. I would also like to thank my advisory committee members, Dr. Troy Harkness, Dr. Keith Bonham, Dr. Scott Stone, and Dr. Yu Luo, who have challenged me and helped me to grow scientifically. Additionally, I am grateful for the guidance of Dr. Nicholas Low and Dr. Anthony Kusalik.

I would also like to thank all those I have met whilst in Saskatoon, making it feel like home, and friends from home who make it feel like I never left. Although there are many who made this thesis possible, through friendship and through scientific support, I particularly want to thank Lily Zehfus and Ashley Sutherland for being there on the good days and the rough ones. I also want to thank members past and present, of the Eskiw lab, Carla Almendáriz-Palacios, Matthew Janzen, Valeria Martinez, Morgan Fleming, Fina Nelson, Michelle Whalen, Kira Wang, Topaza Yu, Wen Yu Ruan, Joshua Pickering, and Dr. Zachary Belak for the wit, encouragement, and discussion.

Finally, thank you to my family, for their love, support, encouragement, and early-morning phone calls when the time difference got too much.

DEDICATION

For Elizabeth Jane Hare

TABLE OF CONTENTS

LIST OF TABLES

LIST OF FIGURES

LIST OF SYMBOLS AND ABBREVIATIONS

-Arg – Arginine Restriction

-Leu – Leucine Restriction

-ArgLeu – Arginine and Leucine Restriction

-GlcPyr – Glucose and Pyruvate Restriction

+0.5 mM Metf – 0.5 mM Metformin

+680 nM Rap – 680 nM Rapamycin

3C – Chromatin conformation capture

A - adenine

AAR – amino acid restriction

AARE – amino acid response elements

ABE – adenine base editors

AMP – adenosine monophosphate

AMPK – adenosine monophosphate kinase

AP1 – activator protein 1

Arf-1 – ADP-ribosylation factor 1

ASO – antisense oligonucleotide

ATF– activating transcription factor

ATG – autophagy related

ATP – adenosine triphosphate

AVV9 – adeno-associated virus serotype 9

bp – base pair

BCAA – branched chain amino acids

BSA – bovine serum albumin

CAAX - cysteine-aliphatic-aliphatic-other

CASTOR1 – cytosolic arginine sensor for mTORC1

CR – caloric restriction

C - cytosine

DamID –DNA adenine methyltransferase identification

DEGs – differentially expressed genes

DEPTOR – DEP domain containing mtor-interacting protein

DisGeNet - Disease-Gene NETwork

DMEM – Dulbelco's Modified Eagles Serum

DMSO – dimethyl sulfoxide

DNA – deoxyribose nucleic acid

DSB – double strand break

EdU – 5-ethynyl-2-deoxyuridine

eIF2α/β- eukaryotic initiation factor 2α/β

ESC – embryonic stem cells

EZH2 – enhancer of zeste homolog 2

FA – formaldehyde

FBS – fetal bovine serum

FGF21 – fibroblast growth factor

FISH – fluorescence *in situ* hybridization

FOXO3a – forkhead box O3

FTI – farnesyl transferase inhibitor

G – guanine

GADD34 – protein phosphatase 1 regulatory subunit 15A

GATOR – GTPase-activating protein toward Rags

GCN2 – general control non-derepressable 2

GDP – guanosine diphosphate

GSEA – gene set enrichment analysis

GTP – guanosine triphosphate

h – hour

H – histone

H3K9me3 – H3 lysine 9 trimethylation

H3K27me3 – H3 lysine 27 trimethylation

HATs – histone acetyltransferases

HDACs – histone deacetyl transferases

HGPS – Hutchinson-Gilford progeria syndrome

HiC – high throughput chromatin conformation capture

HKMT – histone lysine methyltransferases

HMGN5 – high mobility group nucleosome binding domain 5

HP1α – heterochromatin protein 1α

IF – immunofluorescence

IGF1 – insulin growth factor 1

LADs – lamin associated domains

LAP2B - lamina-associated polypeptide 2b

LBR – lamin B receptor

LC3B – light chain 3B

LKB1 – liver kinase B1

MAPK – mitogen activated protein kinase

MCRS1 – microspherule protein 1

min – minutes

mLST8 – mammalian lethal with sec-13

mSin1 – mammalian stress-activated kinase-interacting protein 1

mTOR – mammalian target of rapamycin

mTORC – mammalian target or rapamycin complex

NAD/H – nicotinamide adenine dinucleotide/hydrogen

NE – nuclear envelope

NETs – nuclear envelope transport proteins

NF-κB - nuclear factor κB

NPC – nuclear pore complex

NR – nutrient restriction

NRF2 – nuclear factor, erythroid 2 Like 2

NRM – nutrient restriction mimetic

(pS22) – serine22-phosphorylated

PBS – phosphate buffered saline

PBST – phosphate buffered saline with 0.5% Tween20

PGC-1a - peroxisome proliferator-activated receptor-γ coactivator 1a

PI3K/PDK1/AKT - phosphoinositide 3-kinase/3-phosphoinositide-dependent protein kinase 1/protein kinase B

PRAS40 – proline rich AKT substrate 40 kDa

PRC – polycomb repressor complex

Protor1/2 – protein observed with rictor 1 and 2

PTM – post translational modifications

RagA/B/C/D – ras-related GTP-binding protein A/B/C/D

Raptor – regulatory-associated protein of mTOR

Rce1 – ras-converting enzyme 1

Rcf – relative centrifugal force (rcf)

Rheb – RAS homolog enriched in brain

RICTOR – rapamycin-insensitive companion of mTOR

RIN – RNA integrity number

RT – room temperature

SAM – S-adenosylmethionine

SAMTOR – S-adenosylmethionine sensor upstream of mTORC1

SESN2 – Sestrin 2

shRNA – short hairpinRNA

SIRT1 – sirtuin 1

SPRITE - split-pool recognition of interactions by tag extension

SMP – skimmed milk powder

SSC – saline sodium citrate

SUV39 – suppressor of variegation 3-9

T - thymine

TAD – topologically associated domain

TBC1D7 – Tre-2/Bub2/Cdc16 Domain Family Member 7

TNFα – tumor necrosis factor α

TSC1/2 – tuberous sclerosis complex1/2

V - volts

WB – western blot

WDR5 – WD repeat-containing protein 5

WNT – wingless integration site

YY1 – ying yang 1

γ-H2AX – γ-H2A histone family member X

ZMPSTE24 – zinc metalloprotease related to ste24p

1.0 REVIEW OF THE LITERATURE

1.1 The Genome: Do You Want to Build a Human?

1.1.1 The Basic Structure of the Human Genome

Through alternating arrangements of four nucleotides (adenine (A), guanine (G), cytosine (C), thymine (T)), the genome provides a framework upon which a human can grow, develop, and respond to its environment. These nucleotides base pair (bp) (A to T; C to G) to form a ~3.2 billion bp genome packaged into the nucleus. This packaging is complex and highly regulated; DNA must remain readily and quickly accessible for a multitude of cellular processes essential to life (DNA replication, recombination, transcription, repair). Therefore, numerous levels of genome organization exist, transforming a linear strand of DNA into a three-dimensional, highly organized structure.

Nucleosomes are the first level of genome organization. In these structures, ~147 bp of DNA are supercoiled into ~1.65 left super helical turns of DNA around a histone octamer (Finch *et al.,* 1977; Kornberg 1974; Luger *et al.,* 1997; Noll 1974; Oudet *et al.,* 1975; Richmond *et al.,* 2003). These histones are basic proteins that favour binding of DNA, neutralizing its negative charges, and enable DNA folding. This octamer consists of two copies of each canonical histone: (H) H2A, H2B, H3 and H4. As canonical histones, these proteins contain a conserved, short, C-terminal tail, and a longer, mobile, N-terminal tail that protrudes from the core histone complex. When modified, the N-terminal tail functions as a binding site for other proteins, regulating interactions between proteins, histones, and nucleosomes. Nucleosomes are linked to one another in a "beads-on-a-string"-like structure with the "string" being variable stretches of linker DNA (10-100 bp) (Leuba *et al.,* 1994; Woodcock *et al.,* 1993), and "beads" being the nucleosomes to which the string is bound, and can be rapidly unbound, by H1 (Holde 1995; Olins *et al.,* 1974; Oudet *et al.,* 1975) (Stasevich *et al.,* 2010). Nucleosome spacing (the space between each "bead") is varied in eukaryotes and is likely linked to additional genome regulation and folding (Baldi *et al.,* 2018), with nucleosome positioning in promoter regions of genes important for transcriptional regulation (Richmond *et al.,* 2003). The resultant DNA-protein structure is known as chromatin. Combined, nucleosome spacing, and histone tails play dynamic roles in folding and regulation

of genome function (i.e., transcriptional activation and repression) in response to different cellular and extracellular stimuli.

Nucleosomes are wrapped into higher order structures, such as the theoretical 30 nm fibre 30 nm fibre. There are two proposed models for this packaging, the one-start, and the two-start model. In the one-start model, nucleosomes are organized along the same helical path (Figure 1.1), with interactions occurring between histone cores, while in the two-start model, two opposite nucleosomes connected by linker DNA create an interacting structure of alternate histone cores. As a result, various levels of chromatin compaction exist, including the controversial 30 nm fibre (Kornberg, 1974; Dubochet, et al., 1988; Maeshima and Eltsov, 2008; Maeshima, et al., 2014; Conway and Steven 1999), the 300 nm structure with sub chromosomal domains, and chromatin (reviewed in Cremer and Cremer 2001; Belmont, 2014).

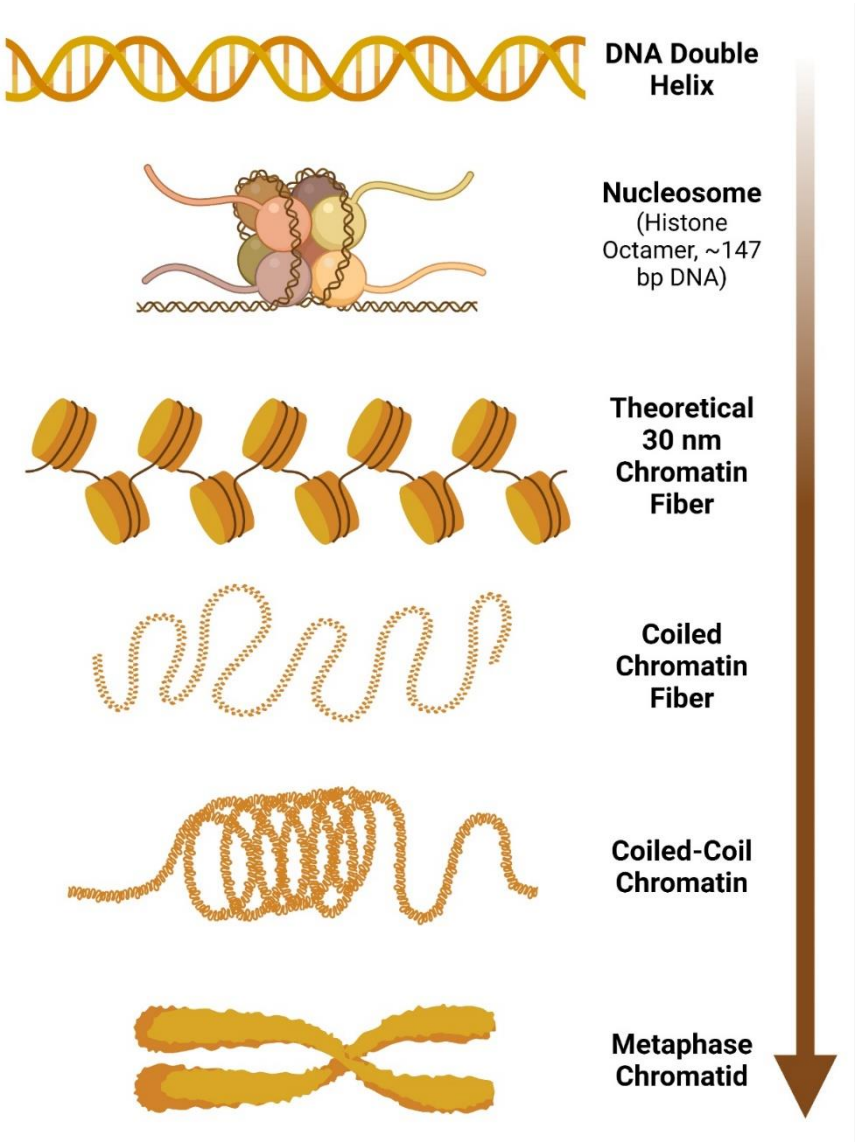

Figure 1.1 Packaging of DNA. ~3.2 billion bp of DNA are packaged into a single nucleus. To achieve this, ~147 bp segments of DNA are wrapped around a core histone octamer, forming nucleosomes. These are then organized and compacted into larger chromatin fibres. In metaphase, this results in the classical metaphase chromatid, whilst in the rest of the cell cycle, the resultant chromatin is organized into distinct chromosome territories. Figure created in Biorender.com.

1.1.2 Post-Translational Modifications, Euchromatin, Heterochromatin and the Epigenome

In recent years, fundamental changes have occurred in how the genome is studied. Instead of focusing on an individual gene and its role in a specific biological process, thousands of genes are now studied simultaneously, with physical interactions, spatial localization, and temporality recognized as essential in the contribution of genes to biological functions. Essential for this paradigm shift was the understanding that organization of DNA into higher order structures, such as chromatin and chromosome territories, was not just important for the packaging of DNA into a limited volume, but necessary for genome regulation and function. Fundamental to this higher-level organization and regulation are core histones, H2A, H2B, H3 and H4. These histones can be post-translationally modified to regulate cellular development, differentiation, and transcriptional activity (Chan *et al.,* 2020; Peng *et al.,* 2021; Ryslava *et al.,* 2013; Van der Laan *et al.,* 2014). Post translational modifications (PTM) occur primarily on the amino acids: lysine, arginine, serine, tyrosine, and threonine of histones. These modifications are usually covalent, and can include: methylation, acetylation, phosphorylation and ubiquitylation (reviewed by (Bannister *et al.,* 2011)).

Histone methylation occurs primarily on the side chains of lysine and arginine (reviewed by (Bannister *et al.,* 2011)). Lysine can be mono-, di- or tri- methylated, whereas arginine can be mono- or symmetrically/asymmetrically di-methylated (reviewed in (Lan *et al.,* 2009; Ng *et al.,* 2009)). Enzymes are responsible for catalyzing the addition of methyl groups to these amino acids, with lysine methylation catalyzed by histone lysine methyltransferases (HKMT), an enzyme that transfers a methyl group from S-adenosylmethionine (SAM) to the lysine sidechain. Each HKMT is specific to the site being methylated, and the number of methyl groups being added (reviewed in (Husmann *et al.,* 2019)). Arginine methylation, on the other hand, is regulated by two key classes of arginine methyltransferases, Type I and Type II (Reviewed by (Wu *et al.,* 2021)). As with lysine methylation, this enzyme uses SAM as a methyl donor; however, the methyl group is transferred to the ω-guanidino group of arginine. Histone demethylation occurs via histone demethylases (Bannister *et al.,* 2002). Like methyltransferases, demethylases are often specific to the site being demethylated. The existence of both methyltransferases and

demethylases has enhanced the understanding of PTMs as dynamic chemical modifications involved in regulating the genome (reviewed in (Dimitrova *et al.,* 2015)).

Histone acetylation occurs primarily on lysine side chains, regulated by histone acetyltransferases (HATs) and histone deacetylases (HDACs). Acetyl-CoA is used as a co-factor by HATs to transfer an acetyl group to the amino group of lysine side chains. The addition of an acetyl group neutralizes the positive charge of lysine, weakening DNA-histone interactions, and thus making chromatin more accessible for transcription. Two classes of HAT exist, Type A and Type B. Type A HATs are localized to the nucleus and contribute to transcriptional regulation via acetylation sites within the histone N-terminal tails of nucleosomes. Type B HATs acetylate free, newly synthesised, histones before incorporation into a larger chromatin structure. Type B marks are removed after histone deposition. Although the majority of acetylation occurs at the histone N-terminal tail, some sites can also be acetylated within the globular histone core (e.g. H3K56, which has a side chain facing the DNA major grove, and therefore its acetylation impacts DNA-histone interactions) (reviewed by (Bannister *et al.,* 2011; Sun *et al.,* 2015)).

Phosphorylation, addition of phosphate groups primarily to N-terminal histone tails of serine, threonine, tyrosine, and histidine, is controlled by kinases and phosphatases. Histone kinases transfer a phosphoryl group from adenosine triphosphate (ATP) to the hydroxyl group of a target amino acid side chain. Phosphorylation can rapidly induce changes in protein function (allosterically or by binding domains) and is essential in the regulation of cellular processes, including transcription, replication, cell metabolism, and response to environment (reviewed in (Karve *et al.,* 2011; Ramazi *et al.,* 2021)).

Methylation, acetylation, and phosphorylation are relatively small modifications of amino acid side chains. Ubiquitination, however, involves addition of ubiquitin, a 76 amino acid polypeptide, to histone lysine. A lysine can be either mono- or poly-ubiquitinated. Addition of ubiquitin is regulated by enzymes E1 (activating), E2 (conjugating), and E3 (ligating). These enzymes determine substrate specificity, as well as the amount of ubiquitination. As with other PTM, ubiquitination is a dynamic process, and promotes cellular homeostasis (Bannister *et al.,* 2011). Numerous other PTM also exist, with roles in regulating various aspects of cellular function.

Post-translation modifications are functionally related to two chromatin states within the nucleus: euchromatic and heterochromatic. Euchromatin is comprised of an "open chromatin" structure within which genes are generally active and chromatin less compact (increased physical space between nucleosomes as well as increased spacing between adjacent chromatin fibres). Not all euchromatin is the same, some is enriched with specific histone modifications, and others devoid of all histone modifications. For example, active transcriptional enhancers contain high levels of H3K4me1 (reviewed in (Hon *et al.,* 2009)), whilst active genes have transcriptional start sites enriched for H3 lysine 4 trimethylation (H3K4me3) (Barski *et al.,* 2007; Schneider *et al.,* 2004). Regions of euchromatin considered enriched for PTM are more likely to be actively involved in transcription and transcriptional regulation (Barski *et al.,* 2007).

Heterochromatin is formed of compact, "closed chromatin", with transcriptionally inactive genes. Heterochromatin can be further sub-divided into facultative and constitutive regions. In facultative chromatin, genes which are differentially expressed during development and differentiation are silenced (for example, the inactive X-chromosome in females). These silenced genes are marked by H3 lysine 27 trimethylation (H3K27me3), which is regulated and maintained by the enhancer of zeste homolog 2 (EZH2) methyltransferase, a member of the polycomb repressor complex (PRC). PRC2 is recruited to sites of DNA replication by H3K27me3, ensuring addition of the histone mark onto newly deposited histones, maintaining facultative heterochromatin (Hansen *et al.,* 2008; Trojer *et al.,* 2007). Constitutive heterochromatin, on the other hand, exists in areas of the genome comprised of permanently silenced genes, such as centromeres and telomeres. These are silenced by H3 lysine 9 trimethylation (H3K9me3) and maintained by the methyltransferase suppressor of variegation 39 (SUV39) (Bannister *et al.,* 2011; Trojer *et al.,* 2007). Therefore, organization of the genome is more complex than just fitting a large amount of genetic material into a limited volume. It is dynamically regulated by post-translational modifications to establish when, and to what degree, various regions of the genome should be expressed or repressed. Consequently, disruption of this regulation and organization frequently results in disease.

1.1.3 Chromosome Territories and Chromatin-Chromatin Interactions

Linear polymers of DNA, as well as its' associated proteins, are the backbone of what we call chromosomes, typically envisioned during metaphase as distinct entities. Although these condensed chromatin structures are iconic, the genome spends relatively little time organized into these structures. On exiting mitosis and the initiation of nucleus reformation, chromosomes decondense into specific chromosome territories. The existence of these territories has been postulated since 1885 (Carl Rabl, 1885) but direct evidence was not available until the development of fluorescence *in situ* hybridization (FISH) and chromosome probes ("paints"). Since, the existence of chromosome territories has been confirmed across numerous types of eukaryotic cells, including human (Croft *et al.,* 1999). The arrangement of chromosome territories is non-random, with gene-rich chromosomes localized more frequently towards the nuclear interior than gene poor chromosomes (Bolzer *et al.,* 2005; Boyle *et al.,* 2001; Cremer *et al.,* 2001). Similarly, within each chromosome, gene rich regions are orientated toward the nuclear interior, and gene poor to the periphery (Boyle *et al.,* 2011; Khalil *et al.,* 2007; Kupper *et al.,* 2007). Each chromosome is further partitioned into chromosomal compartments: euchromatic A and heterochromatic B. Additional, size-dependent, arrangement of chromosome territories has been proposed, with smaller chromosomes localizing closer to the nuclear interior (Bolzer *et al.,* 2005; Maharana *et al.,* 2016; Sun *et al.,* 2000). In line with this arrangement, there is a gradient of transcriptional activity across the nucleus. The highest level of activity is at nuclear speckles (toward the nuclear interior), with activity decreasing towards the nuclear lamina (Chen *et al.,* 2018b). Chromosomes are also organized preferentially, meaning that beyond size distribution, chromosome territories are consistently reported in specific positions in relation to one another and other nuclear structures (Bolzer *et al.,* 2005; Boyle *et al.,* 2001; Branco *et al.,* 2006).

Evidence exists that intermingling of chromosome territories occurs (Branco *et al.,* 2006); however, most interactions between genomic regions have been detected within the same chromosome (Belton *et al.,* 2012; Dekker *et al.,* 2002). Highly conserved across species, this chromatin folding functions to dynamically regulate gene expression. These loop-like structures formed of DNA can range in size from kilobases to megabases, with loops mediating interaction of regulatory elements in the genome (e.g. enhancers with gene

promoters) (Dekker *et al.,* 2015; Halfon 2020; Vermunt *et al.,* 2019). Multiple loops can come together in a cluster to integrate signalling events form multiple inputs on target genes (Halfon 2020; Hnisz *et al.,* 2017). Disruptions of chromatin looping have been observed in disease; therefore, it is necessary to consider how genes associated with disease are organized three-dimensionally in order to fully elucidate disease mechanisms.

Interactions between genomic regions along the same chromosome are referred to as topologically associated domains (TADs). TADs play an important role in mediating transcription, with physical contacts between enhancers and target genes occurring through loop formation of the respective DNA elements. Chromatin loops between regulatory regions predominantly occur within TADs. TADs are bounded by CTCF binding sites orientated convergently (Guo *et al.,* 2015) and housekeeping genes (Dixon *et al.,* 2012). These insulated domains prevent communication between gene and distal gene regulatory elements in different TADs and are formed by ATP-dependent loop extrusion (Fudenberg *et al.,* 2016). To achieve this, a ring-shaped cohesin protein complex is loaded at specific chromosomal positions. Chromatin fibre is progressively fed through the cohesin-complex ring, generating a loop. Chromatin sliding continues until a boundary element is encountered (e.g. CTCF binding sites), inhibiting cohesion progression and generating a loop (de Wit *et al.,* 2015; Guo *et al.,* 2015; Mirny *et al.,* 2019; Nuebler *et al.,* 2018; Sanborn *et al.,* 2015). It is likely that additional chromatin binding proteins and non-coding RNAs also contribute to formation of loops and higher-order genome organization (Quinodoz *et al.,* 2018). Removal of CTCF does not disrupt many TAD boundaries, nor does disruption affect overall segregation of A and B heterochromatin compartments, indicating that alternative CTCF-independent mechanisms also exist for TAD formation (Barutcu *et al.,* 2018; Dixon *et al.,* 2012; Nora *et al.,* 2017; Schwarzer *et al.,* 2017). The extent to which TADs regulate gene expression is also unclear. There is evidence that co-regulated genes are frequently found in the same TAD (Hsieh *et al.,* 2020; Krietenstein *et al.,* 2020) and disruption of TAD boundaries causes dysregulation of these genes within the TAD (Lupianez *et al.,* 2015; Narendra *et al.,* 2015); however, TADs are highly variable between individual cells of the same population (Cattoni *et al.,* 2017; Finn *et al.,* 2019; Nagano *et al.,* 2013), with the exception of mouse embryonic stem cells (ESCs) (Dixon *et al.,* 2015). Additionally, disruption of TAD insulation does not consistently lead to aberrant gene regulation in development (Williamson *et al.,* 2019). Recently these genomic

features have been documented to exhibit a high degree of heterogeneity, with two alleles of the same gene differing in their three-dimensional position and functional status in the same nucleus (Finn *et al.,* 2019). Furthermore, many chromatin-chromatin interactions occur at low frequency within a cell population (Finn *et al.,* 2019; Rodriguez *et al.,* 2019). Therefore, these chromatin domains may not be strong determinants of gene function, but instead provide a framework upon which genes can be regulated, and chromatin-chromatin interactions facilitated (Misteli 2020). The variability of chromatin interactions combined with the non-randomness of its organization, presents numerous unanswered questions for our understanding of genome organization. Non-random patterns indicate the existence of specific mechanisms in regulating gene expression and organization, whilst the variability across cells and genomes suggests that these features are disposable/other mechanisms could be involved and muddy the picture of how genome organization links to transcriptional regulation.

Chromatin-chromatin interactions have been detected between genomic regions of the same chromosome, with long-range interactions identified less frequently than shorter-range interactions; however, longer-range (larger loops) most frequently contribute to genome compaction and regulation of clusters spatially and temporally. This is achieved through sequential association of upstream elements within individual target genes, most frequently observed in development (Darbellay *et al.,* 2016; Vermunt *et al.,* 2019). In rare cases, likely in differentiation or exclusion of DNA damage, long-range chromatin loci have been observed to exhibit directed motion – probably dependent on nuclear actin and myosin (Caridi *et al.,* 2019; Chuang *et al.,* 2006). Although these long-range interactions are rarely detected, there is some debate over whether they exist more rarely or are simply not detectable by the methods available for examining genome organization: chromatin conformation capture (3C)/high throughput HiC or FISH. Computational models appear to support the rarity of longer-range interactions. Computer modelling assumes that chromatin is a self-avoiding polymer that can undergo local constrained diffusion by its polymer nature. Using this assumption, models re-create evidence for chromosome territories, compartmentalization, and chromatin-chromatin interactions proposed via experimental means and recapitulating the classical representation of a chequerboard HiC plot (Barbieri *et al.,* 2012; Bintu *et al.,* 2018; Jost *et al.,* 2014; Parmar *et al.,* 2019). In support of these models, they are also able to

accurately predict local organization of specific gene loci (e.g. Sox9) (Bianco *et al.*, 2018; Falk *et al.*, 2019). Modelling further shows that without the regulation via topoisomerases II (which act to pass chromatin strands) a genome would form an entangled and knotted state, at least at chromosome interfaces; however, this is not the case (Tavares-Cadete *et al.*, 2020). This is due to the ability of chromatin fibers/domains from one chromosome to locally invade another to an extent without becoming topologically linked (Branco *et al.*, 2006; Tavares-Cadete *et al.*, 2020). Therefore, as proposed in transcriptional control by genome organization, additional processes are likely to exist to prevent entanglement.

Many inter-chromosomal interactions that occur at large nuclear bodies are not efficiently captured by HiC since the interactions are at such large distances that they are not close enough for ligation by HiC, nor by FISH. This has recently been overcome by split-pool recognition of interactions by tag extension (SPRITE) – from which data agree with the previously proposed model of transcriptionally active and inactive hubs within chromosome territories. A large portion of these transcriptionally active hubs are associated with nuclear speckles, whilst inactive hubs are associated with the nucleolus (Quinodoz *et al.*, 2018). Though it is obvious that genome organization and genomic interactions play important roles in genome regulation, future work elucidating and finessing the role of these interactions will provide important insights for health and disease.

1.1.4 The Nuclear Lamina in Genome Organization and Function

The nuclear lamina is a complex and highly organized meshwork of proteins essential for the structure and function of the cell. Lamin proteins are expressed in all metazoan cells (Dechat *et al.*, 2010; Gruenbaum *et al.*, 2015) and form part of the nuclear envelope (NE), alongside inner and outer nuclear membranes and nuclear pore complexes (NPCs). Structurally, the lamina meshwork is found under the inner nuclear membrane, and alongside the rest of the NE, separates the inner nuclear and outer cytoplasmic compartments of eukaryotic cells (Dechat *et al.*, 2010; Dechat *et al.*, 2008). The nuclear lamina functions beyond separation of cellular compartments, with roles in maintaining nuclear shape, chromatin organization, cell cycle progression, cell development and differentiation, cell signalling, RNA transcription, DNA replication, and DNA damage repair pathways. The main structural components of the lamina are the lamin proteins. These type V intermediate filament proteins have a short N-terminal head, central alpha-helical coiled-coil rod domain,

and globular tail-domain (Herrmann *et al.,* 2016; Herrmann *et al.,* 2007). The lamina meshwork is formed by polymerization, with lamin dimerization mediated by the coiled-coil rod domain and the head/tail domains mediating head-to-tail polymer assembly. These polymers then associate into fibres and subsequently ordered lattices (Stuurman *et al.,* 1998).

The mammalian genome contains three lamina-encoding genes: *LMNA* (coding for lamin A and lamin C proteins), *LMNB1* (lamin B1) and *LMNB2* (lamin B2). Lamin proteins are assigned to one of two groups (A-type or B-type) dependent on function and expression. *LMNA* (A-type lamins) are primarily expressed in differentiated cells, whilst B-type lamins (*LMNB1/LMNB2*) are expressed in all cells and throughout embryogenesis (Rober *et al.,* 1989; Stewart *et al.,* 1987). These lamin proteins are post-translationally modified in preparation for their specific roles. The precursor of lamin A (prelamin A) and B-type lamins are farnesylated by farnesyltransferases at the cysteine residue of the carboxy-terminal cysteine-aliphatic-aliphatic-other (CaaX) motif (Weber *et al.,* 1989), anchoring these proteins to the inner nuclear membrane (Figure 1.2). Unlike lamin A and B-type lamins, lamin C has no CaaX motif and requires no additional modifications. Following farnesylation, both lamin A and B-type lamins undergo cleavage of the terminal three amino acids of the CaaX motif (-aaX) by either zinc metalloprotease related to ste24p (ZMPSTE24; prelamin A) or ras-converting enzyme 1 (Rce1; B-type lamins). The alpha carboxyl-groups of these proteins are then methylated by isoprenylcysteine carboxyl methyltransferase (Winter-Vann *et al.,* 2005), and unique to prelamin A, the farnesyl group is removed by ZMPSTE24, producing mature lamin A. Unlike lamin A, B-type lamins retain farnesylation, indicating closer association with the inner nuclear membrane than A-type lamins (Nigg 1992). In support of this, A and B-type lamins each form a separate meshwork, with B-type lamins forming irregular, wavy filaments associated with intranuclear membrane structures (Goldberg *et al.,* 2008). Finally, it has been demonstrated that A-type lamins exhibit greater nuclear mobility than B-type lamins (Shimi *et al.,* 2008), supporting the divergent nuclear localization and function of A and B-type lamins.

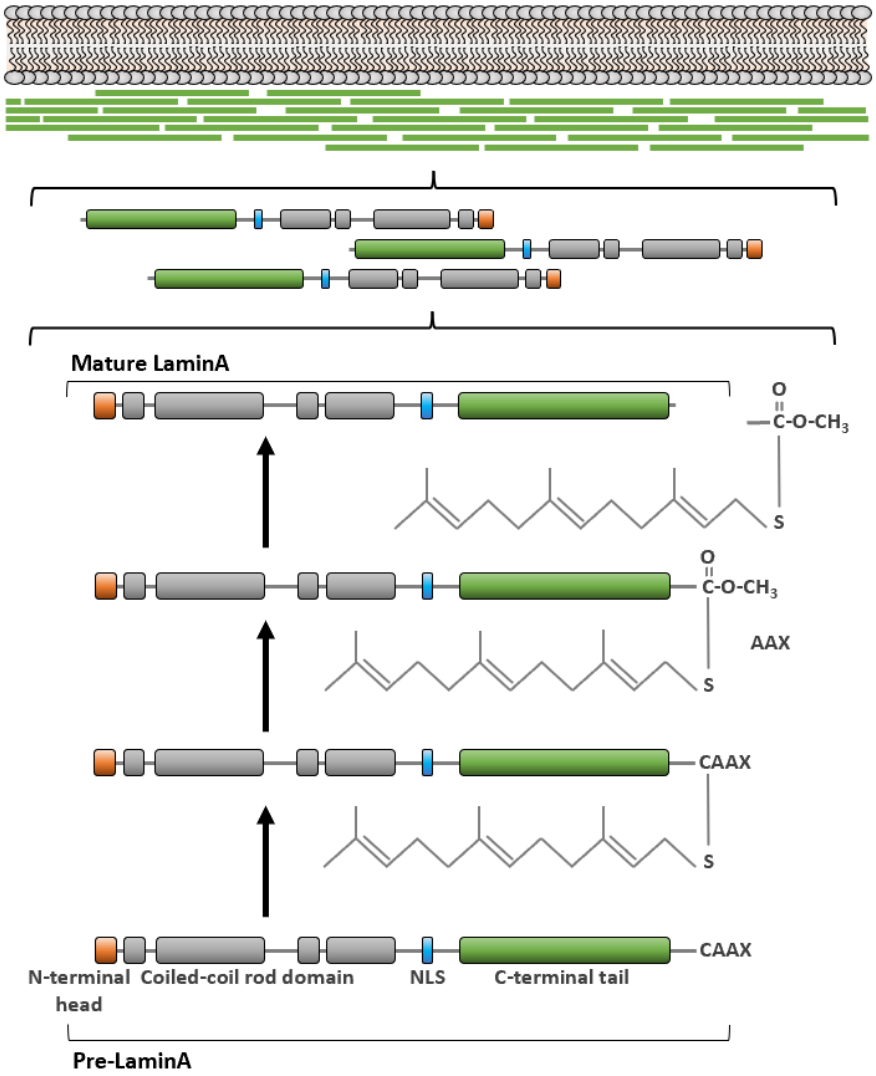

Figure 1.2: Processing of Prelamin A to Mature Lamin A. Prelamin A is encoded for by the *LMNA* gene and can be processed to produce lamin A or lamin C protein. Prelamin A is farnesylated at its CaaX terminal end and anchored to the inner nuclear membrane. -aaX is then cleaved by ZMPSTE24 and the carboxy-group methylated by isoprenylcysteine carboxyl methyltransferase. Finally, the entire farnesyl group is cleaved by ZMPSTE24 and lamin A forms a regular meshwork under the nuclear envelope via polymerisation.

Genomic regions that interact with the nuclear lamina are known as lamina associated domains (LADs). LADs are evolutionarily conserved, having been detected in multiple cell types and organisms, including human fibroblasts (Guelen *et al.,* 2008; Meuleman *et al.,* 2013), mouse ESCs/differentiated astrocytes (Meuleman *et al.,* 2013; Peric-Hupkes *et al.,* 2010), *Drosophila melanogaster* (Pickersgill *et al.,* 2006; van Bemmel *et al.,* 2010), and *Caenorhabditis elegans* (Ikegami et al., 2010). However, the same LADs are not necessarily found in each cell type (Kind *et al.,* 2015) demonstrating that each cell type uses alternative LAD boundaries as a mechanism to control specific gene expression profiles/signatures associated with cell identity. DNA adenine methyltransferase identification (DamID) is a technique used to identify genome-wide DNA-protein interactions, and was used in the initial identification of LADs, finding that 40% of the genome is organized into approximately ~1300 lamin B associated domains, containing genes exhibiting low levels of transcription, are gene poor and enriched in repressive histone marks (Consortium *et al.,* 2007; Guelen *et al.,* 2008; Kind *et al.,* 2013; Peric-Hupkes *et al.,* 2010; Pickersgill *et al.,* 2006; van Bemmel *et al.,* 2010; Wu *et al.,* 2017). Although published data suggests that lamin A and lamin B1 have highly similar DamID profiles (Kind *et al.,* 2014; Meuleman *et al.,* 2013), other researchers have found that sonication levels could influence this, with mild sonication of genomic DNA associated with lamin A and lamin B1 exhibiting association with divergent chromatin domains. Specifically, lamin A exhibited association with transcribed genes and active chromatin marks, whilst lamin B1 associated with gene poor and non-transcribed domains (Gesson *et al.,* 2016). These associations have been documented as functional via knock-out studies, with B-type lamin knockdowns in *Drosophila melanogaster* S2 cells and neuroblasts exhibiting re-localization of genes from the nuclear periphery to the interior (Kohwi *et al.,* 2013; Shevelyov *et al.,* 2009). In mouse embryonic fibroblasts, the same knock-out induced re-localization of chromosome 18, whilst in *Drosophila melanogaster* S2 cells, bulk chromatin detachment and decompaction from the nuclear envelope occurred (Ulianov *et al.,* 2019). This total detachment was not observed following the same loss of lamins in mammalian cells (Zheng *et al.,* 2018). Exactly how LADs are targeted to the nuclear lamina is poorly understood, although many researchers have proposed involvement of various proteins and transcriptional regulators (e.g. H3K9 methyltransferases (Towbin *et al.,* 2012), H3K9me2/3 marked chromatin (Gonzalez-Sandoval *et al.,* 2015), lamin B receptor (LBR) (Solovei *et al.,* 2013), cKrox, ying yang 1 (YY1), HDAC3 (Milon *et al.,* 2012; Poleshko *et*

al., 2017; Zullo *et al.,* 2012), and lamina associated polypeptide 2b (LAP2B) (Harr *et al.,* 2015; Zullo *et al.,* 2012)). Experiments in which specific genomic regions are tethered to the nuclear lamina demonstrate that LADs are associated with gene regulation. Furthermore, upon artificial movement of genes to the LAD, repression is induced (Dialynas *et al.,* 2010; Finlan *et al.,* 2008; Reddy *et al.,* 2008; Wang *et al.,* 2018a). Combined, these findings further signify the importance of the nuclear lamina in normal genome function.

The nuclear lamina and chromatin are extensively associated with one another and cooperate in the regulation of gene expression. Nuclear morphology is also known to be regulated by the nuclear lamina, and more recently, chromatin. Nuclear morphology is an important aspect of cellular function, even if the mechanics behind its maintenance are poorly understood. The cell nucleus is responsive to its microenvironment and is required to protect and organize the genome it encapsulates. Forces upon the nucleus can directly influence gene transcription via positioning and stretching of the genome. Without an ability to respond to its environment, or to function in cell migration (Davidson *et al.,* 2014; Harada *et al.,* 2014), the nucleus would undergo deleterious events, including nuclear rupture and deformations, mixing nuclear and cytoplasmic contents, inducing DNA damage and disrupting gene transcription (De Vos *et al.,* 2011; Shimi *et al.,* 2008; Xia *et al.,* 2018). These environmental stressors subsequently result in irregular nuclear morphology, which has been identified in and used as a marker of aging (Haithcock *et al.,* 2005; Mehta *et al.,* 2007; Pathak *et al.,* 2021), cancer (Fischer 2020) and disease (Hutchinson-Gilford Progeria Syndrome (HGPS) (Goldman *et al.,* 2004); Emery-Dreifuss muscular dystrophy (Roux *et al.,* 2007)). Furthermore, manipulation of nuclear morphology has been linked to various alterations in transcriptional activity. For example, nuclei with reduced volume have been reported to enter a more quiescent state (Damodaran *et al.,* 2018), whilst increasing nuclear volume has been shown to decondense chromatin (Katiyar *et al.,* 2019).

Although the nuclear lamina is often considered the primary contributor to nuclear shape, with cells with perturbed nuclear lamina prone to rupture (Chen *et al.,* 2018a; De Vos *et al.,* 2011; Le Berre *et al.,* 2012; Robijns *et al.,* 2016; Stephens *et al.,* 2017; Stephens *et al.,* 2019; Tamiello *et al.,* 2013; Vargas *et al.,* 2012), there is evidence that chromatin also plays an important role in maintaining nuclear structure independent of the nuclear lamins, having previously been demonstrated as an essential component of nuclear mechanical response

(Banigan *et al.,* 2017; Chalut *et al.,* 2012; Furusawa *et al.,* 2015; Schreiner *et al.,* 2015; Stephens *et al.,* 2017; Stephens *et al.,* 2019). The role of chromatin in maintaining nuclear structure continues to be refined. In 2004, it was hypothesized from studies in *Xenopus* oocytes that chromatin had little to do with the mechanical properties of the nucleus (Dahl *et al.,* 2005); however, it has since been revealed that condensation and decondensation of chromatin leads to nuclear stiffening and softening respectively (Dahl *et al.,* 2005; Erdel *et al.,* 2015; Krause *et al.,* 2013; Mazumder *et al.,* 2008; Neubert *et al.,* 2018; Pajerowski *et al.,* 2007; Schreiner *et al.,* 2015; Shimamoto *et al.,* 2017; Stephens *et al.,* 2017). Additionally, embryonic stem cells do not express A-type lamins but have a characteristic ovoid nucleus. Lamins may instead have a greater role in mediating mechanical strength and link the nucleus to the cytoplasm through nuclear envelope transport proteins (NETs). The nuclear lamina and chromatin have been identified to regulate diverging aspects of nuclear response to external forces. Chromatin regulates resistance to small deformations, whilst lamin A mediates resistance to large deformations (Stephens *et al.,* 2017).

In general, chromatin histone modifications that result in abnormally increased euchromatin or decreased heterochromatin (overall a more open-chromatin structure) result in weakened nuclear rigidity, with cells exhibiting irregular nuclear morphology which are prone to rupture (Stephens *et al.,* 2017). For example, cells lacking lamin B1, containing a lamin A mutant, or those of HGPS patients, exhibit irregular nuclei and nuclear blebs which contain histone modifications and loss of chromatin condensation (Stephens *et al.,* 2017). Disruption of histone modifiers similarly disrupt nuclear morphology and transcriptional activity. Overexpression of high mobility group nucleosome binding domain 5 (HMGN5) disrupts histone linker H1, decreasing chromatin compaction and increasing nuclear instability and blebbing (Furusawa *et al.,* 2015), whilst WD repeat-containing protein 5 (WRD5), regulator of euchromatic mark H3K4me3, has also been demonstrated to regulate nuclear deformity (Wang *et al.,* 2018a). In mammalian epithelial cells, increased nuclear stiffness and increased levels of histone deacetylases induced tumorigenicity (Stowers *et al.,* 2019). Significantly for disease, these perturbations may be reversible. In lamin B1 knock-out cells, lamin A mutants, and HGPS patient fibroblasts, it was possible to partially rescue nuclear morphology with the use of histone demethylase inhibitors, increasing heterochromatin levels and improving nuclear stiffness (Stephens *et al.,* 2017; Stephens *et al.,*

2019). Chromatin condensation has also been reported to coincide with bleb reabsorption in lamin A/C knock-out human fibrosarcoma cells (Robijns *et al.,* 2016). Therefore, chromatin histone modifications and their contribution to nuclear rigidity act as a major determinant of nuclear blebbing and morphology. Thus, loss of heterochromatin, as seen in both HGPS and normal aging, is associated with increased cellular senescence.

1.2 Hutchinson-Gilford Progeria Syndrome

1.2.1 Hutchinson-Gilford Progeria Syndrome: A Laminopathy

Hutchinson-Gilford Progeria Syndrome (HGPS) belongs to a group of diseases known as laminopathies; diseases that result from mutations in the genes encoding the proteins of the nuclear lamina. HGPS is a rare laminopathy, affecting approximately 1 in 4 million live births, causing children to age roughly eight times faster than normal. As a result, children with HGPS usually succumb to heart failure or stroke by ~14 years of age (range 8-21 years old) (Baker *et al.,* 1981; Capell *et al.,* 2006; Csoka *et al.,* 2004b; De Sandre-Giovannoli *et al.,* 2003). Although children with this disease die young, they are rarely diagnosed before their third birthday (Hennekam 2006). This is likely the result of the progressive accumulation of a mutant of the lamin A protein, progerin, generated following introduction of a single point mutation (G608G; GGC > GGT) in the *LMNA* gene (De Sandre-Giovannoli *et al.,* 2003; Eriksson *et al.,* 2003a). This point mutation activates a cryptic splice site in *LMNA* exon 11, causing a 50 amino acid deletion in the C-terminal tail domain, including the ZMPSTE24 proteolytic cleavage site, resulting in retention of a farnesyl group (Goldman *et al.,* 2004). This anchors progerin to the nuclear membrane, resulting in progerin accumulation within the lamina (Figure 1.3). Accumulation of progerin also occurs due to increased rates of translation in HGPS cells, further contributing to disruption of protein homeostasis within the lamina (Buchwalter *et al.,* 2017).

Progerin accumulation is considered the primary driver of HGPS and its phenotypes. This accumulation induces a number of cellular defects, including irregular nuclear morphology (Goldman *et al.,* 2004), mis-localization of entire regions of the genome (chromosome territories) (Mehta *et al.,* 2011), decreased rates of DNA repair (Scaffidi *et al.,* 2006; Scaffidi *et al.,* 2008), global disruption of gene expression patterns and loss of heterochromatin marks (Csoka *et al.,* 2004a; Goldman *et al.,* 2004; McCord *et al.,* 2013;

Shumaker *et al.*, 2006). As a culmination of these cellular defects, the rate at which cells enter senescence is increased (Baker *et al.*, 1981; DeBusk 1972). Patients, therefore, often exhibit characteristics associated with aging, such as poor growth, alopecia, loss of subcutaneous fat, and arthritis, as well as delayed wound healing (Gordon *et al.*, 2005).

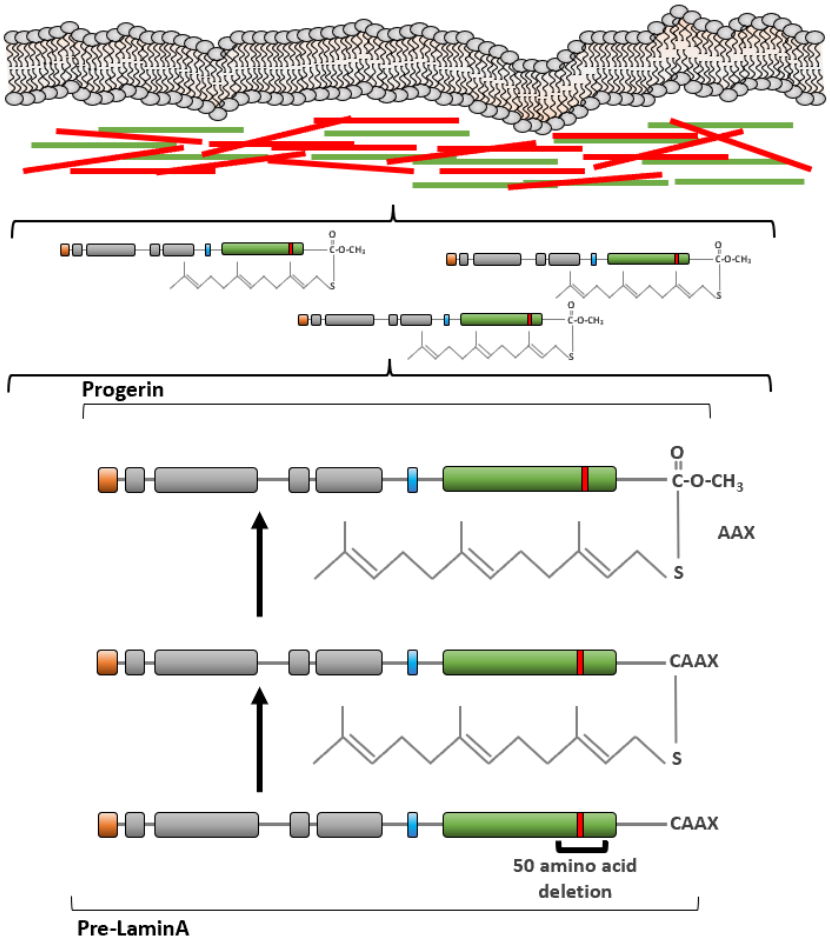

Figure 1.3: Production of Mutant Protein Progerin from Prelamin A. In production of progerin, a 50 amino acid deletion is introduced into prelamin A. This deletion is the result of a single point mutation (G608G; GGC > GGT) and activates a cryptic splice site – which results in removal of the 50 amino acid region during post-translational processing. As a result, its ZMPSTE24 cleavage site is lost. Therefore, while prelamin A is farnesylated at the CaaX motif and the -aaX cleaved as usual, the farnesyl group can no longer be removed. Progerin then accumulates under the nuclear envelope, alongside lamin A and C, creating aggregates and disrupting the normally regular lattice-like structure.

In spite of the severe manifestations of HGPS in some tissues, other tissues remain unaffected. This is likely the result of divergent expression of *LMNA* or *LMNB* in differentiation or development respectively (Rober *et al.*, 1989; Stewart *et al.*, 1987), as well as different levels of the lamin A or lamin C production. For example, progerin has not been detected in cells of the nervous system in HGPS patients and is probably the reason patients exhibit no cognitive defects, nor dementias, usually found in an aging phenotype (Merideth *et al.*, 2008). This is likely due to the usually low levels of lamin A in these tissues. In the brain, there is evidence that the brain-specific micro-RNA-9 (mir-9) prevents prelamin A processing (Nissan *et al.*, 2012), and instead the tissue exhibits higher levels of lamin C (Jung *et al.*, 2012), enabling preservation of nuclear morphology.

HGPS is a multifactorial disease, both at the organismal and cellular level, making it difficult to identify the order of disease progression at the molecular level. It is known that progerin accumulates under the nuclear envelope, likely burying chromatin binding sites, altering LAD structure, and preventing post-translational modifications (Chojnowski *et al.*, 2015; Scaffidi *et al.*, 2006; Shumaker *et al.*, 2006). It is unknown exactly what accumulation of this mutant protein perturbs first. Initial evidence into the progression of HGPS was provided when immortalization of human dermal fibroblasts expressing progerin prevented premature senescence (Cao *et al.*, 2011a; Chojnowski *et al.*, 2015) but did not correct alterations in heterochromatin and nuclear morphology (Chojnowski *et al.*, 2015). Additionally, changes in chromatin structure occur before increases in irregular nuclei in HGPS models (Shumaker *et al.*, 2006), whilst progerin accumulation alone is not sufficient to cause previously observed increases in levels of DNA damage when cells are arrested in G1. It was further demonstrated that changes in the heterochromatin of HGPS cells could occur before cell cycle progression (Chojnowski *et al.*, 2020). These data suggest that disruption of heterochromatin may be an initial step in HGPS disease progression. Combined, these reports suggest that alterations in chromatin structure are the primary step in HGPS pathogenesis, triggered by progerin accumulation. Subsequent disruptions in nuclear morphology, DNA damage repair rates, and cellular senescence, are downstream of this initial disruption.

1.2.2 Epigenetic Alterations in Hutchinson-Gilford Progeria Syndrome

The transcriptome of HGPS fibroblasts is divergent to that of non-diseased fibroblasts. For over a decade it has been reported that HGPS fibroblasts, as well as cell types from various *in vitro* and *in vivo* models, exhibit alterations in histone marks which have previously been associated in regulating chromatin accessibility and gene expression. Histone methylation is one mechanism by which gene expression can be controlled. In 2006, Shumaker and colleagues identified loss of the repressive mark H3K27me3 in HGPS fibroblasts (Shumaker *et al.,* 2006). Specifically, this was examined on the inactive X chromosome of female HGPS fibroblasts. Since, overall decreases in H3K27me3 have been recapitulated in male and female fibroblasts from multiple HGPS patients (Cao *et al.,* 2011b; McCord *et al.,* 2013; Shah *et al.,* 2013). If variations in the amount of H3K27me3 exist because of sex-differences and the inactive X chromosome is unclear; however, given differences between male and female transcriptome of HGPS patients, this could provide one explanation. Loss of H3K27me3 is usually specific, with gene poor regions and CpG islands of the HGPS genome more likely to lose this epigenetic mark (McCord *et al.,* 2013). Furthermore, there is evidence that loss and gain of H3K27me3 at different genomic regions in HGPS fibroblasts is also involved in disease progression (Shah *et al.,* 2013). EZH2, a methyltransferase that specifically mediates H3K27me3, is also reduced in HGPS cells, as is *EZH2* mRNA (McCord *et al.,* 2013). It is possible that changes in H3K27me3 levels is one of the first alterations in nuclei of progerin positive cells, occurring before nuclei exhibit irregular blebbing (Chojnowski *et al.,* 2020; Sebestyen *et al.,* 2020; Shumaker *et al.,* 2006).

H3K9me3 is an epigenetic mark associated with pericentric heterochromatin. Reduction of this mark is detected specifically in late passage HGPS fibroblasts, particularly in nuclei exhibiting disrupted morphology (Chojnowski *et al.,* 2020; Columbaro *et al.,* 2005; Sebestyen *et al.,* 2020; Shumaker *et al.,* 2006); however, association with its binding partner heterochromatin protein 1α (HP1α) is decreased before extensive nuclear lobulation and H3K9me3 loss (Shumaker *et al.,* 2006). Cells expressing progerin and lacking heterochromatin marks H3K27me3 or H3K9me3 are then more likely to accumulate DNA damage during DNA replication (Chojnowski *et al.,* 2020). Others have reported changes/decreases in H3K9me3 levels, dependent on model and HGPS fibroblast cell line (Kohler *et al.,* 2020; Liu *et al.,* 2013). Further examination revealed prelamin A/progerin and

passage number have opposing effects on SUV39H levels; the primary methyltransferase responsible for maintaining H3K9me3. Prelamin A has a higher binding constant than lamin A and C to SUV39H, stabilizing the methyltransferase and preventing its proteasomal degradation resulting in increasing H3K9me3 levels. In contrast, in HGPS and non-progeroid fibroblasts, H3K9me3 levels decrease with increasing passage/cellular 'aging' in culture (Liu *et al.,* 2013). These findings highlight the importance of passage and age matching HGPS fibroblasts and controls. Another pericentric heterochromatin mark and mark of telomeric chromatin, H4K20me3, is also increased in late passage HGPS fibroblasts (Liu *et al.,* 2013) and following ectopic progerin expression (Shumaker *et al.,* 2006). This has been associated with dysfunction of telomeres in HGPS cells (Cao *et al.,* 2011b).

In contrast to the repressive histone marks H3K27me3 and H3K9me3, the histone mark H3K4me3 associated with transcriptional start sites and gene activation, has also been studied in HGPS. Of note, H3K4me3 can occupy the same promoter as the repressive H3K27me3, creating a bivalent domain (Bernstein *et al.,* 2006). Although the role of these domains is unclear, it is proposed that these play an important role in inactivating developmental genes but keeping these genes ready for rapid transcription (Lauberth *et al.,* 2013; Voigt *et al.,* 2013). In HGPS, H3K4me3 is enriched, but at different locations to control cell lines (Shah *et al.,* 2013), although this could be due to the different cell line sampling locations (HGPS fibroblasts vs non-diseased lung tissue). Further relationships between H3K27me3 and H3K4me3 can be elucidated, with H3K27me3 having stronger association with the nuclear lamina than H3K4me3 (McCord *et al.,* 2013), supporting these marks respective roles in gene activation and repression.

Epigenetic changes result in altered chromatin organization. Accordingly, HGPS fibroblasts exhibit loss of chromatin organization, specifically compartmentalization of active and inactive chromatin regions at late passages (Chandra *et al.,* 2015; Goldman *et al.,* 2004; McCord *et al.,* 2013). LADs are proposed to be involved in regulating these changes in chromatin organization, which is logical given anchoring of progerin at the nuclear periphery as a result of its farnesyl group and subsequent disruption of the nuclear lamina. Heterochromatin is usually found anchored to the nuclear periphery, in LADs. These have been documented to dissociate from the nuclear lamina in HGPS, with fewer lamin associated regions identifiable (McCord *et al.,* 2013; Sebestyen *et al.,* 2020). When compared to non-

diseased fibroblasts, HGPS fibroblasts gained 282 LADs and lost 353 LADs (Ikegami *et al.*, 2020). Other changes in chromatin organization were identified by Kohler and colleagues, (Kohler *et al.*, 2020) identifying 545 regions of differential chromatin accessibility in HGPS fibroblasts compared to control, 397 regions of chromatin were more open (accessible) while 148 regions exhibited compaction. These changes were non-random and associated with LADs (Kohler *et al.*, 2020). Variation in LAD identification could be the result of computational analyses conducted, as well as experimental resolution. This change in LAD-specific chromatin accessibility correlated with changes in gene expression, identifying 343 genes differentially expression in HGPS compared to control cells, 160 up-regulated and 183 down-regulated. 21 of these genes also exhibited changes in chromatin accessibility and were localized in, or close to, LADs (Kohler *et al.*, 2020). Although LADs are key in gene repression in normal genome regulation, the low number of genes changing expression in HGPS that are associated with LADs indicates other mechanisms may be involved. Serine22-phosphorylated (pS22) lamin A/C has been identified as a player in this alternate mechanism (Ikegami *et al.*, 2020). Localized to the interior of the nucleus throughout the cell cycle in human fibroblasts, pS22 lamin A/C has been shown to interact with the genome at sites outside of LADs, at putative active enhancers, particularly in association with accessible chromatin and histone mark H3 lysine 27 acetylation (H3K27ac) (Ikegami *et al.*, 2020). This contrasts lamin A/C, which is generally strongly enriched at LADs. Ikegami and colleagues further identified strong correlation between pS22 lamin A/C binding sites and HGPS highly transcribed genes. It is proposed that misdirection of pS22 lamin A/C in HGPS (due to direct interaction between progerin and lamin A/C (Lee *et al.*, 2016b) results in binding of otherwise unbound enhancer regions, inducing abnormal transcriptional activation of genes associated with HGPS patient phenotypes.

DNA methylation is another modification essential to epigenetic regulation; however, its role in HGPS is less defined. DNA methylation profiles, as with histone marks, have also been associated LADs and are altered in HGPS (Kohler *et al.*, 2020; Liu *et al.*, 2011). Although heterochromatic, LADs are not associated with high levels of DNA/cytosine methylation, but instead tend to overlap with partially methylated domains (Berman *et al.*, 2011; Xie *et al.*, 2017). Although DNA methylation is poorly understood in HGPS, techniques studying DNA methylation, as well as current understanding of DNA methylation in context

of human aging are well established. To this end, accurate epigenetic clocks for predicting age from DNA methylation profiles have been developed (Horvath *et al.*, 2018). The skin and blood epigenetic clock centered on DNA methylation profiles revealed that HGPS males were epigenetically older than females with HGPS (Horvath *et al.*, 2018). Application of the epigenetic clock to newly contributed DNA methylation profiles of HGPS patients revealed two patient sub-groups, one of which was epigenetically older than the other (Horvath *et al.*, 2018; Kohler *et al.*, 2020). These groups could not be separated on sex, age, passage, body site of sampling, or strength of progerin expression; however, the epigenetically older group had higher levels of partial DNA methylation, mostly at intergenic regions (Kohler *et al.*, 2020). However, given the divergence of DNA methylation profiles of normal aging vs HGPS, the accuracy of the epigenetic clock in this application is unclear. DNA methylation profiling of HGPS fibroblasts also revealed an increase in average methylation levels associated with lamin A (Kohler *et al.*, 2020), counterintuitive to increased chromatin accessibility reported. These changes may be the result of relocation of former LADs to the nuclear interior to increase gene expression. Despite changes in DNA methylation, no changes were identified between control and HGPS fibroblasts at CpG islands (Kohler *et al.*, 2020). Combined, these data suggest that changes in DNA methylation in HGPS are not random and occur primarily at lamina-associated regions that are partially methylated.

1.2.3 The Transcriptome of Hutchinson-Gilford Progeria Syndrome

Accumulation of the mutant protein progerin perturbs chromatin, chromatin-interactions, and chromosome territory localization. Therefore, it is unsurprising that the transcriptome of HGPS patients is also altered. Understanding how exactly transcription is disrupted, beyond the production of progerin, could be useful in identifying treatment targets and determining HGPS disease progression. Csoka and colleagues first sequenced the transcriptome of HGPS fibroblasts in 2004, identifying 361 differentially expressed genes (DEGs) when compared to non-diseased controls (Csoka *et al.*, 2004a). Computational analyses of these DEGs identified genes associated atherosclerosis, as well as down-regulation of those involved in DNA replication, chromatin remodeling and heterochromatin silencing, whilst histone deacetylase HDAC9 was up-regulated (Csoka *et al.*, 2004a). RNA sequencing of six HGPS fibroblast patient cell lines and three controls identified 364 DEGs altered in HGPS, overlapping those previously identified (Csoka *et al.*, 2004a). Gene set

enrichment analysis (GSEA) of these datasets (considering changes across the transcriptome) identified enrichment of Hippo and NOTCH signalling, extracellular matrix receptor interactions, and UV response pathways, as well as enrichment of AP1 target genes (Kohler *et al.,* 2020). Furthermore, it was noted that HGPS patients <8 years of age exhibited variation to those >8 years of age, with younger patients exhibiting enrichment in more pathways associated with development (Kohler *et al.,* 2020). Ikegami and colleagues recapitulated the finding that HGPS patients exhibit divergent transcriptomes to those of non-diseased individuals and conducted bioinformatic analyses focused around disease ontology terms in DisGeNet (Disease-Gene NETwork) (Ikegami *et al.,* 2020), identifying overrepresentation of HGPS up-regulated DEGs associated with coronary artery disease, cardiomegaly, middle cerebral artery infraction, hypertension, arthritis, and congenital femoral hypoplasia. Ikegami and colleagues therefore linked genes dysregulated in progeria-patient fibroblast lines with clinical presentations of HGPS. Another meta-analysis identified 525 DEGs, revealing "hub-genes" involved in the altered HGPS pathways, including fibroblast growth factor 2, dexorin, matrix metallopeptidase 2 and FOS protooncogene AP-1 transcription factor (Wang *et al.,* 2020). Pathways in cancer and PI3K-AKT signalling were also identified as having DEG overrepresentation (Wang *et al.,* 2020), not surprising given the association of many growth and proliferation genes with HGPS, and the numerous age-linked genes associated with cancer.

It is evident from transcriptome analyses of HGPS cells that signalling pathways altered in this disease are numerous. The number of these pathways, and their interdependence on one another, have generated difficulties in distinguishing direct targets of progerin from subsequent secondary effects. Nuclear factor, erythroid 2 like 2 (NRF2) is a transcription factor associated with longevity (Lewis *et al.,* 2015) and is up-regulated in response to many promising anti-aging compounds (Calabrese *et al.,* 2021a; Calabrese *et al.,* 2021b; Fang *et al.,* 2018; Han *et al.,* 2012; Hosseini *et al.,* 2020; Kim *et al.,* 2018; Lewis *et al.,* 2015; Robida-Stubbs *et al.,* 2012). Its primary function is to activate expression of antioxidant genes via binding to antioxidant promoter elements of genes. NRF2 promoter sites have been repeatedly identified in down-regulated HGPS DEGs (Kohler *et al.,* 2020; Kubben *et al.,* 2016). To establish if changes in NRF2 transcription factor binding drives HGPS phenotypes, Kubben and colleagues examined nuclear localization of NRF2, identifying accumulation of the

transcription factor at the nuclear envelope in HGPS cells. It was further confirmed that NRF2 was preferentially bound by progerin over lamin A, likely sequestering the transcription factor at the nuclear periphery and preventing its interaction with NRF2-linked antioxidant pathway genes (Kubben *et al.*, 2016).

As with NRF2, nuclear factor kappa B (NF-κB) regulates gene expression in mammalian aging (Adler *et al.,* 2007) and accumulates at the nuclear envelope in HGPS mouse-model cells. This accumulation is proposed to activate the NF-κB signalling pathway, increase inflammation, and contribute to the senescence associated phenotype (Osorio *et al.,* 2012), and therefore premature senescence, of HGPS cells. Inhibition of NF-kB increases lifespan of HGPS mouse-models (Osorio *et al.,* 2012). NF-κB signalling and NRF2 expression are closely associated, with NF-κB modulating NRF2 transcription and activity, whilst absence of NRF2 increases NF-κB activity (reviewed in Warden, et al., 2015).

Other molecular pathways dysregulated in HGPS can be more directly linked to physical characteristics of the disease. Disruption of WNT/β-catenin signalling is associated with brittle bones in HGPS patients (Choi *et al.,* 2018; Hernandez *et al.,* 2010), whilst mitochondrial disruption contributes to loss of skeletal mass and function (Aliper *et al.,* 2015; Marzetti *et al.,* 2013). Additionally, disruption of the EGFR pathway is associated with delayed wound healing (Aliper *et al.,* 2015), and disrupted TGF-β signalling has been linked to features of skin aging (Aliper *et al.,* 2015). Other altered pathways include, but are not limited to, caspase cascade pathway, ERK pathway, mammalian target of rapamycin (mTOR) signalling and insulin growth factor-1 (IGF-1) signalling. The extensive nature of this list, alongside with the physical characteristics associated with misregulation of these pathways, highlight the extent to which accumulation of progerin perturbs normal cellular function and contributes to HGPS progression.

1.2.5 Current and Experimental Treatment Strategies for Hutchinson-Gilford Progeria Syndrome

Hutchinson-Gilford Progeria Syndrome is a rare disease with no cure. Despite its rarity, intensive research has examined numerous avenues of treating this disease, perhaps due to its striking resemblance to the normal aging process, the severity of the HGPS phenotype, or even the potential to apply proven methods to other rare diseases. Numerous

small molecule compounds have been tested in the treatment of HGPS across model organisms, including various farnesyl transferase inhibitors (FTI) (FTI-276 (Wang *et al.*, 2010); FTI 277 (Bikkul *et al.*, 2018; Mehta *et al.*, 2011). Although numerous avenues have been explored, from drug repurposing to genome editing, just one compound has recently been approved by the FDA to treat HGPS – the FTI lonafarnib (also known as Sarasar or Zokinvy) (Dhillon 2021). FTIs function by preventing the addition of a farnesyl group to progerin, reducing progerin accumulation at the nuclear membrane, promoting progerin degradation and ameliorating the induction of cellular defects associated with HGPS, with evidence at the cellular level (Capell *et al.*, 2005; Glynn *et al.*, 2005; Mallampalli *et al.*, 2005; Yang *et al.*, 2005) and from studies in progeroid-like model organisms, in which lifespan was also extended (Capell *et al.*, 2008; Fong *et al.*, 2006; Takenaka *et al.*, 2000a; Yang *et al.*, 2005; Yang *et al.*, 2008). The first clinical trials of Lonafarnib in 25 HGPS patients (aged between 3-16 years) were approved, and following a minimum of two years of treatment, it was reported that patients exhibited maintained or improved weight gain, reduced vascular stiffness (Gordon *et al.*, 2012) a mean increase in survival of 1.6 years (Gordon *et al.*, 2012) and a potential decrease in mortality rate (Gordon *et al.*, 2012).

Although FTIs have been approved for clinical use, and show promising results *in vitro* and *in vivo*, caution is still required, and additional research needed. This compound does not reverse all HGPS phenotypes, and many of the improvements seen in animal models were not transferable to human trials. Furthermore, FTIs only extended lifespan by ~11% (based on the average life expectancy of an HGPS patient being 14 years old). This could be due to FTIs inhibiting other molecular pathways that require farnesylation to properly function, for example in Ras signalling (Gysin *et al.*, 2011). It has also been reported that in the absence of farnesyl transferases, progerin is alternatively prenylated by geranylgeranyltransferase I. Although not approved as a co-treatment by the FDA, HGPS mouse models treated with an FTI and a GeranylGeranylTransferase I inhibitor had extended lifespans, with improved physical findings to untreated controls (preventing weight loss, growth retardation, lipodystrophy, hair loss, and bone defects) (Varela *et al.*, 2008). FTIs have also been demonstrated to exhibit severe side effects in HGPS models when used long-term, including neurotoxicity to the hippocampus neurons of rat embryos (Kim *et al.*, 2010). In non-progeroid mice, accumulation of prelamin A results in lethal cardiomyopathy, without

expression of any HGPS phenotypes, suggesting that accumulation of prelamin A in those treated with FTIs could also generate dangerous side-effects (Davies *et al.,* 2010). Therefore, despite the approval of FTIs in the treatment of HGPS, there is a long way to go in generating a more effective treatment strategy that decreases the impact of HGPS phenotypes, has fewer risky side effects, and has the potential to further extend the health and lifespan of HGPS patients. Although several cellular phenotypes have been restored by FTIs, including chromosome territory localization (Mehta *et al.,* 2011), the global impact of these compounds in re-establishing normal genome function and structure, such as the effect on heterochromatin marks and transcription, have not been evaluated.

HGPS is a rare disease; however, investigations into genetic therapies for this condition are numerous. A plethora of attempts at modifying the genome in model organisms have been made to correct or ameliorate the HGPS phenotype, including prenatal genetic manipulation (Griveau *et al.,* 2018; Ibrahim *et al.,* 2013; Liu *et al.,* 2013; Ocampo *et al.,* 2016; Osorio *et al.,* 2012; Strandgren *et al.,* 2015), antisense oligonucleotide (ASO) therapy (Aguado *et al.,* 2019; Lee *et al.,* 2016a; Osorio *et al.,* 2011), CRISPR-Cas9 (Beyret *et al.,* 2019; Santiago-Fernandez *et al.,* 2019), and base editing (Koblan *et al.,* 2021).

ASOs are short, chemically synthesized, DNA sequences (12-30 nucleotides) that are designed to target and bind specific RNA sequences, to promote its degradation or sterically hinder its translation (reviewed in (Bennett 2019)). Osorio, et al., provided initial evidence that ASOs could be used in the treatment of HGPS, using an ASO to target the *LMNA/C* pre-mRNA, ameliorating HGPS phenotypes and extending lifespan in HGPS-model mice (Osorio *et al.,* 2011). ASOs have since been used to ameliorate specific HGPS defects (such as the DNA damage response (Aguado *et al.,* 2019)) and its clinical effects (e.g. aortic pathology (Lee *et al.,* 2016a)). In complementary works, Erdos et al., and Puttaraju, et al., screened novel ASOs for their therapeutic potential in HGPS mice models, demonstrating significant decreases in progerin transcript and protein levels, and increased mouse lifespan (61.6 % and 33% respectively). ASO therapy started at 2 weeks by Erdos and colleagues also rescued the vascular phenotypes of HGPS – significant given the primary cause of death is linked to vascular decline in HGPS patients (Erdos *et al.,* 2021; Koblan *et al.,* 2021). However, some tissue abnormalities were observed in the kidney tissue of mice, suggesting potential toxicity as a result of ASO treatment. An increase in treatment dose by Puttaraju and colleagues

resulted in just 19% lifespan extension, compared to lower dose at 33%, also hinting at potential ASO toxicity (Puttaraju *et al.,* 2021). Furthermore, discrepancies in these findings may be the result of age of treatment onset (2 weeks vs 5-6 weeks), with earlier treatment aligning with the greater lifespan extension. This is supported that in mice, there is an age at which stem cells lose their ability to repopulate the tissue, meaning the tissue damage caused by progerin is irreversible (Rosengardten *et al.,* 2011). Although more research is needed, ASO's may prove a future option given approval by the FDA already in the treatment of other genetic diseases.

Clustered regularly interspaced short palindromic repeats (CRISPR)-Cas9 is a popular technology for genome editing and investigating treatment of genetic disease. As such, CRISPR-Cas9 has been investigated as a potential *in vivo* strategy for treating HGPS. Using adeno-associated virus serotype 9 (AVV9) as a delivery system (due to its safety profile, FDA approval, and broad tissue tropism) Santigao-Fernandez and team targeted a single guide RNA to *LMNA* exon 11 upstream of the HGPS mutation, introducing a frame shift mutation to prevent progerin production in HGPS-model mice. Although it was possible to detect a significant reduction of progerin-positive nuclei in liver, heart, and skeletal muscle, it was not possible to reliably detect a global decrease in progerin mRNA. Furthermore, lung, kidney, and aorta showed no decrease in progerin-positive nuclei, likely due to lower tropism of AAV9 in these organs (Santiago-Fernandez *et al.,* 2019). Regardless, it was important that this method involved postnatal application of genome editing and did extend the lifespan of injected mice. Similarly, and in the same model but genetically modified to be hemizygous for the *Cas9* transgene, Beyret and team implemented CRISPR-Cas9, but targeted lamin A downstream of lamin C, which also increased lifespan of the HGPS mouse-model (Beyret *et al.,* 2019).

A recent method for genetic manipulation, base editing, has also been applied in the treatment of HGPS fibroblasts and HGPS-model mice. Specifically, adenine base editors (ABEs) convert targeted A-T base pairs to G-C pairs (Anzalone *et al.,* 2020; Gaudelli *et al.,* 2017). Koblan and colleagues used an ABE to directly correct the HGPS mutation, introducing the ABE *in vitro* using AAV9 postnatally (Koblan *et al.,* 2021). A single injection of AAV9 encoding the ABE durably (6 months post-injection) corrected the HGPS mutation between 20-60% across organs, with lower levels of progerin detected. Vascular pathology

of mice was also rescued, and lifespan was increased from 215 to 510 days (Koblan *et al.*, 2021).

Many potential HGPS treatments are based on administration of small-molecule compounds and pharmaceuticals, with an abundance of treatment strategies examined in recent years. Of these, a number are already established in promotion of health and lifespan. For example, quercetin (a plant pigment/flavonoid) extends lifespan in worms (Kampkotter *et al.*, 2008; Pietsch *et al.*, 2009), fungi (Warnsmann *et al.*, 2018), yeast (Alugoju *et al.*, 2018) and mice (Geng *et al.*, 2019a). Similarly, resveratrol extends lifespan in silkworms (Song *et al.*, 2020) and turquoise killifish (Valenzano *et al.*, 2006) but has mixed effects in flies (Abolaji *et al.*, 2018; Staats *et al.*, 2018; Wang *et al.*, 2013). Quercetin was demonstrated to decrease senescence in HGPS human mesenchymal stem cells (Geng *et al.*, 2019b). Resveratrol extends lifespan in HGPS-model zmpste24−/− mice, improving bone mineral density and slowing down weight loss (Liu *et al.*, 2012); however, a subsequent study documented only improvement in dental defects (Strandgren *et al.*, 2015). This variation in data is likely due to the use of different HGPS-mouse models or perhaps different age of treatment onset. Both quercetin and resveratrol can be found naturally in the diet, and modulate the adenosine monophosphate kinase (AMPK) and mammalian target of rapamycin (mTOR) signalling pathways, major nutrient signalling hubs, to achieve health and lifespan promotion.

Rapamycin, a compound that is commonly used as an immunosuppressant following organ transplants, has also been demonstrated to reverse nuclear defects observed in HGPS patient fibroblasts, including improving nuclear morphology, decreasing progerin levels, promoting autophagy (Cao *et al.*, 2011b; Graziotto *et al.*, 2012) and DNA damage repair (Bikkul *et al.*, 2018). In an alternative HGPS model, DNA repair deficient mice, rapamycin failed to extend health or lifespan (Birkisdottir *et al.*, 2021). Rapamycin has also been demonstrated to promote health and lifespan in primary human cells and model organisms, with these benefits attributed to its inhibition of mTOR nutrient sensing pathway (Miller *et al.*, 2014; Neff *et al.*, 2013; Wilkinson *et al.*, 2012). As with FTIs, rapamycin may induce severe side effects (Baur *et al.*, 2011; Ekberg *et al.*, 2010), including delayed growth and development in pediatric patients – a major barrier in treated HGPS patients already

exhibiting growth delays. Therefore, identifying additional mTOR targets not associated with such side-effects is desirable.

1.3 Utilizing Nutrient Restriction and Nutrient Restriction Mimetics to Treat Hutchinson-Gilford Progeria Syndrome

1.3.1 Parallels Between Hutchinson-Gilford Progeria Syndrome and the Normal Aging Process

Children with HGPS have a striking resemblance to the elderly, exhibiting aged-looking and thinning skin, prominent veins, hair loss, loss of fat under the skin, and musculoskeletal deformities, including a narrow nose and chin (DeBusk 1972). Clinically, these children also exhibit conditions of aging: osteoporosis and atherosclerotic cardiovascular disease (Baker *et al.,* 1981; Gordon *et al.,* 2011; Merideth *et al.,* 2008; Prakash *et al.,* 2018). Despite these aging-features, HGPS patients do not exhibit developmental delays or signs of neurodegeneration (Nissan *et al.,* 2012; Ullrich *et al.,* 2015). Given commonalities between HGPS and the elderly, researchers examined various cells and tissues from normally aging individuals for the presence of progerin, detecting it in samples from 1 month to 97 years (Cao *et al.,* 2011a; Luo *et al.,* 2013; McClintock *et al.,* 2007; Olive *et al.,* 2010; Scaffidi *et al.,* 2006). Cells exhibiting progerin isolated from non-diseased individuals also exhibited irregular nuclear morphology, increased levels of the DNA damage marker γ-H2AX (McClintock *et al.,* 2007), and decreased H3K9me3/HP1 levels (Scaffidi *et al.,* 2006). Even though progerin was detectable in normally aging individuals, levels were much higher in children with HGPS. It is possible that with age, splicing machinery loses efficiency, and more frequently incorrectly targets the cryptic splice site for progerin production. Another feature of the aging process is the accrual of cellular defects which induce cells to senesce, with accumulation of senescent cells associated with numerous age-linked diseases. This is also observed in HGPS patient fibroblasts, but at a faster rate than the normal aging process. Clearance of these cells has been demonstrated to delay and improve age-related phenotypes (Baar *et al.,* 2017; Baker *et al.,* 2011; Walaszczyk *et al.,* 2019). Telomere length has also been linked to organismal lifespan, with longer telomeres proposed to result in longer lifespan of an organism. In HGPS, telomere length is on average less than those in non-diseased fibroblasts (Decker *et al.,* 2009); however, in HGPS cells that do not express *LMNA*, telomeres were of equal length to age-matched controls (Benson *et al.,* 2009). Telomere

length may be directly linked to progerin levels, with its ectopic expression inducing telomere shortening (Benson *et al.*, 2009), and damage to telomeres in non-disease fibroblasts inducing progerin accumulation (Cao *et al.*, 2011a). Finally, various attempts have been made at creating epigenetic clocks that accurately predict age. Using one of these models, HGPS patient fibroblasts were demonstrated to exhibit similar DNA methylation profiles to fibroblasts from individuals middle-aged and older (Aliper *et al.*, 2015). In spite of these similarities, whole-transcriptome meta-analyses of multiple HGPS fibroblast patients compared to age-matched controls, as well as normally aged individuals, revealed HGPS patient fibroblast transcriptomes more closely resembled that of the age-matched controls than the elderly, suggesting HGPS gene expression is divergent to that of physiological aging (Kohler *et al.*, 2020).

Though commonalities exist between HGPS and normal aging, the aging process is complex, and although progerin has been detected in HGPS and in normally aging individuals, the death of average humans before the accumulation of HGPS-equivalent levels of progerin indicates that other molecular mechanisms may be involved. Nevertheless, the similarities between HGPS and aging implicate strategies proven successful in the treatment of aging/promotion of health and lifespan as potential treatment opportunities for HGPS.

1.3.2 Caloric Restriction: The Original Method of Extending Health and Lifespan

For as long as humans have understood the association between aging and death, they have searched for methods to promote immortality; although most modern-day scientists are more realistic in searching for methods to extend lifespan and/or health span, as opposed to achieving immortality. One such method of lifespan and health span extension is caloric restriction (CR), the reduction of nutritional intake by 60-80% of *ad libitum* without inducing malnutrition. CR has been repeatedly demonstrated to extend health and lifespan across numerous model organisms, from the unicellular to non-human primates (yeast (Jiang *et al.*, 2000), fruit flies (Mair *et al.*, 2011), nematodes (Lakowski *et al.*, 1998), crustaceans (Ingle *et al.*, 1937; Weeks 2020), spiders (Austad 1989), lab mice/rats (McCay *et al.*, 1935; Weindruch *et al.*, 1986) and monkeys (Colman *et al.*, 2014; Mattison *et al.*, 2017; Mattison *et al.*, 2012). Trials in humans have also proven effective in preventing and improving outcomes of age-linked pathologies such as cancer (Brandhorst *et al.*, 2015; Mercken *et al.*, 2013). One

mechanism by which CR may achieve these results is through the reduction of senescent cells, as demonstrated in cell culture and model organisms (Csiszar *et al.*, 2009; Fontana *et al.*, 2018; Makino *et al.*, 2021; Messaoudi *et al.*, 2006; Shinmura *et al.*, 2011). CR has also been documented to delay and prevent age-associated cellular changes shared between the elderly and HGPS patients, including genomic instability, telomere shortening, epigenetic changes, loss of proteostasis, mitochondrial dysfunction, and dysregulated free-radical scavenging (Blanc *et al.*, 2003; Cabelof *et al.*, 2003; Hambly *et al.*, 2005; Heilbronn *et al.*, 2006; Il'yasova *et al.*, 2018; Ke *et al.*, 2020; Redman *et al.*, 2018; Um *et al.*, 2003; Vermeij *et al.*, 2016; Wang *et al.*, 2018b).

With age, and in HGPS, changes in intracellular and nutrient sensing have been reported. Higher levels of insulin and decreased insulin sensitivity are a major aging-phenotype – with decreased insulin sensitivity (Barinda *et al.*, 2020) identified in HGPS model-mice, and early onset type II diabetes observed in some HGPS patients (Holder *et al.*, 2020; Shalev *et al.*, 2007). CR decreases levels of circulating glucose and insulin, increasing insulin sensitivity (Dao *et al.*, 2018; Granado *et al.*, 2019; Kannan *et al.*, 2013; Zhang *et al.*, 2014). This decrease in glucose and insulin levels/increase in insulin sensitivity promote maintenance and repair in mice (Mitchell *et al.*, 2016), with unclear results in short-term human trials (Belsky *et al.*, 2017; Fontana *et al.*, 2016; Fontana *et al.*, 2008). Limited research into CR as a treatment for HGPS has demonstrated that it is also effective at ameliorating HGPS-associated pathologies in DNA repair-deficient Ercc1 Δ/− mice (Vermeij *et al.*, 2016), tripling median and maximal lifespan, reducing γ-H2AX DNA damage foci and promoting genome stability.

At the centre of CR reversing these hallmarks of aging, reducing inflammation and incidence of age-linked diseases, is signalling to the mammalian target of rapamycin (mTOR) pathway – a major hub integrating multiple sources of information on cellular nutrient status to shift cellular state from growth and proliferation to maintenance and repair, inducing autophagy (molecule recycling) and decreasing protein translation.

1.3.2.1 The Mammalian Target of Rapamycin Pathway

The target of rapamycin (TOR) pathway detects nutrient levels from multiple sources to determine subsequent cellular functions and has been identified as a key target in the promotion of health and lifespan at the cellular and organismal level. Under conditions of

plentiful nutrients, cell growth and proliferation are promoted via changes in the mTOR pathway and its downstream components, whilst under nutrient restriction the cellular state will shift to energy conservation, autophagy induction, and repair (reviewed in (Almendariz-Palacios *et al.,* 2020)). In mammals the mTOR pathway is composed of two complexes, mammalian target of rapamycin complex (mTORC)1 and mTORC2 (Kim *et al.,* 2019b). mTORC1 is comprised of seven proteins (DEP domain containing mTOR-interacting protein (DEPTOR), regulatory-associated protein of mTOR (Raptor), mammalian lethal with sec-13 (mLST8), tti1/tel2, and proline rich AKT substrate 40 kDa (PRAS40)). mTORC2 is also composed of DEPTOR, mLST8 and tti1/tel2, but diverges from mTORC1 by the inclusion of rapamycin-insensitive companion of mTOR (RICTOR), protein observed with rictor 1 and 2 (Protor 1/2) and mammalian stress-activated kinase-interacting protein 1 (mSin1). mTORC1 is well characterized and is directly involved in mediating cellular responses to nutrient levels, whilst until recently, mTORC2 had only been identified as involved in regulating cytoskeletal organization. However, there is new evidence that mTORC2 is also nutrient sensitive (Kazyken *et al.,* 2019), suggesting that this complex may also have a currently undefined role in cellular responses to nutrient levels.

Upstream of mTORC1, multiple growth factor pathways (such as the insulin/insulin-like growth factor 1 pathway) converge at the tuberous sclerosis complex (TSC; a heterotrimeric complex of TSC1, TSC2 and Tre-2/Bub2/Cdc16 Domain Family Member 7 (TBC1D7)) (Dibble *et al.,* 2012) (Figure 1.4). In the presence of growth factors, the phosphoinositide 3-kinase/3-phosphoinositide-dependent protein kinase 1/protein kinase B (PI3K/PDK1/AKT) pathway inhibits the TSC via multisite phosphorylation of TSC2, dissociating the TSC from the lysosomal membrane (Menon *et al.,* 2014). This enables GTP-loading of RAS homolog enriched in brain (Rheb), also partially localized to the lysosome, enabling its phosphorylation of mTORC1. Up-regulated mTORC1 promotes downstream pathways (e.g. nucleotide, lipid and protein synthesis) involved in cellular growth and proliferation (reviewed by (Liu *et al.,* 2020)) (Figure 1.4). Other growth factor pathways converging at the TSC include receptor tyrosine kinase-dependent Ras signaling, wingless-related integration site (WNT), and tumor necrosis factor α (TNFα), although exactly how the TSC integrates the input of these various pathways is unknown (reviewed in (Liu *et al.,* 2020; Saxton *et al.,* 2017)). In the absence of growth-factor signalling, TSC sequesters Rheb at the

surface of the lysosomal membrane, preventing up-regulation of mTOR, and instead shifting cellular processes toward maintenance and repair, promoting autophagy (reviewed by (Almendariz-Palacios *et al.,* 2020)).

As with many mTOR inhibitors, CR does not directly inhibit the mTOR pathway, but modulates upstream energy-sensing complexes (Figure 1.5). In response to CR, the ratio of adenosine monophosphate (AMP):ATP is altered, with an increase in AMP levels indicating nutrient scarcity. This altered ratio activates the adenosine monophosphate activated protein kinase (AMPK; reviewed in (Almendariz-Palacios *et al.,* 2020)). AMPK is a heterotrimeric serine/threonine kinase comprised of a catalytic α-subunit and regulatory β- and γ- subunits. These subunits each have tissue-dependent isoforms, with key differences in these isoforms including the degree of AMP dependence exhibited (Burkewitz *et al.,* 2014; Gowans *et al.,* 2014). AMPK is allosterically activated by AMP binding to its γ-subunit and by phosphorylation. This phosphorylation is promoted by AMP binding, and conformational changes of AMPK as the result of AMP binding the γ-subunit inhibits dephosphorylation of AMPK by protein phosphatases. Therefore, AMPK can be activated not just by CR, but any stress that can increase AMP:ATP ratios (e.g. hypoxia). Key upstream kinases known to phosphorylate AMPK include the liver kinase B1 (LKB1) complex. The role of AMPK activation is to promote catabolic pathways and increase cellular energy status, inhibiting anabolic pathways that are not essential for cell survival, and thus inhibits mTOR indirectly, preventing protein synthesis (Bolster *et al.,* 2002; Horman *et al.,* 2002) (Figure 1.5). AMPK achieves this by both phosphorylation of Raptor (an mTORC1 component) and of TSC2. AMPK activation has also been associated with increased nicotinamide adenine dinucleotide $(NAD)^+$ levels - achieved by CR. This molecule induces deacetylation of peroxisome proliferator-activated receptor-γ coactivator 1α (PGC-1α) by sirtuin 1 (SIRT1), with PGC-1α key in regulating mitochondrial biogenesis, disruption of which results in shortened lifespans, and promotion of PGC-1α increasing health and lifespan. Specifically, AMPK phosphorylates PGC-1α at two sites (Thr177 and Ser538) proceeding deacetylation of PGC-1α by SIRT1, therefore activating PGC-1α. Furthermore, increasing SIRT1 levels have also been documented to increase health and lifespan (Longo *et al.*, 2006).

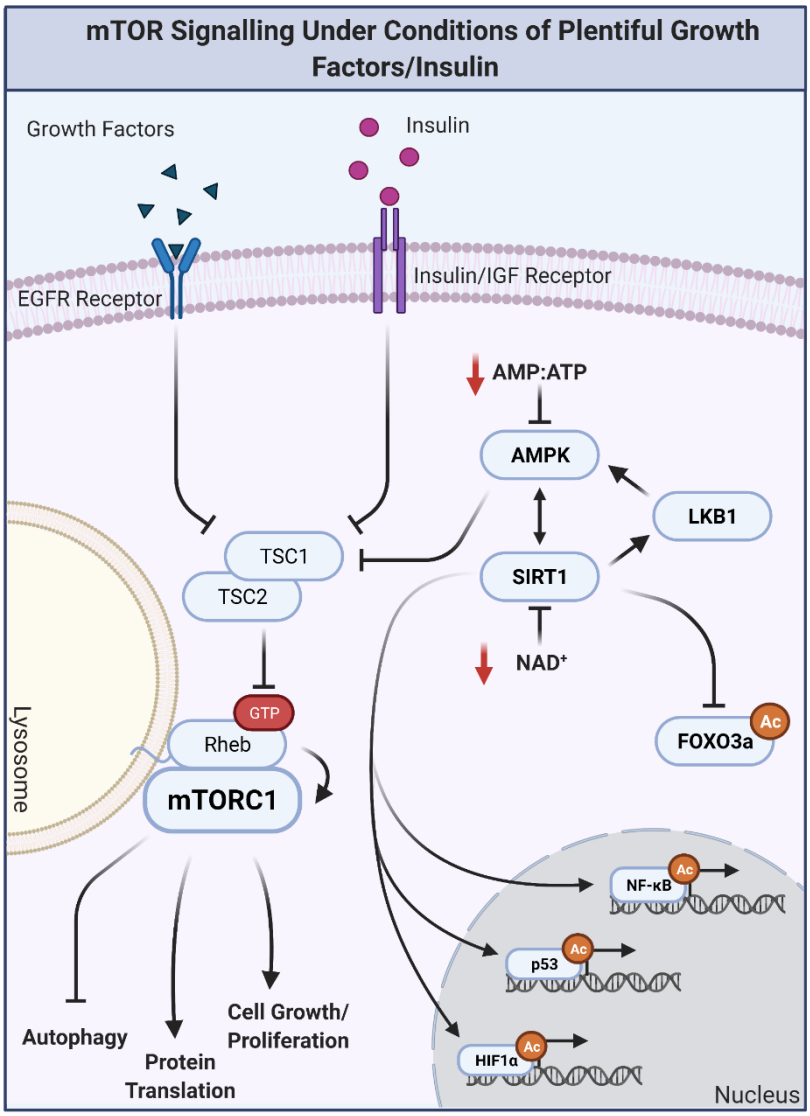

Figure 1.4: mTOR Signalling in Response to Conditions of Plentiful Growth Factors/Insulin. mTORC1 integrates signals from nutrients and growth factors to regulate cell function. When plentiful growth factors and insulin are available, TSC1/2 are inhibited, preventing GTP loading of Rheb and subsequent activation of mTORC1. Under these conditions mTORC1 signals downstream to promote cell growth, proliferation, and protein translation, while down-regulated pathways such as autophagy. Under conditions of plentiful nutrients, ATP is increased and AMP:ATP ratio decreased. Theis results in AMPK inhibition, which also contributes to inhibition of TSC1/2 and subsequent mTORC1 activation. AMPK also modulates AMPK-SIRT1-LKB1 feedback loop, down-regulating expression of FOXO3a and promoting synthesis of genes/proteins involved in the cell cycle. Figure created in BioRender.com and reprinted with permission (Almendariz-Palacios *et al.*, 2020).

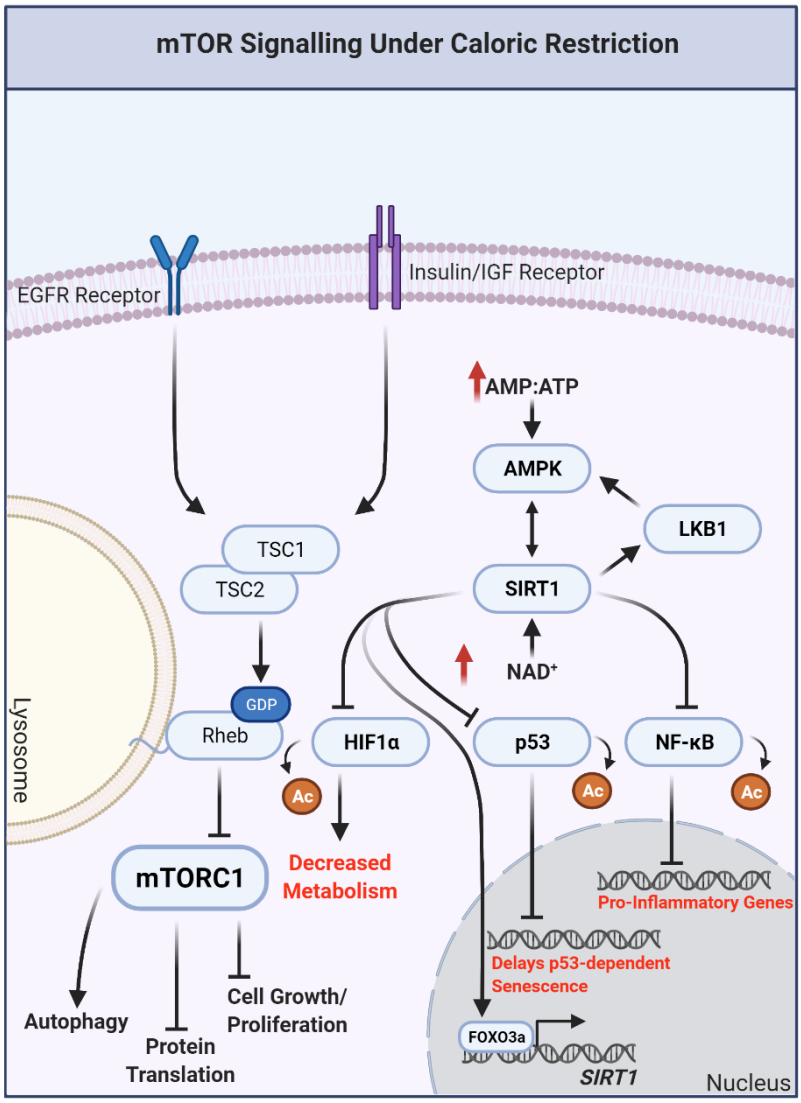

Figure 1.5: mTOR Signalling in Response to Caloric Restriction. In the absence of plentiful nutrients (or under conditions of CR), TSC1/2 are activated, GDP loading rheb and enabling dissociation of mTORC1 from the lysosomal surface. As a result, protein translation, cell growth and proliferation are inhibited, whilst autophagy is up-regulated to recycle cellular components to be used in mTORC1 activation or fulfil other biosynthetic needs. ATP levels decrease, increasing AMP:ATP ratios and activating AMPK, which then contributes to mTORC1 inhibition, as well as modulating SIRT1-LKB1-AMPK feedback loop, decreasing metabolism while also upregulating pro-longevity factors. Figure created in BioRender.com and reprinted with permission (Almendariz-Palacios *et al.*, 2020).

1.3.3 Amino Acid Restriction as an Alternative to Caloric Restriction in Extending Health and Lifespan

Although CR is promising in extending health and lifespan, it is hard to achieve. Nearly 40% of the Worlds population are overweight (World Health Organization, 2020). Therefore, considering alternative strategies in which specific elements of the diet are reduced could be appealing and more achievable. CR is non-specific. It may be possible to remove specific elements of the diet and still achieve prolonged health and lifespan. Like CR, restriction of just amino acids has been documented to extend lifespan in yeast (Cheon Lee *et al.,* 2014; Jiang *et al.,* 2000), ants (Arganda *et al.,* 2017) and flies (Cheon Lee *et al.,* 2014; Min *et al.,* 2006). Furthermore, removing only amino acids from the diet is sufficient to modulate mTORC1 function (Beugnet *et al.,* 2003; Carroll *et al.,* 2016; Hara *et al.,* 1998; Long *et al.,* 2005). Multiple amino-acid restriction regimes have been studied. For example, restriction of branched chain amino acids (BCAAs) in mice has been reported to be as beneficial as total amino acid restriction (Xiao *et al.,* 2014). Furthermore, removal of BCAAs improves metabolic health of mice (Cummings *et al.,* 2018), and extends male-mouse lifespan (Richardson *et al.,* 2021). In rats, removal of essential amino acids (leucine, lysine, methionine and threonine), and total AAR, reduced IGF-1 levels (Takenaka *et al.,* 2000b), also associated with promoting health and lifespan.

1.3.3.1. Amino Acid Sensing

Another key indicator of cellular nutrient status to which mTOR responds is the presence of amino acids (Beugnet *et al.,* 2003; Carroll *et al.,* 2016; Hara *et al.,* 1998; Long *et al.,* 2005). Some organisms can synthesize all amino acids required for survival; mammals must rely on extracellular sources for a subset of amino acids (essential amino acids). Although it has been established that mTOR activity can be modulated by amino acid levels, exactly how these signalling inputs are integrated into the mTOR pathway is unclear, with potentially distinct upstream receptors for each amino acid. Only a few of these amino acid receptors have been identified, those for arginine, leucine, and methionine (Chantranupong *et al.,* 2016; Saxton *et al.,* 2016a; Saxton *et al.,* 2016b), and an amino acid specific regulator identified for glutamine and asparagine. Furthermore, it has been proposed that amino acids modulate mTORC1 activity through two distinct pathways, the RAG-GTPase pathway and the RAG-GTPase independent pathway (Almendariz-Palacios *et al.,* 2020; Meng *et al.,* 2020).

In response to eight amino acids (alanine, arginine, histidine, leucine, methionine, serine, threonine, and valine) and under the Rag-GTPase pathway, mTORC1 is localized to the lysosomal surface (Sancak *et al.,* 2010). Due to the presence of amino acids, Ras-related GTP-binding protein (Rag)A/B and RagC/D form stable dimers, which are targeted to the lysosome via Ragulator. RagC/D is GDP loaded, and RagA/B guanosine triphosphate (GTP) loaded. This promotes interaction with the raptor subunit of mTORC1, maintaining localisation to the lysosomal surface and promoting cell growth, proliferation, and protein translation (Figure 1.6) (Almendariz-Palacios *et al.,* 2020; Sancak *et al.,* 2008). Although it has been demonstrated that eight amino acids function through the Rag-GTPase pathway, only three of these amino acids (arginine, leucine, and methionine) have known upstream sensors that interact with the Rag-GTPase pathway. Arginine and leucine are bound by their respective sensors, cytosolic arginine sensor for mTORC1 (CASTOR) and sestrin2 (Chantranupong *et al.,* 2016; Saxton *et al.,* 2016a; Saxton *et al.,* 2016b; Wolfson *et al.,* 2016). This prevents association of these sensors with GTPase-activating protein toward Rags (GATOR)2, and GATOR1. In the presence of Rag-GTPase dependent amino acids, GATOR2 suppresses association of GATOR1 with the lysosome. Rag GTPases, which are primarily controlled by GATOR1/2, form active heterodimers (RagA/B-GTP and RagC/D-guanosine diphosphate (GDP)) which recruit mTORC1 to the lysosomal surface, where mTORC1 is activated by Rheb. Localization of Rheb can also be regulated by amino acid signalling, promoting an amino-acid dependent interaction of Rheb with microspherule protein 1 (MCRS1), maintaining Rheb localization to the lysosome. Similarly, methionine is indirectly detected by the S-adenosylmethionine sensor upstream of mTORC1 (SAMTOR) via binding of its metabolite, S-adenosylmethionine. Upon binding of SAM, SAMTOR is dissociated from GATOR1, and following the Rag GTPase-dependent pathway, upregulates mTOR activity (Figure 1.6) (Kim *et al.,* 2019b). In the absence of these amino acids, GATOR2 is bound by the leucine and arginine sensors, enabling association of GATOR1 with the lysosomal membrane via KICSTOR, down-regulating mTOR activity. SAMTOR functions in a similar way, binding GATOR1 instead of GATOR2 (Figure 1.7).

Unlike arginine, leucine and methionine, mTOR-associated responses to asparagine and glutamine function via the Rag-GTPase independent pathway, require lysosomal H+ATPase (v-ATPase), and vesicle trafficking ADP ribosylation factor (Arf-1 GTPase)

(Duran *et al.*, 2012; Jewell *et al.*, 2015; Meng *et al.*, 2020; Stracka *et al.*, 2014). This sensor acts independently of GATOR and RagA/B/C/D, although the processes linking Arf-1 to mTOR promotion are still unknown. Amino acids can also be detected from the lysosome, for example, SLC39A9 is a lysosomal arginine sensor that interacts with the Rag-GTPase-Ragulator-v-ATPase complex, promoting mTORC1 activity (Kim *et al.*, 2019b). It is likely that this couples release of essential amino acids from the lysosome (generated during proteolysis) to mTORC1 activity.

The responses of mTORC1 to amino acid levels have become optimized to detect sufficient amino acid levels; however, a second pathway centralized to the general control non-derepressable 2 (GCN2) responds specifically to a lack of amino acids or amino acid imbalance. As intracellular levels of amino acids decrease, so do levels of charged tRNA. Uncharged tRNA levels increase, binding and activating the protein kinase GCN2 which phosphorylates its target, eukaryotic initiation factor 2α (eIF2α). eIF2α then inhibits eIF2β, slowing the rate at which eIF2α is reloaded with GTP, reducing the GTP-GDP rates necessary for mRNA translation re-initiation, decreasing global levels of translation (Kilberg *et al.*, 2012). Despite the overall decrease in translation, a subset of mRNAs, generally with upstream open reading frames, increase translation rates, increasing levels of activating transcription factor (ATF)2, ATF4, ATF5 and DNA damage inducible protein phosphatase 1 regulatory subunit 15A (GADD34) (Lee *et al.*, 2009). ATF4 translocates to the nucleus, where it promotes transcription of genes containing amino acid response elements (AAREs), upregulating expression of amino acid transporters, metabolic regulators, antioxidant defences, and other processes involved in re-establishing homeostatic cellular conditions. A subset of autophagy-related (ATG)4-up-regulated genes, usually those that do not respond to other amino acid response-liked transcription factors, also require phosphorylation of ATF2, while GADD34 enables feedback signalling to permit the translation of these GCN2-linked genes (Chaveroux *et al.*, 2009; Novoa *et al.*, 2003).

The GCN2 and mTOR pathways communicate with one another to promote cellular homeostasis. A key protein in this interaction is fibroblast growth factor (FGF)21. FGF21 is up-regulated by ATF2/4 in the absence of amino acids (De Sousa-Coelho *et al.*, 2012; Maruyama *et al.*, 2016), and activates the mTORC1 pathway via mitogen activator protein kinase (MAPK) (Minard *et al.*, 2016). Given that FGF21 is primarily secreted by the liver,

this molecule could act as a signal of global energy status across tissues, promoting energy-saving states across various cell types. FGF21 could be key in mediating beneficial responses to dietary restriction and amino acid restriction. Administration of FGF21 has been documented to alleviate biological features associated with osteoarthritis (Lu *et al.*, 2021), and extend lifespan in mice (Zhang *et al.*, 2012). FGF21 has also been documented as essential in cellular response to methionine restriction in preventing cognitive decline (Ren *et al.*, 2021), as well as response to dietary restriction (Fujii *et al.*, 2019), logical given that restriction of dietary intake also includes restriction of amino acids. Therefore, restriction of individual amino acids may be as effective as whole dietary restriction, via activation of the mTOR-linked GCN2 pathway.

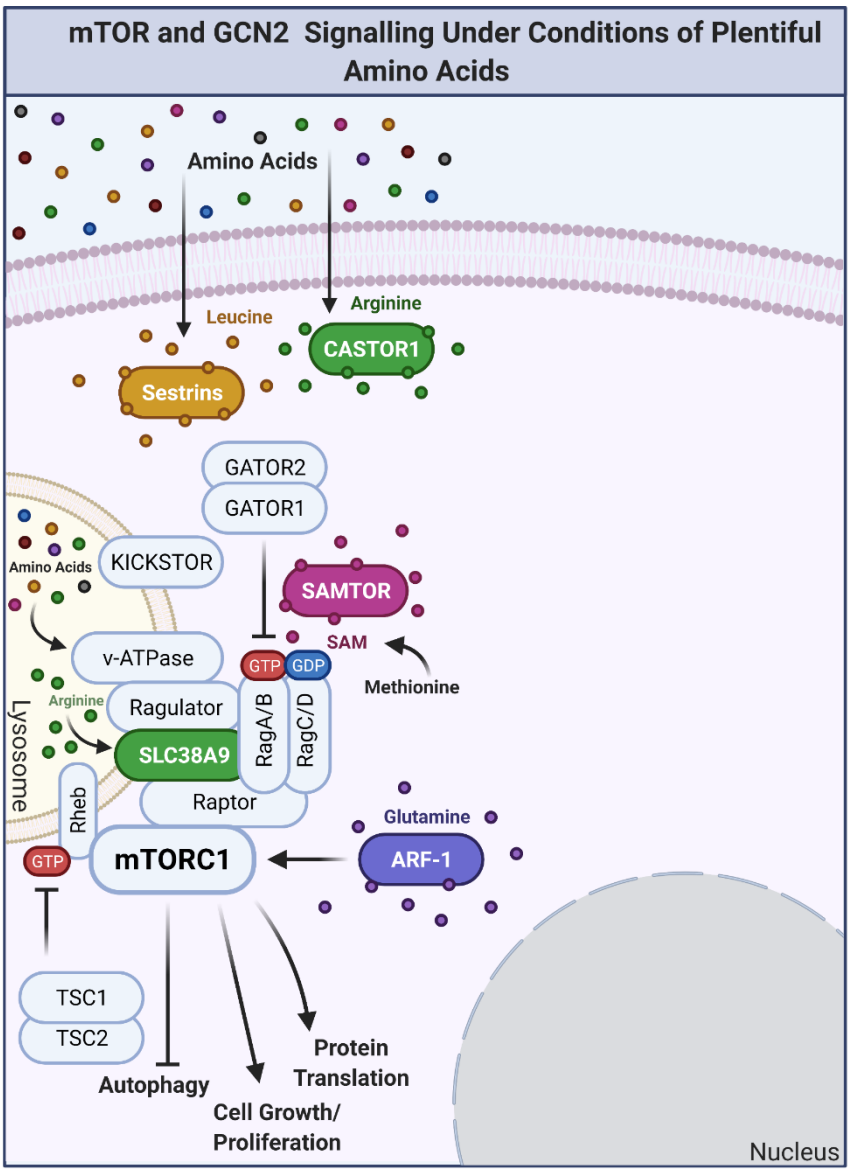

Figure 1.6: mTOR and GCN2 Signalling in Response to Conditions of Plentiful Amino Acids. In the presence of amino acids, mTORC1 integrates signals from a variety of amino acid sensors. In the cases of arginine, leucine, methionine, and glutamine, these amino acids bind their respective amino acid sensors (CASTOR1, Sestrins, SAMTOR, ARF-1) preventing formation of complexes necessary for mTOR inactivation. mTORC1 also receives input from lysosomal amino acid levels via lysosomal amino acid sensor v-ATPase, with SLC38A9 the lysosomal sensor of arginine. While amino acids are binding their respective sensors, mTORC1 remains active, promoting cell growth and proliferation. Figure created in BioRender.com and reprinted with permission (Almendariz-Palacios *et al.*, 2020).

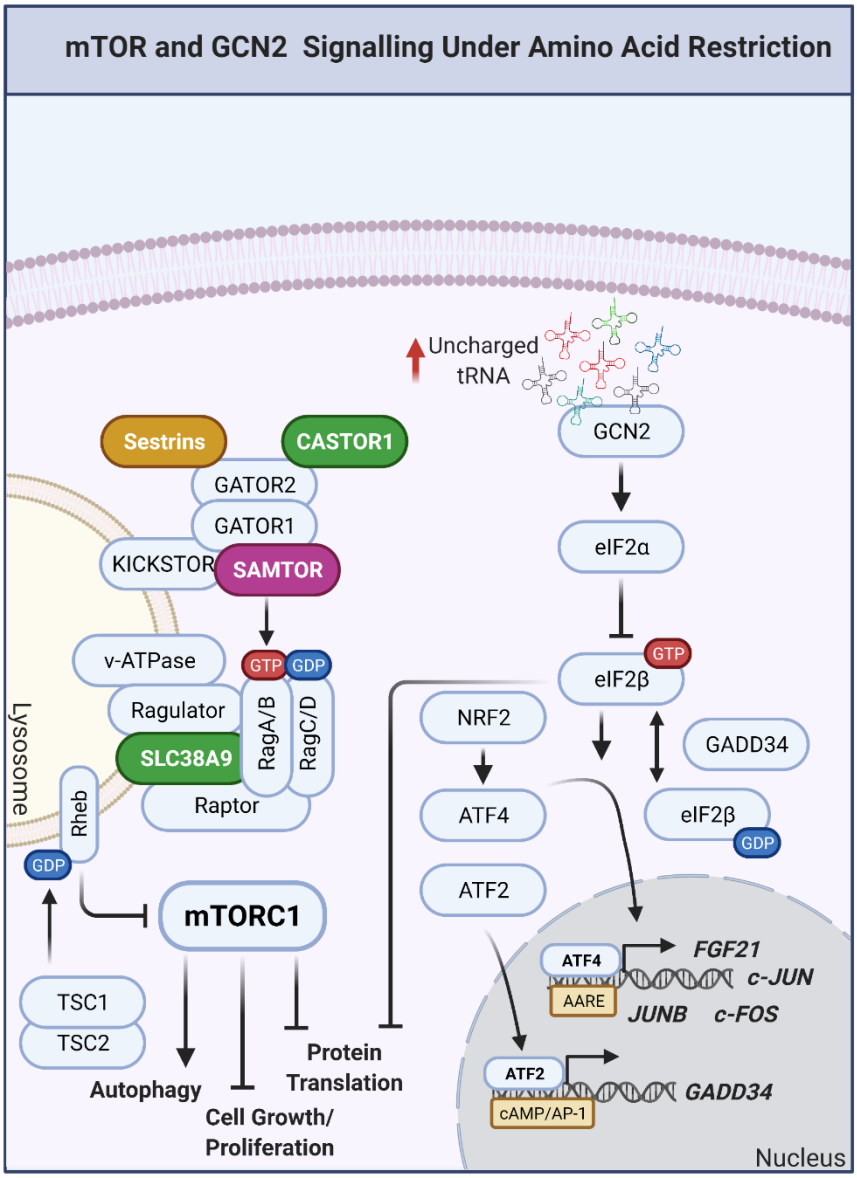

Figure 1.7: mTOR and GCN2 Signalling in Response to Amino Acid Restriction. In the absence of amino acids, mTORC1 is inhibited, promoting various cellular maintenance, repair, and longevity pathways. CASTOR1 and sestrins can bind GATOR2, generating a downstream signalling cascade which results in mTORC1 dissociating from the lysosomal surface. Unbound tRNA levels increase, binding GCN2 and upregulating the integrated stress response. eIF2α is converted to eIF2β, which cycles between GTP- and GTP-loaded states. This process is regulated by GADD34. This process promotes translocation of ATF2/4 to the nucleus where they upregulate genes containing amino acid response elements. Figure created in BioRender.com and reprinted with permission (Almendariz-Palacios *et al.*, 2020).

1.3.4. Metformin as a Potential Treatment for Hutchinson-Gilford Progeria Syndrome

Metformin, (*N*,*N*-dimethylimidodicarbonimidic diamide), derived from the French Lilac (*G. officinalis*) a compound normally used in the treatment of type II diabetes, has also been documented to extend lifespan across model organisms (worms (Cabreiro *et al.,* 2013; Chen *et al.,* 2017), silkworms (Song *et al.,* 2019), and mice (Martin-Montalvo *et al.,* 2013). Like CR, metformin is proposed to prolong health and lifespan via increased AMP:ATP ratios, activating AMPK and inhibiting mTORC1. Metformin likely achieves its health and lifespan promoting properties by regulating mitochondrial metabolism (Andrzejewski *et al.,* 2014; Anedda *et al.,* 2008; Jing *et al.,* 2018; Rena *et al.,* 2017). Furthermore, metformin mediates levels of inflammation-linked cytokines (Gillespie *et al.,* 2019; Saisho 2015; Ustinova *et al.,* 2019), increases insulin sensitivity (Cree-Green *et al.,* 2019), and decreases IGF-1 levels (Yang *et al.,* 2020). Mediation of these pathways has been linked to pro-longevity transcription factors FOXO3a and AP-1, both of which regulate cytokine levels. The ATF2 transcription factor network was also enriched in response to metformin treatments (Gillespie *et al.,* 2019), further linking this pathway to pro-longevity mechanisms.

2.0 HYPOTHESIS AND OBJECTIVES

HGPS is a devastating childhood disease with a short life expectancy. Currently, no treatments exist for HGPS that effectively extend the health and lifespan of patients without severe side effects (FTI's, rapamycin). The effectiveness of rapamycin has been attributed to inhibition of the mammalian target of rapamycin (mTOR) pathway (Cao *et al.*, 2011b). Inhibition of the mTOR pathway through nutrient restriction has also been extensively reported. Given the life and health span promoting effects of nutrient restriction, using this strategy to modulate mTOR could provide a novel avenue for treating HGPS. Specifically, inhibition of mTOR through amino acid depletion (arginine, leucine), glucose restriction, or treatment with nutrient restriction mimetic metformin, could restore genome function (gene expression) and organization of HGPS fibroblasts, restoring rates of DNA damage repair, chromosome mis-localization, and nuclear morphology to that of non-diseased fibroblasts.

Hypothesis: Amino acid (arginine or leucine) restriction, glucose restriction, or metformin treatment will inhibit mTOR signaling, leading to decreased progerin levels and the re-establishment of normal genome organization and function in HGPS cells.

The following specific objectives will be addressed to test this hypothesis:

(1) Determine if arginine or leucine depletion, glucose restriction, or metformin treatment can decrease progerin levels and rates of cellular senescence in HGPS cells by monitoring:

(a) cell growth (doubling) before senescence

(b) progerin levels

(c) changes in cell morphology

(2) Determine if arginine or leucine depletion, glucose restriction, or metformin treatment restore normal genome function and organization in HGPS cells by monitoring:

(d) changes in chromosome territory positioning

(e) the ability of cells to repair their genetic material (DNA)

(f) the re-establishment of heterochromatin marks and compartments

(g) the restoration of non-diseased gene expression profiles

3.0 MATERIALS AND METHODS

3.1 Cell Culture

Primary human dermal fibroblast cell lines (FSF, 2DD) and HGPS primary human dermal fibroblast cell lines AG03513 (Coriell Institute), HGADFN003, HGADFN167, HGADFN169, HGADFN271 (The Progeria Research Foundation) were cultured in 4.5 mg/ml glucose Dulbelco's Modified Eagles Media (DMEM; Corning, Cat #: ca45000-304) containing 15% (v:v) fetal bovine serum (FBS; Gibco, Thermo Fisher Scientific, Cat #: 12483-020) and 1% (v:v) penicillin-streptomycin (GE Healthcare Life Sciences, Cat #: SV30010). Incubator conditions were 37^{o}C, 5% CO_2 (Fisher Scientific, Marietta, OH, USA). To prevent contact inhibition, cultures were not allowed to exceed 70% confluence. Fibroblasts were passaged using TrypLE Xpress (Life Technologies, Cat #: 12604013) to induce dissociation from culture flasks. TrypLE Xpress was deactivated by addition of 15% FBS, 1% penicillin-streptomycin, DMEM, and cells pelleted at 174 relative centrifugal force (rcf) for 3 min (Eppendorf, Hamburg, Germany). The supernatant was aspirated, and pellet gently resuspended in DMEM solution (with 15% FBS, 1% penicillin-streptomycin). Cell counts were conducted using a haemocytometer (Tiefe 0.100 mm, 0.0025 mm2; Neubauer Improved, EM Sciences, Hatfield, PA, USA). Total cell numbers were calculated, and non-diseased fibroblasts (FSF, 2DD) re-seeded at 3000 cells/cm^2, whilst HGPS fibroblasts were re-seeded at 4500 cells/cm^2. Media was changed every 3-4 days until 70% confluence. For experimental assays, HGPS and non-diseased fibroblasts were passage-matched and grown in identical environments. Only fibroblasts between passage 11-14 were used.

3.2 Treatment Conditions

To achieve conditions of nutrient restriction, in house media was made to the same specifications of commercial DMEM. In house DMEM was used for control conditions, and the same recipe with either arginine, leucine, both arginine and leucine, or glucose and pyruvate removed were used. Metformin (Santa Cruz Biotechnology, sc-202000a) was dissolved in nuclease free H_2O. Metformin was added to in house DMEM for a final concentration of 0.5 mM when treating fibroblasts. Rapamycin (LC Laboratories, R-5000) was dissolved in dimethyl sulfoxide (DMSO) and added to in house media for a final concentration of 680 nM. 1% (v:v) of penicillin-streptomycin was added to in house DMEM.

To control for amino acid and batch variation of FBS, 15% knock-out serum (Fisher Scientific, A3181502) was used.

3.3 Cell Counts and Cell Survival

To assess the impact of treatment conditions on cell numbers (population doubling times) and cell viability, cell counts and Trypan Blue (VWR International, USA, CA97063-702) staining were conducted following of 72 h of treatment. For cell counts, media was aspirated, and cells dissociated in TrypLE Xpress. 0.4% Trypan Blue stain was added to cell suspension 1:1 (v:v) and incubated for 5 min. Cell counts were conducted using a Cell Countess (Thermo Scientific Invitrogen Countess II). Cell counts and numbers of Trypan Blue positive cells were recorded. Technical counts were conducted in quadruplet and a minimum of three biological replicates used per cell line.

For long-term cell survival assays in culture, treatments assessed included: combined arginine and leucine restriction, 0.5 mM metformin treatment, 680 nM rapamycin treatment, and restriction of arginine and leucine with 0.5 mM metformin. Arginine and leucine restriction was conducted by cycling 7 days arginine and leucine restricted, followed by 7 days normal growth conditions. 0.5 mM metformin was examined under both cycling and continuous conditions. 680 nM rapamycin was examined by treating continuously until the end of the assay. To prevent contact inhibition and ensure every condition was handled equally, cell counts, and passaging were conducted when one condition reached 70% confluency. Passaging and treatments continued until cell numbers were no longer sufficient for passaging. Cells were also grown as described for five weeks before protein extraction.

3.4 Transfections/shRNA Knockdown

shRNA were reconstituted according to manufacturer's instructions (Santa Cruz) in nuclease free H_2O. Non-disease fibroblasts (FSF) were grown to 70% confluence and HGPS (HGADFN169) fibroblasts were grown to 90% confluence before transfection of shRNA in 6-well plates. To prepare the transfection reaction, 3.75 μl Lipofectamine 3000 reagent (ThermoFisher Scientific, L3000001) was added to 125 μl Opti-MEM medium (ThermoFisher Scientific, 31985062) in an Eppendorf tube (tube 1). In a second Eppendorf (tube 2), 5 μl P3000 reagent and 75 pmol shRNA were added to 125 μl Opti-MEM. Each solution was gently mixed by pipetting before adding tube 2 to tube 1 and mixing well.

Solution was incubated for 15 min, RT. Cells were washed twice with Opti-MEM, and 1 ml Opti-MEM added to the well. Following incubation, transfection reaction was added dropwise to the well and incubated for 6 h 37ºC, 5% CO_2. 1 ml of 2x DMEM (30% FBS, 2% penicillin streptomycin) was added back following incubation. Cells were left in these conditions overnight and media changed the following morning. To maintain consistency between experiments, samples were given 48 h to achieve knock-down before 72 h of respective treatment conditions were applied (untreated, arginine restricted, leucine restricted, combined arginine leucine restricted, metformin treated, or rapamycin treated). Following 72 h of treatment, protein extracts were harvested, and knockdown examined by western blot. shRNA used: shATG5 (shAGP5; Santa Cruz Biotechnology, sc-41445-SH), shCASTOR1 (shGATSL3; Santa Cruz Biotechnology, sc-75555), shSESN2 (sc-106544-SH) and Control shRNA Plasmid-A (Santa Cruz Biotechnology, sc-108060).

3.5 DNA Damage Assays

To access levels of DNA damage and cellular response to DNA damage induction, non-diseased (FSF, 2DD) and HGPS (HGADFN003, HGADFN167, HGADFN169, AG03513) were grown under normal growth conditions, under restricted amino acid conditions (arginine restriction, leucine restriction, combined arginine and leucine restriction), restricted glucose and pyruvate, or in the presence of 0.5 mM metformin or 680 nM rapamycin for 72 h. Each sample was then exposed to 150 μM H_2O_2 for 30 min. Following H_2O_2 exposure, media was replaced with 4.5 mg/ml glucose DMEM containing 15% FBS and 1% penicillin-streptomycin. Protein extractions were conducted at 0 h, 1 h and 6 h post-exposure.

3.6 Immuno-labelling and Image Analysis

Cells were grown as described on glass coverslips for 72 h. Media was aspirated and cells were fixed in 4% formaldehyde (FA) in 1x phosphate buffered saline (PBS) for 10 min, RT. Fibroblasts attached to coverslips were dehydrated in ethanol series (70%, 90%, 100%) and rehydrated before permeabilization in 0.5% TritonX-100/1x PBS for 10 min, RT. Samples were blocked in 1% Bovine Serum Albumin (BSA)/1x PBS for 20 minutes before incubation with primary antibody 1:200 (v:v) in 1% BSA/1x PBS (mouse anti-progerin (Abcam, ab66587); mouse anti-H3K27me3 (Abcam, 6002); mouse anti-laminAC (Santa Cruz Biotechnologies, sc-376248)) and then secondary in 1:200 (v:v) 1% BSA/1x PBS (goat anti-

mouse a488 (Jackson ImmunoResearch, 115-545-062), goat anti-mouse cy3 (Jackson ImmunoResearch, 115-165-062) for 1 h each, RT. All antibodies were diluted in 1% BSA/1x PBS. Chromatin was counterstained using Vectashield with DAPI (Vector Laboratories, H-1200) and mounted onto glass slides.

For quantification of fluorescence intensity (Progerin, H3K27me3) all images for immunofluorescence were collected at 40X magnification with constant exposure times. Gray-scale images were imported into ImageJ (https://imagej.nih.gov/ij/) and converted to RGB files. Nuclei were identified using particle analyzer and fluorescence intensity of each nucleus measured. A minimum of 50 nuclei per sample replicate, and a minimum of three biological replicates, were conducted for each cell line.

For quantification of nuclear morphology (LaminAC), all images were collected at 20X magnification with constant exposure times. Image sets were double blinded and assessed for irregular nuclear morphology. A minimum of 100 nuclei per sample per replicate, and a minimum of three biological replicates, were conducted for each cell line.

3.7 5-ethynyl-2-deoxyuridine (EdU) Incorporation and Image Analysis

Cells were grown under conditions described in 3.1. Following 72 h, 5 μM EdU was added and incubated for 2 h before media was aspirated, and cells were fixed in 4% FA/1x PBS for 10 min, RT. Samples were washed in 1X PBS for 5 minutes and then permeabilized in 0.5% Triton X-100 for 10 min RT. Samples then underwent washes of 1x PBS, dH2O x 2, 0.05% Triton X-100 each for 5 min RT. Click-It reaction mix was made fresh from reagent stocks to a final 1x solution (10x reaction buffer (500 mM 1M citrate buffer, 250 mM 1M sodium ascorbate), 100x copper sulfate solution (400 mm copper sulfate), 100x Cy3-azide dye solution (2 mM in DMSO) with remaining volume made up with dH_2O. Samples were incubated in reaction mixture for 1 h RT, washed 5 min, RT dH_2O twice, and mounted using DAPI. Cells were imaged at 20X. A minimum of 100 nuclei were imaged for each sample, with three biological replicates. Any cell with signal was considered positive for EdU.

3.8 Protein Extraction, Quantification, and Western Blotting

Whole protein lysates were collected by scraping into 1x Laemmli Buffer without bromophenol blue (62.5 mM Tris-HCl pH 6.8, 2% SDS (w:v), 10% glycerol (v:v), 100 mM beta-mercaptoethanol, 1x protease inhibitor cocktail 2 (ThermoFisher Scientific, P187785),

1x phosphatase inhibitor cocktail 2 (Millipore Sigma, p5726) and protein concentration determined by Nanodrop™ 2000 Spectrophotometer (Thermo Fisher, Wilmington, DE, USA) at 280 nm before addition of bromophenol blue. Protein samples were denatured for 5 min, 95°C (protein equivalents were loaded, 30-60 μg per well) and separated on a 5% polyacrylamide stacking gel and subsequently a 6-15% polyacrylamide resolving gel in 1X SDS-PAGE running buffer (25mM Tris base, 192 mM glycine, and 0.1% SDS) at 125 volts (V). Proteins were transferred to a nitrocellulose membrane (Bio-Rad, 1620112) or in the case of H3K27me3, to polyvinylidene fluoride membrane (Bio-Rad, 1620177) using 1x transfer buffer (25 mM Tris base, 192 mM glycine, and 20% methanol (v:v) with a Trans-Blot® SD semi-dry transfer cell (Bio-Rad Laboratories) at 25 V. Membranes were blocked in 5% skimmed-milk powder in 1x PBS-0.5% Tween20 (SMP/PBST) for 1 h, RT. Primary and secondary antibodies were diluted in 2.5% SMP/PBST. Primary antibodies: mouse anti-progerin (1:500, Abcam, ab66587); mouse anti-H3K27me3 (1:500, Abcam, 6002); mouse anti-laminAC (1:1000, Santa Cruz Biotechnologies, sc-376248), mouse anti-(p)-mTOR (1:200, Santa Cruz, sc-293133), mouse anti-mapLC3B (1:1000, SantaCruz, sc-271625,) rabbit anti-EZH2 (1:1000; Abcam, ab191250), mouse anti-ATG5 (1:500, Santa Cruz, sc-133158) mouse anti-CASTOR1 (1:500, Santa Cruz, sc-377114), mouse anti-SESN2 (1:500, Santa Cruz, sc-393195), mouse anti-γ-H2AX (1:1000, Santa Cruz, sc-517348). Secondary antibodies: goat anti-mouse horse radish peroxidase (HRP) (1:2500, Jackson ImmunoResearch, 115-035-146), goat anti-rabbit HRP (1:2500, Jackson ImmunoResearch, 111-035-003). Primary antibody incubations were overnight at 4°C, washed 3x in 5% SMP/PBST, 5 min/wash, and incubated in secondary antibody at 1:100 2.5% SMP/PBST for 1 h at RT. Following secondary incubation, membranes were washed 3x in 5% SMP/PBST, once in 1x PBST and once in 1x PBS, 5 min/wash. Membranes were developed using enhanced chemiluminescence reagent (100 mM Tris-HCl pH 8.5, 0.2 mM p-coumaric acid, 1.25 mM luminol, and 0.1% H_2O_2 (v:v)) and images collected using Biorad VersaDoc system. Densitometry measurements were taken for each protein band using ImageJ. Equal loading was confirmed by Coomassie staining. Biological triplicates of proteins were collected, and western blots conducted for each of these replicates. Images and densitometry presented are representative of replicates.

3.9 Fluorescence In-Situ Hybridization and Chromosome Painting

Cells were grown for 72 h under conditions described above. Probe generation was conducted as described in (Mehta *et al.*, 2010) using degenerative oligo primer-PCR of chromosomes containing biotinylated uridine residues (biotin-16-UTP, Roche). Cells were grown on coverslips for 72 h and media aspirated. Coverslips were washed in ice-cold 1x PBS and then fixed by adding ice-cold 3:1 (v:v) methanol:acetic acid dropwise to each coverslip (enough to cover the bottom of the dish). Samples were then incubated for 1 h at 4^{o}C before washing 3 x in 3:1 methanol:acetic acid (5 min/wash). All supernatant was aspirated, and coverslips aged at RTP for 2 days then dehydrated in 70%, 90%, 100% ethanol series. To denature chromatin, coverslips were pre-warmed then incubated for 2 min at 70^{o}C in 70% formamide, 2x saline sodium citrate (SSC). Coverslips were immediately placed in ice cold 70% ethanol (5 min), and then 90% (5 min, RT) and 100% (5 min, RT) ethanol wash series. Coverslips were air dried at RT and kept warm. Cells on coverslips were placed on 15 μl of probe (chromosome X, 10, or 18) and sealed with rubber cement before overnight incubation in a humidity chamber (37^{o}C). The rubber cement was removed, coverslips lifted and washed in wash buffer A (45^{o}C; 50% formamide, 2 x SSC) for 15 min and then wash buffer B (60^{o}C; 0.5 X SCC) for 15 min. Coverslips were transferred to 1x PBS and underwent immuno-labelling for goat anti-streptavidin-Cy3 (1:200; Vector laboratories, USA, cat #: Ba-0500) for 1 h, goat anti-streptavidin conjugated to biotin (1:200; Cedarlane, UK, cat #: 111-065-003) 1 h and then a second goat anti-streptavidin-Cy3 for 1 h. A 2 min 0.05% TritonX-100/1x PBS wash was conducted between each antibody incubation. Samples were mounted in DAPI. Nuclei were imaged in grey scale and were false coloured in Adobe Photoshop (CS6). Smart Capture VP V1.4, a Leica fluorescence microscope with Plan Fluor 100x oil-immersion lens was used to collect images. Software called the Cell Nucleus Analyzer for nuclear segmentation and analysis was used to divide the DAPI image into five concentric shells of equal area, the first being the most peripheral and innermost denoting the interior of the nucleus. The script measures pixel intensity of DAPI and the chromosome probe in these five shells. Normalization of the probe signal was conducted by dividing the percentage of the probe by the percentage of DAPI signal in each shell. For each condition, ≥ 35 nuclei were measured for each chromosome. Ratios from each shell were averaged and the standard error of the mean calculated.

3.10 RNA Extraction

Media was aspirated and cells dissociated from culture dishes in Tryple Xpress. The Tryple Xpress-cell suspension was pelleted (174 g, 3 min) and supernatant aspirated. Cell pellet was resuspended in 1 ml of Trizol RNA extraction reagent (38% phenol, 0.8 M guanidine thiocyanate, 0.4 M ammonium thiocyanate, 0.1 M sodium acetate and 5% glycerol (v:v)), vortexed, and incubated for 5 min, RT. 200 µl of chloroform was added, and samples vortexed before pelleting (12,000 g, 5 min, 4°C). Aqueous phase was collected in a new Eppendorf and 1/10th volume 3M sodium acetate (pH 5.2) and 1x volume ice cold isopropanol added. Samples were incubated on ice for 30 min, RNA pelleted (12,000 g, 10 min, 4°C), and supernatant aspirated. Pellets were washed in 1 ml ice-cold 70% ethanol/nuclease free water and re-pelleted (12,000 g, 10 min, 4°C). Samples were then DNase treated. Pellets were air-dried and resuspended in 88 µl nuclease free water, 1 µl of RNaseOUT, 10 µl 10X DNase recombinant buffer and 1 µl DNase I. Samples were incubated for 20 min, 37°C. 100 µl Ambion 5:1 acid phenol: chloroform (pH 4.5) was added, samples vortexed and pelleted at 12,000 g, 10 min, 4°C. The aqueous phase was transferred to a new Eppendorf, and RNA precipitated with 1/10th volume 3M sodium acetate (pH 5.2) and 3x volume ice cold 100% ethanol (30 min, ice). RNA was again pelleted (12,000 g, 30 min, 4°C), supernatant aspirated and air-dried (10 min, RTP). Pellets were resuspended in 41.5 µl nuclease free water and 1 µl of RNaseOUT. RNA quality checked by NanoDrop2000 (A_{260}/A_{280}: 1.6-1.8, A_{260}/A_{230}: >2) and gel electrophoresis.

3.11 RNA Sequencing and Alignment

RNA integrity number (RIN) was determined by Bioanalyzer, and RNA with RIN above 8.0 was used for sequencing. RNA from FSF and HGADFN169 grown under standard conditions, arginine and leucine restricted, or in the presence of 0.5 mM metformin, for 5 weeks. Each set of samples (FSF and HGADFN169) were passage-matched and expanded from a single culture flask to avoid variation in culture age. Libraries were stranded poly(A) mRNA prepared and sequenced at the Toronto Centre for Applied Genomics (TCAG) using the Illumina HiSeq2500 sequencer. Reads were 100 base pairs in length and paired-end. The raw reads were quality checked using FastQC (https://www.bioinformatics.babraham.ac.uk/projects/fastqc/) and adaptors/poor quality sequences trimmed using Trim Galore!, removing 13 base pairs (e.g. trim_galore --phred33 -

-paired --illumina --clip_R1 13 --clip_R2 13 --length 80 <forward_read> <reverse_read>). Sequence quality was then re-examined by FastQC. Trimmed reads were mapped to human genome reference GRCh38 using HISAT2 (v. 2.2.0; (Kim *et al.*, 2019a)) and a pre-assembled index available at the HISAT2 website (https://genome-idx.s3.amazonaws.com/hisat/grch38_snptran.tar.gz, accessed January 2021). Example alignment command: hisat2 -x grch38_snptran.gz -p 2 -1 forward_read_trimmed.fq.gz -2 reverse_read_trimmed.fq.gz | samtools view -bS -o alignedfile.hisat.bam. Datasets were imported into Seqmonk (v1.47.2) and normalized to one another. Seqmonk was used to generate DEG lists of fold change and PCA plots. DEGs were input into Cytoscape (v3.8.2) with ReactomeFI to conduct pathway enrichment analyses. Dot plots were constructed in R using ggplot2.

3.12 Statistical Analyses

The primary question to be answered in this data was whether a specific treatment condition could induce changes in the dependent variable (e.g., progerin levels) against control. Students T-test with Bonferroni correction for multiple testing were utilized in assessing data from population doubling times, total population doublings, cell survival, EdU assays, nuclear morphology, and assays inspecting fluorescence intensity (progerin, H3K27me3). In these instances, the corrected p-value threshold for significance is 0.0083.

4.0 Nutrient Restriction and Nutrient Restriction Mimetics Ameliorate the Cellular Hallmarks of Hutchinson-Gilford Progeria Syndrome Fibroblasts and Decrease Levels of the Mutant Protein Progerin.

4.1 Nutrient Restriction and Nutrient Restriction Mimetics Slow Growth Rates of Non-Diseased and HGPS Fibroblasts in Cell Culture.

The overall hypothesis of this work is that nutrient restriction (NR) via restriction of arginine, leucine, combined arginine and leucine, glucose and pyruvate, or the nutrient restriction mimetic (NRM) metformin will significantly ameliorate cellular phenotypes of HGPS and restore genome function and organization. Changes in cellular growth and proliferation have been associated with various pro-longevity compounds (Belak *et al.,* 2020; Gillespie *et al.,* 2015; Gillespie *et al.,* 2019; Wang *et al.,* 2019; Zehfus *et al.,* 2021). Therefore, cellular growth and survival were examined under conditions of NR and NRM in HGPS patient fibroblasts HGADFN003, HGADFN167, HGADFN169, and AG03513 (Figures 4.1-4.4). In addition to metformin, rapamycin was also examined as an NRM and positive control, having previously been demonstrated to decrease progerin levels and reduced pathologic hallmarks of HGPS (Bikkul *et al.,* 2018; Cao *et al.,* 2011b; Gabriel *et al.,* 2016; Kawakami *et al.,* 2019; Liao *et al.,* 2016), as well as having been examined in non-disease primary fibroblasts (Gillespie *et al.,* 2015). Concentrations of metformin and rapamycin (0.5 mM and 680 nM respectively) were selected based on previous literature (Cao *et al.,* 2011b; Gillespie *et al.,* 2019). Given limited research availability on amino acid restriction, identical assays were also conduced in two non-diseased human primary fibroblast cell lines (FSF, 2DD) (Figures 4.1-4.4). Fibroblasts were grown under NR and NRM conditions for 72 h, cell counts conducted and population doubling times calculated. Furthermore, Trypan Blue was used to assess cell survival. FSF fibroblasts (human neonate; Figure 4.1A) demonstrated subtle increases in population doubling times (PDT; Figure 4.1 and Table 4.1) in response to each treatment condition compared to untreated cells. 2DD fibroblasts (human juvenile; Figure 4.1A and Table 4.1) also exhibited increased PDT in response to all conditions, with increases greater than those observed in FSF. PDT corresponded with fewer total population doublings (TPD) (Figure 4.1A and 4.2A, Table 4.2). Both 2DD and FSF were assessed for cell survival by Trypan Blue staining, with no significant decrease in survival detected (Figure 4.3A, Table

4. 3), providing evidence that changes in PDT and TPD are the result of changes in rates of cell proliferation, not the result of decreased cell survival.

On average, HGPS fibroblasts exhibit significantly (p-value = 0.000002) slower population doubling times than non-diseased counterparts (FSF: 29.2 h, 2DD: 43.7 h, HGADFN003: 71.0 h, HGADFN167: 68.1 h, HGADFN169: 84.6 h, AG03513 82.1 h) not attributable to passage number (p) in culture (p11-p14 for all cell lines). HGPS fibroblast cell-lines HGADFN003, HGADFN167, and HGADFN169 frequently exhibited greater than 100 h increases in PDT compared to untreated counterparts in response to NR and NRM (Figure 4.1B, Table 4.1). In general, AG03513, the oldest cell-line examined, exhibited far greater variability in replicates than other tested primary HGPS fibroblasts. TPD were consistent with PDT in all cell lines (Figure 4.2, Table 4.2). As with non-diseased fibroblasts, each HGPS patient-derived cell line was also examined for cell survival, by Trypan Blue staining. No significant changes were identified (Figure 4.3B, Table 4.3).

To further confirm fibroblasts were progressing more slowly through the cell cycle, and perhaps entering a state of cellular maintenance and repair, cells were treated with 5-ethynyl-2'-deoxyuridine (EdU), a thymidine analog which only incorporates into actively replicating DNA, and Click-iT^{TM} chemistry used to visualize EdU positive nuclei by fluorescence microscopy. If nuclei are EdU positive, the cell is in S-phase. Of all fibroblast samples, FSF exhibited the highest percentage of S-phase cells under control (Untreated) conditions (16.45%), whilst -Arg, -Leu, -ArgLeu, +0.5 mM Metf, and +680 nM Rap resulted in significantly ($p < 0.0083$) fewer EdU positive nuclei than untreated FSF. Though the percentage of S-phase nuclei was lower than FSF in Untreated 2DD (6.87%), all treatment conditions exhibited a lower percentage of nuclei actively replicating DNA, in line with increases observed in PDT (Figure 4.4, Table 4.4). HGPS fibroblasts under the same NR and NRM conditions as non-diseased fibroblasts also exhibited decreased percentages of S-phase cells, with the exception of AG03513 restricted of arginine for 72 h. These findings are consistent with PDT/TPD. Combined, these data demonstrate that all conditions tested are decreasing cell proliferative rates and rates of DNA replication without inducing cell death.

Table 4.1: Population doubling times of cells for four HGPS (HGADFN003, HGADFN167, HGADFN169, AG03513) and two non-diseased (FSF, 2DD) fibroblast cell lines grown under defined NR and NRM treatment conditions for 72 h. [1, 2]

Cell Line	Treatment Condition						
	Untreated	-Arg	-Leu	-ArgLeu	-GlcPyr	+0.5 mM Metf	+680 nM Rap
HGADFN003 (2y0m)	70.95 ± 8.19	334.50 ± 94.13	203.53 ± 43.06	174.81 ± 24.09	229.61 ± 45.71	175.52 ± 32.39	118.60 ± 29.12
HGADFN167 (8y5m)	68.7 ± 4.52	153.69 ± 24.49	221.82 ± 65.02	179.68 ± 37.31	348.05 ± 197.83	115.17 ± 16.69	172.13 ± 43.44
HGADFN169 (8y6m)	84.63 ± 11.84	307.37 ± 104.38	297.40 ± 118.58	200.67 ±44.59	133.32 ± 21.82	221.07 ± 117.40	175.87 ± 46.10
AG03513 (13y)	82.06 ± 11.19	103.98 ± 9.14	134.31 ± 32.35	88.83 ± 15.49	207.67 ± 47.91	273.74 ± 176.44	199.72 ± 25.09
FSF (Neonate)	29.23 ± 2.53	33.94 ± 5.03	33.93 ± 5.04	35.92 ± 5.66	33.71 ± 5.97	30.91 ± 5.20	54.95 ± 16.03
2DD (Juvenile)	43.71 ± 1.58	64.58 ± 7.66*	99.10 ± 15.04*	86.64 ± 11.52*	73.57 ± 6.67*	59.70 ± 8.71	61.07 ± 5.12*

[1]Population doubling time reported in hours (h)
[2]Mean ± standard error of the mean of at least three replicates
* $p < 0.0083$ by students T-test corrected for multiple testing

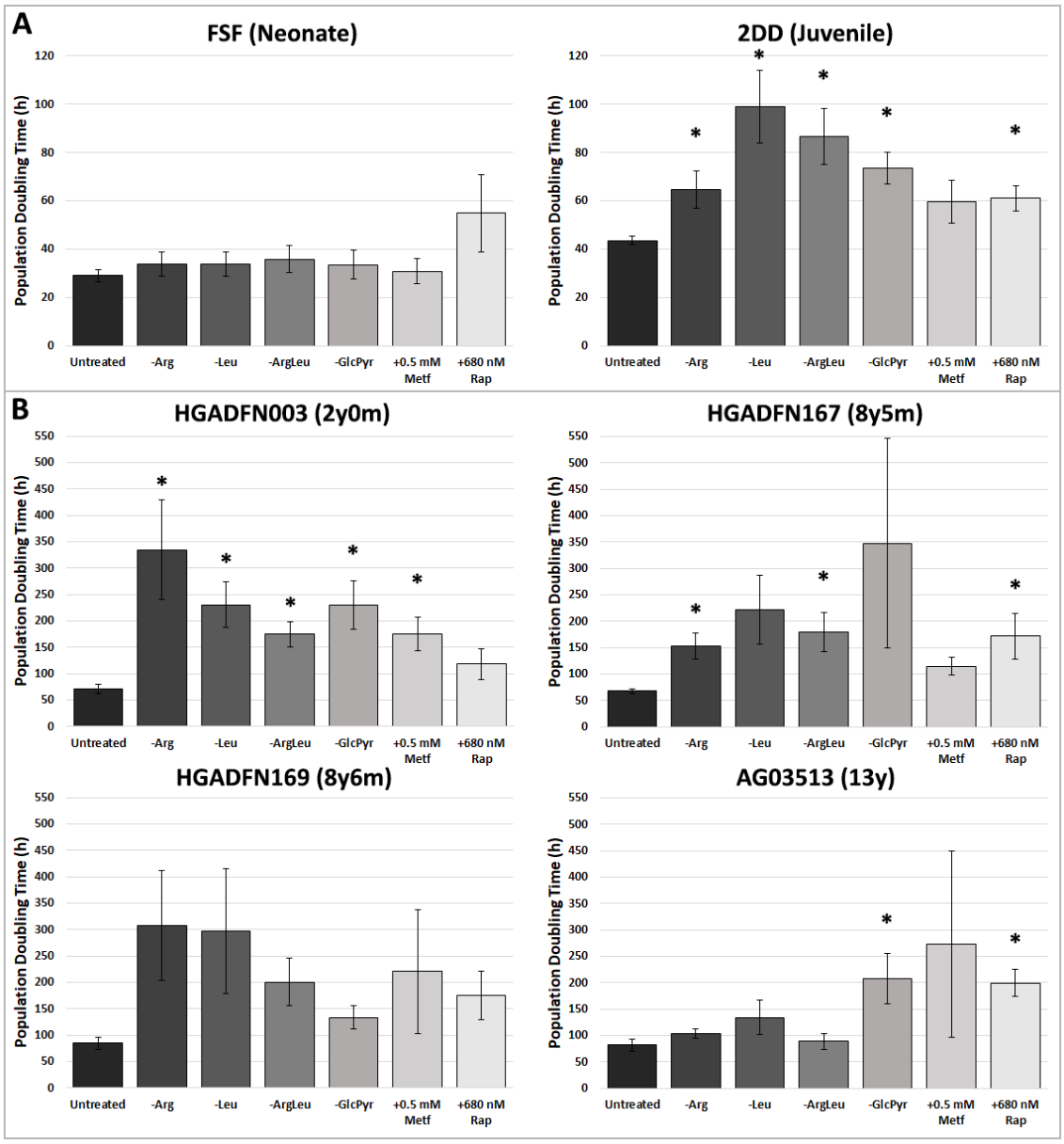

Figure 4.1: Population Doubling Times of Non-Diseased and HGPS Fibroblasts in Response to NR and NRM. Non-diseased (A) FSF, 2DD and (B) HGPS HFADFN003, HGADFN167, HGADFN169, AG03513 fibroblasts were grown under standard culture conditions (Untreated) or under conditions of arginine restriction (-Arg), leucine restriction (-Leu), combined arginine and leucine restriction (-ArgLeu), glucose and pyruvate restriction (-GlcPyr) or in the presence of either 0.5 mM metformin (+0.5 mM Metf) or 680 nM rapamycin (+680 nM Rap) (X-Axis) for 72 h. Cell numbers were monitored and population doubling times calculated (Y-Axis). A minimum of three replicates for each cell line were conducted. Error bars = standard error of the mean (SEM). * $p < 0.0083$ by students T-test corrected for multiple testing.

Table 4.2: Total population doublings of cells for four HGPS (HGADFN003, HGADFN167, HGADFN169, AG03513) and two non-diseased (FSF, 2DD) fibroblast cell lines grown under defined NR and NRM treatment conditions for 72 h. [1, 2]

Cell Line	Treatment Condition						
	Untreated	-Arg	-Leu	-ArgLeu	-GlcPyr	+0.5 mM Metf	+680 nM Rap
HGADFN003 (2y0m)	1.19 ± 0.05	0.38 ± 0.12*	0.38 ± 0.08*	0.46 ± 0.07*	0.41 ± 0.08*	0.48 ± 0.08*	0.69 ± 0.17
HGADFN167 (8y5m)	1.10 ± 0.08	0.48 ± 0.08*	0.53 ± 0.10*	0.47 ± 0.08*	0.51 ± 0.08*	0.76 ± 0.12*	0.47 ± 0.09*
HGADFN169 (8y6m)	1.21 ± 0.14	0.51 ± 0.17	0.47 ± 0.10*	0.58 ± 0.12*	0.79 ± 0.11	0.65 ± 0.14	0.65 ± 0.16
AG03513 (13y)	1.02 ± 0.13	0.72 ± 0.07	0.70 ± 0.15	0.96 ± 0.15	0.42 ± 0.10*	0.79 ± 0.21	0.40 ± 0.06*
FSF (Neonate)	3.47 ± 0.36	3.03 ± 0.45	3.03 ± 0.44	2.88 ± 0.46	3.15 ± 0.58	3.36 ± 0.51	2.02 ± 0.46
2DD (Juvenile)	1.66 ± 0.06	1.17 ± 0.15*	0.80 ± 0.16*	0.87 ± 0.10*	1.01 ± 0.10*	1.27 ± 0.14*	1.20 ± 0.10*

[1]Total population doublings
[2]Mean ± standard error of the mean of at least three replicates
* $p < 0.0083$ by students T-test corrected for multiple testing

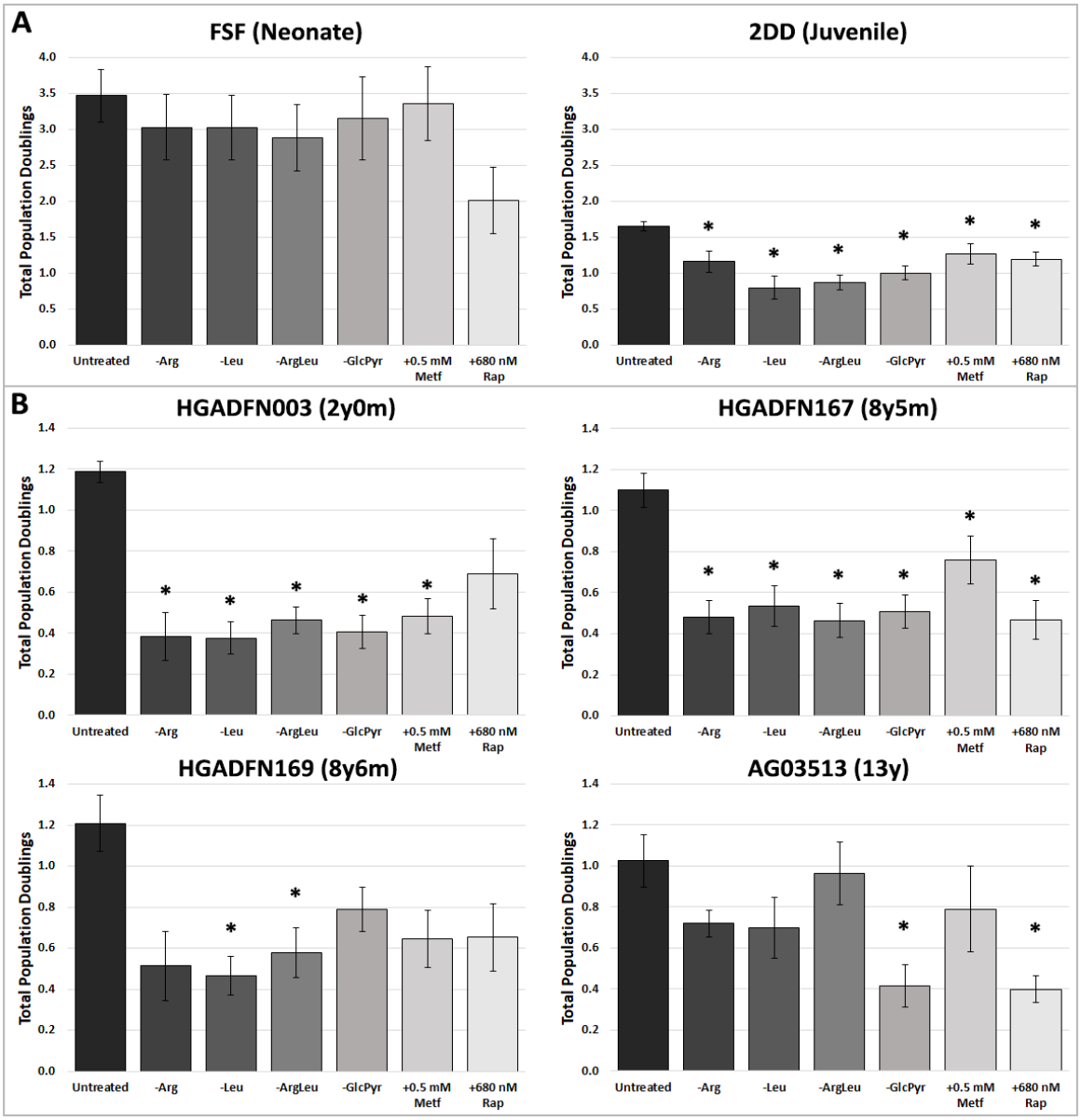

Figure 4.2: Total Population Doublings of Non-Diseased and HGPS Fibroblasts in Response to NR and NRM. Non-diseased (A) FSF, 2DD and (B) HGPS HFADFN003, HGADFN167, HGADFN169, AG03513 fibroblasts were grown under standard culture conditions (Untreated) or under conditions of arginine restriction (-Arg), leucine restriction (-Leu), combined arginine and leucine restriction (-ArgLeu), glucose and pyruvate restriction (-GlcPyr) or in the presence of either 0.5 mM metformin (+0.5 mM Metf) or 680 nM rapamycin (+680 nM Rap) (X-Axis) for 72 h. Cell numbers were monitored and total population doublings calculated (Y-Axis). A minimum of three replicates for each cell line were conducted. Error bars = standard error of the mean (SEM). * $p < 0.0083$ by students T-test corrected for multiple testing.

Table 4.3: Cell survival as determined by trypan blue of for four HGPS (HGADFN003, HGADFN167, HGADFN169, AG03513) and two non-diseased (FSF, 2DD) fibroblast cell lines grown under defined NR and NRM treatment conditions for 72 h. [1, 2]

Cell Line	Treatment Condition						
	Untreated	-Arg	-Leu	-ArgLeu	-GlcPyr	+0.5 mM Metf	+680 nM Rap
HGADFN003 (2y0m)	93.38 ± 3.09	95.50 ± 0.33	95.76 ± 0.87	95.21 ± 0.88	94.21 ± 0.13	95.73 ± 0.37	94.67 ± 3.18
HGADFN167 (8y5m)	96.82 ± 0.27	97.51 ± 0.39	96.31 ± 0.39	96.75 ± 0.20	93.59 ± 1.41	96.23 ± 0.07	96.50 ± 0.59
HGADFN169 (8y6m)	96.34 ± 1.03	96.38 ± 0.44	96.58 ± 0.22	96.45 ± 0.16	95.61 ± 0.88	97.15 ± 2.15	95.61 ± 0.92
AG03513 (13y)	96.91 ± 1.80	92.01 ± 4.30	95.95 ± 2.36	93.46 ± 2.35	91.95 ± 3.56	91.30 ± 4.19	94.59 ± 3.03
FSF (Neonate)	96.45 ± 1.04	94.08 ± 2.19	94.02 ± 1.07	92.22 ± 1.86	94.58 ± 1.19	93.13 ± 2.25	100.00 ± 0.00
2DD (Juvenile)	97.11 ± 1.10	96.78 ± 0.17	96.90 ± 0.35	98.27 ± 0.14	97.58 ± 0.04	97.81 ± 0.70	97.93 ± 1.18

[1]Reported as percentage
[2]Mean ± standard error of the mean of at least three replicates
* $p < 0.0083$ by students T-test corrected for multiple testing

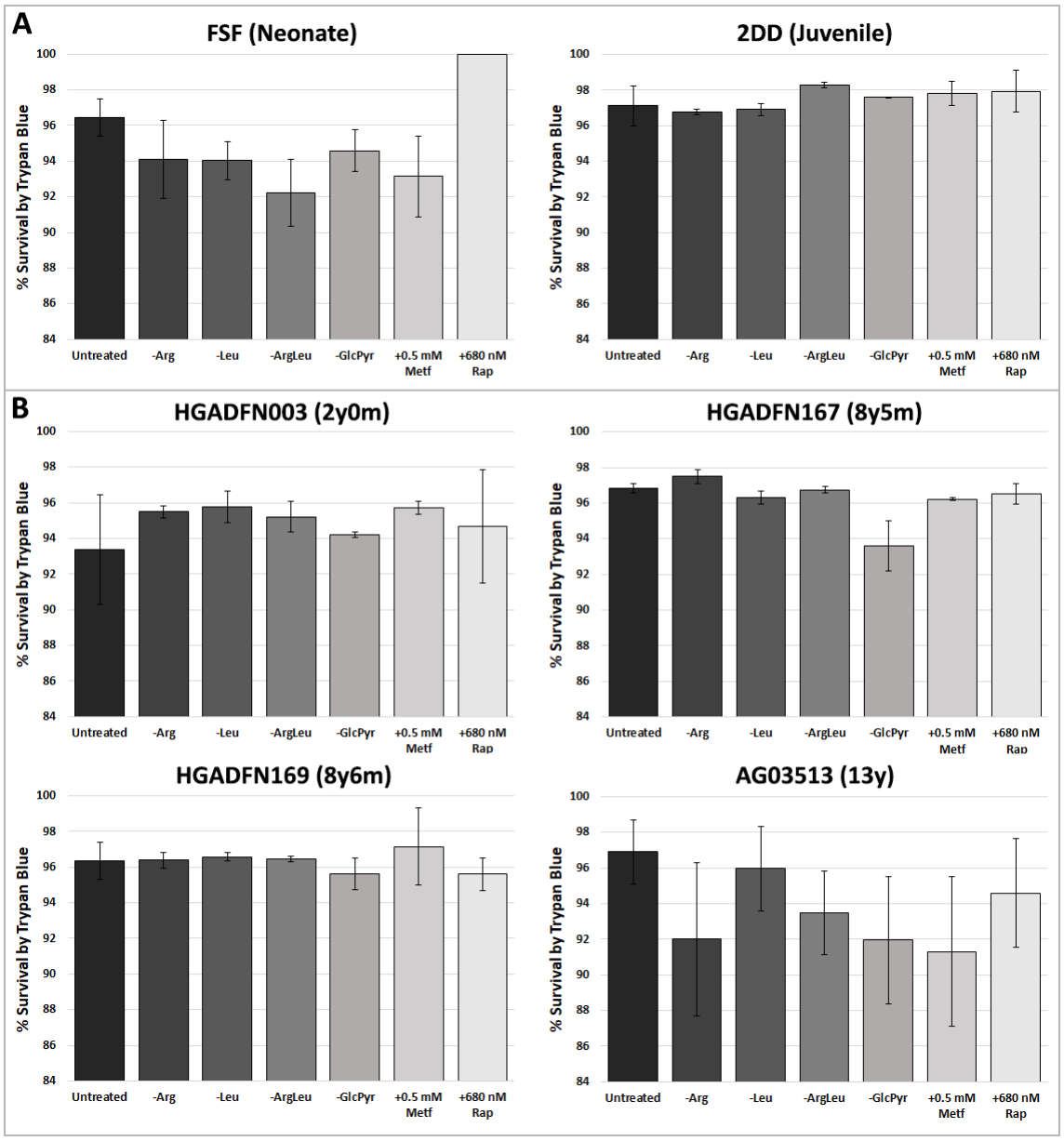

Figure 4.3: Cell Survival by Trypan Blue of Non-Diseased and HGPS Fibroblasts in Response to NR and NRM. Non-diseased (A) FSF, 2DD and (B) HGPS HFADFN003, HGADFN167, HGADFN169, AG03513 fibroblasts were grown under standard culture conditions (Untreated) or under conditions of arginine restriction (-Arg), leucine restriction (-Leu), combined arginine and leucine restriction (-ArgLeu), glucose and pyruvate restriction (-GlcPyr) or in the presence of either 0.5 mM metformin (+0.5 mM Metf) or 680 nM rapamycin (+680 nM Rap) (X-Axis) for 72 h. Following treatments, cells were stained with Trypan Blue and percent survival calculated (Y-Axis). A minimum of three replicates for each cell line were conducted. Error bars = standard error of the mean (SEM). * $p < 0.0083$ by students T-test corrected for multiple testing.

Table 4.4: Mean percentage of EdU positive nuclei for four HGPS (HGADFN003, HGADFN167, HGADFN169, AG03513) and two non-diseased (FSF, 2DD) fibroblast cell lines in response to defined NR and NRM treatment conditions. [1, 2]

Cell Line	Treatment Condition						
	Untreated	-Arg	-Leu	-ArgLeu	-GlcPyr	+0.5 mM Metf	+680 nM Rap
HGADFN003 (2y0m)	8.93 ± 0.93	4.50 ± 2.15	1.70 ± 0.80*	1.09 ± 0.65*	1.95 ± 1.49*	4.41 ± 0.43*	ND
HGADFN167 (8y5m)	6.32 ± 0.88	1.19 ± 0.22*	0.59 ± 0.32*	1.08 ± 0.17*	5.08 ± 2.65	4.04 ± 1.87	1.73 ± 0.11*
HGADFN169 (8y6m)	5.39 ± 1.62	1.46 ± 0.67	1.04 ± 0.43	1.38 ± 0.33	0.56 ± 0.56	0.55 ± 0.34	0.00 ± 0.00
AG03513 (13y)	7.03 ± 1.48	8.52 ± 0.35	6.25 ± 1.53	5.76 ± 1.72	4.35 ± 1.27	6.18 ± 1.66	1.42 ± 0.78
FSF (Neonate)	16.45 ± 1.79	6.45 ± 1.84*	4.96 ± 1.56*	2.18 ± 0.18*	11.49 ± 3.57	8.91 ± 1.13*	5.20 ± 1.92*
2DD (Juvenile)	6.87 ± 0.89	3.26 ± 1.42	1.60 ± 0.63*	2.26 ± 0.63*	1.89 ± 0.57*	2.01 ± 0.20*	1.55 ± 0.80*

[1]Reported as percentage
[2]Mean ± standard error of the mean of at least three replicates
* $p < 0.0083$ by students T-test corrected for multiple testing

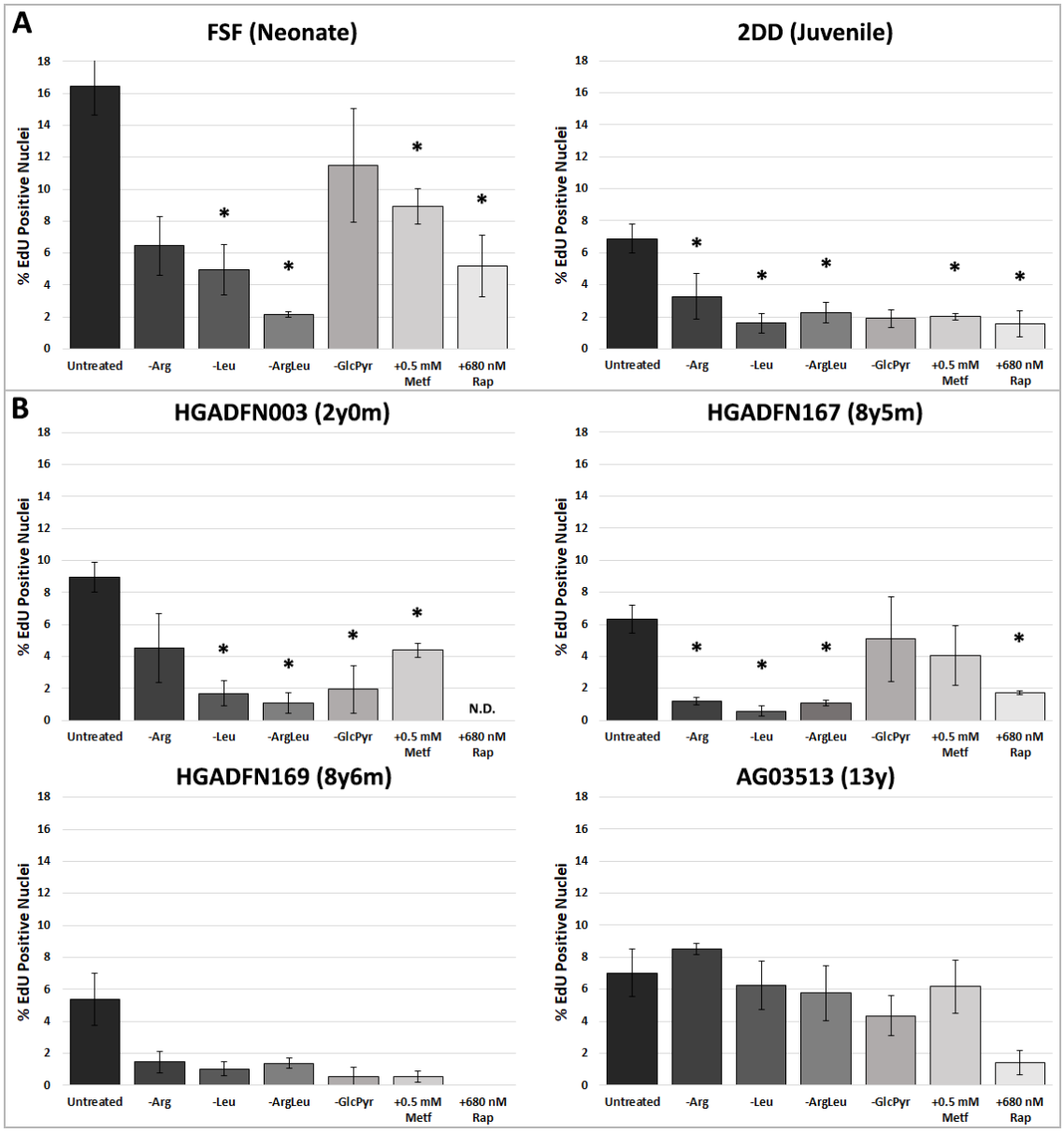

Figure 4.4: Active DNA Replication by EdU of Non-Diseased and HGPS Fibroblasts in Response to NR and NRM Corresponds with Changes in PDT and TPD. Non-diseased (A) FSF, 2DD and (B) HGPS HFADFN003, HGADFN167, HGADFN169, AG03513 fibroblasts were grown under standard culture conditions (Untreated) or under conditions of arginine restriction (-Arg), leucine restriction (-Leu), combined arginine and leucine restriction (-ArgLeu), glucose and pyruvate restriction (-GlcPyr) or in the presence of either 0.5 mM metformin (+0.5 mM Metf) or 680 nM rapamycin (+680 nM Rap) (X-Axis) for 72 h. Percentage of EdU positive fibroblasts were calculated (Y-Axis) for each condition and cell line. A minimum of three replicates for each cell line were conducted. Error bars = standard error of the mean (SEM). * $p < 0.0083$ by students T-test corrected for multiple testing.

4.2 Progerin Levels are Reduced in Hutchinson-Gilford Progeria Syndrome Fibroblasts Treated with NR and NRM.

Progerin is the mutant protein driving the HGPS phenotype (Cao *et al.,* 2007; Dechat *et al.,* 2007; Glynn *et al.,* 2005; Goldman *et al.,* 2004), with its removal resulting in improvements in cellular characteristics and physiological phenotypes. To determine if NR or NRM result in decreased levels of this mutant protein in HGPS patient fibroblasts, progerin levels were examined by immunofluorescence (IF) and western blot (WB) following 72 h of treatment. Hallmarks of HGPS, including number of irregular nuclei, rate of DNA damage repair, levels of inactive chromatin, and chromosome territory localization, were also examined.

Three HGPS patient fibroblast cell lines were examined by IF (HGADFN003, HGADFN167, HGADNF169) (Table 4.1, Figures 4.5-4.7 B and C) with an additional cell line examined by WB (AG03513; Figure 8A). Of the six NR/NRM conditions tested, -Arg significantly decreased progerin levels in all tested HGPS cell lines by IF ($p < 0.001$) and three of four (HGADFN003, HGADFN169, AG03513) tested cell lines by WB of whole protein lysates. Unlike -Arg, -Leu only decreased progerin levels by IF in HGADFN003, but achieved this in WB in HGADFN003, HGADFN169 and AG03513. Combined, -ArgLeu decreased progerin in two HGPS cell lines by IF ($p < 0.001$) and all patient fibroblasts tested by WB. -GlcPyr significantly decreased progerin levels by IF in HGADFN003 and HGADFN169, but increased levels in HGADFN167 ($p < 001$). By WB, -GlcPyr treated fibroblasts also exhibited increased progerin levels in HGADFN167 and AG03513. Of NRM tested, metformin is more novel, whilst rapamycin is currently entering clinical trials for HGPS treatment. Both compounds significantly decreased progerin levels in two of three cell lines by IF. Metformin treatment resulted in decreased levels of progerin in all tested HGPS patient lines, while rapamycin achieved this in three of four cell lines. In general, the HGADFN167 (8y5m) was least responsive to NR/NRM. Finally, changes in progerin levels were also reflected in WB for the non-mutant lamin A/C alongside mutant progerin (Table 4.1, Figures 4.5-4.7B and C, Figure 4.8A)., whilst no changes were observed in lamin A/C protein levels in non-diseased 2DD and FSF (Figure 4.9 A and C). In general, every NR and NRM condition tested demonstrated an ability to decrease progerin protein levels when assayed by immunofluorescence and western blot.

Previously, inhibition of the mammalian target of rapamycin (mTOR) pathway and up-regulation of autophagy have been associated with health and lifespan extending benefits of NR and NRM. Although these pathways have been of interest in terms of how compounds degrade progerin, research is limited on the role of the mTOR pathway and its status in HGPS. Therefore, mTOR phosphorylated at serine 2448 ((p)-mTOR) and LC3B were used as markers to examine endogenous levels of mTOR inhibition and autophagy induction in HGPS fibroblasts. In comparison to non-diseased FSF fibroblasts, (p)-mTOR protein levels were increased in three HGPS cell lines (HGADFN003, HGADFN167 and HGADFN169), and decreased in AG03513. LC3B levels were also higher in three HGPS cell lines (HGADFN003, HGADFN169 and AG03513) and decreased compared to non-diseased controls in HGADFN167 (Figure 4.5-4.8 D and E, Figure 4.9 C-E).

In response to -Arg, the youngest HGPS patient-derived cell line tested exhibited an increase in (p)-mTOR, all other HGPS fibroblasts exhibited a decrease (Figure 4.5-4.8 D and E). In response to -Leu, however, HGADFN003 (2y0) exhibited roughly the same levels of (p)-mTOR as untreated controls. Again, in all other HGPS fibroblasts tested, -Leu decreased (p)-mTOR levels, but to a lesser extent than -Arg. Combined, -ArgLeu drastically decreased levels of (p)-mTOR in HGADFN003 but maintained the lower levels of (p)-mTOR observed in -Arg or -Leu. GlcPyr restriction resulted in half of tested HGPS samples increasing (p)-mTOR levels, whilst the other half decreased (p)-mTOR levels. In three of four patient cell lines, metformin increased or elicited no change in (p)-mTOR levels, with the remaining line exhibiting a decrease. Surprisingly, rapamycin elicited a decrease in (p)-mTOR levels across all patient lines tested. In non-diseased fibroblasts, a mix of decreases and increases of (p)-mTOR protein levels were also observed dependent on cell line and treatment condition (Figure 4.9 B and D). No obvious patterns were present in terms of cell-line specific responses to explain these varied levels of (p)-mTOR, nor any obvious trends in response to treatment type; however, it is possible that (p)-mTOR is no longer the ideal method of assessing mTOR activity (Figueiredo *et al.,* 2017).

The LC3B marker of autophagy was expected to increase in association with increased (p)-mTOR levels (and therefore increased mTOR inactivation). In two of four HGPS cell lines, -Arg or -Leu increased LC3B levels, whilst in the remaining lines, no change was observed in one and a decrease observed in the other. Together, -ArgLeu-treated fibroblasts

exhibited increased LC3B levels in three of four lines tested, with a decrease in the oldest line tested (AG03513, 13y). Though -GlcPyr was the least successful condition in inducing progerin degradation, it consistently increased LC3B levels, whilst metformin mimicked findings observed in response to -Arg/-Leu. Rapamycin, contrary to expectations, resulted in lower LC3B levels across all HGPS primary fibroblasts tested (Figure 4.5-4.8E). In non-diseased FSF counterparts, decreases were observed in LC3B levels in response to all tested conditions (Figure 4.9E). Therefore, the expected coupling of mTOR inactivation and autophagy upregulation associated with progerin clearance was not observed, though sole upregulation of autophagy was seen in most treatments that decreased progerin levels.

Table 4.5: Mean fluorescence intensity of progerin by immunofluorescence in three HGPS patient fibroblast cell lines (HGADFN003, HGADFN167, HGADFN169) in response to defined NR and NRM conditions. [1, 2]

Cell Line	Treatment Condition						
	Untreated	-Arg	-Leu	-ArgLeu	-GlcPyr	+0.5 mM Metf	+680 nM Rap
HGADFN003 (2y0m)	22.50 ±0.88	18.51 ±0.55*	17.08 ±0.47*	19.04 ±0.64*	18.52 ±0.74*	20.45 ±0.62*	15.24 ±0.49*
HGADFN167 (8y5m)	6.27 ±0.21	5.15 ±0.21*	6.34 ±0.19	6.57 ±0.19	8.15 ±0.25*	6.62 ±0.17	5.80 ±0.24
HGADFN169 (8y6m)	36.90 ±1.46	27.87 ±1.70*	37.60 ±1.67	23.26 ±1.07*	28.92 ±1.26*	18.82 ±1.37*	25.79 ±1.61*

[1]Reported as Arbitrary Units
[2]Mean ± standard error of the mean of triplicates of at least 30 nuclei
* $p < 0.0083$ by students T-test corrected for multiple testing

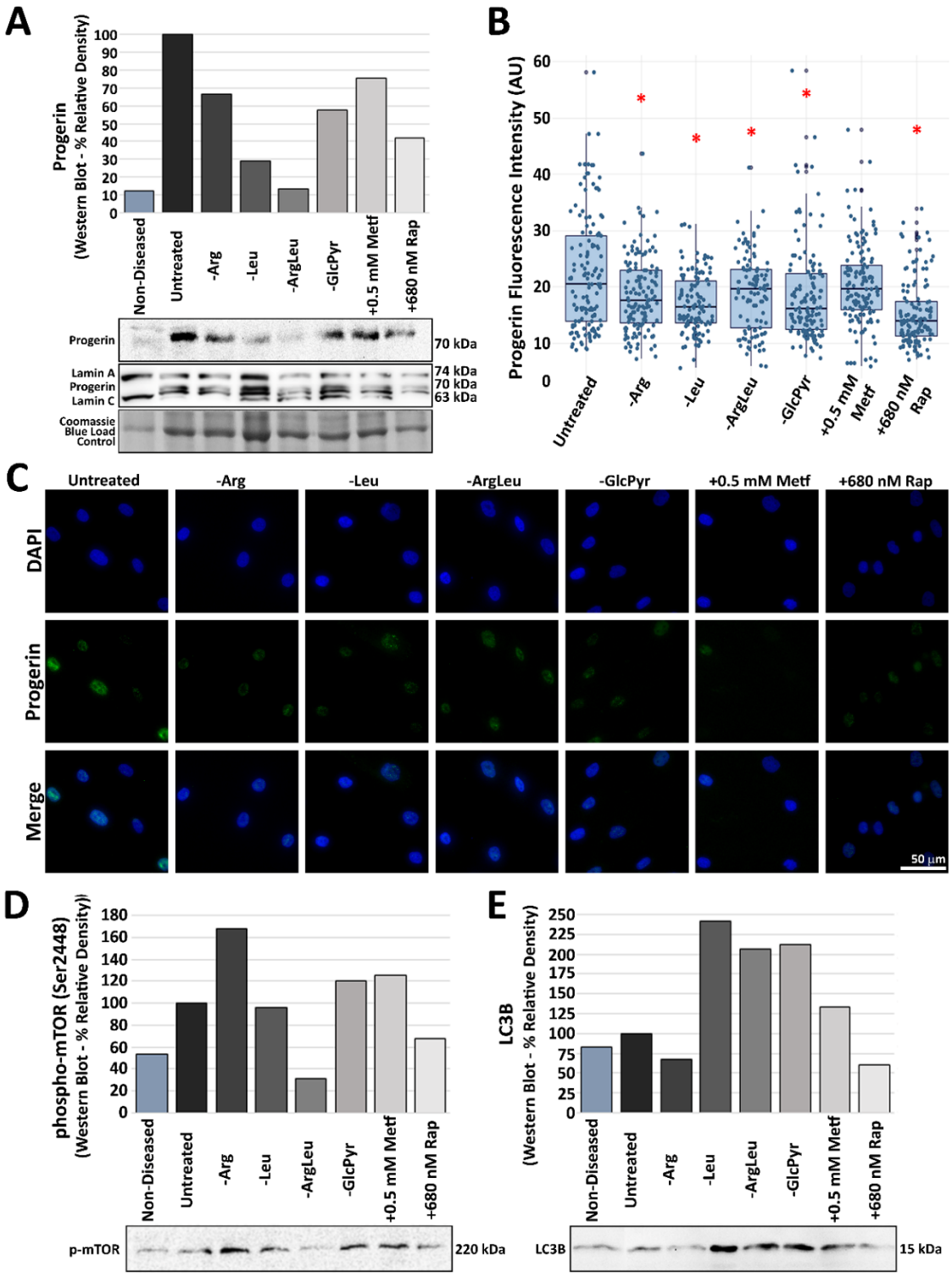

Figure 4.5: Response of Progerin Levels to NR and NRM in HGADFN003 (HGPS; 2y0m). (A) Bar graph for relative densitometry (%, Y-axis) of progerin levels by western blot following 72 h of treatment (X-axis; FSF untreated (Non-Diseased) untreated HGPS (Untreated), arginine restricted HGPS (-Arg), leucine restricted HGPS (-Leu), -ArgLeu,

glucose and pyruvate restricted HGPS (-GlcPyr), HGPS treated with 0.5 mM metformin (+0.5 mM Metf) and HGPS treated with 680 nM rapamycin (+680 nm Rap). Western blots for progerin (70 kDa) and lamin A/C (74 kDa and 63 kDa respectively) are presented below the bar graph. All densities were compared to untreated HGPS in all western blots presented. Every western blot was conducted in biological triplicates, with representative blots presented. Coomassie load controls apply to each protein replicate and therefore are shown once for each cell line and time point. (B) Box and whisker distribution of fluorescence intensity for progerin in response to each of the above treatment conditions (X-axis). One dot represents fluorescence intensity (arbitrary units, AU; Y-axis) of progerin in one nucleus. A minimum of 30 nuclei were measured per condition per replicate (n=3). * $p < 0.0083$ by students T-test corrected for multiple testing (C) Representative images of nuclei stained for DAPI (blue; top) and immunolabelled for progerin (green; middle) for each treatment condition. Merged image (bottom). Scale bar = 50 μm. (D) Bar graph of western blot densitometry relative to HGPS untreated (%, Y-axis) for phosphorylated mTOR ser2448 ((p)-mTOR) in response 72 h of each treatment condition (X-axis) with western blot displayed below. (p)-mTOR = 289 kDa. (E) Bar graph of western blot densitometry relative to HGPS untreated (%, Y-axis) for LC3B in response 72 h of each treatment condition (X-axis) with western blot displayed below. LC3B = 15 kDa.

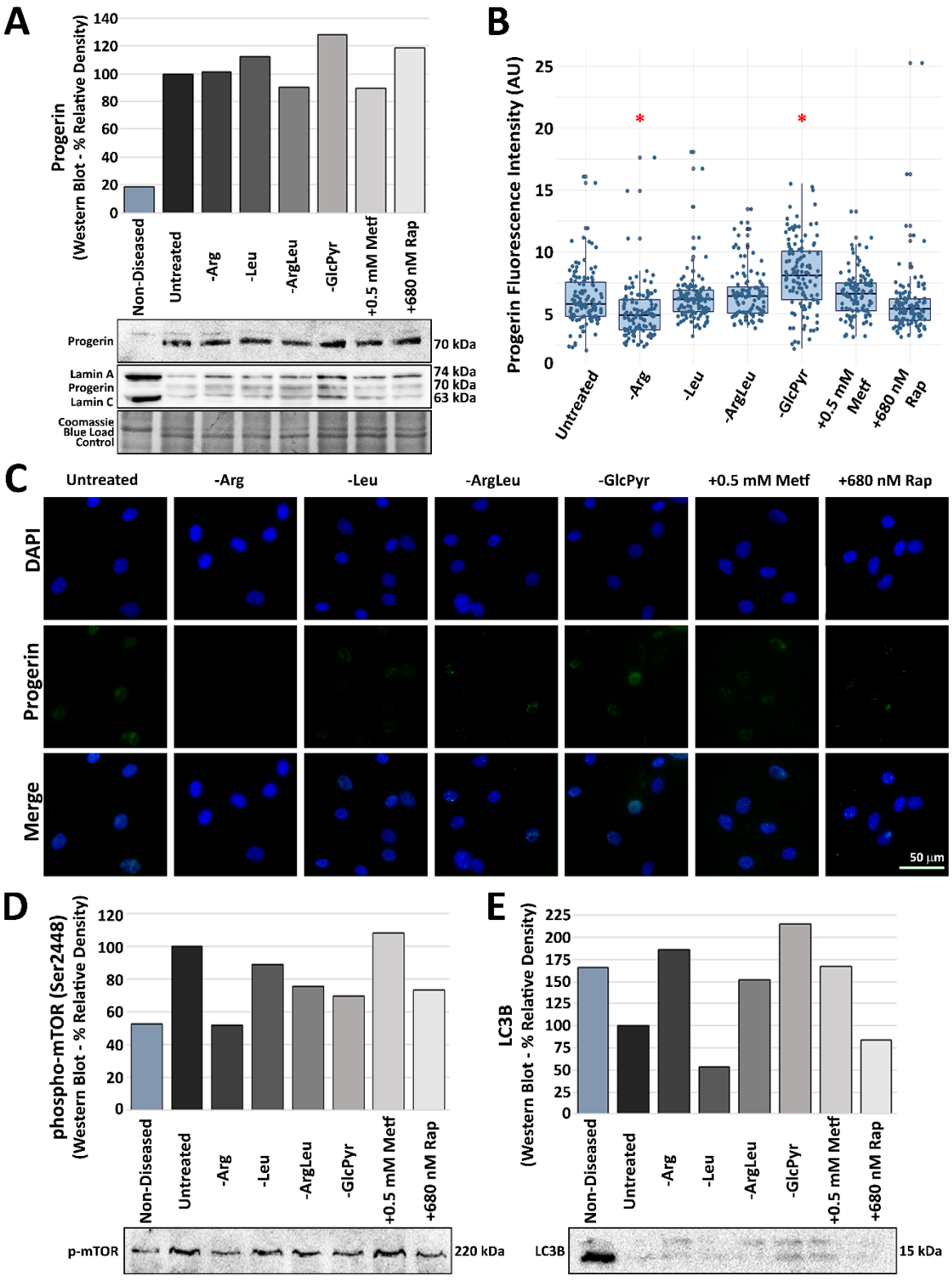

Figure 4.6: Response of Progerin Levels to NR and NRM in HGADFN167 (HGPS; 8y5m). (A) Bar graph for relative densitometry (%, Y-axis) of progerin levels by western blot following 72 h of treatment (X-axis; FSF untreated (Non-Diseased) untreated HGPS

(Untreated), arginine restricted HGPS (-Arg), leucine restricted HGPS (-Leu), -ArgLeu, glucose and pyruvate restricted HGPS (-GlcPyr), HGPS treated with 0.5 mM metformin (+0.5 mM Metf) and HGPS treated with 680 nM rapamycin (+680 nm Rap). Western blots for progerin (70 kDa) and lamin A/C (74 kDa and 63 kDa respectively) are presented below the bar graph. All densities were compared to untreated HGPS in all western blots presented. Every western blot was conducted in biological triplicates, with representative blots presented. Coomassie load controls apply to each protein replicate and therefore are shown once for each cell line and time point. (B) Box and whisker distribution of fluorescence intensity for progerin in response to each of the above treatment conditions (X-axis). One dot represents fluorescence intensity (arbitrary units, AU; Y-axis) of progerin in one nucleus. A minimum of 30 nuclei were measured per condition per replicate (n=3). * $p < 0.0083$ by students T-test corrected for multiple testing (C) Representative images of nuclei stained for DAPI (blue; top) and immunolabelled for progerin (green; middle) for each treatment condition. Merged image (bottom). Scale bar = 50 μm. (D) Bar graph of western blot densitometry relative to HGPS untreated (%, Y-axis) for phosphorylated mTOR ser2448 ((p)-mTOR) in response 72 h of each treatment condition (X-axis) with western blot displayed below. (p)-mTOR = 289 kDa. (E) Bar graph of western blot densitometry relative to HGPS untreated (%, Y-axis) for LC3B in response 72 h of each treatment condition (X-axis) with western blot displayed below. LC3B = 15 kDa.

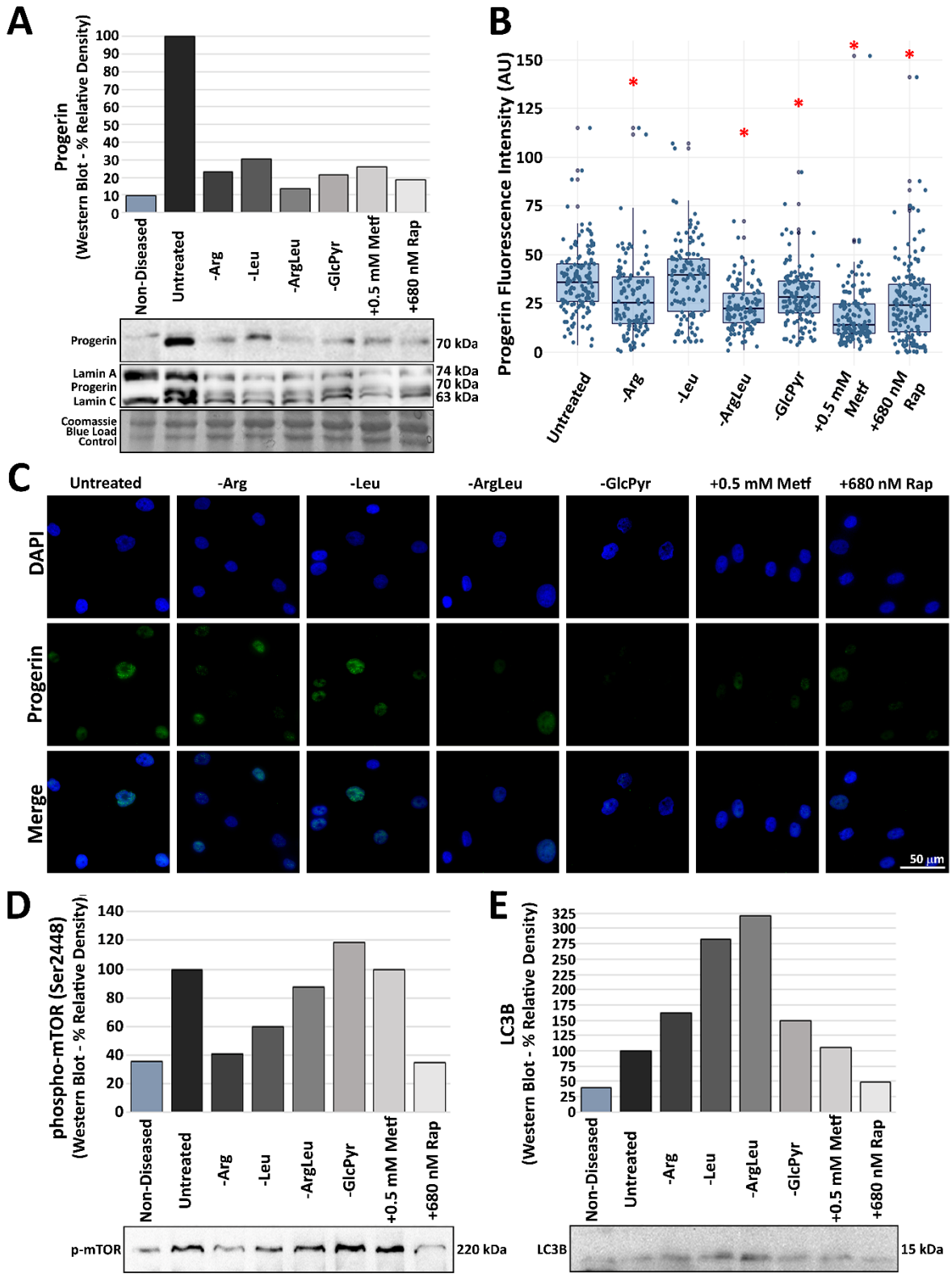

Figure 4.7: Response of Progerin Levels to NR and NRM in HGADFN169 (HGPS; 8y6m). (A) Bar graph for relative densitometry (%, Y-axis) of progerin levels by western blot following 72 h of treatment (X-axis; FSF untreated (Non-Diseased) untreated HGPS

(Untreated), arginine restricted HGPS (-Arg), leucine restricted HGPS (-Leu), -ArgLeu, glucose and pyruvate restricted HGPS (-GlcPyr), HGPS treated with 0.5 mM metformin (+0.5 mM Metf) and HGPS treated with 680 nM rapamycin (+680 nm Rap). Western blots for progerin (70 kDa) and lamin A/C (74 kDa and 63 kDa respectively) are presented below the bar graph. All densities were compared to untreated HGPS in all western blots presented. Every western blot was conducted in biological triplicates, with representative blots presented. Coomassie load controls apply to each protein replicate and therefore are shown once for each cell line and time point. (B) Box and whisker distribution of fluorescence intensity for progerin in response to each of the above treatment conditions (X-axis). One dot represents fluorescence intensity (arbitrary units, AU; Y-axis) of progerin in one nucleus. A minimum of 30 nuclei were measured per condition per replicate (n=3). * $p < 0.0083$ by students T-test corrected for multiple testing (C) Representative images of nuclei stained for DAPI (blue; top) and immunolabelled for progerin (green; middle) for each treatment condition. Merged image (bottom). Scale bar = 50 μm. (D) Bar graph of western blot densitometry relative to HGPS untreated (%, Y-axis) for phosphorylated mTOR ser2448 ((p)-mTOR) in response 72 h of each treatment condition (X-axis) with western blot displayed below. (p)-mTOR = 289 kDa. (E) Bar graph of western blot densitometry relative to HGPS untreated (%, Y-axis) for LC3B in response 72 h of each treatment condition (X-axis) with western blot displayed below. LC3B = 15 kDa.

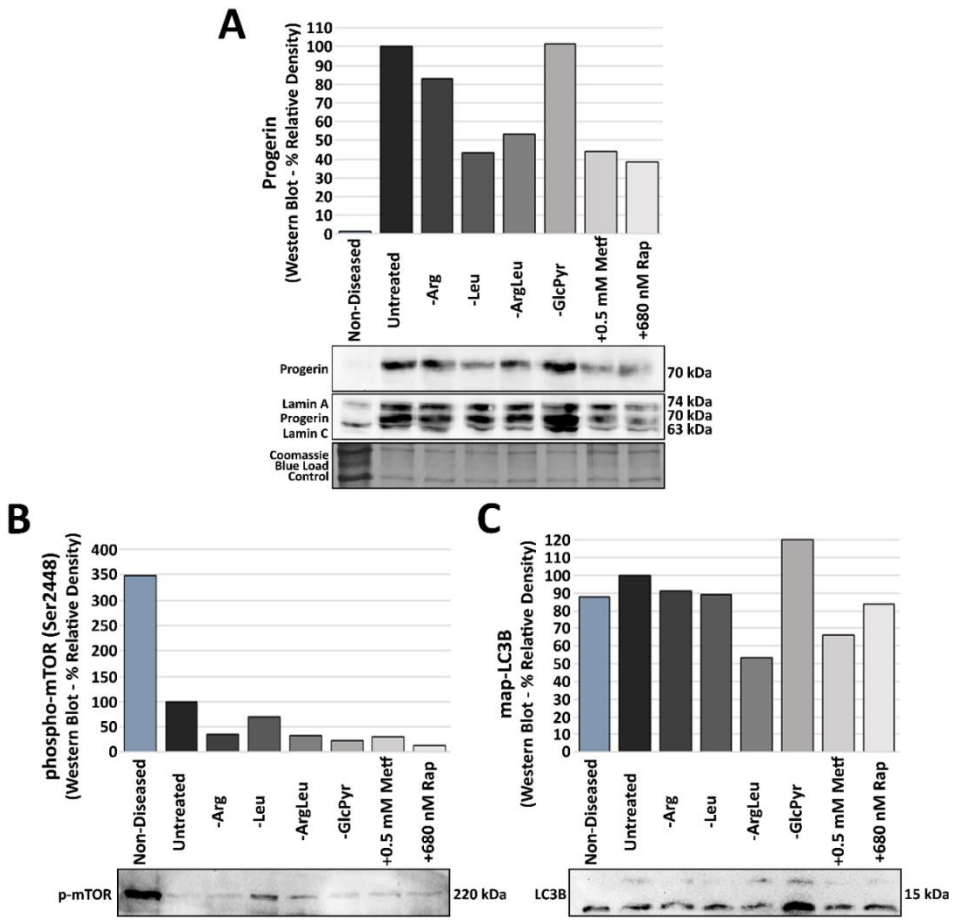

Figure 4.8: Response of Progerin Levels to NR and NRM in AG03513 (HGPS; 13y). (A) Bar graph for relative densitometry (%, Y-axis) of progerin levels by western blot following 72 h of treatment (X-axis; FSF untreated (Non-Diseased) untreated HGPS (Untreated), arginine restricted HGPS (-Arg), leucine restricted HGPS (-Leu), -ArgLeu, glucose and pyruvate restricted HGPS (-GlcPyr), HGPS treated with 0.5 mM metformin (+0.5 mM Metf) and HGPS treated with 680 nM rapamycin (+680 nm Rap)). Western blots for progerin (70 kDa) and lamin A/C (74 kDa and 63 kDa respectively) are presented below the bar graph. All densities were compared to untreated HGPS in all western blots presented. Every western blot was conducted in biological triplicates, with representative blots presented. Coomassie load controls apply to each protein replicate and therefore are shown once for each cell line and time point. **(B)** Bar graph of western blot densitometry relative to HGPS untreated (%, Y-axis) for phosphorylated mTOR ser2448 ((p)-mTOR) in response 72 h of each treatment condition (X-axis) with western blot displayed below. (p)-mTOR = 289 kDa. **(C)** Bar graph of western blot densitometry relative to HGPS untreated (%, Y-axis) for LC3B in response 72 h of each treatment condition (X-axis) with western blot displayed below. LC3B = 15 kDa.

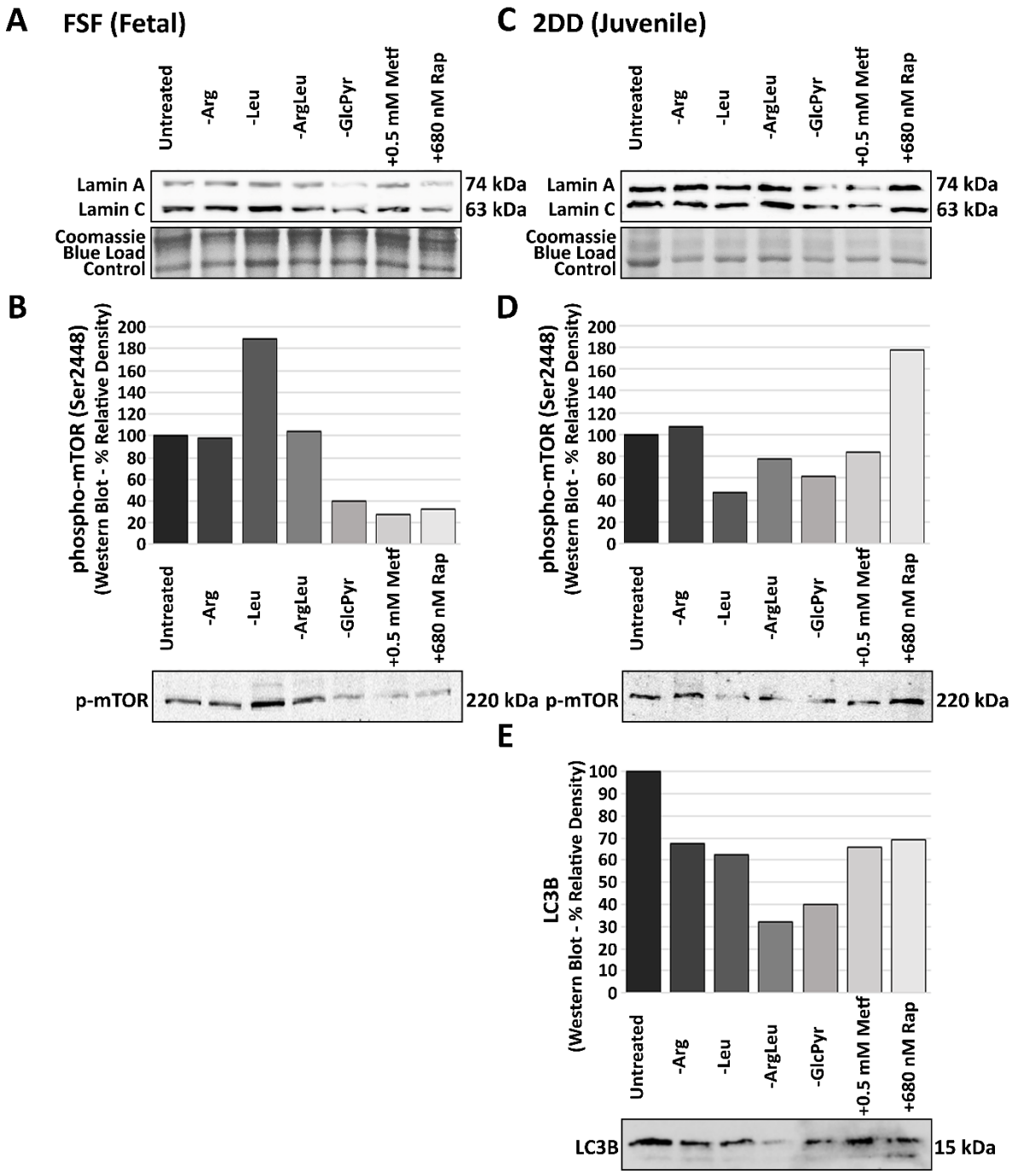

Figure 4.9: Response of Non-Diseased Fibroblasts (FSF and 2DD) to NR and NRM. (A) Western blot for lamin A/C (74 kDa and 63 kDa respectively) in untreated FSF (Untreated), arginine restricted FSF (-Arg), leucine restricted FSF (-Leu), -ArgLeu, glucose restricted FSF (-GlcPyr), FSF treated with 0.5 mM metformin (+0.5 mM Metf) and FSF treated with 680 nM rapamycin (+680 nM Rap). Every western blot was conducted in biological triplicates,

with representative blots presented. Coomassie load controls apply to each protein replicate and therefore are shown once for each cell line and time point. **(B)** Bar graph for relative densitometry (%, Y-axis) compared to untreated FSF for phosphorylated mTOR ser2448 ((p)-mTOR) in response to 72 h of each treatment condition (X-axis). Analyzed western blot displayed below the bar graph. (p)-mTOR = 289 kDa**. (C)** Western blot for laminAC in 2DD with the same conditions listed in (A). **(D)** Bar graph for relative densitometry (%, Y-axis) compared to untreated 2DD for phosphorylated mTOR ser2448 ((p)-mTOR) in response to 72 h of each treatment condition (X-axis). Analyzed western blot displayed below the bar graph. **(E)** Bar graph of western blot densitometry relative to untreated 2DD (%, Y-axis) for LC3B in response 72 h of each treatment condition (X-axis) with western blot displayed below. LC3B = 15 kDa.

4.3 Decreases in Progerin Levels in HGPS Fibroblasts Occurs via Autophagy Dependent and Independent Mechanisms

Progerin is depleted in response to NR and NRM; however, in this model, it is unclear exactly how this progerin depletion is occurring. It was hypothesised that conditions of NR or treatment with NRM would result in inactivation of mTOR (therefore an increase in (p)-mTOR) and activation of autophagy (and therefore an increase in LC3B). However, when levels of these proteins were examined by western blot, data were mixed. Therefore, to determine the role of autophagy in the decrease of progerin in patient HGPS fibroblasts (HGADFN169) and non-diseased fibroblasts (FSF), ATG5, a protein associated with the formation of the autophagosome, was knocked down using shRNA. Arginine sensor CASTOR1 and leucine sensor SESN2, both upstream of mTORC1, were also knocked down to establish the role of these sensors in this process (Figure 4.10).

ATG5 knock-down was achieved in FSF, with lower levels of ATG5 protein detected by western blot. As predicted, LC3B levels also decreased in FSF across NR/NRM conditions examined (-Arg, -Leu, -ArgLeu, +0.5 mM Metf, +680 nM Rap) at 72 h (Figure 4.10A). In HGPS fibroblasts, ATG5 levels were also decreased following ATG5 knock-down; all treatment conditions still exhibited a decrease in progerin levels compared to untreated HGPS, with no obvious changes in (p)-mTOR levels or LC3B (Figure 4.10D). Therefore, progerin degradation could be achieved using mechanisms alternate to ATG5-dependent autophagy.

In non-diseased fibroblasts with knocked-down arginine sensor CASTOR1, -Arg-treated fibroblasts exhibited levels of (p)-mTOR and LC3B similar to that of untreated fibroblasts, as expected. -Leu also appeared dependent on CASTOR1 to elicit changes in mTOR activity and autophagy. In the absence of CASTOR1, other NR/NRM conditions (-ArgLeu, +0.5 mM Metf, +680 nM Rap) induced a subtle increase in (p)-mTOR levels and a concordant increase in LC3B protein levels. Therefore, these conditions are able to elicit response independent of CASTOR1 (Figure 4.10B). In HGPS fibroblasts these changes were not observed; however, only -ArgLeu exhibited a decrease in progerin levels compared to untreated HGPS control. Furthermore, +0.5 mM Metf and +680 nM Rap treatment of these knockdowns exhibited increased progerin levels. These data suggest an essential role for CASTOR1 in mediating progerin degradation in response to -NR and NRM in HGPS fibroblasts (Figure 4.10E).

Knockdown of leucine sensor SESN2 resulted in decreased LC3B protein levels in non-diseased fibroblasts treated with -Leu, in line with no longer responding to NR. No change was observed in -Arg, or in NRM; however combined -ArgLeu still exhibited an increase in LC3B (Figure 4.10C). Unexpectedly, levels of progerin were still decreased in HGPS fibroblasts with decreased SESN2. In response to -Arg, progerin levels were increased, suggesting the beneficial impacts of -Arg not only require intact arginine sensing, but also depend on cellular ability to detect leucine levels using SESN2. To support this, progerin levels in -ArgLeu exhibited no change (Figure 4.10F). Metformin had no change in progerin levels in the absence of SESN2, whilst rapamycin was still able to induce progerin degradation. Combined, these knockdowns indicate that the pathways governing progerin loss in response to NR and NRM is not solely the result of mTOR inactivation and autophagy, and that the beneficial effects of -Arg and -Leu may be dependent on SESN2 sensing.

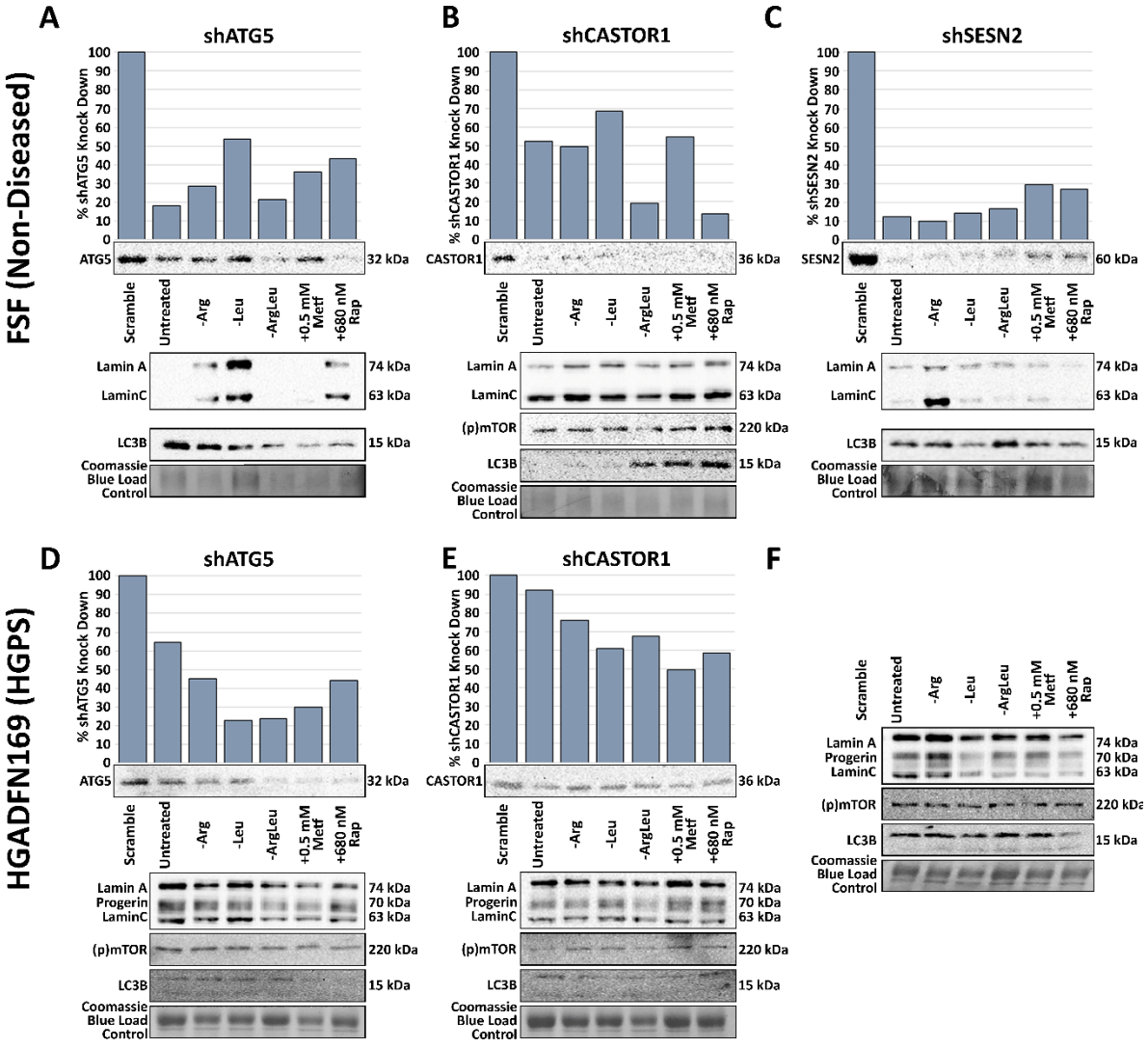

Figure 4.10: Knock-Down of Autophagy-Associated ATG5, Arginine Sensor CASTOR1 and Leucine Sensor Sestrin2 in Non-Diseased and HGPS Fibroblasts. (A) Densitometry of shATG5 in FSF fibroblasts for Scrambled, Untreated, arginine (-Arg) restricted, leucine restricted (-Leu), arginine and leucine restricted (-ArgLeu), +0.5 mM metformin treated (+0.5 mM Metf) and +680 nM rapamycin treated (+680 nM Rap). Lamin AC (top; Lamin A (74 kDa) and Lamin C (63 kDa)), and LC3B (bottom; 15 kDa) western blots are shown below to demonstrate the impact of this knockdown on markers of interest. **(B)** As with A but for shCASTOR1 and containing an additional western blot for (p)-mTOR (middle; 289 kDa). **(C)** As for A but for shSESN2. **(D)** Densitometry of shATG5 in HGADFN169 HGPS fibroblasts for Scrambled, Untreated, arginine (-Arg) restricted, leucine restricted (-Leu), arginine and

leucine restricted (-ArgLeu), +0.5 mM metformin treated (+0.5 mM Metf) and +680 nM rapamycin treated (+680 nM Rap). Lamin AC (top; Lamin A (74 kDa), Progerin (70 kDa) and Lamin C (63 kDa)), (p)-mTOR (middle; 289 kDa) and LC3B (bottom; 15 kDa) western blots are shown below to demonstrate the impact of this knockdown on markers of interest. **(E)** As with D but for shCASTOR1. **(F)** As for D but for shSESN2.

4.4 NR and NRM Alter Molecular Pathologies Associated with Hutchinson-Gilford Progeria Syndrome

4.4.1 Irregular Nuclei are Significantly Reduced in Response to NR and NRM in Hutchinson-Gilford Progeria Syndrome Fibroblasts

Having established the promise of these treatment conditions in decreasing progerin levels across patient cell lines, other molecular characteristics were assessed. Irregular nuclear morphology is a classic cellular phenotype of HGPS, with improved nuclear morphology associated with improved physiological patient outcomes. Nuclear morphology was examined by immunolabelling nuclei for lamin AC. When comparing non-diseased fibroblasts to HGPS fibroblasts, 73.31% of HGPS fibroblast nuclei on average were irregular compared to 12.74% in non-diseased counterparts. As with decreasing progerin levels, all NR and NRM conditions exhibited an ability to decrease the number of irregular nuclei in patient fibroblasts. In fact, -Arg, -Leu, -ArgLeu, -GlcPyr and +0.5 mM Metf decreased irregular nuclei in every patient cell line tested (Table 4.2, Figure 4.11 and 4.12). Rapamycin treatment also decreased number of irregular nuclei across patient cell lines, but to a lesser extent. Importantly, non-diseased fibroblasts treated with NR/NRM exhibited no statistically significant increase in irregular nuclei. In FSF, 12.00% of nuclei were identified as irregular in untreated samples, with NR/NRM conditions altering this number by ± 3.23% (Table 4.2, Figure 4.13 and 4.14). In juvenile fibroblasts, all conditions exhibited a decrease, except for rapamycin, which resulted in an increase from 13.48% to 23.65% (Table 4.2). Therefore, NR and NRM are capable of robustly decreasing the number of irregular nuclei in HGPS patient-cell populations without compromising non-diseased counterparts.

Table 4.6: Mean percentage of irregular nuclei as determined using cells labelled by immunofluorescence by lamin AC. Samples were double blinded and determined number of irregular nuclei in each sample for four HGPS (HGADFN003, HGADFN167, HGADFN169, AG03513) and two non-diseased (FSF, 2DD) fibroblast cell lines in response to defined NR and NRM treatment conditions. [1, 2]

Cell Line	Treatment Condition						
	Untreated	-Arg	-Leu	-ArgLeu	-GlcPyr	+0.5 mM Metf	+680 nM Rap
HGADFN003 (2y0m)	80.42 ± 3.53	54.50 ± 8.33	67.42 ± 5.12	67.32 ± 5.15	70.83 ± 1.82	58.97 ± 2.87*	74.13 ± 3.69
HGADFN167 (8y5m)	54.39 ± 3.87	34.88 ± 6.40	31.38 ± 4.21*	34.38 ± 2.56*	26.62 ± 3.54*	34.26 ± 5.45	36.28 ± 3.92
HGADFN169 (8y6m)	80.54 ± 3.65	67.19 ± 1.10	64.70 ± 0.98	53.71 ± 0.97*	62.71 ± 2.02*	52.97 ± 2.31*	68.81 ± 1.34
AG03513 (13y)	77.88 ± 5.35	53.44 ± 1.37	54.44 ± 1.22	56.10 ± 1.44	61.60 ± 2.99	51.06 ± 2.25*	75.91 ± 5.06
FSF (Neonate)	12.00 ± 1.40	15.23 ± 2.40	10.83 ± 2.25	11.00 ± 1.64	12.90 ± 2.77	10.51 ± 1.39	14.48 ± 2.55
2DD (Juvenile)	13.48 ± 3.66	2.56 ± 1.84	4.41 ± 2.08	3.76 ± 1.32	5.23 ± 1.46	6.10 ± 1.56	23.65 ± 2.21

[1]Reported as percentage
[2]Mean ± standard error of the mean of triplicates of at least 100 nuclei
* $p < 0.0083$ by students T-test corrected for multiple testing

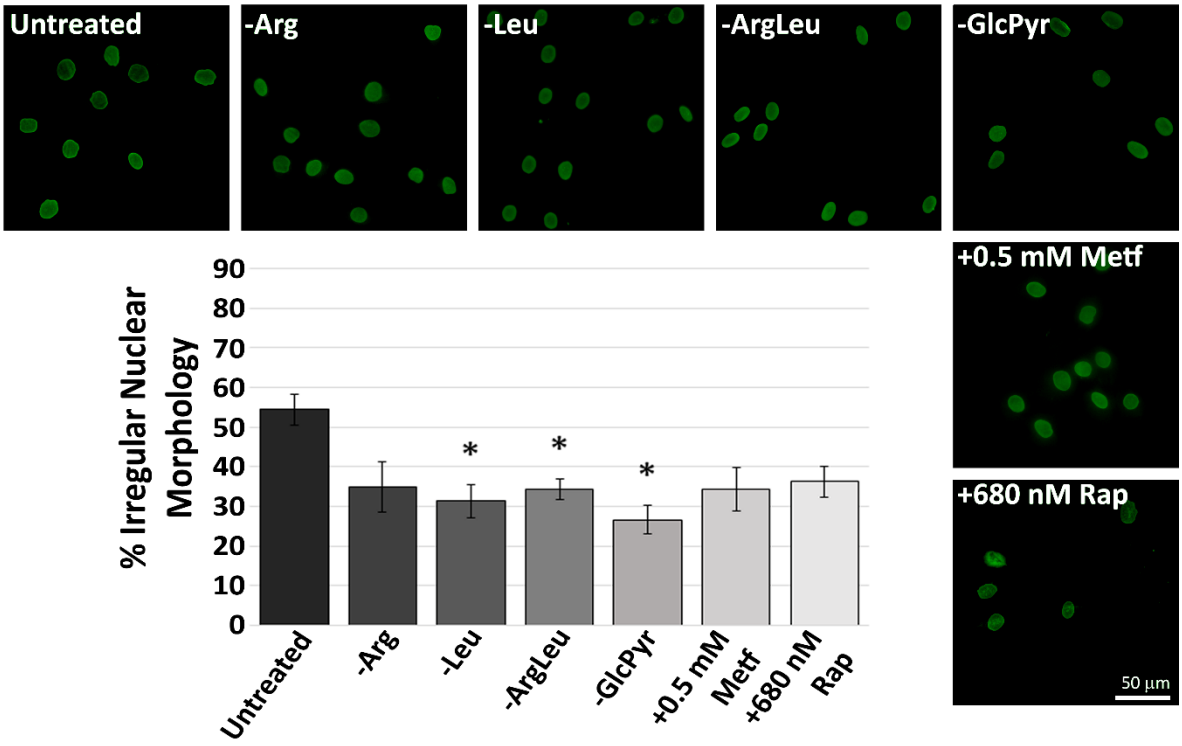

Figure 4.11: Nuclear Morphology of HGADFN167 is Improved in Response to Nutrient Restriction and Nutrient Restriction Mimetics. Representative images are presented for Untreated, arginine restricted (-Arg), leucine restricted (-Leu), arginine and leucine restricted (-ArgLeu), glucose and pyruvate restricted (-Glcpyr), treated with 0.5 mM metformin (+0.5 mM Metf) or 680 nM rapamycin (+680 nM Rap). Nuclei are labelled for lamin AC (green). Scale bar = 50 µm. Bar graph summarises data from three replicates. Percent irregular nuclei (Y-axis) for each condition (X-axis) are presented. * $p < 0.0083$ by students T-test corrected for multiple testing. All data were analyzed blinded to reduce bias in identification of irregular nuclei.

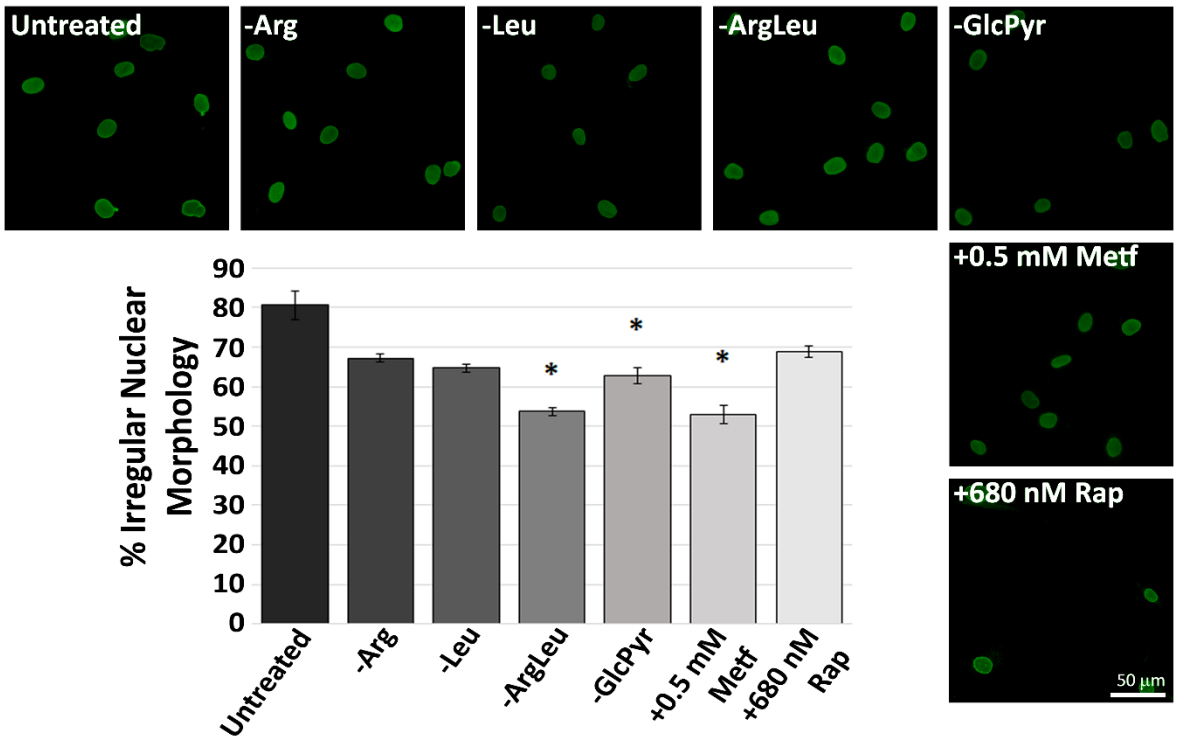

Figure 4.12: Nuclear Morphology of HGADFN169 is Improved in Response to Nutrient Restriction and Nutrient Restriction Mimetics. Representative images are presented for Untreated, arginine restricted (-Arg), leucine restricted (-Leu), arginine and leucine restricted (-ArgLeu), glucose and pyruvate restricted (-Glcpyr), treated with 0.5 mM metformin (+0.5 mM Metf) or 680 nM rapamycin (+680 nM Rap). Nuclei are labelled for lamin AC (green). Scale bar = 50 µm. Bar graph summarises data from three replicates. Percent irregular nuclei (Y-axis) for each condition (X-axis) are presented. * $p < 0.0083$ by students T-test corrected for multiple testing. All data were analyzed blinded to reduce bias in identification of irregular nuclei.

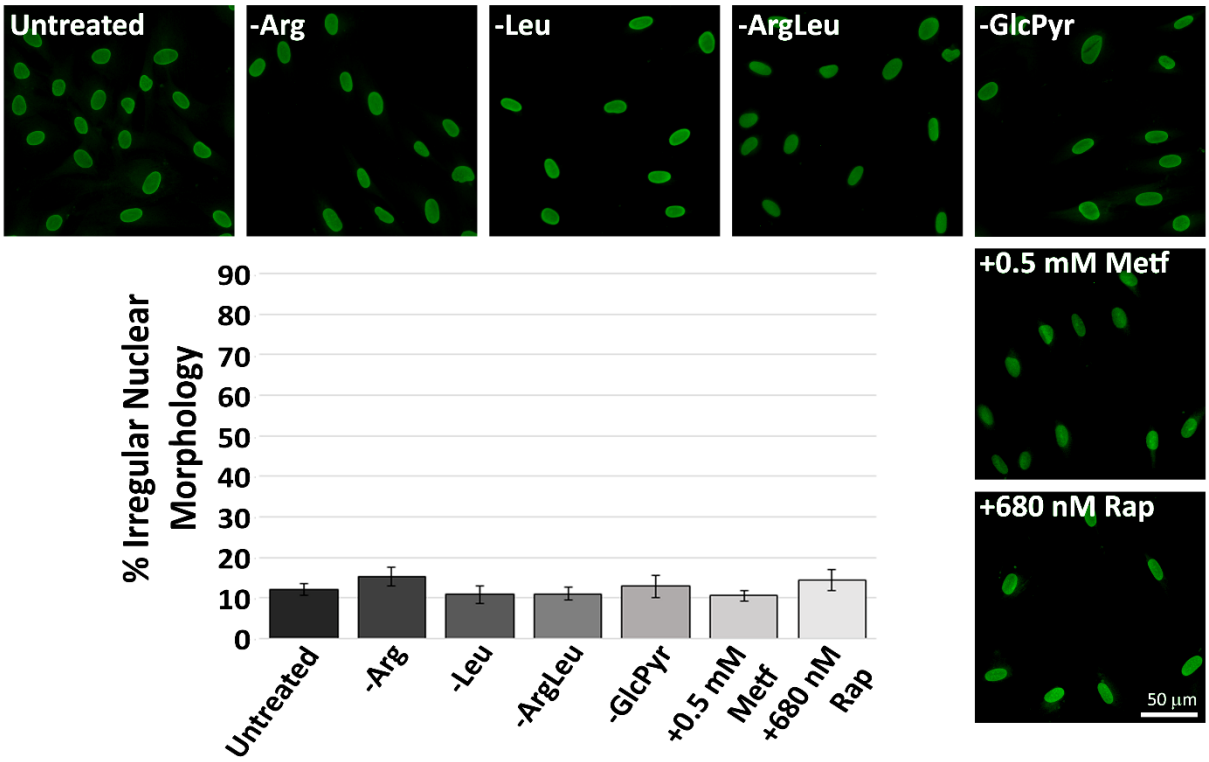

Figure 4.13: Nuclear Morphology of FSF is Maintained in Response to Nutrient Restriction and Nutrient Restriction Mimetics. Representative images are presented for Untreated, arginine restricted (-Arg), leucine restricted (-Leu), arginine and leucine restricted (-ArgLeu), glucose and pyruvate restricted (-Glcpyr), treated with 0.5 mM metformin (+0.5 mM Metf) or 680 nM rapamycin (+680 nM Rap). Nuclei are labelled for lamin AC (green). Scale bar = 50 µm. Bar graph summarises data from three replicates. Percent irregular nuclei (Y-axis) for each condition (X-axis) are presented* $p < 0.0083$ by students T-test corrected for multiple testing. All data were analyzed blinded to reduce bias in identification of irregular nuclei.

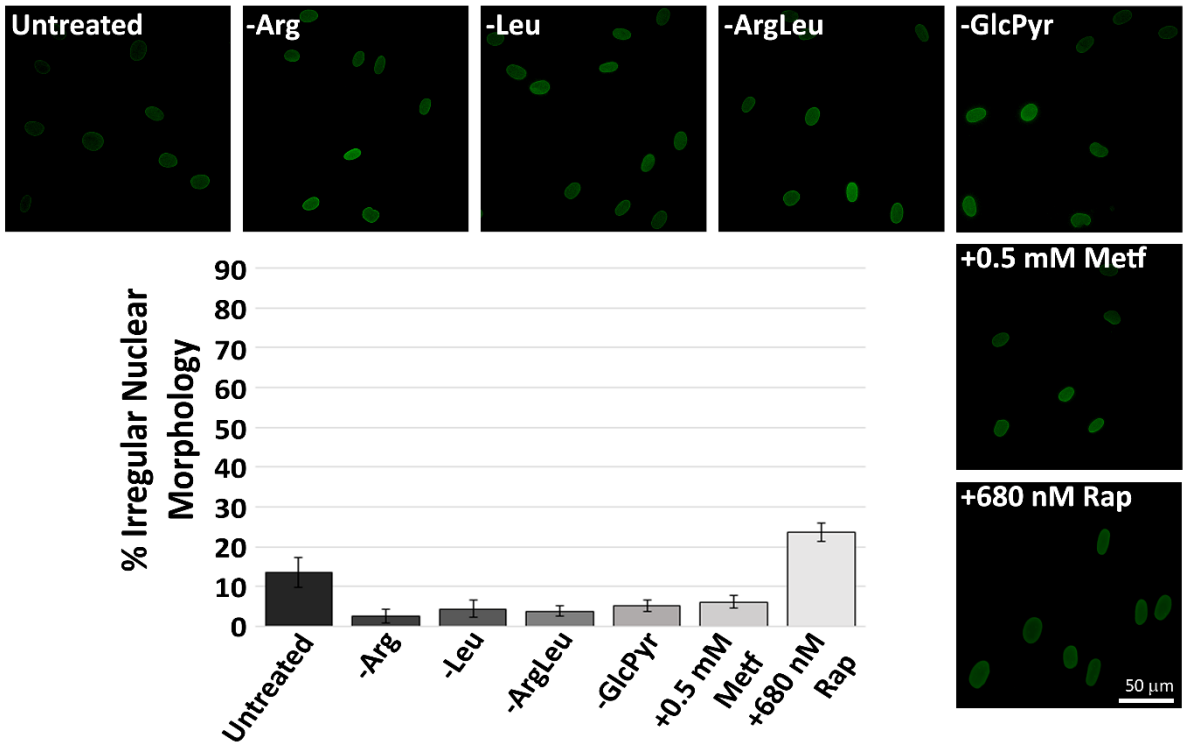

Figure 4.14: Nuclear Morphology of 2DD is Maintained in Response to Nutrient Restriction and Nutrient Restriction Mimetics. Representative images are presented for Untreated, arginine restricted (-Arg), leucine restricted (-Leu), arginine and leucine restricted (-ArgLeu), glucose and pyruvate restricted (-Glcpyr), treated with 0.5 mM metformin (+0.5 mM Metf) or 680 nM rapamycin (+680 nM Rap). Nuclei are labelled for lamin AC (green). Scale bar = 50 µm. Bar graph summarises data from three replicates. Percent irregular nuclei (Y-axis) for each condition (X-axis) are presented. * $p < 0.0083$ by students T-test corrected for multiple testing. All data were analyzed blinded to reduce bias in identification of irregular nuclei.

4.4.2 DNA Damage Repair is Improved in Response to NR and NRM in Hutchinson-Gilford Progeria Syndrome Fibroblasts

HGPS fibroblasts have been documented to exhibit dysregulation of DNA damage and repair. The marker of unrepaired double strand breaks, γ-H2AX, has classically been used to identify this disruption in HGPS fibroblasts, with greater levels of γ-H2AX in HGPS cells and models compared to their respective controls (Chojnowski *et al.,* 2020; Liu *et al.,* 2006; Liu *et al.,* 2008; Richards *et al.,* 2011), a finding replicated here. The ability of HGPS fibroblasts to repair DNA following induction of DNA damage was examined by growing cells for 72 h under NR or NRM before inducing double strand breaks with H_2O_2. γ-H2AX levels were examined at 0 h, 1 h and 6 h (Figure 4.15) post-DSB induction. By 6 h, HGADFN003, HGADFN169 and AG03513 exhibited lower levels of DSB than untreated counterparts in response to -Arg, -Leu, -ArgLeu, +0.5 mM Metf and +680 nM Rap. In response to -GlcPyr, HGADFN003 and AG03513 also exhibited lower levels of γ-H2AX at 6 h. In the HGADN167 cells, only -ArgLeu and +0.5 mM Metf resulted in lower γ-H2AX levels (Figure 4.15b). In non-diseased fibroblasts, findings were varied, with some treatments resulting in higher levels of γ-H2AX following 6 h of recovery compared to untreated samples (for example, in FSF only treatment with metformin resulted in lower detectable γ-H2AX, whilst in 2DD this was the case for -Arg, -Leu, +0.5 mM Metf and +680 nM Rap) (Figure 4.16). Finally, γ-H2AX levels are lower than at the point of DNA damage induction following 6 h recovery, demonstrating that DNA damage repair is improved in response to the NR conditions arginine and/or leucine as well as metformin or rapamycin treatment.

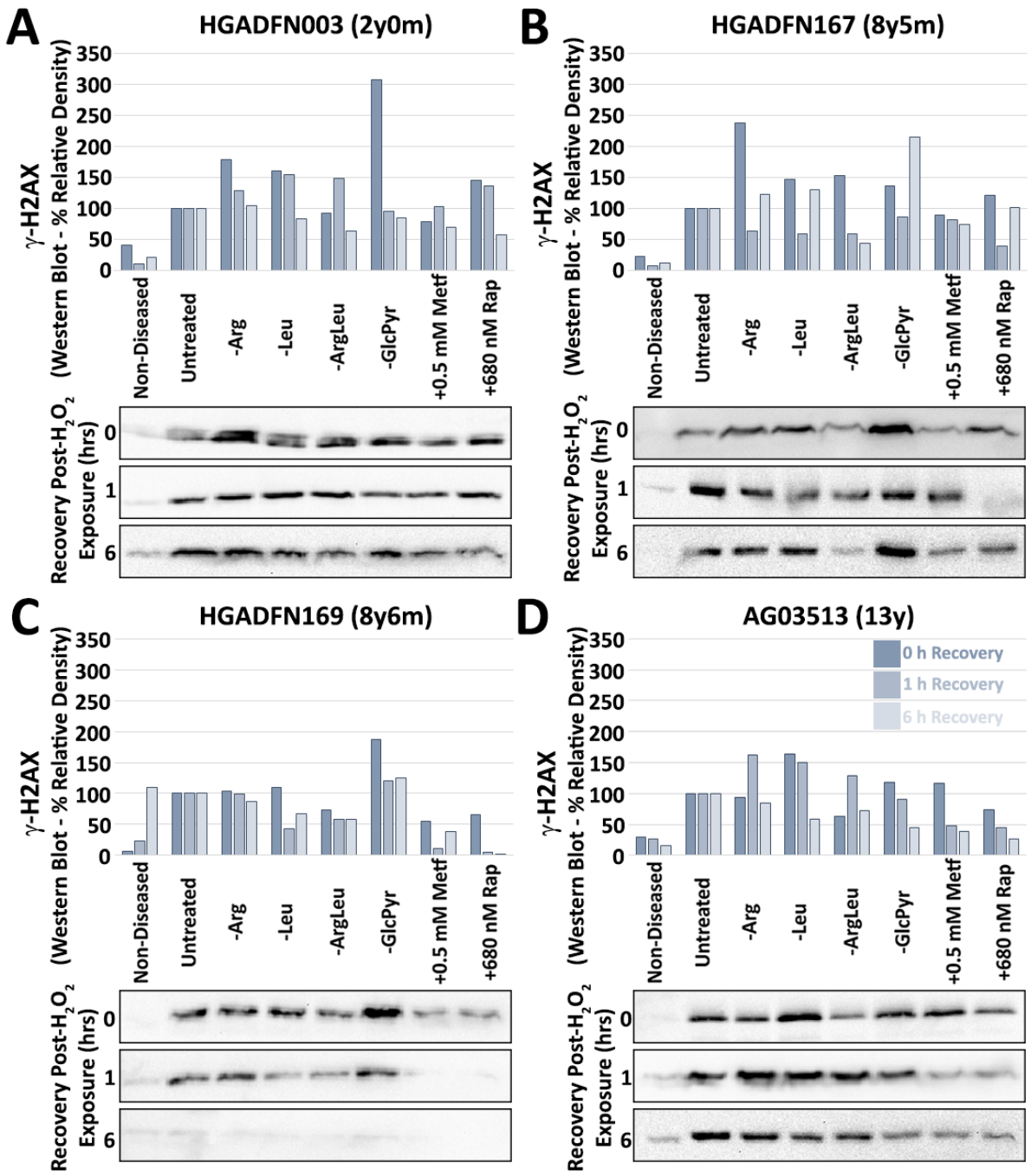

Figure 4.15: Altered Protein Levels of the DNA Damage Marker γ-H2AX in HGPS Fibroblasts Following Treatment with NR and NRM. Densitometry for γ-H2AX (15 kDa) is presented as bar graphs with corresponding western blots presented below at 0 h, 1 h, and 6 h following exposure to 150 μM H_2O_2. HGPS patient fibroblasts **(A)** HGADFN003, **(B)** HGADFN167, **(C)** HGADFN169, **(D)** AG03513 were grown for 72 h under regular growth conditions (Untreated), arginine restricted (-Arg), leucine restricted (-Leu), arginine and

leucine restricted (-ArgLeu), glucose and pyruvate restricted (-GlcPyr) or treated with 0.5 mM metformin (+0.5 mM Metf) or 680 nM rapamycin (+680 nM Rap) (X-axis) before exposure to H_2O_2 for thirty minutes. Protein used in western blots are from whole-cell lysates. A non-diseased control lysate is presented alongside HGPS lysates. All densitometry is compared back to untreated HGPS fibroblasts and presented as a percentage of untreated conditions (Y-axis).

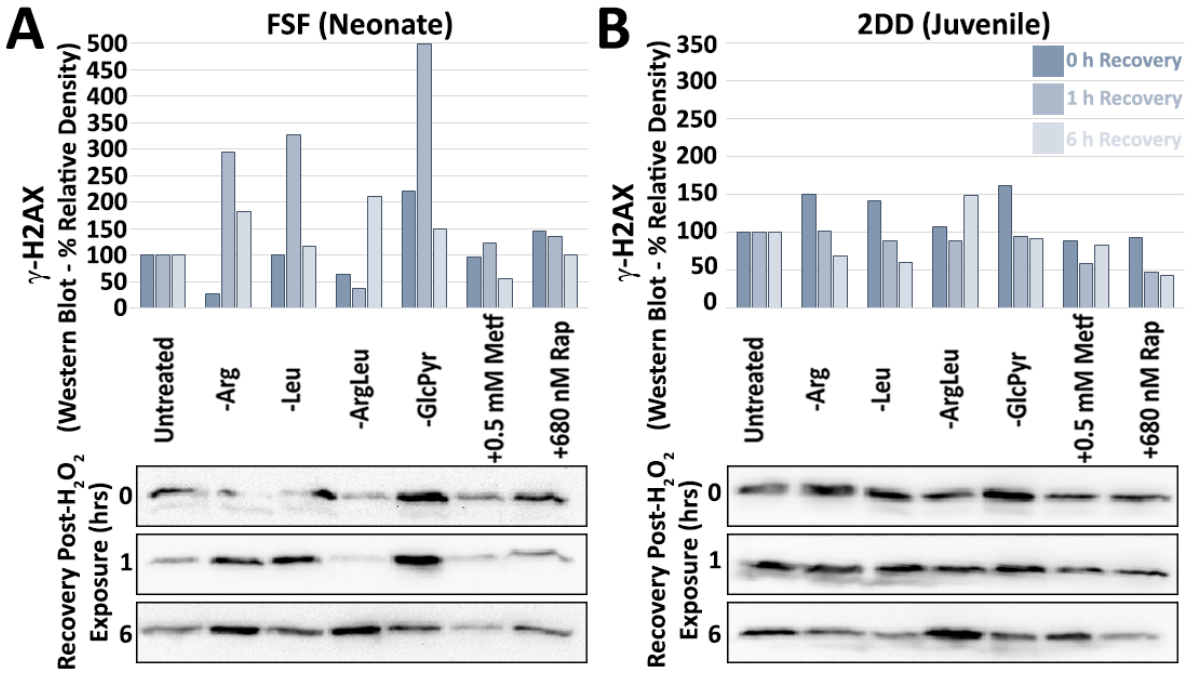

Figure 4.16: Altered Protein Levels of the DNA Damage Marker γ-H2AX in Non-Diseased Fibroblasts Following Treatment with NR and NRM. Densitometry for γ-H2AX (15 kDa) is presented as bar graphs with corresponding western blots presented below at 0 h, 1 h, and 6 h following exposure to 150 μM H_2O_2. HGPS patient fibroblasts **(A)** FSF and **(B)** were grown for 72 h under regular growth conditions (Untreated), arginine restricted (-Arg), leucine restricted (-Leu), arginine and leucine restricted (-ArgLeu), glucose and pyruvate restricted (-GlcPyr) or treated with 0.5 mM metformin (+0.5 mM Metf) or 680 nM rapamycin (+680 nM Rap) (X-axis) before exposure to H_2O_2 for thirty minutes. Protein used in western blots are from whole-cell lysates. All densitometry is compared back to untreated HGPS fibroblasts and presented as a percentage of untreated conditions (Y-axis).

4.4.3 NR and NRM Result in Divergent Changes in H3K27me3 Levels in Hutchinson-Gilford Progeria Syndrome Fibroblasts

Among the numerous cellular characteristics associated with HGPS is loss of inactive chromatin, indicated by a decrease in the repressive mark H3K27me3. This decrease in H3K27me3 was recapitulated when comparing non-diseased and HGPS fibroblasts here (Figures 4.17-4.19C). It was hypothesised that H3K27me3 levels will increase in response to NR and NRM. Protein levels of H3K27me3 were examined by immunofluorescence (IF) and western blot (WB) following 72 h of NR or NRM. In data collected by IF, -Arg decreased levels of H3K27me3 in two of three HGPS fibroblast lines tested, whilst -Leu, combined -ArgLeu, and -GlcPyr decreased levels of H3K27me3 in all three of these cell lines (Table 4.3, Figures 4.17-19A and B). By IF, the NRM metformin reduced levels of H3K27me3 in two of the three diseased lines, whilst rapamycin achieved this reduction across all lines. In non-diseased fibroblasts, -ArgLeu significantly increased H3K27me3 levels, but otherwise all other NR/NRM conditions tested decreased levels, as with HGPS fibroblasts. By WB, -Arg data coincided with IF findings, with decreased H3K27me3 levels in two (HGADFN003, HGADFN169) patient fibroblast samples (Figures 4.17-19C). -Leu, was also decreased in line with IF as reported in two of the three HGPS samples; however, an increase was noted in HGADFN167. Contrary to IF, -ArgLeu and -GlcPyr induced increased H3K27me3 levels in two of the three HGPS cell lines tested (HGADFN167, HGADFN169). Metformin results by WB were in line with IF, demonstrating two cell-lines exhibited lower levels of H3K27me3 than untreated controls. Rapamycin achieved this decrease in H3K27me3 protein levels as in the case of metformin-treated fibroblasts, whilst a small increase was observed in HGADFN169. Non-diseased fibroblasts exhibited greater divergence in techniques, with all treatments but rapamycin increasing H3K27me3 in FSF, while only -ArgLeu achieved this by IF (Table 4.3, Figure 4.20 A-C). In summary, the majority of treatments under NR/NRM conditions are inducing a reduction in H3K27me3 levels, with fewer instances of increased H3K27me3 reported by either assay. Therefore, NR/NRM are able to alter the inactive chromatin environment of HGPS patient fibroblasts.

EZH2 is the methyltransferase primarily responsible for H3K27 methylation. In HGPS cells, it has previously been reported that levels are lower than non-diseased counterparts (McCord *et al.*, 2013; Shumaker *et al.*, 2006). However, in these HGPS

fibroblasts, when compared to neonate control, EZH2 protein levels are higher (Figures 4.16-18D). In response to -Arg, -Leu and -ArgLeu, EZH2 protein levels increase following 72 h of treatment in two of the three HGPS cell-lines examined, whilst in all other conditions (-GlcPyr, +0.5 mM Metf, +680 nM Rap) a decrease is observed. In non-diseased FSF, levels of EZH2 are low across all conditions, compared to HGPS, with a potential increase in response to -Leu. In general, in conditions under which H3K27me3 is being decreased, EZH2 levels are increasing.

Table 4.7 Mean fluorescence intensity of H3K27me3 by immunofluorescence in three HGPS patient fibroblast cell lines (HGADFN003, HGADFN167, HGADFN169) and two non-diseased cell lines (FSF) in response to defined NR and NRM conditions. [1, 2]

Cell Line	Treatment Condition						
	Untreated	-Arg	-Leu	-ArgLeu	-GlcPyr	+0.5 mM Metf	+680 nM Rap
HGADFN003 (2y0m)	38.90 ± 1.30	31.32 ± 1.25*	22.48 ± 0.90*	24.75 ± 1.45*	30.95 ± 1.59*	23.50 ± 0.94*	19.75 ± 0.71*
HGADFN167 (8y5m)	6.75 ± 0.20	7.31 ± 0.28	5.57 ± 0.15*	6.62 ± 0.17	6.12 ± 0.15*	4.97 ± 0.13*	5.66 ± 0.21*
HGADFN169 (8y6m)	8.04 ± 0.24	7.76 ± 0.23	7.50 ± 0.21	7.52 ± 0.27	7.14 ±40	9.54 ± 0.37*	7.00 ± 0.18*
FSF (Neonate)	18.14 ± 0.23	15.07 ± 0.26*	16.66 ± 0.38*	24.00 ± 0.53*	13.65 ± 0.42*	14.95 ± 0.35*	15.84 ± 0.42*

[1]Reported as percentage
[2]Mean ± standard error of the mean of triplicates of at least 100 nuclei
* $p < 0.0083$ by students T-test corrected for multiple testing

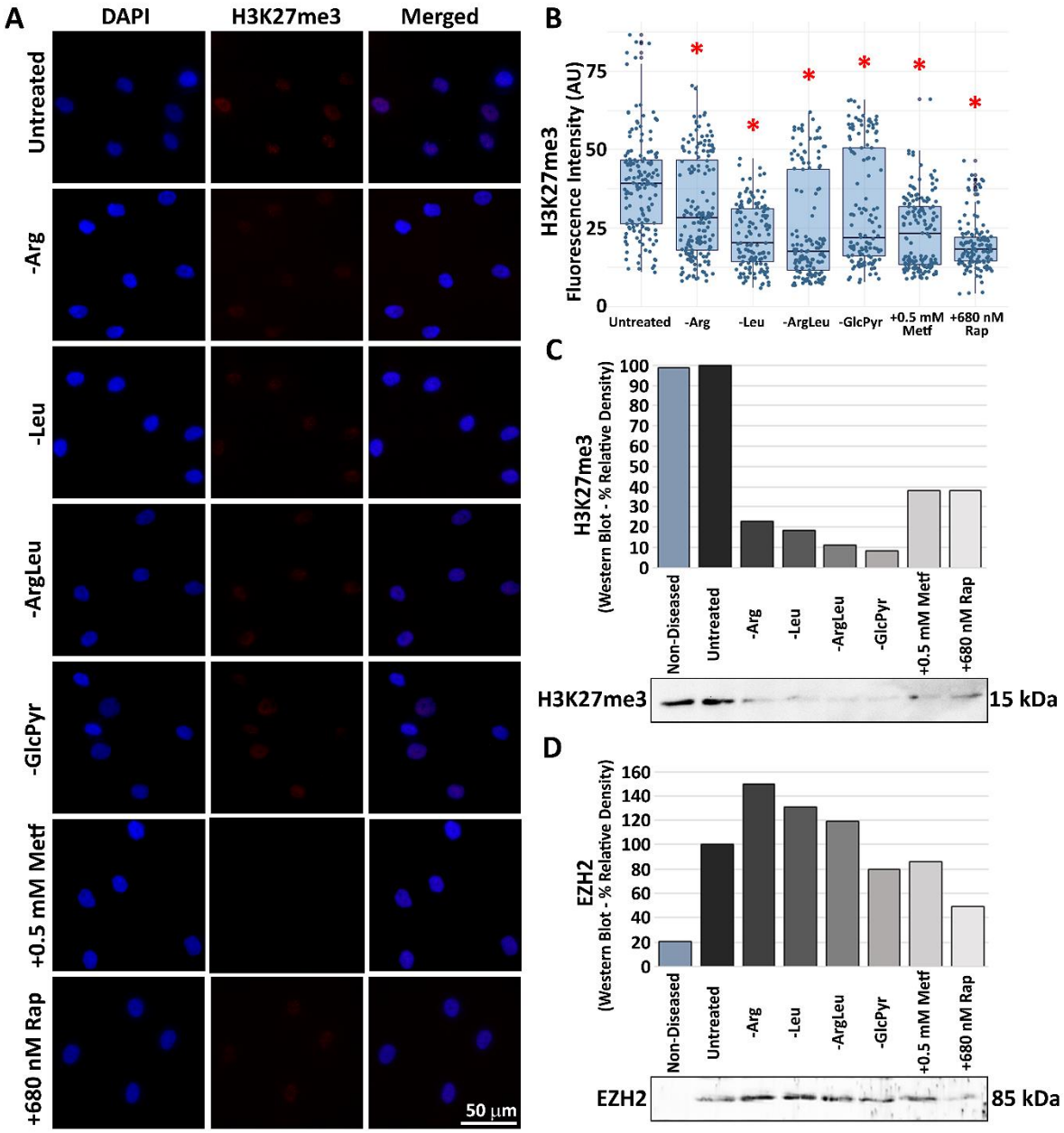

Figure 4.17: Alterations in Inactive Chromatin in Response to NR and NRM in HGADFN003 (HGPS; 2y0mo). (A) Representative images of nuclei stained for DAPI (blue; left) and immunolabelled for H3K27me3 (red; middle) for each treatment condition. Merged image (right). Treatment conditions listed along the left-hand side: 72 h of standard growth conditions (Untreated), arginine restricted (-Arg), leucine restricted (-Leu), -ArgLeu, glucose and pyruvate restricted (-GlcPyr), treated with 0.5 mM metformin (+0.5 mM Metf) and treated with 680 nM rapamycin (+680 nm Rap). Scale bar = 50 µm. **(B)** Box and whisker distribution of fluorescence intensity for progerin in response to each of the above treatment conditions (X-axis). One dot represents fluorescence intensity (arbitrary units, AU; Y-axis) of

H3K27me3 in one nucleus. A minimum of 30 nuclei were measured per condition per replicate (n=3). * $p < 0.0083$ by students T-test corrected for multiple testing. **(C)** Bar graph for relative densitometry (%, Y-axis) of progerin levels by western blot following 72 h of treatment (X-axis; FSF untreated (Non-Diseased) untreated HGPS (Untreated), and HGPS under -Arg, -ArgLeu, -GlcPyr, +0.5 mM Metf, +680 nM Rap. Western blot for H3K27me3 (~17 kDa) below the bar graph. All densities were compared to untreated HGPS in all western blots presented. **(D)** Bar graph of western blot densitometry relative to HGPS untreated (%, Y-axis) for EZH2 (~85 kDa) in response 72 h of each treatment condition in (C; X-axis) with western blot displayed below. All western blots were biologically replicated a minimum of three times, with representative western blots presented. All proteins were equally loaded as determined by Coomassie blue, presented alongside previously shown progerin western blots.

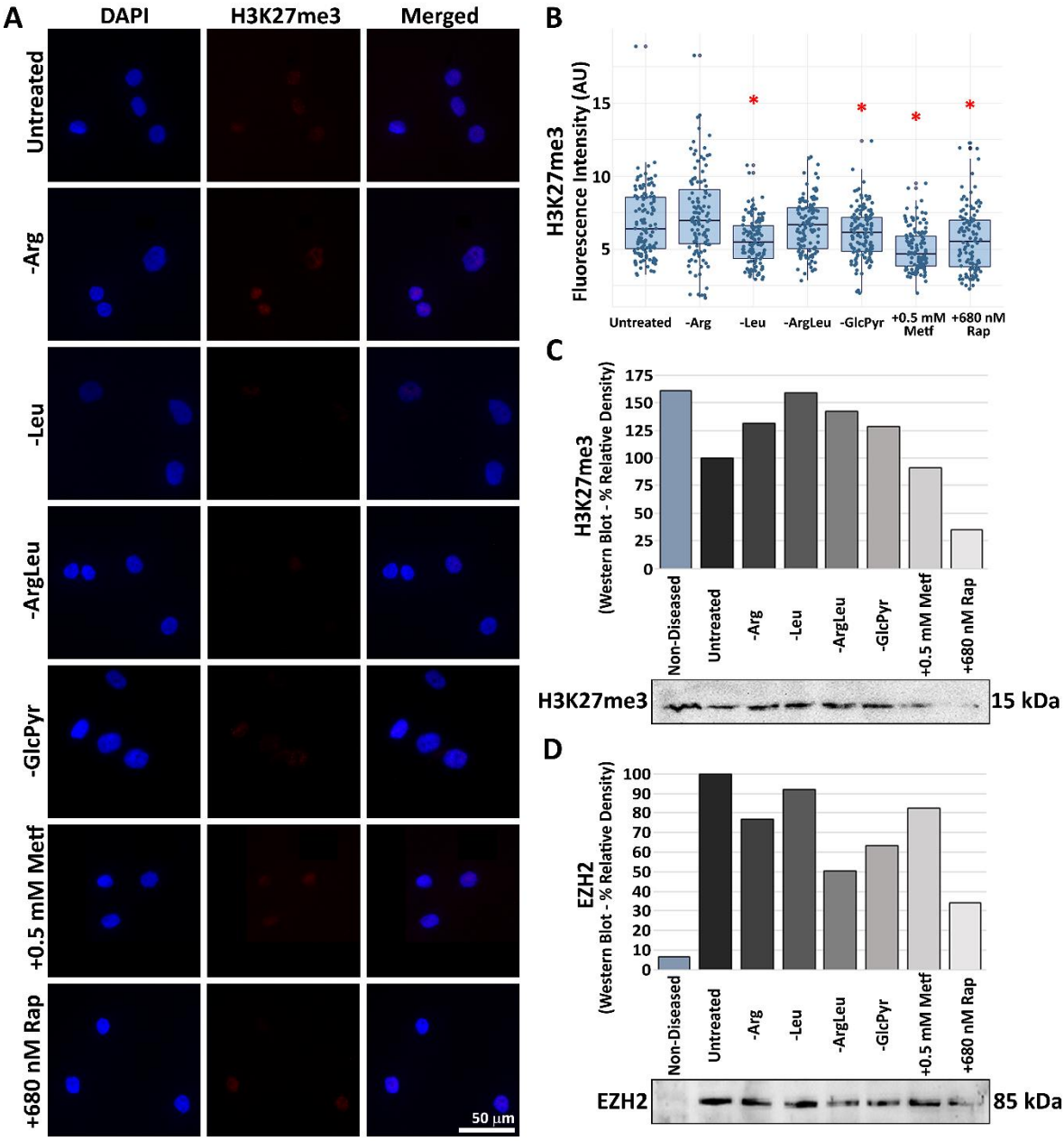

Figure 4.18: Alterations in Inactive Chromatin in Response to NR and NRM in HGADFN167 (HGPS; 8y5mo). (A) Representative images of nuclei stained for DAPI (blue; left) and immunolabelled for H3K27me3 (red; middle) for each treatment condition. Merged image (right). Treatment conditions listed along the left-hand side: 72 h of standard growth conditions (Untreated), arginine restricted (-Arg), leucine restricted (-Leu), -ArgLeu, glucose and pyruvate restricted (-GlcPyr), treated with 0.5 mM metformin (+0.5 mM Metf) and treated with 680 nM rapamycin (+680 nm Rap). Scale bar = 50 μm. **(B)** Box and whisker distribution of fluorescence intensity for progerin in response to each of the above treatment conditions

(X-axis). One dot represents fluorescence intensity (arbitrary units, AU; Y-axis) of H3K27me3 in one nucleus. A minimum of 30 nuclei were measured per condition per replicate (n=3). * $p < 0.0083$ by students T-test corrected for multiple testing**. (C)** Bar graph for relative densitometry (%, Y-axis) of progerin levels by western blot following 72 h of treatment (X-axis; FSF untreated (Non-Diseased) untreated HGPS (Untreated), and HGPS under -Arg, -ArgLeu, -GlcPyr, +0.5 mM Metf, +680 nM Rap. Western blot for H3K27me3 (~17 kDa) below the bar graph. All densities were compared to untreated HGPS in all western blots presented. **(D)** Bar graph of western blot densitometry relative to HGPS untreated (%, Y-axis) for EZH2 (~85k Da) in response 72 h of each treatment condition in (C; X-axis) with western blot displayed below. All western blots were biologically replicated a minimum of three times, with representative western blots presented. All proteins were equally loaded as determined by Coomassie blue, presented alongside previously shown progerin western blots.

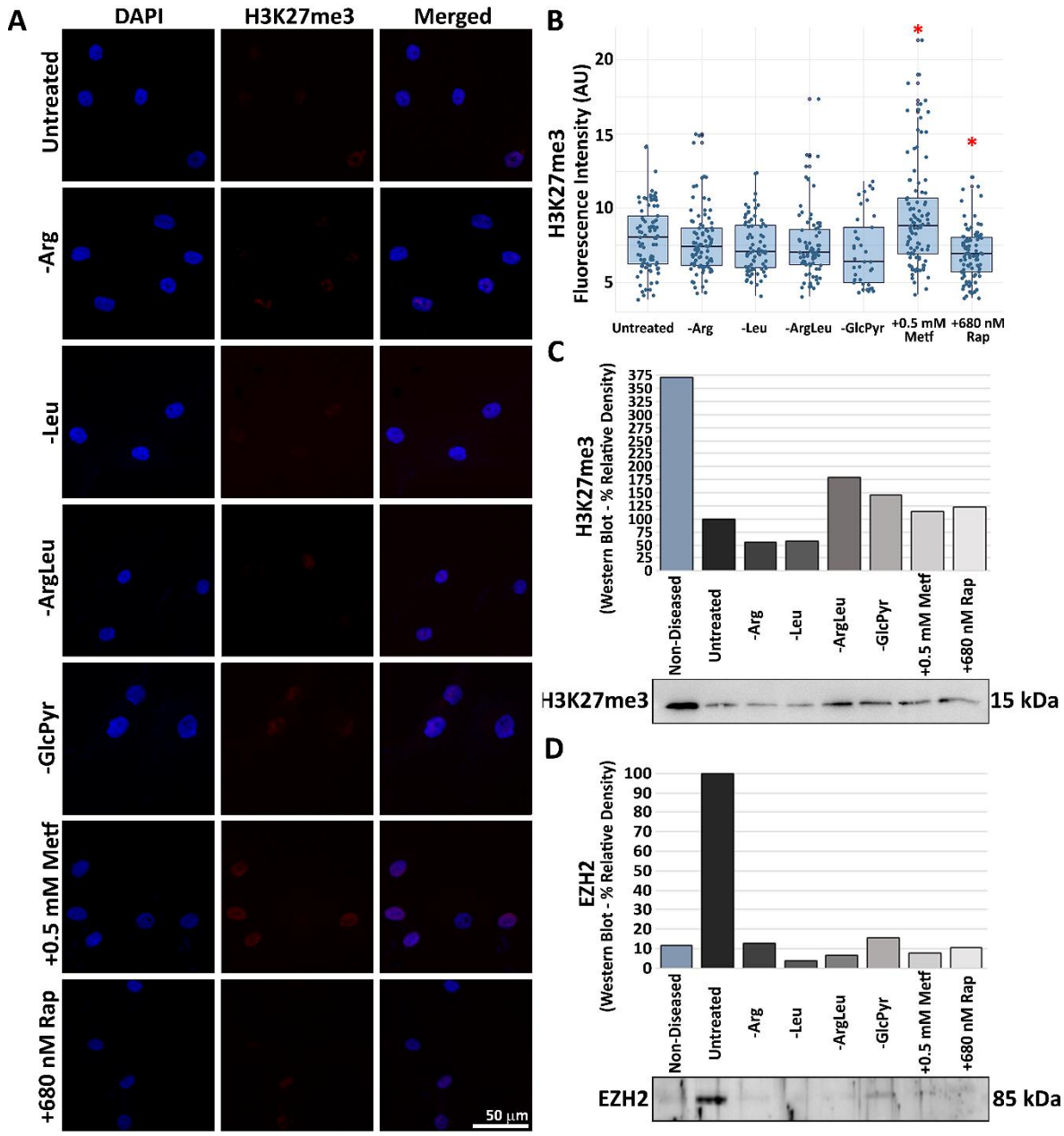

Figure 4.19: Alterations in Inactive Chromatin in Response to NR and NRM in HGADFN169 (HGPS; 8y6mo). (A) Representative images of nuclei stained for DAPI (blue; left) and immunolabelled for H3K27me3 (red; middle) for each treatment condition. Merged image (right). Treatment conditions listed along the left-hand side: 72 h of standard growth conditions (Untreated), arginine restricted (-Arg), leucine restricted (-Leu), -ArgLeu, glucose and pyruvate restricted (-GlcPyr), treated with 0.5 mM metformin (+0.5 mM Metf) and treated with 680 nM rapamycin (+680 nm Rap). Scale bar = 50 µm. **(B)** Box and whisker distribution of fluorescence intensity for progerin in response to each of the above treatment conditions

(X-axis). One dot represents fluorescence intensity (arbitrary units, AU; Y-axis) of H3K27me3 in one nucleus. A minimum of 30 nuclei were measured per condition per replicate (n=3). * $p < 0.0083$ by students T-test corrected for multiple testing**. (C)** Bar graph for relative densitometry (%, Y-axis) of progerin levels by western blot following 72 h of treatment (X-axis; FSF untreated (Non-Diseased) untreated HGPS (Untreated), and HGPS under -Arg, -ArgLeu, -GlcPyr, +0.5 mM Metf, +680 nM Rap. Western blot for H3K27me3 (~17 kDa) below the bar graph. All densities were compared to untreated HGPS in all western blots presented. **(D)** Bar graph of western blot densitometry relative to HGPS untreated (%, Y-axis) for EZH2 (~85 kDa) in response 72 h of each treatment condition in (C; X-axis) with western blot displayed below. All western blots were biologically replicated a minimum of three times, with representative western blots presented. All proteins were equally loaded as determined by Coomassie blue, presented alongside previously shown progerin western blots.

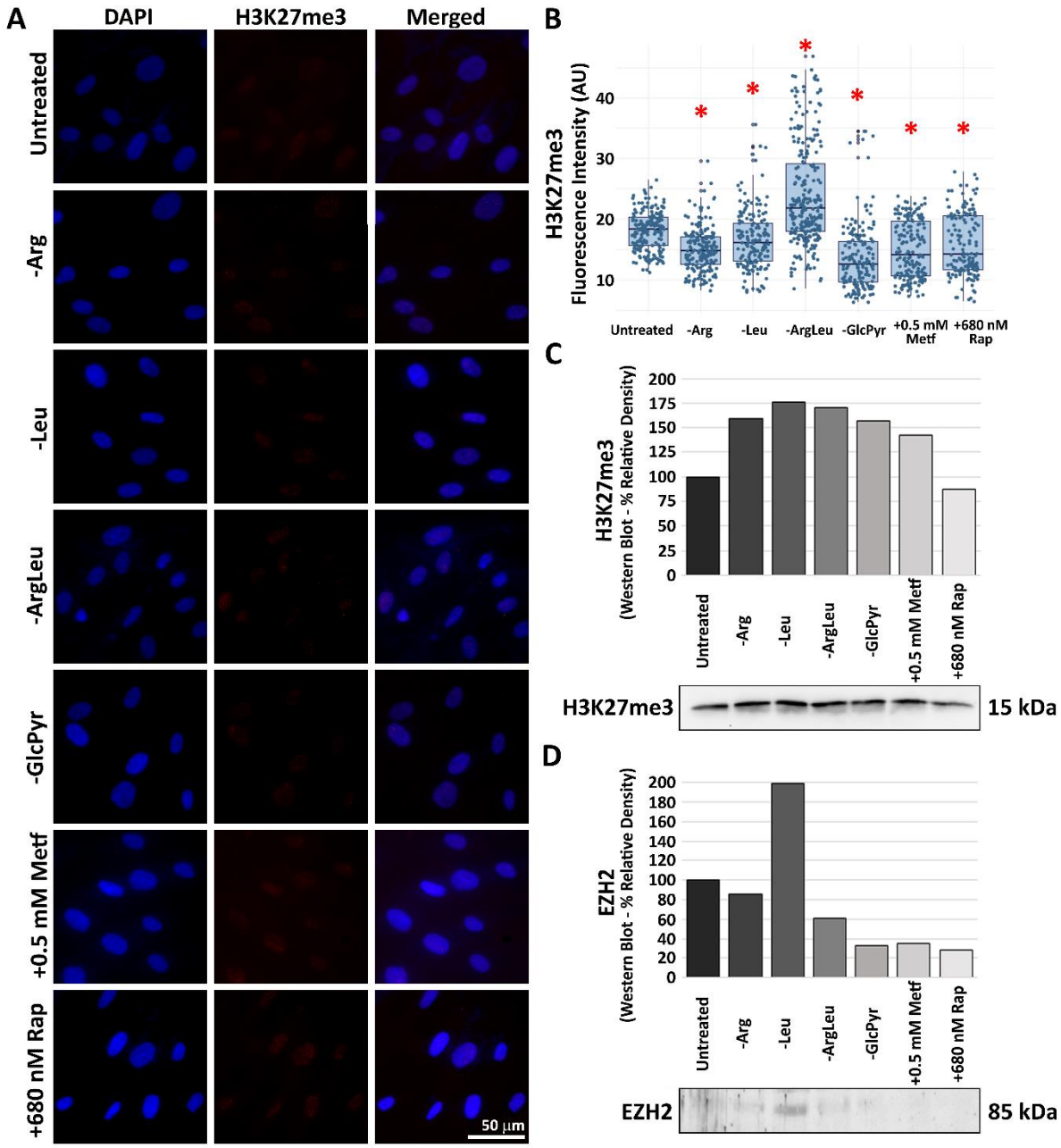

Figure 4.20: Alterations in Inactive Chromatin in Response to NR and NRM in FSF (Non-Diseased; Neonate). (A) Representative images of nuclei stained for DAPI (blue; left) and immunolabelled for H3K27me3 (red; middle) for each treatment condition. Merged image (right). Treatment conditions listed along the left-hand side: 72 h of standard growth conditions (Untreated), arginine restricted (-Arg), leucine restricted (-Leu), -ArgLeu, glucose and pyruvate restricted (-GlcPyr), treated with 0.5 mM metformin (+0.5 mM Metf) and treated with 680 nM rapamycin (+680 nm Rap). Scale bar = 50 µm. **(B)** Box and whisker distribution of fluorescence intensity for progerin in response to each of the above treatment conditions

(X-axis). One dot represents fluorescence intensity (arbitrary units, AU; Y-axis) of H3K27me3 in one nucleus. A minimum of 30 nuclei were measured per condition per replicate (n=3). * $p < 0.0083$ by students T-test corrected for multiple testing**. (C)** Bar graph for relative densitometry (%, Y-axis) of H3K27me3 levels by western blot following 72 h of treatment (X-axis: FSF Untreated, -Arg, -ArgLeu, -GlcPyr, +0.5 mM Metf, +680 nM Rap). Western blot for H3K27me3 (~17 kDa) below the bar graph. All densities were compared to untreated FSF. **(D)** Bar graph of western blot densitometry relative to FSF untreated (%, Y-axis) for EZH2 (~85kDa) in response 72 h of each treatment condition in (C; X-axis) with western blot displayed below. All western blots were biologically replicated a minimum of three times, with representative western blots presented. All proteins were equally loaded as determined by Coomassie blue, presented alongside previously shown FSF lamin AC western blots.

4.4.4 Chromosome Territory Localization

Chromosome territory positions in HGPS fibroblasts are mis-localized (Meaburn *et al.,* 2007; Mehta *et al.,* 2011), with mis-localization representative of altered genome organization and gene regulation. Fluorescence in-situ hybridization (FISH) was used to probe for chromosomes 10, 18 and X in non-diseased (FSF) and HGPS (AG03513, HGADFN003) fibroblasts. Subsequent analyses using the cell nucleus analyzer (a software that breaks nuclei into five concentric rings of equal area and calculates signal ratio of probe:chromatin (Gillespie *et al.,* 2019)) were conducted to determine chromosome localization. Chromosome X is used as a control and maintains localization at the nuclear periphery in all cell-lines and conditions tested. Analyses were conducted on untreated non-disease and HGPS fibroblasts to recapitulate previous findings, confirming altered localization of chromosomes 10 and 18 in HGPS (AG03513, HGADFN003) (Meaburn et al. 2007, Mehta et al. 2011) (Figures 21 and 22).

Previously, compounds that mimic NR have been documented to alter positions of chromosomes 10 and 18 in fibroblasts (Bikkul *et al.,* 2018; Gillespie *et al.,* 2015; Gillespie *et al.,* 2019); however, it is unknown if amino-acid restriction could also achieve this re-location. In non-diseased fibroblasts (FSF) restricted of arginine or leucine, or both, for 72 h, no significant repositioning of chromosome 18 occurred, with subtle changes in localization of chromosome 10 to the nuclear interior in response to leucine deprivation. Additionally, 72 h of 0.5 mM metformin treatment induced repositioning of chromosome 10 to the nuclear periphery (as previously reported in (Gillespie *et al.,* 2019)) and no significant changes in chromosome 18 localization (although ratios indicate a shift to the nuclear interior). These changes were likely more subtle due to the shorter treatment time compared to literature. However, these findings indicate no significant impact on genome organization in response to amino acid restriction in non-diseased fibroblasts.

Having established that HGPS fibroblasts exhibit mis-localization of chromosomes 10 and 18, and that NR via amino acid restriction has no significant impacts on localization in non-diseased cells, HGPS fibroblasts (AG03513, HGADFN003) were treated with the same conditions (72 h -Arg, -Leu, -ArgLeu, or 0.5 mM Met) to determine if NR/NR mimetics have the potential to alter or restore chromosome territory positions to those of non-diseased passage-matched fibroblasts. Chromosome 10 showed significant relocation to the nuclear

periphery in AG03513 cells (Figure 20). This relocation was not corrected in response to leucine deprivation or metformin treatment, both of which demonstrated the same significant difference as the untreated AG03153 cells when compared to control. Arginine restriction of AG03513 demonstrated no significant difference to non-diseased control fibroblasts, suggesting restoration of chromosome localization, whilst treatment with arginine and leucine deprivation resulted in chromosome 10 having more intermediate localization, with no obvious preference for the interior or periphery of the nucleus. Localization of chromosome 18 in AG03513 was more obviously different to that of non-diseased control fibroblasts, preferring an interior localization. Following 72 h treatment with arginine deprivation or 0.5 mM metformin, no significant differences were detected between treated fibroblasts and control, with 0.5 mM metformin treated fibroblasts appearing highly parallel to non-diseased localization. Both leucine deprivation and combined arginine/leucine deprivation also decreased differences between treated progeria and non-diseased control cells, and although localization was not restored to that of non-diseased fibroblasts, it was more intermediate (Figure 21). In HGADFN003 fibroblasts, both 72 h arginine and leucine promoted positioning of chromosome 10 to the nuclear interior (more than that of the FSF), whilst combined -ArgLeu showed no significant differences between non-diseased and HGADFN003 fibroblasts. For all NR assessed in HGADFN003, chromosome 18 was significantly positioned to the exterior (Figure 22). These findings indicate that 72 h of NR can restore chromosome territory localization to that of non-diseased human fibroblasts, suggesting alterations in genome function and regulation.

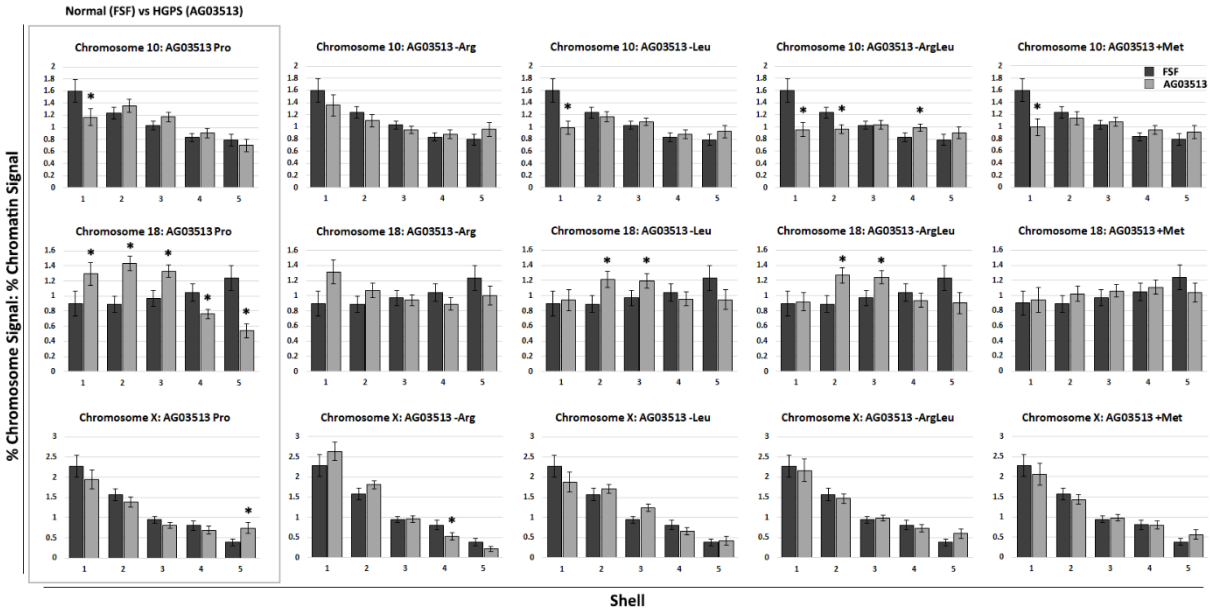

Figure 4.21: Chromosome Territories Re-localize in Response to NR/NRM in HGPS AG03513 (13y) Fibroblasts. Chromosomes 10 (top), 18 (middle) and X (bottom) were identified in 72h proliferative (Pro), arginine (-Arg), leucine (-Leu), and combined arginine and leucine deprived (-ArgLeu) and 0.5 mM metformin (+Met) treated AG03513 (HGPS) fibroblasts. Cell nucleus analyser (CNA) broke nuclei into five concentric shells of area, 1 being the most exterior and 5 the most interior (X-axis). Y-axis is the ratio of % chromosome signal/% DAPI signal in each shell. Error bars = S.E.M. * = $p \leq 0.05$ by students T-test, comparing AG03513 (Light grey) to FSF Control (Dark grey).

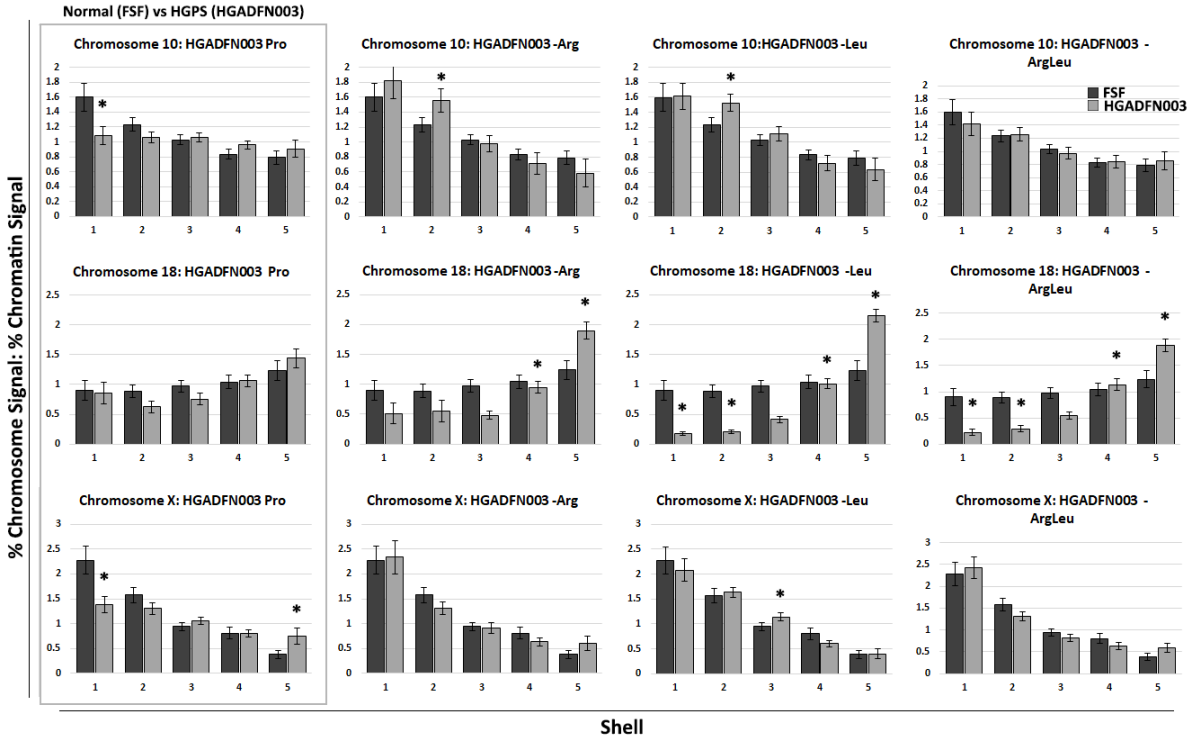

Figure 4.22: HGADFN003 Chromosome Territories Re-localize in Response to NR/NRM in HGPS HGADFN003 Fibroblasts. Chromosomes 10 (top), 18 (middle) and X (bottom) were identified in 72h proliferative (Pro), arginine (-Arg), leucine (-Leu), and combined arginine and leucine deprived (-ArgLeu) and 0.5 mM metformin (+Met) treated AG03513 (HGPS) fibroblasts. Cell nucleus analyser (CNA) broke nuclei into five concentric shells of area, 1 being the most exterior and 5 the most interior (X-axis). Y-axis is the ratio of % chromosome signal/% DAPI signal in each shell. Error bars = S.E.M. * = $p \leq 0.05$ by students T-test, comparing AG03513 (Light grey) to FSF Control (Dark grey).

4.5 Discussion

These data demonstrate for the first time in HGPS patient fibroblasts (ranging in age from 2 to 13 years) that restriction of specific amino acids from the diet induce progerin degradation. Treatment with the NRMs metformin and rapamycin were similarly able to result in decreased progerin levels. Furthermore, these data demonstrate that combined arginine and leucine restriction reduce progerin levels to a greater extent than rapamycin, the current gold standard entering clinical trials. This is particularly important when considering NR and metformin have fewer life-altering side effects than rapamycin and could provide a better quality of life, as well as an extended lifespan, for HGPS patients. In addition to reduction of progerin, NR of arginine and/or leucine and NRM also altered or ameliorated HGPS cellular phenotypes, including improved nuclear morphology, altered DNA damage repair responses, and changes in genome structure, without any negative effects in non-diseased counterparts (i.e., decreased cell survival or increased numbers of irregular nuclei).

Though the ability of NR and NRM to decrease progerin levels in HGPS fibroblasts is obvious from these data, exactly how progerin is depleted is not. Previous work identified rapamycin as inducing progerin degradation via mTOR inhibition and autophagy induction, with knock-down of autophagy via ATG7 (a protein essential for autophagosome formation in autophagy) preventing progerin degradation (Cao *et al.*, 2011b). As NR and NRM strategies have also been demonstrated to inhibit mTOR activity (reviewed in (Almendariz-Palacios *et al.*, 2020)), it was expected that these conditions would function in a similar manner. Surprisingly, though generally decreases in progerin were associated with increases of the autophagy marker LC3B, no clear association could be made with (p)-mTOR levels. To dissect this response, ATG5 (key in formation of autophagic membranes and essential for autophagy (Arakawa *et al.*, 2017) was knocked down in non-diseased and HGPS fibroblasts which subsequently underwent 72 h of arginine and/or leucine restriction, treatment with 0.5 mM metformin or 680 nM rapamycin. LC3B levels were reduced across conditions in non-diseased and HGPS fibroblasts; however, lower levels of progerin were still maintained. This disconnect between the mechanism of progerin degradation via rapamycin here and previously published findings are likely the result of model used; the work by Cao and colleagues utilized a HeLa cell model expressing progerin. It is possible that given the short time these cells expressed progerin (compared to years in HGPS patients), and their cancerous

background, cells functioned to remove proteins differently in response to rapamycin (Cao *et al.,* 2011b). Furthermore, the proteasome has been reported as disrupted in HGPS fibroblasts, and levels of autophagy and autophagic regulation appear to change with age, passage number, and model (Cenni *et al.,* 2011; Gabriel *et al.,* 2016; Gabriel *et al.,* 2015; Pan *et al.,* 2020). These factors could contribute to divergent responses to NR and NRM reported. Alterations in LC3 levels could also be attributed to fibroblast aging *in vitro* (Demirovic *et al.,* 2015); however, age-matching of fibroblasts in this assay, alongside parallel growth conditions and passage numbers for diseased and non-diseased fibroblasts, make this an unlikely cause of LC3 levels presented here. Additional mechanisms of progerin depletion could also play a role, such as ubiquitination (Borroni *et al.,* 2018) and splicing regulation (Harhouri *et al.,* 2017). Finally, since depletion of progerin in response to NR/NRM in the absence of ATG5 is persistent, and that ATG5/7 independent methods of proteasomal degradation have been identified (Arakawa *et al.,* 2017; Goebel *et al.,* 2020; Nishida *et al.,* 2009), (p)-mTOR/LC3 independent mechanisms of progerin-degradation should be considered. Additional elucidation of autophagic/proteasomal pathways in HGPS and subsequent assays in HGPS fibroblasts would be required to identify exactly how these conditions are inducing progerin degradation.

To further examine cellular response to NR/NRM, amino acid sensors CASTOR1 (arginine) and SESN2 (leucine) were also knocked down. As with ATG5, if signalling were occurring solely through these proteins, mTOR signalling, autophagy, and progerin levels would no longer be responsive to treatment conditions. Arginine sensing is required for depletion in response to both -Arg and -Leu, whilst -ArgLeu still promoted decreased progerin levels, whilst in the absence of leucine sensor SESN2, arginine restriction no longer induces progerin depletion. Therefore, there is an interplay between these two amino acid sensors required for progerin depletion. Interestingly, metformin requires both CASTOR1 and SESN2 to induce progerin degradation, whilst rapamycin requires CASTOR1. This is unexpected as treatment with metformin likely functions via activation of AMPK (Almendariz-Palacios *et al.,* 2020; Rena *et al.,* 2017), whilst rapamycin acts directly on the mTORC1 complex (Choi *et al.,* 1996). This structure-function link to the importance of CASTOR1 and SESN2 in response to these compounds will require further investigation.

In addition to progerin degradation, NR and NRM slowed cellular growth and improved nuclear morphology of HGPS fibroblasts. Non-diseased counterparts similarly exhibited slowing of growth profiles and either no change or improved number of regular nuclei. Neither patient nor control cell-lines exhibited decreased cell survival in response to NR and NRM. Another classical feature of HGPS patient cells is disrupted DNA damage response (Musich *et al.,* 2009; Musich *et al.,* 2011). Our data were concordant with previous reports of increased γ-H2AX in HGPS, with the NRMs metformin (Park *et al.,* 2017) and rapamycin (Bikkul *et al.,* 2018) decreasing γ-H2AX levels. Furthermore, metformin concentration used to achieve this here is lower than previously reported (Park *et al.,* 2017). Significantly, these data examine the ability of cells to repair DNA following DNA damage induction, and not just endogenous levels following treatment, as has previously been done. Finally, for the first time, NR conditions of arginine and/or leucine were shown to decrease γ-H2AX levels following DSB induction when compared to untreated counterparts, indicating increased DNA damage repair.

HGPS patients exhibit substantial alterations in genome architecture and function. H3K27me3 is often decreased in HGPS patient fibroblasts and models, and general gene expression altered. It is generally accepted that an increase in H3K27me3 in HGPS is desirable given its loss is an initial step in progression of HGPS at a molecular level. However, HGPS patient fibroblasts treated for 72 h with NR/NRM exhibit no consistent increase in H3K27me3 for any one condition, surprising given other improvements in cellular health in response to these treatments. Data in other models are varied, such as cancer cell-lines cells (restriction of (Fontana *et al.,* 2013; Tang *et al.,* 2018; Tang *et al.,* 2015), elderly human dermal fibroblasts (Cuyas *et al.,* 2018), HGPS model cell-lines (Chojnowski *et al.,* 2020), and flies (Ma *et al.,* 2018), with increases/decreases in H3K27me3 both reported and associated with better/worse outcomes in response to NR/NRM or aging. Recently, H3K27me3 has been identified as essential in three-dimensional gene regulation (Cai *et al.,* 2021). EZH2, responsible for H3K27 tri-methylation, was demonstrated to be up-regulated in HGPS and down-regulated in response to NR/NRM, but still expressed at far greater levels than untreated counterparts. From these reports and data here, it is likely that H3K27me3, in conjunction with EZH2, is involved in dynamic regulation of the genome, with specific regions of H3K27me3 enrichment/depletion more important that global gain/loss. H3K27me3 will

require further examination in HGPS fibroblasts to determine how NR/NRM function to promote progerin depletion and healthy cellular phenotypes in HGPS.

In contribution to the alterations in genome function exhibited by HGPS patient fibroblasts is the mis-localization of chromosome territories. First, this mis-localization was recaptured here in a comparison between untreated HGPS fibroblasts and non-diseased fibroblasts. Surprisingly, the HGPS cell-line HGADFN003 (which has not previously been examined for chromosome localization) exhibited re-positioning to a much lesser extent than AG03513. These discrepancies could be due to age of the patient when samples were taken (2y0m and 13y respectively). The phenotypes of HGPS are attributed to accumulation of progerin, patients fail to meet growth milestones and are typically diagnosed at ~2 years old, therefore it is possible that chromosomal mis-localizations at this stage of the disease are not as prominent as older patients with HGPS. Additional analyses will be required to confirm this in age and passaged matched HGPS cell-lines. Furthermore, it was established that changes in chromosome territory positioning were occurring in HGPS fibroblasts in response to NR/NRM, and that in multiple instances differences could no longer be identified between non-diseased and HGPS fibroblasts. Chromosome territory localization has been associated with maintaining appropriate gene-gene interactions and genome regulation. Therefore, this data indicates the possibility that NR/NRM can alter, and restore, genome organization and function in HGPS fibroblasts.

5.0 Molecular Pathways Associated with Hutchinson-Gilford Progeria Syndrome and the Cellular Lifespan-Extending Effects of NR and NRM

5.1 NR and NRM Increase Cellular Lifespan of Non-Diseased and Hutchinson-Gilford Progeria Syndrome Fibroblasts in Cell Culture

Children suffering from HGPS have significantly shortened lifespans of ~14 years (Baker *et al.,* 1981; Csoka *et al.,* 2004b; De Sandre-Giovannoli *et al.,* 2003; Eriksson *et al.,* 2003b). This shortened lifespan is recapitulated in tissues affected by HGPS, with cells entering senescence prematurely (Cao *et al.,* 2011a). To determine if restriction of amino acids, or treatment with metformin, can maintain lower levels of progerin over longer periods of time, cells from both non-diseased (2DD, FSF) and HGPS (HGADFN271, HGADFN003, HGADFN169, AG03153) patients were maintained under control conditions or treated with intermittent (Int; 7 days treated, 7 days control) arginine/leucine (-ArgLeu) deprivation, intermittent 0.5 mM metformin (+0.5 mM Metf), continuous (Cont.) +0.5 mM Metformin (0.5 mM Met Cont.) or continuous +680 nM Rapamycin (+680 nM Rap; included as a positive control). At 5 weeks, protein extracts were collected, and western blots conducted for progerin (Figure 5.1), H3K27me3 (Figure 5.2), and EZH2 (Figure 5.3). These treatments were selected due to their ability to decrease progerin levels and improve nuclear morphology across HGPS patient cell-lines at 72 h. Following 5 weeks, -ArgLeu maintained lower levels of progerin except for in HGADFN003. Metformin treatment, regardless of intermittent/continuous treatment, maintained lower progerin levels across all cell lines tested. Finally, rapamycin maintained lower progerin levels in HGADFN003 and HGADFN167 at 5 weeks. Notably, at 72 h, HGADFN167 progerin levels were unresponsive to NR or NRM; however, following 5 weeks of these protocols, progerin levels were decreased. Combined treatment of NR and NRM (-ArgLeu +0.5 mM Metf(Cont.)) also reduced progerin levels across all lines tested. Therefore, longer-term strategies for reducing progerin levels via NR and NRM are successful in HGPS patient fibroblasts.

Global levels of H3K27me3 were examined at 72 h and exhibited mixed responses in response to each NR/NRM condition tested. As a dynamic process, it was possible that this was examined during a phase of chromatin remodelling, therefore these levels were also examined at 5 weeks under the previously defined long-term conditions. At this time point,

H3K27me3 protein levels by western blot were lower than untreated HGPS controls in two patient samples, while in the third cell line tested, no obvious increase or decrease was observed. In FSF non-diseased counterparts, metformin, and rapamycin increased levels of H3K27me3, whilst in 2DD non-diseased fibroblasts, rapamycin was the only condition in which an increase was not observed (Figure 5.2). EZH2 protein levels were also examined. In HGADFN003, -ArgLeu and -ArgLeu combined with metformin exhibited greater EZH2 levels than other conditions. In AG03513, metformin (cont.) and rapamycin resulted in EZH2 increases. In non-diseased 2DD, both intermittent and continuous metformin treatments increased EZH2 (Figure 5.3). FSF levels of EZH2 were not detectable across any condition (data not shown). Therefore, levels of chromatin inactivation appear more consistent across treatment groups at 5 weeks; however, EZH2 levels are still in flux.

Progerin levels were maintained at lower levels for a minimum of 5 weeks, therefore it was examined if this could be associated with an increase in cellular lifespan under the same conditions. HGPS fibroblasts survived fewer days in culture than non-diseased counterparts, an average of 96.5 days compared to 140.8 days (Figure 5.4). In three of the four HGPS patient fibroblast samples examined, -ArgLeu significantly increased days in culture (HGADFN003 from 96.5 days to 135.5 days, HGADFN169 from 127 days to 149 days, AG03513 from 84 days to 144 days). No significant change was observed in HGADFN271 in response to -ArgLeu (Control: 60 days, -ArgLeu: 58 days). +0.5 Metf(Int.) significantly increased days in culture in HGADFN169 only (127 days to 149 days). Other HGPS cell lines exhibited no significant changes in response to +0.5 mM Metf(Int.) (HGADFN271: 58 days, HGADFN003: 100 days, AG03513 86 days). Of the three HGPS cell-lines examined for response to +0.5 mM Metf(Cont.) all exhibited significant increases in days in culture (HGADFN271: 151 days, HGADFN003: 111 days, HGADFN169: 125 days). Similarly, in the same cell lines, +680 nM Rap(Cont.) also significantly increased days in culture (HGADFN271: 151 days, HGADFN003: 224 days, HGADFN169: 194 days), as previously reported (Cao *et al.*, 2011b) (Figure 5.4). On average, -ArgLeu and +0.5 mM Met(Cont.) increased the number of days HGPS fibroblasts survived in culture from 96 days to 122 days and 129 days, respectively.

In 2DD, +0.5 mM Metf(Int.) and +680 nM Rap(Cont.) significantly ($p < 0.05$) extended time in culture from 128 days to 158 and 207 days respectively, whilst +0.5 mM

Metf(Cont.) decreased cellular time in culture (100 days; Figure 5.4). -ArgLeu had no impact on days in culture of 2DD. In the second non-diseased fibroblast cell line, FSF, -ArgLeu significantly ($p < 0.05$) extended cellular lifespan from 147.25 days to 187.5 days, whilst +0.5 mM Metf(Int.) and + 0.5 mM Metf(Cont.) had no significant impact on cell survival in culture (143.25 days and 149 days respectively). On average, -ArgLeu and +680 nM Rap significantly increased days in culture of non-diseased fibroblasts, whilst both +0.5 mM Metf(Int.) and (Cont.) had no significant impact on days in culture (Figure 5.4). These conditions were therefore selected for RNA sequencing to establish if genome function was also restored.

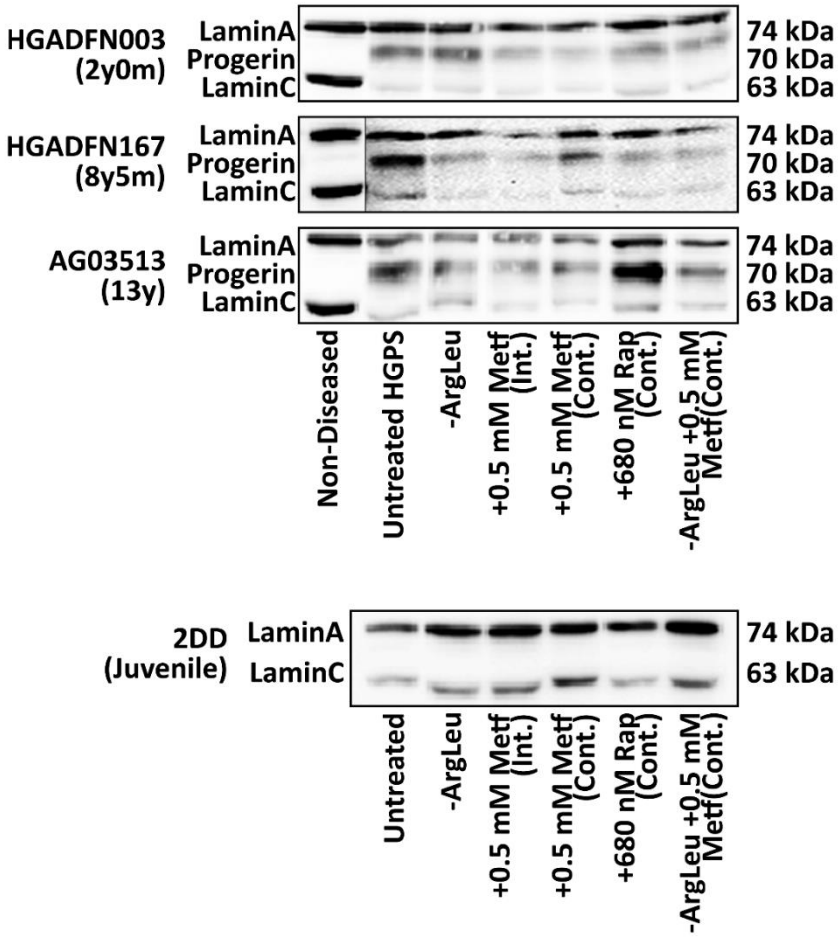

Figure 5.1: Decreases in Progerin Levels Persist at 5 Weeks in HGPS Fibroblasts in Response to Combinations of Arginine and Leucine Restriction, Metformin, and Rapamycin. Western blots conducted on whole cell lysates of HGPS (HGADFN003, HGADFN167, AG03513) and 2DD fibroblasts following 5 weeks of growth under standard conditions (Untreated), arginine and leucine restriction (-ArgLeu), intermittent (Int.) or continuous (Cont.) treatment with metformin +0.5 mM Metf, continuous rapamycin treatment (+680 nM Rap(Cont.)) or combined -ArgLeu (Int) + 0.5 mM Metf(Cont). Extracts were immunoblotted for lamin A/C (74 kDa and 63 kDa respectively), which also binds progerin (70 kDa). Bands are identified to the left of the western blot. Non-diseased FSF were run along with every HGPS cell-line. HGADFN167 non-diseased is from a lower exposure time to avoid saturation. Each western blot was conducted in biological triplicate and representative images are presented. Coomassie blue load controls for these samples are shown with H3K27me3 western blots (Figure 5.2).

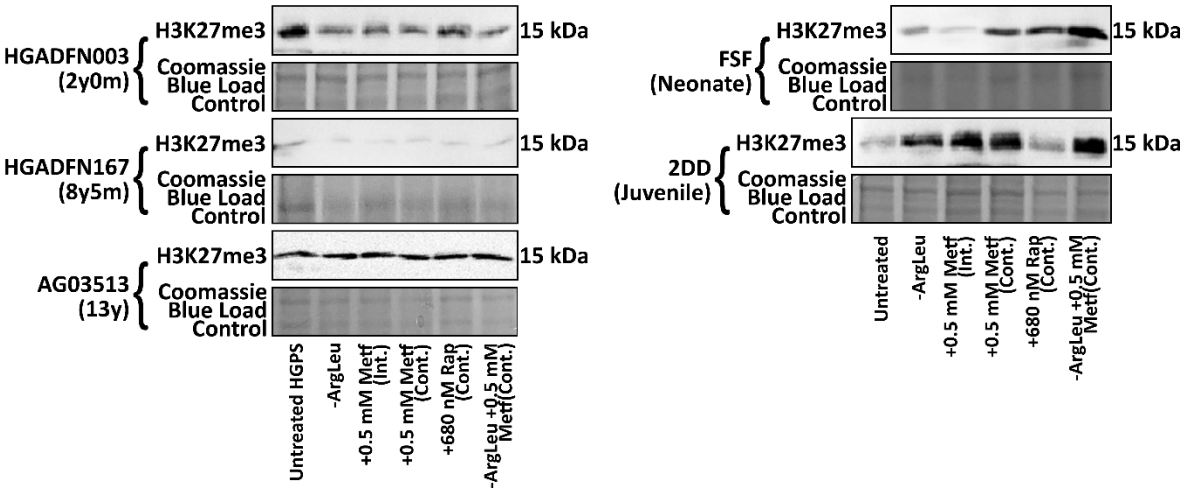

Figure 5.2: H3K27me3 Levels Remain Altered at 5 weeks in HGPS and Non-Diseased Fibroblasts in Response to Combinations of Arginine and Leucine Restriction, Metformin, and Rapamycin. Western blots conducted on whole cell lysates of HGPS (HGADFN003, HGADFN167, AG03513) and non-diseased (FSF and 2DD) fibroblasts following 5 weeks of growth under standard conditions (Untreated), arginine and leucine restriction (-ArgLeu), intermittent (Int.) or continuous (Cont.) treatment with metformin (+0.5 mM Metf), continuous rapamycin treatment (+680 nM Rap(Cont.) or combined -ArgLeu (Int) + 0.5 mM Metf(Cont). Extracts were immunoblotted for H3K27me3 (15 kDa). Bands are identified to the left of the western blot. Non-diseased FSF were run along with every HGPS cell-line. Each western blot was completed in biological triplicate and representative images presented.

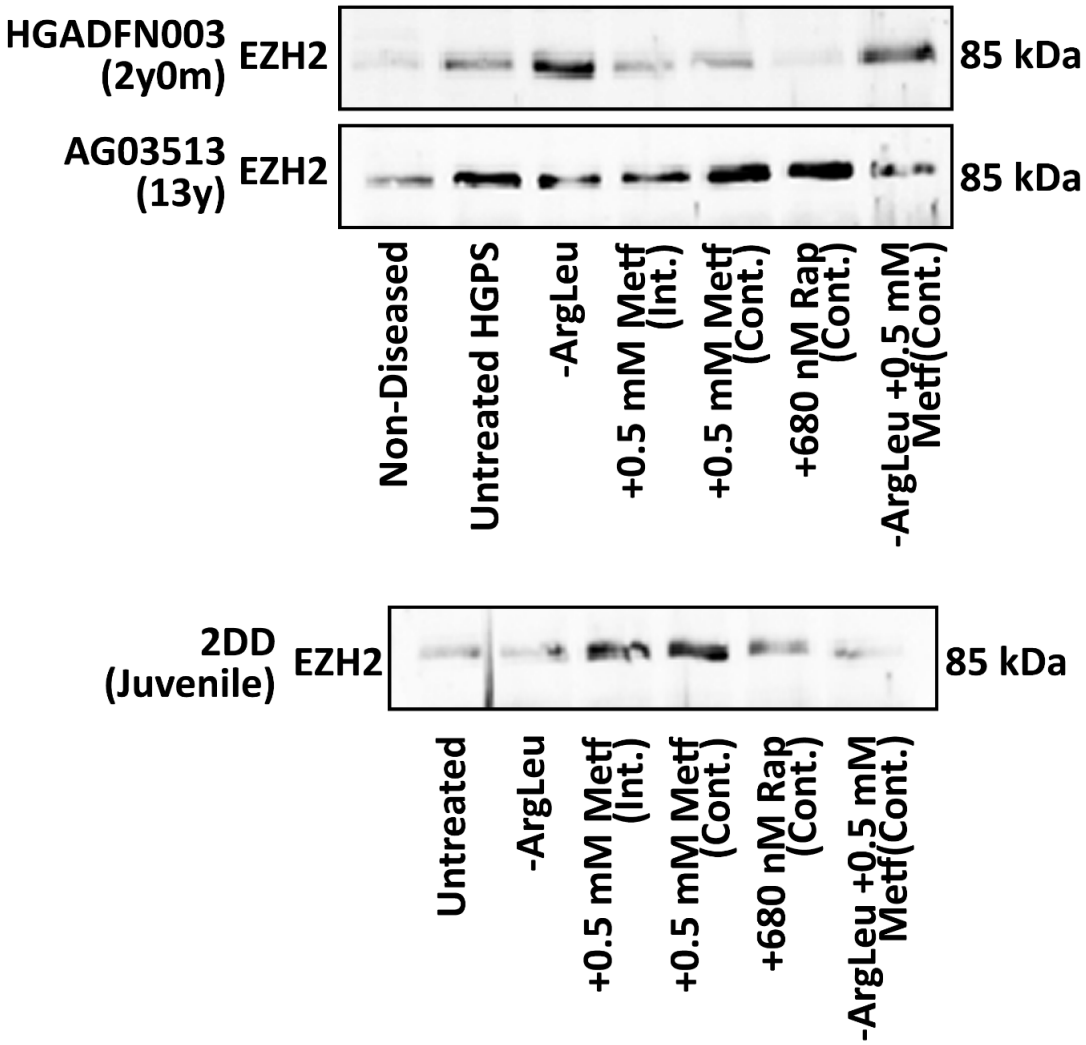

Figure 5.3: EZH2 Levels Remain Altered at 5 Weeks in HGPS and Non-Diseased Fibroblasts in Response to Combinations of Arginine and Leucine Restriction, Metformin, and Rapamycin. Western blots conducted on whole cell lysates of HGPS (HGADFN003, AG03513) and non-diseased (2DD) fibroblasts following 5 weeks of growth under standard conditions (Untreated), arginine and leucine restriction (-ArgLeu), intermittent (Int.) or continuous (Cont.) treatment with metformin (+0.5 mM Metf), continuous rapamycin treatment (+680 nM Rap(Cont.) or combined -ArgLeu (Int) + 0.5 mM Metf(Cont). Extracts were immunoblotted for EZH2 (85 kDa). Bands are identified to the left of the western blot. Non-diseased FSF were run along with every HGPS cell-line. Each western blot was run in biological triplicate and representative images shown. Correlating Coomassie blue load controls for these samples are show in Figure 5.2.

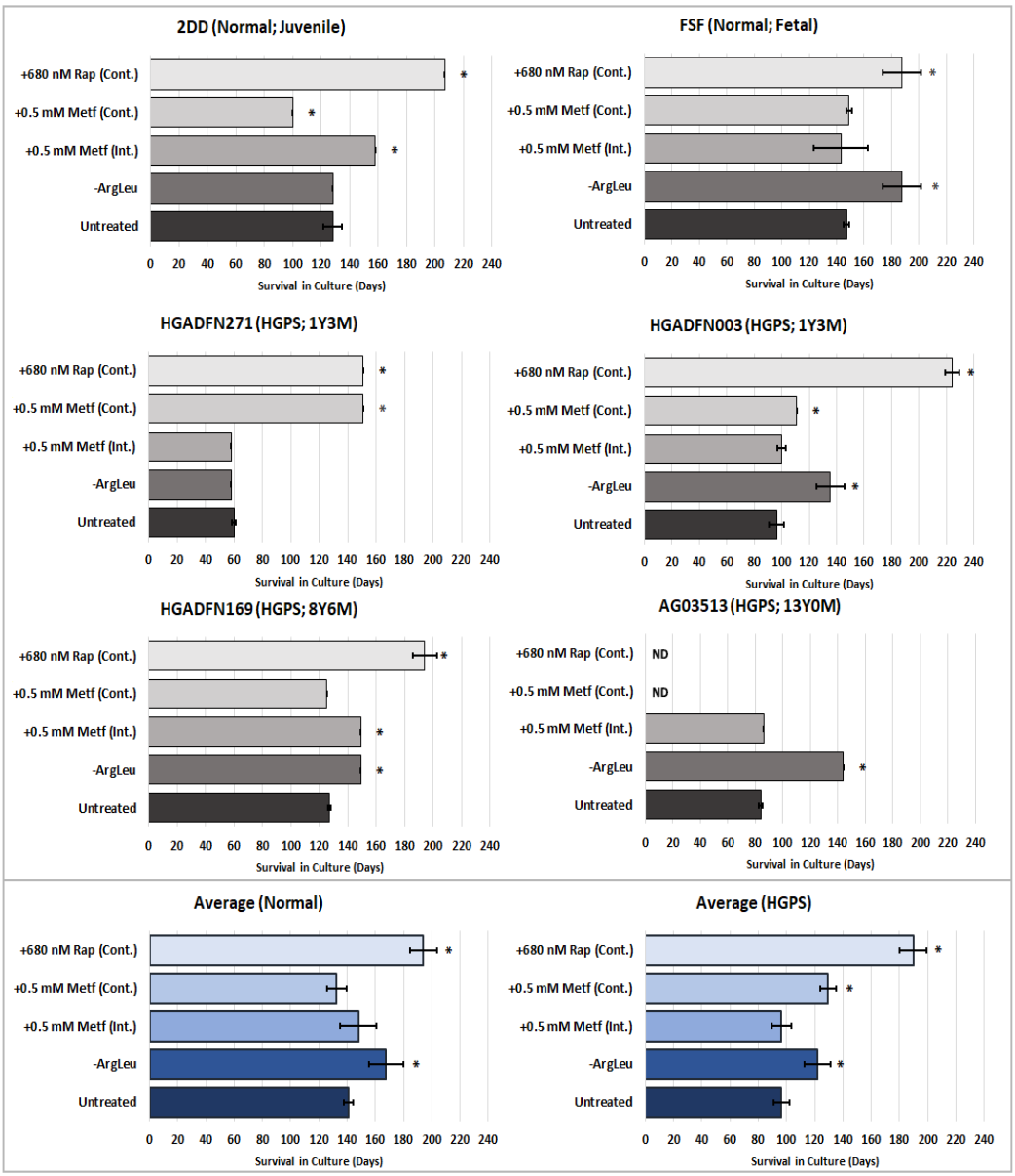

Figure 5.4: NR and NRM Extend HGPS Cell Lifespan in Culture. Bar graphs representing days in culture for non-diseased (2DD, FSF) and HGPS (HGADFN271, HGADFN003, HGADFN169, AG03513) fibroblasts. Each patient cell-line was grown under control conditions or treated with intermittent (Int; 7 days treated, 7 days control) arginine/leucine (-ArgLeu) deprivation, intermittent 0.5 mM metformin (+0.5 mM Metf), continuous (Cont.) +0.5 mM Metformin (0.5 mM Met Cont.) or continuous +680 nM Rapamycin (+680 nM Rap). Cells were grown and passaged until minimum plating values (3000 cells/cm^2) could be achieved, and days in culture recorded (X axis). Blue bar graphs represent averages of time in culture for non-diseased and HGPS cells. ND = not determined. Error bars = standard error of the mean. * $p < 0.0083$ by students T-test corrected for multiple testing.

5.2 Hutchinson-Gilford Progeria Syndrome Fibroblasts Exhibit Enrichment of Cytokine-Cytokine Receptor Signalling and Transforming Growth Factor-β Signalling Pathways

To confirm that the transcriptome of HGPS fibroblasts is divergent to that of non-diseased control fibroblasts, RNAseq data was processed and analysed following five weeks of growth in culture. Replicates of each cell line correlated well, with R scores (correlation value) of 0.997 (FSF non-diseased) and 0.945 (HGPS) respectively; however, when comparing non-diseased and HGPS fibroblasts, correlation was much lower, averaging an R score of 0.796 (Figure 5.5A). Data were analyzed with DESeq2, identifying 4450/35805 probes as significantly changing ($p < 0.05$) between non-diseased and HGPS fibroblasts, confirming alterations in the transcriptome between these samples (Figure 5.5B). Genes changing expression ≥5-fold in HGPS fibroblasts were identified (901 up-regulated, 1257 down-regulated), with subsequent analyses analysing gene lists for changes in biological function (Figure 5.5C). Cytokine-cytokine receptor interaction pathway was enriched in genes up-regulated in HGPS, as were the transforming growth factor (TGF)-beta signalling pathway and pathways involved in development (activation of anterior HOX genes in hindbrain development during early embryogenesis). No pathway enrichment was identified in genes ≥5-fold down-regulated in HGPS compared to control. The large number of genes changing expression, but the lack of enrichment could be a result of the lack of genome function regulation in HGPS fibroblasts. GO terms were reflective of these alterations in pathway enrichment, identifying terms associated with changes in transcription, inflammatory responses, and development (GO Biological Process, GO Molecular Function) (Figure 5.6). Terms associated with ≥5-fold down-regulated genes included GO Biological Process for regulation of development of the cardiovascular and respiratory system (Figure 5.6). Analysis of gene lists using DisGeNET identified the genes changing as associated with HGPS, as well as cardiovascular, diabetic, and arthritic conditions.

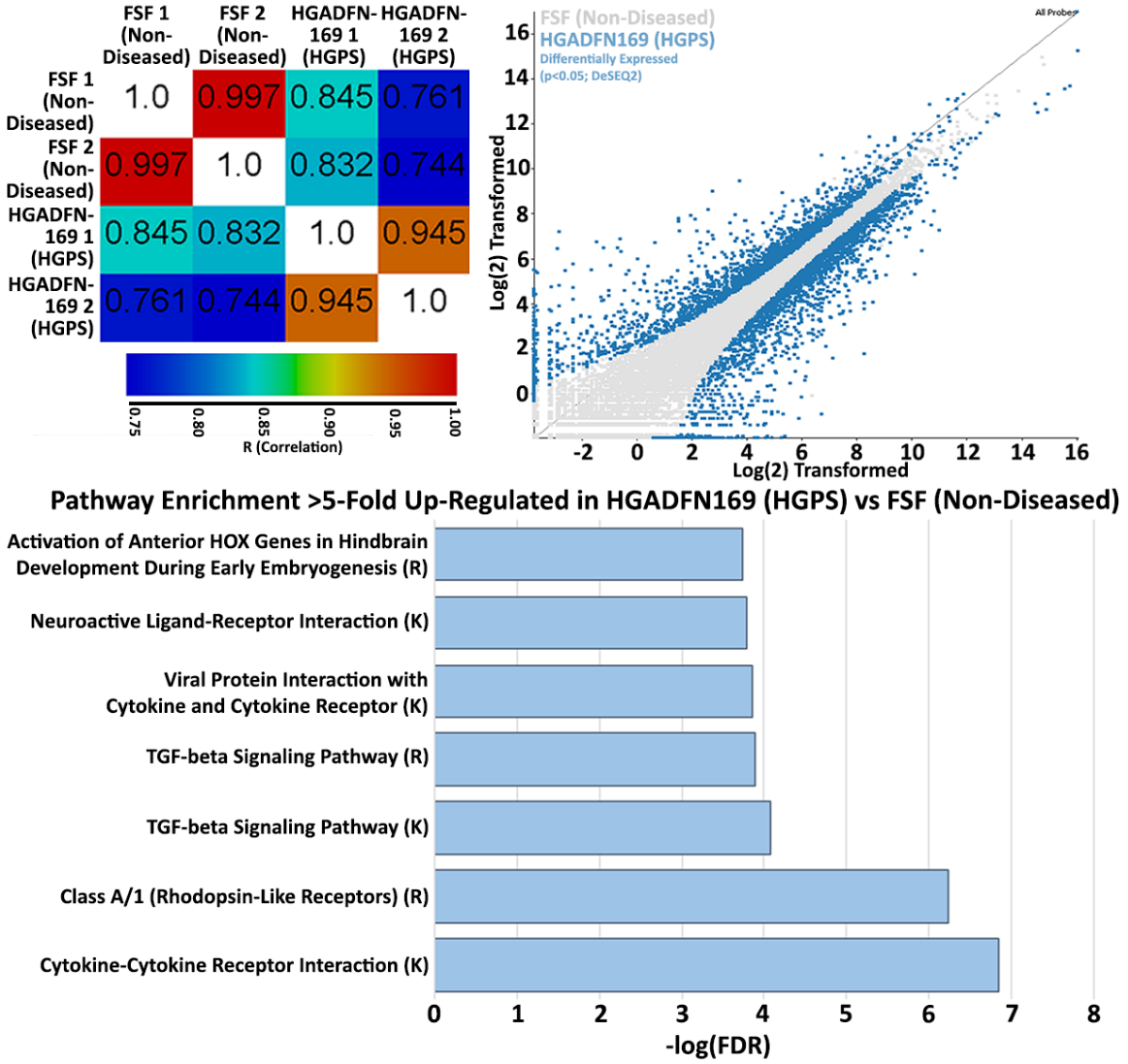

Figure 5.5: HGPS Fibroblasts Exhibit Differential Transcript Profiles to Non-Diseased Fibroblasts. (A) Correlation matrix of FSF (Non-Diseased) and HGADFN169 (HGPS) RNA sequencing replicates (1, 2) based on raw reads. R values are given, with higher correlation indicated with warmer colours, and lower correlation by cooler colours (colour-correlation key under the matrix). R values of 1.0 are highlighted in white. **(B)** DESeq2 used to identify genes that significantly statistically different ($p < 0.05$) between FSF (Non-Diseased; grey) and HGADFN169 (HGPS; blue). Raw reads were log(2) transformed using SeqMonk and plotted on a scatter graph. **(C)** Bar graph demonstrating pathway enrichment of genes up-regulated ≥5-fold in HGADFN169 (HGPS) compared to FSF (Non-Diseased). X axis is the -log(False Discovery Rate (FDR)) and Y-axis lists enriched pathways. The larger the -log(FDR) the greater the confidence in pathway enrichment. All pathways p-value <0.05, FDR<0.05.

Figure 5.6: Gene Ontology (GO) Terms Associated with Genes ≥5-fold Altered in HGPS Fibroblasts. Dot plots representing alterations in GO terms between HGPS and Non-Diseased fibroblasts. Size of dot represents number of genes from the GO Term network in relation to the networks size (Ratio of Genes from Network) and colour represents -log(FDR) (scales top right). GO terms are listed to the left of the dot plot. All p-value and FDR <0.05 for displayed terms.

5.3 Restriction of Arginine and Leucine, or Treatment with Metformin, Does Not Restore Non-Diseased Genome Profiles in Hutchinson-Gilford Progeria Syndrome (HGPS) Fibroblasts but Does Repress Disease-Associated Molecular Pathways of HGPS

It has previously been reported that the HGPS transcriptome is divergent to that of non-diseased, age matched fibroblasts (Kreienkamp *et al.*, 2018; Kubben *et al.*, 2016; McCord *et al.*, 2013; Prokocimer *et al.*, 2013); however, there is limited evidence of whether treatments that reduce progerin levels also restore the transcriptome of HGPS cells to that of fibroblasts isolated from healthy donors (non-diseased). Furthermore, the impacts of long-term amino acid restriction or treatment with metformin in the transcriptomes of HGPS and non-diseased fibroblasts are unknown. Principal component analysis (PCA) of HGADFN169 (HGPS) fibroblasts grown for 5 weeks under control (Untreated), -ArgLeu or +0.5 mM Metf(Cont.) and FSF (non-diseased) fibroblasts grown for 5 weeks under control conditions reveal divergence between non-diseased fibroblasts and HGPS, providing evidence that the transcriptome is not restored to that of non-diseased fibroblasts (Figure 5.7A). Although the genome of treated HGPS fibroblasts does not resemble that of non-diseased fibroblasts, average correlation values of probes for -ArgLeu (R = 0.787) and +0.5 mM Metf(Cont.; 0.804) treated HGPS fibroblasts indicate that treatments do alter gene expression profiles, and that these are different to untreated HGPS (R = 0.796) (Figure 5.7B). DESeq2 analysis for identification of DEGs support this, with 7018 genes changing expression in response to -ArgLeu and 4636 in response to +0.5 mM Metf(Cont.) when compared to untreated FSF controls (Figure 5.7 C and 4D).

It is possible that DEGs are different to those altered in response to untreated disease state. Gene lists were generated from genes ≥5-fold up- or down-regulated for HGPS untreated, HGPS -ArgLeu and HGPS +0.5 mM Metf(Cont.) compared to non-diseased untreated fibroblasts. In response to -ArgLeu, 606 genes were common between up-regulated lists, and 691 common in down-regulated lists (Figure 5.7). Therefore, -ArgLeu did not prevent expression of many HGPS-associated genes; however, 692 genes were solely ≥5-fold up-regulated and 292 solely ≥5-fold down-regulated by -ArgLeu. 295 and 565 genes respectively, were unique to HGPS disease phenotype compared to non-diseased fibroblasts and were not found in treated fibroblasts (Figure 5.7). In +0.5 mM Metf(Cont.)-treated HGPS

fibroblasts, as with -ArgLeu, subsets of genes changing ≥5-fold were common between +0.5 mM Metf(Cont.) and Untreated (497 up-regulated, 936 down-regulated), some were unique to HGPS (404 up-regulated, 320 down-regulated) and some were unique to +0.5 mM Metf(Cont.) (241 up-regulated, 442 down-regulated) (Figure 5.7).

Genes changing only in response to treatment may be responsible for the positive effects observed on cellular lifespan, therefore additional pathway analyses were conducted on these genes. No pathways were significantly enriched in genes up-regulated ≥5-fold in response to -ArgLeu, but in the down-regulated gene list, pathways included those involved in chemokine signalling (CXCR3-mediated signalling events, class A/1 (rhodopsin-like receptors) and cell cycle regulation (activation of PKC through G-protein coupled receptors, PLK1 signalling events), as well as the advanced glycation end-product/receptor advanced glycation end products (AGE-RAGE) signalling pathway in diabetic complications (Figure 5.8). Thus, -ArgLeu is down-regulating pathways associated with chemokine and cytokine signalling that were identified as associated with HGPS-disease phenotype (class A/1 (rhodopsin-like receptors), viral protein interaction with cytokine and cytokine receptor) as well as pathways whose down-regulation may be pro-longevity specific. These analyses did not reveal any pathways potentially involved in the ability of metformin to improve phenotypes and lifespan of HGPS fibroblasts (Figure 5.8).

Although genes were still common between HGPS untreated and treated fibroblasts, it is possible that these are still exhibiting changes in gene expression levels that may be significant to HGPS disease progression. Analysis of these genes revealed that 388/606 (64%) genes were up-regulated compared to HGPS untreated, with the remainder (36%) down-regulated. No pathway enrichment was identified in the up-regulated shared genes; however, common down-regulated genes exhibited enrichment of signalling by Type 1 Insulin-like Growth Factor 1 Receptor, and notably, enrichment of TGF-beta signalling pathway (a pathway up-regulated in untreated HGPS). Fewer changes in expression levels were observed in down-regulated common genes, with 420/691 (61%) not changing in response to -ArgLeu; and no pathway enrichment in the 101 (15%) genes further decreasing expression. 170 (25%) genes increased expression, which were enriched in the inflammatory mediator regulation of TRP channels, thus this pathway was also down-regulated by -ArgLeu.

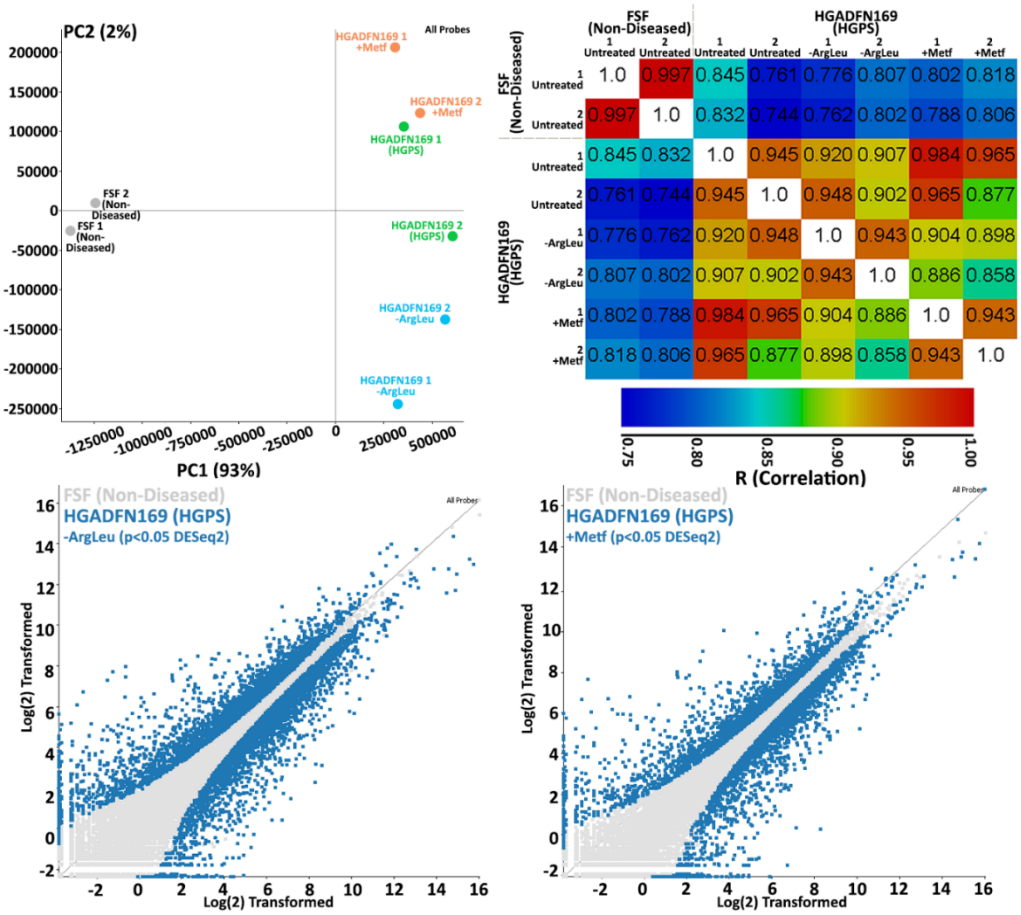

Figure 5.7: Changes in Gene Expression in HGPS Fibroblasts Restricted of Arginine and Leucine or Treated with 0.5 mM Metformin for 5 Weeks. (A) Principal component analysis (PCA) of HGADFN169 (HGPS) fibroblasts grown for 5 weeks under control (green), -ArgLeu (blue) or +Metf (orange) and FSF (non-diseased) fibroblasts (grey) grown for 5 weeks under control conditions. **(B)** Correlation matrix for two replicates (1, 2) of untreated FSF (Non-Diseased), HGADFN169 (169 HGPS), HGADFN169 restricted of arginine and leucine (169 -ArgLeu) and HGADFN169 treated with 0.5 mM metformin (169 +Metf) for 5 weeks. R values are given, with higher correlation indicated with warmer colours, and lower correlation by cooler colours (colour-correlation key under the matrix). R values of 1.0 are highlighted in white. **(C)** DESeq2 used to identify genes that significantly statistically different ($p < 0.05$) between FSF (non-diseased; grey) and HGADFN169 -ArgLeu (HGPS; blue). Raw reads were log(2) transformed using SeqMonk and plotted on a scatter graph. **(D)** DESeq2 was used to identify genes that significantly statistically different ($p < 0.05$) between FSF (Non-Diseased; grey) and HGADFN169 +Metf (HGPS; blue). Raw reads were log(2) transformed using SeqMonk and plotted on a scatter graph.

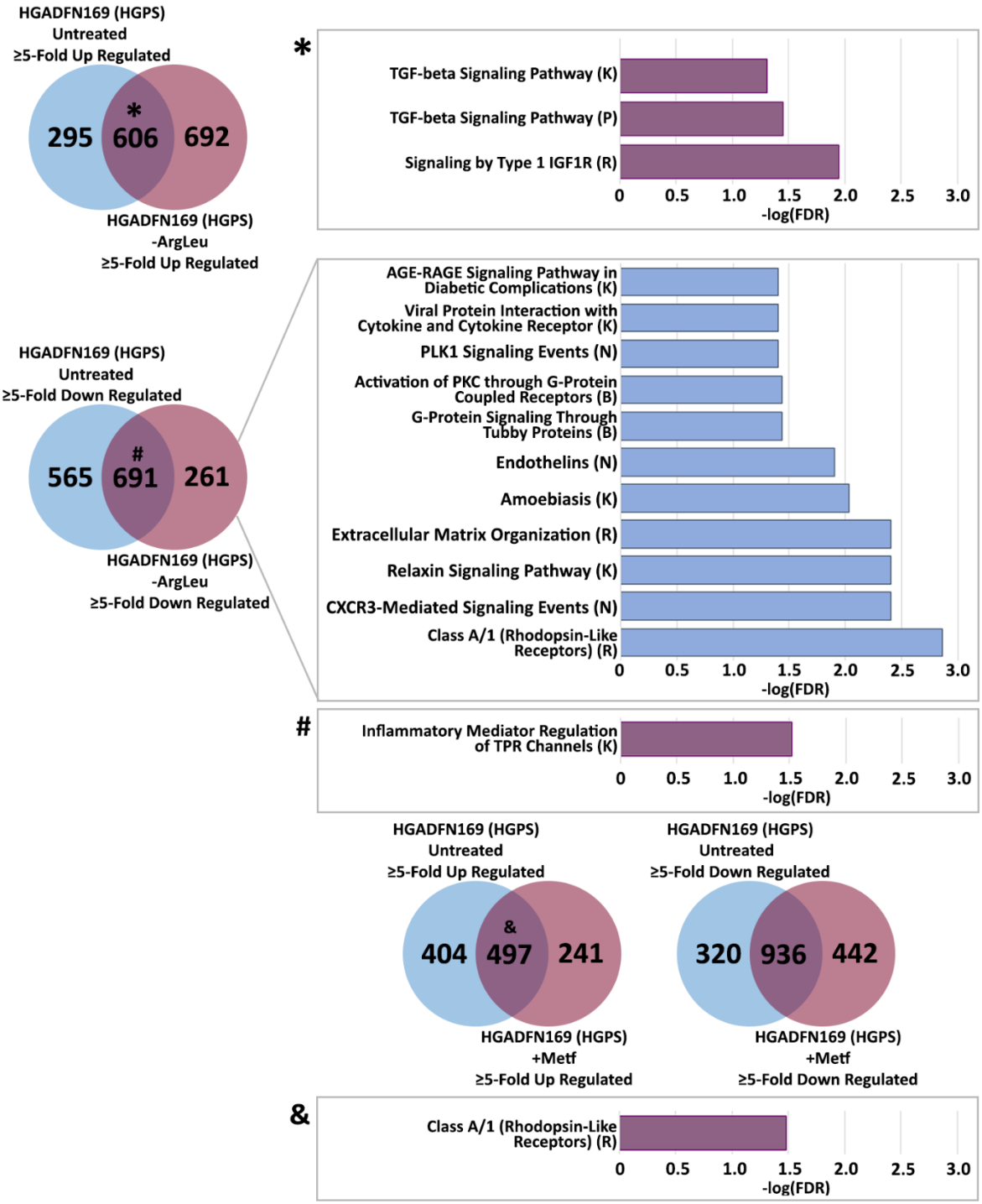

Figure 5.8: Mediation of Pathways Associated with HGPS Disease Phenotype in Response to Restriction of Arginine and Leucine or Treatment with Metformin. Venn Diagrams of genes changing ≥5-fold in HGPS control fibroblasts or HGPS fibroblasts treated with -ArgLeu or +Metf when compared to untreated (FSF) fibroblasts. Bar graphs are linked to the appropriate portion of the venn diagram analysed with marker. *: Pathways enriched in

genes down-regulated by -ArgLeu (but still meeting criteria for ≥5-fold). Inset: Pathway enrichment of genes uniquely down-regulated ≥5-fold in HGADFN169 (HGPS) -ArgLeu compared to FSF (non-diseased). #: Pathways enriched in genes increasing expression but still down-regulated ≥5-fold and in common between HGADN169 Control and HGADFN169 -ArgLeu. &: Genes down-regulated but still ≥5-fold up-regulated by +Metf common between HGADFN169 Control and -ArgLeu. X axis is the -log(False: Discovery Rate (FDR)) and Y-axis lists enriched pathways. Larger the -log(FDR) the greater the confidence in pathway enrichment. All pathways p-value <0.05, FDR<0.05. If no bar graphs are presented, no pathway enrichment was detected in the gene lists.

5.4 Restriction of Arginine and Leucine or Treatment with Metformin Induces Transcriptional Changes in Non-Diseased Fibroblasts

HGPS fibroblasts treated for 5 weeks with either intermittent -ArgLeu or +0.5 mM Metf(Cont.) do not exhibit the same transcriptome as that of non-diseased, untreated, human fibroblasts. Previously, the transcriptome of non-diseased dermal human fibroblasts has been demonstrated to change in response to treatment with metformin, as well as other compounds that impact central nutrient sensing pathways, such as mTOR. Therefore, it is possible that the transcriptome of -ArgLeu or +0.5 mM Metf(Cont.) treated HGPS fibroblasts could instead exhibit similar gene expression profiles to equivalently treated non-diseased foreskin fibroblasts. Principal component analysis of these profiles revealed that although -ArgLeu and +0.5 mM Metf(Cont.) treatments do induce divergent gene expression profiles to that of FSF, these are also different to the profiles observed in response to the same treatments in HGPS (Figure 5.9A), with 6056 DEG between FSF -ArgLeu and HGPS -ArgLeu (Figure 5.9B), and 3719 DEG between FSF +0.5 mM Metf(Cont.) and HGPS +0.5 mM Metf(Cont.) (Figure 5.9C).

Although more genes were found to be changing when comparing like-treated HGPS and non-diseased fibroblasts, genes shared between these datasets could identify pathways involved in extending health and lifespan of cells in non-diseased and disease states. Genes changing ≥5-fold in each condition were examined and shared genes identified (Figure 5.9D). In -ArgLeu, only 41 (2.9%) up-regulated genes and 56 (5.7%) down-regulated genes were

common between the non-diseased and HGPS cells under identical treatment conditions. In +0.5 mM Metf(Cont.), 4 (0.4%) genes were common in up-regulated and 26 (1.7%) in down-regulated between disease and non-diseased. Pathway enrichment of these shared genes was conducted using Cytoscape 3.8.2 and ReactomeFI, with networks linked to cell cycle (mitotic prometaphase, cell cycle checkpoints, mitotic metaphase and anaphase, PLK1 signalling events) identified in response to genes common between ≥5-fold in down-regulated non-diseased and HGPS +0.5 mM Metf(Cont.) treated samples (Figure 5.9E). No pathway enrichment was detected in other overlaps.

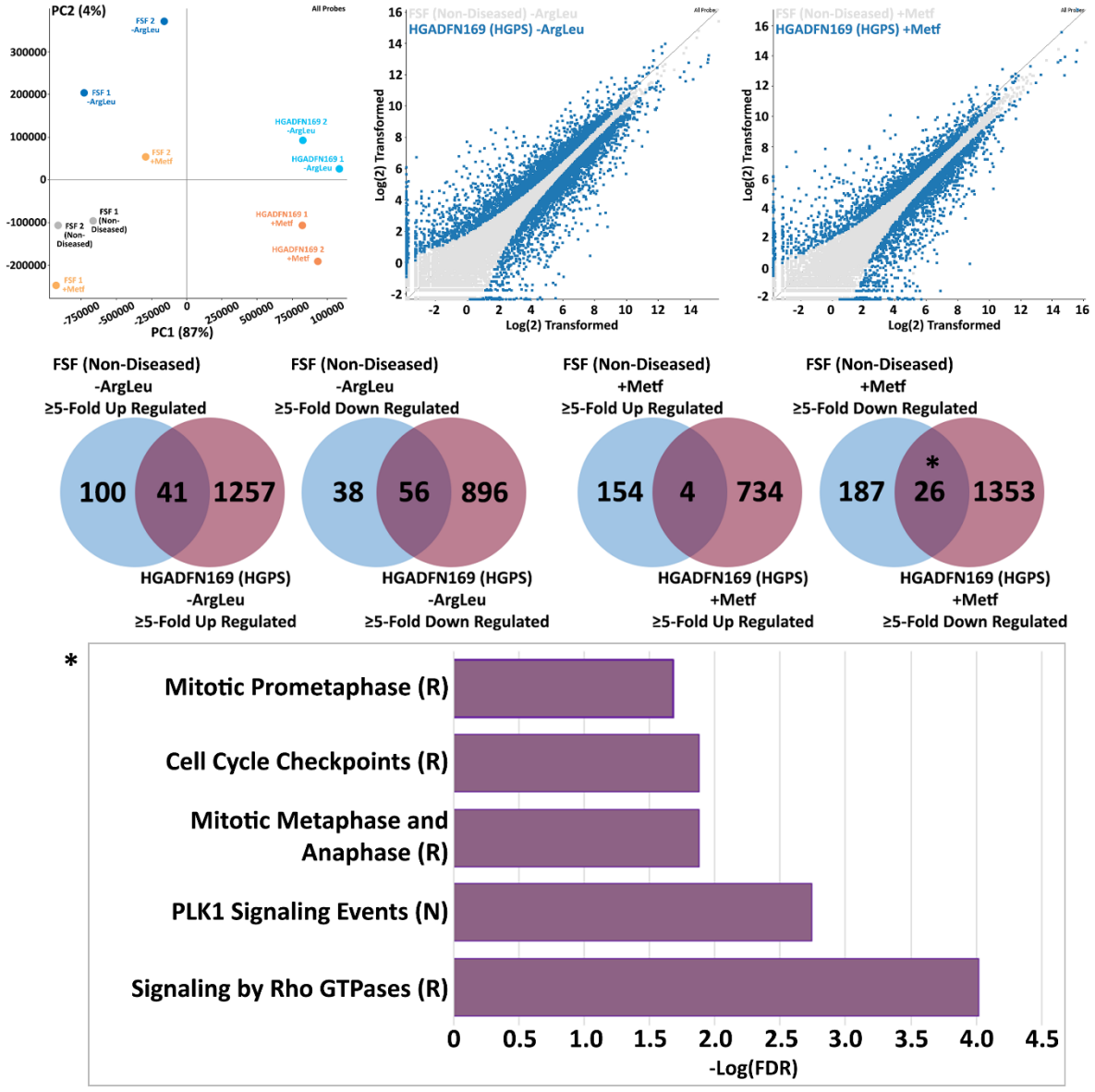

Figure 5.9: NR and NRM Induce Transcriptional Changes in Non-Diseased Fibroblasts.

(A) Principal component analysis (PCA) of HGADFN169 (HGPS) fibroblasts grown for 5

weeks under -ArgLeu (blue) or +Metf (orange) conditions and FSF (Non-Diseased) fibroblasts (grey) grown for 5 weeks under control, -ArgLeu (dark blue) or +Metf (yellow) conditions. **(B)** DESeq2 used to identify genes that significantly statistically different ($p < 0.05$) between FSF -ArgLeu (non-diseased; grey) and HGADFN169 -ArgLeu (HGPS; blue). Raw reads were log(2) transformed using SeqMonk and plotted on a scatter graph. **(C)** Venn Diagrams of genes changing ≥5-fold in HGPS control fibroblasts or HGPS fibroblasts treated with -ArgLeu or +Metf when compared to Untreated (FSF) fibroblasts. Bar graphs are linked to the appropriate portion of the venn diagram analysed with marker. **(D) *:** Genes commonly down-regulated by +Metf in FSF and HGADFN169. X-axis is the -log(False: Discovery Rate (FDR)) and Y-axis lists enriched pathways. Larger the -log(FDR) the greater the confidence in pathway enrichment. All pathways p-value <0.05, FDR<0.05. If no bar graphs are given, no pathway enrichment was detected in the gene lists.

5.5 Are Different Pathways Promoting Cellular Longevity in Response to NR or NRM Non-Diseased and Hutchinson-Gilford Progeria Syndrome Fibroblasts?

Maintenance of FSF (non-diseased) and 2DD (non-diseased) fibroblasts under -ArgLeu or +0.5 mM Metf(Cont.) extended cellular lifespan in culture. Therefore, these treatments are inducing changes at the cellular level that promote cellular lifespan. Although treated HGPS do not exhibit the same transcriptome as non-diseased cells, analysis of genomic changes in response to -ArgLeu or +0.5 mM Metf(Cont.) may provide insight into how to extend health and lifespan. Therefore, DEGs changing ≥3-fold (467 up-regulated, 316 down-regulated) in response to -ArgLeu and 497 up-regulated, and 651 down-regulated in response to +0.5 mM Metf(Cont.) were examined. No pathway enrichment was identified in genes down-regulated in FSF -ArgLeu, but pathways involved in cell proliferation and modulation of immune responses (TNF signalling pathway, toll-Like receptor signalling pathway, interferon alpha/beta signalling and cytokine-cytokine receptor interaction) were identified in up-regulated genes (Figure 5.10A). Metformin up-regulated genes also showed enrichment in toll-like receptor signalling pathway, interferon alpha/beta signalling and cytokine-cytokine receptor interaction (Figure 5.10B). Cytokine-cytokine receptor interaction was also enriched in metformin down-regulated genes (Figure 5.10B). Visualization of GO terms for -ArgLeu and +0.5 mM Metf(Cont.) up-regulated genes highlighted the similarity of biological impacts of these conditions despite varied changes in gene expression (GO

Biological Process: Figure 5.11; GO Molecular Function: Figure 5.12). Most of these terms were associated with regulation of inflammation/immune response or cell proliferation.

Thus far, analyses of the HGPS have focused on comparisons back to the non-diseased fibroblast gene expression profiles from both 2DD and FSF cells. To identify any other biological processes that might be changing in response to -ArgLeu or +0.5 mM Metf(Cont.) in HGPS, treated samples were compared to controls, with 2452 (1711 up, 741 down) genes and 1938 (754 up, 1184 down) genes identified as changing expression ≥3-fold respectively. In addition to inflammatory and cell proliferative pathways previously identified in response to -ArgLeu or +Metf, pathways associated with DNA damage were also down-regulated in response to -ArgLeu (Figure 5.10C) and additional cell signalling/growth pathways were identified as down-regulated in response to +0.5 mM Metf(Cont.) (Figure 5.10D). Unlike non-diseased fibroblasts, -ArgLeu and +0.5 mM Metf(Cont.) exhibited limited similarity between pathway analyses, GO Biological Process (Figure 5.11), and GO Molecular Function (Figure 12). Although discrepancy in metabolic processes of HGPS fibroblasts was not examined in this assay, these findings hint at altered or dysregulated response to dietary input compared to non-diseased counterparts.

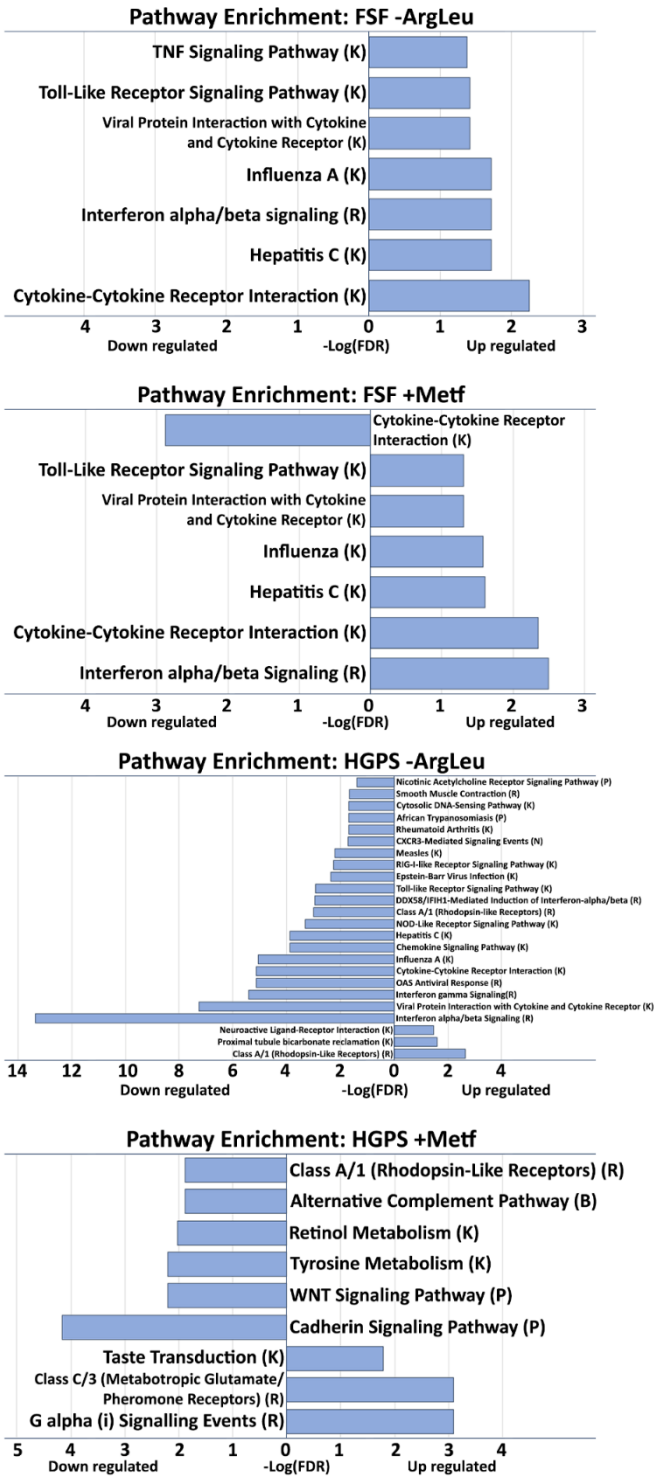

Figure 5.10: Pathway Enrichment of Non-Diseased and HGPS Fibroblasts Restricted of Arginine and Leucine or Treated with Metformin. (A) Bar graph demonstrating pathway enrichment of up-regulated and down-regulated genes changing ≥3-fold in FSF -ArgLeu compared to FSF (non-diseased). **(B)** Bar graph demonstrating pathway enrichment of up-

regulated and down-regulated genes changing ≥3-fold in FSF +Metf compared to FSF (non-diseased). **(C)** Bar graph demonstrating pathway enrichment of up-regulated and down-regulated genes changing ≥3-fold in HGPS -ArgLeu compared to HGPS Untreated. **(D)** Bar graph demonstrating pathway enrichment of up-regulated and down-regulated genes changing ≥3-fold in HGPS +Metf compared to HGPS Untreated. X-axis is the -log(False Discovery Rate (FDR)) and Y-axis lists enriched pathways. Larger the -log(FDR) the greater the confidence in pathway enrichment. No significant pathway enrichment in genes uniquely changed by metformin. All pathways p-value <0.05, FDR<0.05.

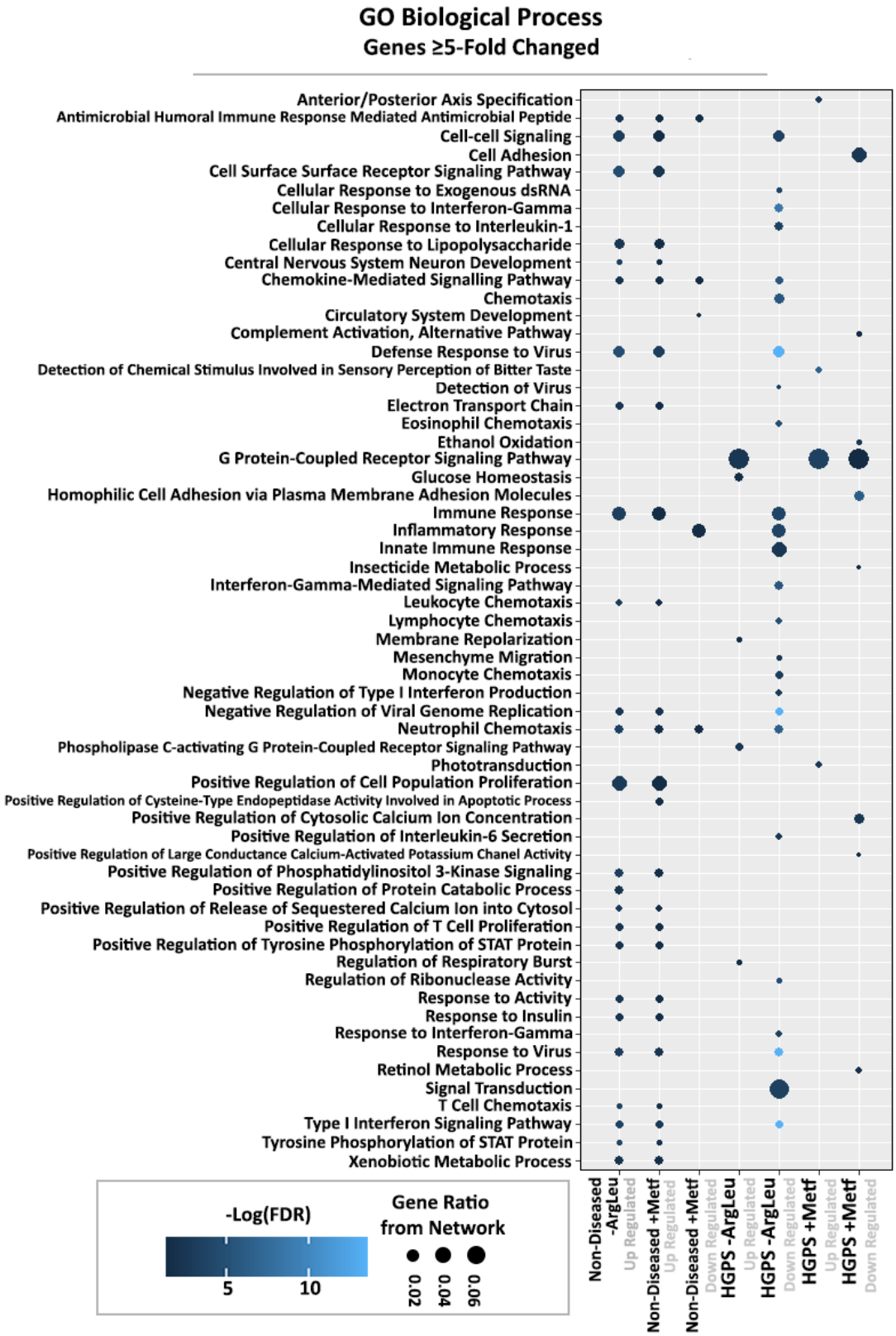

Figure 5.11: Gene Ontology of Biological Processes Comparing Non-Diseased and HGPS Fibroblasts Restricted of Arginine and Leucine or Treated with Metformin. Dot plots of gene ontology (GO) biological process associated with genes ≥3-fold altered in HGPS

and non-diseased fibroblasts under -ArgLeu or +Metf. Size of dot represents number of genes from the GO Term network in relation to the networks size (Ratio of Genes from Network) and colour represents -log(FDR) (Scales top right). GO terms are listed to the left of the dot plot. All p-value and FDR <0.05 for displayed terms.

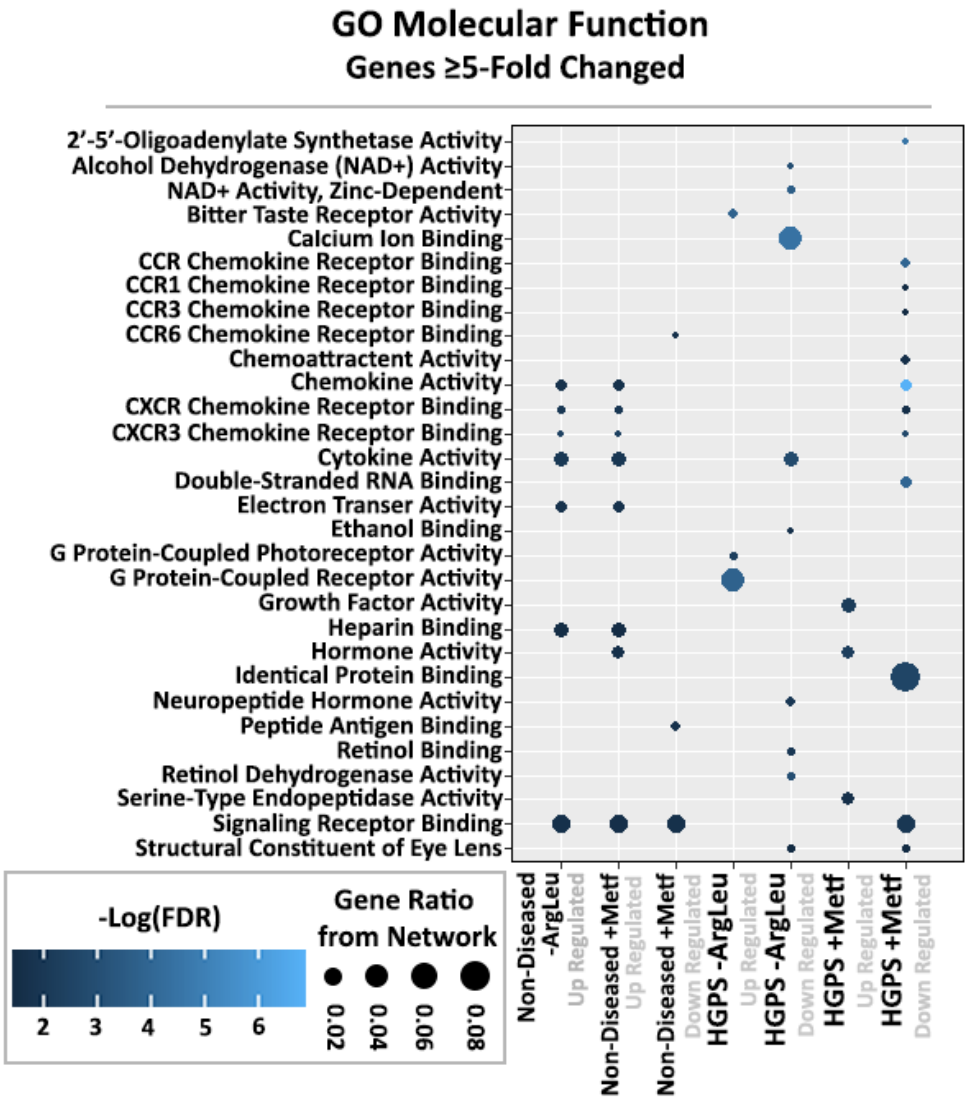

Figure 5.12: Gene Ontology of Molecular Function Comparing Non-Diseased and HGPS Fibroblasts Restricted of Arginine and Leucine or Treated with Metformin. Dot plots of gene ontology (GO) molecular function associated with genes ≥3-fold altered in HGPS and non-diseased fibroblasts under -ArgLeu or +Metf. Size of dot represents number of genes from the GO Term network in relation to the networks size (Ratio of Genes from Network) and colour represents -log(FDR) (Scales top right). GO terms are listed to the left of the dot plot. All p-value and FDR <0.05 for displayed terms.

5.8 Discussion

For decades, it has been known that restriction of nutrients can extend health and lifespan across model organisms, but only recently have researchers begun to refine which aspects of the diet can be removed or retained to achieve these effects. Simultaneously, a new class of drugs, dietary restriction mimetics (DRM), have been generated which are proposed to achieve the same benefits as nutrient restriction without the need for dietary restrictions. Hutchinson-Gilford Progeria Syndrome, HGPS, a disease in which children age prematurely, has no cure or effective treatments; therefore, application of amino acid restriction (specifically removal of arginine and leucine from the diet) or treatment with the proposed DRM metformin are promising avenues for reversing the features of this devastating disease, including the dysregulated genome.

RNA sequencing of non-diseased (FSF) and progeroid (HGADFN169) cells treated for 5 weeks in culture with intermittent arginine and leucine restriction (-ArgLeu) or continuous 0.5 mM metformin (+0.5 mM Metf(Cont.)) was conducted and bioinformatic analyses completed. Initial analyses confirmed previous findings that HGPS fibroblasts do exhibit divergent transcript profiles to those of non-diseased fibroblasts (Csoka *et al.,* 2004a; Kohler *et al.,* 2020; Kreienkamp *et al.,* 2018; Kubben *et al.,* 2016; McCord *et al.,* 2013; Prokocimer *et al.,* 2013). Specifically, we also identified up-regulation of the Transforming Growth Factor-β signalling pathway (Aliper *et al.,* 2017) which is known in HGPS to resemble this pathways expression in the elderly. TGF-β is a cytokine involved in regulating numerous processes in the body, including cell growth, division, and homeostasis. Upregulation of TGF-β signalling has been associated with cellular senescence and aging (reviewed in (Tominaga *et al.,* 2019)). Pathway enrichment analyses also identified up-regulation of other cytokine-linked pathways, including Class A/1 (Rhodopsin-Like Receptors) and Cytokine-Cytokine Receptor Interaction. It is well known that inflammation is a key promoter of aging; however, exactly how these pathways are linked beyond chemokine and cytokine expression/regulation still needs to be examined. Other researchers have also identified up-regulation of inflammatory pathways, including stat-1 regulated interferon like response in HGPS fibroblasts (compared to parental controls (Kreienkamp *et al.,* 2018) and NF-kB transcriptional profiles in HGPS mice (Osorio *et al.,* 2012), with down-regulation of these profiles linked to improved cellular pathologies and HGPS mouse

lifespans (Kreienkamp *et al.,* 2018). Our findings correlate with the literature, providing additional inflammation-linked pathways associated with HGPS.

Treatment of HGPS fibroblasts with -ArgLeu or +0.5 mM Metf(Cont.) failed to restore gene expression profiles of HGPS to non-diseased fibroblasts; however, as cellular lifespan is increased in response to these conditions, it is likely that changes occurring in response to these conditions could be important in understanding how to treat this disease. Treatment with -ArgLeu was able to reverse many of the up-regulated pathways associated with HGPS, including of Class A/1 (Rhodopsin-Like Receptors) and Viral Protein Interaction with Cytokine and Cytokine Receptor. Furthermore, although genes associated with TGF-β signalling were still up-regulated, these were expressed at much lower levels than in untreated controls. The remaining pathways are no longer enriched in up-regulated genes. Therefore, though the gene expression profiles of the HGPS -ArgLeu is different to that of non-diseased cells, treatment has repressed up-regulation of HGPS-associated pathways. -ArgLeu also down-regulated expression of additional cytokine/chemokine-linked pathways. Genes associated with the Class A/1 (Rhodopsin-Like Receptors) are also down-regulated by metformin treatment and no other pathways were detected in comparison to non-diseased fibroblasts, again mediating HGPS-associated pathway enrichment. This supports the findings that inflammatory genes are involved in HGPS cellular pathology, and down-regulation of these pathways can improve cellular phenotype.

Other pathways were also enriched in HGPS -ArgLeu down-regulated genes, including PLK-1 signalling events. This pathway has previously been associated with TGF-β signalling, with down-regulation of TGF-β signalling linked to down-regulation of PLK-1 signalling events (Shin *et al.,* 2020). PLK-1 signalling has also been linked to activation of the anaphase promoting complex (APC) (Hansen *et al.,* 2004), with down-regulation of PLK-1 signalling likely down-regulating the APC. Substrates of the APC are often overexpressed in cancers (VanGenderen *et al.,* 2020), however, down-regulation of PLK-1 can induce cellular senescence of human dermal fibroblasts (Kim *et al.,* 2013). Furthermore, in some circumstances up-regulation of the APC may be pro-longevity (reviewed in (Harkness 2018)). It is possible that the APC is poorly regulated in HGPS, and homeostasis needs to be re-established to promote longevity. Gene expression profiles of HGPS -ArgLeu or +0.5 mM Metf(Cont.) were also dissimilar to their non-diseased fibroblast counterparts, with very few

genes in common. It was postulated that common genes may be central to promoting health and lifespan, as both cell lines exhibited significant increases in time in culture under these conditions; however, pathway enrichment was only detectable in down-regulated genes shared between metformin-treated cells. Despite these limited findings, this analysis identified further cell-cycle and APC-linked pathways (including PLK-1 signalling events), further supporting the role of these processes in promoting longevity in non-diseased and HGPS fibroblasts.

The impact of amino acid restriction (specifically of -ArgLeu) on the genome of human dermal fibroblasts is unknown. Analysis of gene expression profiles again identified cytokine-cytokine receptor interactions, and other inflammation-linked pathways, as up- and down-regulated in response to -ArgLeu. The appearance of these pathways in both up- and down-regulated lists suggests that careful regulation of cytokines and inflammation linked genes is required to promote health and lifespan. Similar findings were found in response to metformin treatment and are in line with previously published data. Overall, numerous genes are divergently up/down-regulated across treatment groups – perhaps an indicator of genome dysregulation of HGPS. Although it seems sufficient to down-regulate HGPS-linked pathways to promote cellular longevity of HGPS-fibroblasts, re-establishing regulation of the genome to mitigate these altered profiles could be important in establishing a lifespan equal to that or non-diseased fibroblasts. Finally, two groups of pathways warrant further investigation in promoting health and lifespan, those associated with the APC/Cell cycle progression, and those involved in orchestrating the balance of inflammation-linked genes.

6.0 CONCLUSIONS AND FUTURE DIRECTIONS

Hutchinson-Gilford progeria syndrome is a catastrophic disease, with accumulation of progerin associated with defects in basic cellular function. For the first time, we have demonstrated that it is possible to induce progerin degradation by restricting HGPS patient fibroblasts of arginine or leucine for just 72 h. These same conditions successfully improved nuclear morphology, rates of DNA damage repair, and restored a level of genome organization (via positioning of chromosome territories). Although increases in H3K27me3 were not observed, depleted levels of progerin continued in longer-term assays, with HGPS fibroblasts exhibiting significantly extended lifespan in culture. Analysis of the transcriptome further demonstrated the ability of arginine and leucine restriction to ameliorate pathways associated with HGPS disease pathogenesis. Surprisingly, this form of nutrient restriction often performed better in depleting progerin levels and extending cellular lifespan than the current standard, rapamycin. Metformin, a nutrient restriction mimetic, achieved similar results to arginine and leucine restriction. RNA sequencing analyses further demonstrate that HGPS fibroblasts exhibit an altered metabolism, responding divergently to arginine and leucine restriction, and metformin treatment, whereas non-diseased counterparts exhibited similar responses to both. This further solidifies metformin as a nutrient restriction mimetic and provides insight into the mechanism of action of metformin, functioning via similar pathways as restriction of amino acids. Additionally, knock-down studies of autophagy associated transcript reveal that autophagy-independent mechanisms of progerin degradation are being induced. This provides new evidence on the function of metformin and rapamycin – determining that amino acid sensors are involved in achieving progerin degradation in HGPS in response to these compounds (particularly surprising for rapamycin given its direct binding of mTORC1 downstream of these sensors).

The impact of amino acid restriction in non-diseased fibroblasts is also unknown. Here we demonstrated that no negative phenotypes or decrease in cell viability were observed in response to arginine and leucine restriction; however, I do acknowledge that this is a cell culture environment and that other tissues or systems, such as muscle, may suffer adverse effect. As such, further validation of this approach needs to be conducted in additional cell lines and model organisms. We demonstrated these conditions can alter chromosome territory

localization; the first-time genome organization has been examined in response to amino acid restriction. Analysis of RNA sequencing data for both non-diseased and diseased fibroblasts identified commonly up-regulated pathways not associated with HGPS disease progression and instead likely associated with promoting longevity. Therefore, although devastating, HGPS has provided researchers with the ability to better understand genome function and organization and how dysregulation of the genome and its organization are heavily linked to disease. These data have further enabled modelling of how nutrient restriction, or nutrient restriction mimetics, can be utilized not only to treat a fatal condition, but provide proof of principle in the ability of restriction of individual amino acids from a cellular diet to alter genome function and organization for the better. As discussed, HGPS is a multifaceted disease with correlations to the aging process in non-diseased individuals. Understanding the mechanisms of HGPS disease progression, as well as how interventions can treat HGPS, could also have important implications for the normal aging process. In the case of HGPS, arginine and leucine restriction, or treatment with metformin, are interventions with far fewer serious side effects, and should be considered for treatment of HGPS and other diseases with age-like phenotypes.

Additional research directions building on this foundation are numerous. NR via restriction of total amino acids has previously been tested in human subjects for short periods of time, whilst metformin has been prescribed to millions as a treatment for type 2 diabetes. Given the already identified safety of these interventions, minor clinical studies should be conducted in animal models to confirm cellular findings, before considering clinical trials for HGPS disease treatment. The caveat of this is that there are limited number of patients suffering HGPS and many will be enrolled in multiple clinical trials and prescribed various medications. Many HGPS model organisms utilized in study of potential treatments are associated with loss of the ZMPSTE24 enzyme, and do not exactly recapitulate the HPGS phenotype. Recently, a CRISPR-cas9 model was generated by Sanchez-Lopez and colleagues which more precisely recapitulates the HGPS phenotype (Sanchez-Lopez *et al.*, 2021). Therefore, this mouse model is well suited for use in a trial of arginine and leucine restriction, or treatment with metformin, ahead of patient trials. Mice of both sexes should be examined, monitoring both molecular (nuclei shape, progerin levels, DNA damage) and physiological (weight, height, muscle mass, cardiovascular health, bone mass, blood chemistry, lifespan)

features of HGPS. Additionally, RNA sequencing and chromatin immunoprecipitation (ChIP)-sequencing should be performed on various tissues extracted from mice at different time points of treatment. These data will help identify the mechanism by which arginine and leucine restriction, or treatment with metformin, are able to induce progerin degradation. Commonly identified target molecules or genomic regions across tissues could then be subject to genetic manipulations to prove mechanism, contributing to understanding of HGPS as a disease, and to NR and NRM as treatments. Analyses will provide important insight into the influence of disease on genome function, and how NR and NRM can reverse or alter genome structure and function. Identified molecules could further be examined as druggable anti-aging targets. If successful in improving molecular and physiological aspects of HGPS, trials should be carried forward into HGPS patients. A trial of NR in otherwise healthy adults would also be informative for the possibility of this as an anti-aging intervention, following similar experimental protocols to those discussed above. Though tissue RNA and ChIP-sequencing is not likely a possibility in these trials, examination of participants blood by these techniques could be informative. Assays in other diseases with accelerated aging-phenotypes and laminopathies, such as Werner Syndrome, would expand the utilization of these interventions and provide further evidence of the applicability of these findings across diseases. Furthermore, some trials have been conducted in cancer following various amino acid restriction strategies, whilst general caloric restriction has been examined in humans for defined periods of time. To specifically examine a modified diet restricted of arginine and leucine or supplemented with metformin could provide valuable insight onto the applicability of these conditions as pro-longevity interventions, in addition to treatment of disease.

Although it is obvious that NR and NRM are having beneficial impacts on cellular health and lifespan in fibroblasts from HGPS patients, one molecular characteristic has raised numerous questions. H3K27me3 has been classically considered as globally lost in the normal aging process, with the same loss reported in HGPS fibroblasts in age-matched counterparts. Therefore, restoration of this mark would logically have been the desired outcome. Although these data recapitulate the loss of H3K27me3 in HGPS fibroblasts compared to non-diseased counterparts, levels of this histone modification were further reduced in response to NR/NRM. Various assays could be conducted to better understand this process. Firstly, there is evidence that repression of specific genes in the aging process is more important than global

gene repression, therefore conducting ChIP-Seq on HGPS fibroblasts treated with NR/NRM could assist in identification of regions of the genome that are necessary for promoting longevity, regardless of overall chromatin inactivation by H3K27me3. Assuming identification of regions of enrichment and depletion of H3K27me3, the importance of these regions could be confirmed by knock-down assays by siRNA or CRISPR-Cas9 in cell and animal models. These experiments would provide important information on the mechanism of NR/NRM in regulating the genome and could identify genes and regulatory regions essential in promoting health and lifespan. Data may also provide novel targets for anti-aging therapies. In the future, these data could contribute to genetically induce NR/NRM-like states via knock-down of identified targets in patients; however, it is generally agreed that the technology is not yet able to effectively knock-down genes in all target tissues, with too many unknowns for safe use in humans. To extend this work, additional histone modifications, such as H3K9me3, should be examined by immunofluorescence, western blot, and ChIP-seq. Analysis should consider interaction of these other histone modifications with one another and with H3K27me3, as well as other features of genome regulation (such as LADs and TADs).

It is known that genome organization plays an essential role in human aging and disease. Furthermore, organization of the genome in HGPS is severely perturbed, as examined by HiC and ATAC-seq. Conducting these assays following NR and NRM, combined with data from ChIP-seq and RNA-seq, would provide a complete database upon which to examine features of genome regulation (i.e. transcription factors) and organization (folding of the genome in three-dimensional space). These data could provide insight into regulatory elements, as well as co-regulated or co-localised genes. This could provide insight into the mechanisms governing HGPS disease progression, and how exactly NR/NRM are able to counteract this. Inclusion of non-diseased datasets across age-ranges for both sexes would further expand the functionality of this dataset. Though some sequencing data already exist for a range of individuals of a variety of ages from non-diseased and HGPS backgrounds, these data do not examine NR/NRM. To build on the RNA-seq conducted in this thesis, transcription factor binding sites enriched for in DEGs should be identified computationally. This would provide additional targets for functional studies in cell models and model organisms.

7.0 REFERENCES

Abolaji, A.O., Adedara, A.O., Adie, M.A., Vicente-Crespo, M. and Farombi, E.O. (2018). Resveratrol prolongs lifespan and improves 1-methyl-4-phenyl-1,2,3,6-tetrahydropyridine-induced oxidative damage and behavioural deficits in *Drosophila melanogaster*. Biochem Biophys Res Commun. *503*, 1042-1048.

Adler, A.S., Sinha, S., Kawahara, T.L., Zhang, J.Y., Segal, E. and Chang, H.Y. (2007). Motif module map reveals enforcement of aging by continual NF-kappaB activity. Genes Dev. *21*, 3244-3257.

Aguado, J., Sola-Carvajal, A., Cancila, V., Revechon, G., Ong, P.F., Jones-Weinert, C.W., Wallen Arzt, E., Lattanzi, G., Dreesen, O., Tripodo, C., Rossiello, F., Eriksson, M. and d'Adda di Fagagna, F. (2019). Inhibition of DNA damage response at telomeres improves the detrimental phenotypes of Hutchinson-Gilford Progeria Syndrome. Nat Commun. *10*, 4990.

Aliper, A., Jellen, L., Cortese, F., Artemov, A., Karpinsky-Semper, D., Moskalev, A., Swick, A.G. and Zhavoronkov, A. (2017). Towards natural mimetics of metformin and rapamycin. Aging. *9*, 2245-2268.

Aliper, A.M., Csoka, A.B., Buzdin, A., Jetka, T., Roumiantsev, S., Moskalev, A. and Zhavoronkov, A. (2015). Signaling pathway activation drift during aging: Hutchinson-Gilford Progeria Syndrome fibroblasts are comparable to normal middle-age and old-age cells. Aging. *7*, 26-37.

Almendariz-Palacios, C., Mousseau, D.D., Eskiw, C.H. and Gillespie, Z.E. (2020). Still Living Better through Chemistry: An Update on Caloric Restriction and Caloric Restriction Mimetics as Tools to Promote Health and Lifespan. Int J Mol Sci. *21*,

Alugoju, P., Janardhanshetty, S.S., Subaramanian, S., Periyasamy, L. and Dyavaiah, M. (2018). Quercetin Protects Yeast Saccharomyces cerevisiae pep4 Mutant from Oxidative and Apoptotic Stress and Extends Chronological Lifespan. Curr Microbiol. *75*, 519-530.

Andrzejewski, S., Gravel, S., Pollak, M. and St-Pierre, J. (2014). Metformin directly acts on mitochondria to alter cellular bioenergetics. Cancer Metab. *2*, 1-14.

Anedda, A., Rial, E. and Gonzalez-Barroso, M.M. (2008). Metformin induces oxidative stress in white adipocytes and raises uncoupling protein 2 levels. Journal of Endocrinology. *199*, 33-40.

Anzalone, A.V., Koblan, L.W. and Liu, D.R. (2020). Genome editing with CRISPR-Cas nucleases, base editors, transposases and prime editors. Nat Biotechnol. *38*, 824-844.

Arakawa, S., Honda, S., Yamaguchi, H. and Shimizu, S. (2017). Molecular mechanisms and physiological roles of Atg5/Atg7-independent alternative autophagy. Proc Jpn Acad Ser B Phys Biol Sci. *93*, 378-385.

Arganda, S., Bouchebti, S., Bazazi, S., Le Hesran, S., Puga, C., Latil, G., Simpson, S.J. and Dussutour, A. (2017). Parsing the life-shortening effects of dietary protein: effects of individual amino acids. Proc Biol Sci. *284*,

Austad, S.N. (1989). Life extension by dietary restriction in the bowl and doily spider, *Frontinella Pyramitela*. Exp Gerontol. *24*, 83-92.

Baar, M.P., Brandt, R.M.C., Putavet, D.A., *et al.* (2017). Targeted Apoptosis of Senescent Cells Restores Tissue Homeostasis in Response to Chemotoxicity and Aging. Cell. *169*, 132-147 e116.

Baker, D.J., Wijshake, T., Tchkonia, T., LeBrasseur, N.K., Childs, B.G., van de Sluis, B., Kirkland, J.L. and van Deursen, J.M. (2011). Clearance of $p16^{Ink4a}$-positive senescent cells delays ageing-associated disorders. Nature. *479*, 232-236.

Baker, P.B., Baba, N. and Boesel, C.P. (1981). Cardiovascular abnormalities in progeria. Case report and review of the literature. Arch Pathol Lab Med. *507*, 384-386.

Baldi, S., Krebs, S., Blum, H. and Becker, P.B. (2018). Genome-wide measurement of local nucleosome array regularity and spacing by nanopore sequencing. Nat Struct Mol Biol. *25*, 894-901.

Banigan, E.J., Stephens, A.D. and Marko, J.F. (2017). Mechanics and Buckling of Biopolymeric Shells and Cell Nuclei. Biophys J. *113*, 1654-1663.

Bannister, A.J. and Kouzarides, T. (2011). Regulation of chromatin by histone modifications. Cell Res. *21*, 381-395.

Bannister, A.J., Schneider, R. and Kouzarides, T. (2002). Histone Methylation: Dynamic or Static? Cell. *109*, 801-806.

Barbieri, M., Chotalia, M., Fraser, J., Lavitas, L.M., Dostie, J., Pombo, A. and Nicodemi, M. (2012). Complexity of chromatin folding is captured by the strings and binders switch model. Proc Natl Acad Sci U S A. *109*, 16173-16178.

Barinda, A.J., Ikeda, K., Nugroho, D.B., Wardhana, D.A., Sasaki, N., Honda, S., Urata, R., Matoba, S., Hirata, K.I. and Emoto, N. (2020). Endothelial progeria induces adipose tissue senescence and impairs insulin sensitivity through senescence associated secretory phenotype. Nat Commun. *11*, 481.

Barski, A., Cuddapah, S., Cui, K., Roh, T.Y., Schones, D.E., Wang, Z., Wei, G., Chepelev, I. and Zhao, K. (2007). High-resolution profiling of histone methylations in the human genome. Cell. *129*, 823-837.

Barutcu, A.R., Maass, P.G., Lewandowski, J.P., Weiner, C.L. and Rinn, J.L. (2018). A TAD boundary is preserved upon deletion of the CTCF-rich Firre locus. Nat Commun. *9*, 1444.

Baur, B., Oroszlan, M., Hess, O., Carrel, T. and Mohacsi, P. (2011). Efficacy and Safety of Sirolimus and Everolimus in Heart Transplant Patients: A Retrospective Analysis. Transplant Proc. *43*, 1853-1861.

Belak, Z.R., Pickering, J.A., Gillespie, Z.E., Audette, G., Eramian, M., Mitchell, J.A., Bridger, J.M., Kusalik, A. and Eskiw, C.H. (2020). Genes responsive to rapamycin and serum deprivation are clustered on chromosomes and undergo reorganization within local chromatin environments. Biochem Cell Biol. *98*, 178-190.

Belsky, D.W., Huffman, K.M., Pieper, C.F., Shalev, I. and Kraus, W.E. (2017). Change in the Rate of Biological Aging in Response to Caloric Restriction: CALERIE Biobank Analysis. J Gerontol A Biol Sci Med Sci. *73*, 4-10.

Belton, J.M., McCord, R.P., Gibcus, J.H., Naumova, N., Zhan, Y. and Dekker, J. (2012). Hi-C: a comprehensive technique to capture the conformation of genomes. Methods. *58*, 268-276.

Bennett, C.F. (2019). Therapeutic Antisense Oligonucleotides Are Coming of Age. Annu Rev Med. *70*, 307-321.

Benson, E.K., Lee, S.W. and Aaronson, S.A. (2009). Role of progerin-induced telomere dysfunction in HGPS premature cellular senescence. J. Cell Sci. *123*, 2605-2612.

Berman, B.P., Weisenberger, D.J., Aman, J.F., Hinoue, T., Ramjan, Z., Liu, Y., Noushmehr, H., Lange, C.P., van Dijk, C.M., Tollenaar, R.A., Van Den Berg, D. and Laird, P.W. (2011). Regions of focal DNA hypermethylation and long-range hypomethylation in colorectal cancer coincide with nuclear lamina-associated domains. Nat Genet. *44*, 40-46.

Bernstein, B.E., Mikkelsen, T.S., Xie, X., Kamal, M., Huebert, D.J., Cuff, J., Fry, B., Meissner, A., Wernig, M., Plath, K., Jaenisch, R., Wagschal, A., Feil, R., Schreiber, S.L. and Lander, E.S. (2006). A bivalent chromatin structure marks key developmental genes in embryonic stem cells. Cell. *125*, 315-326.

Beugnet, A., Tee, A.R., Taylor, P.M. and Proud, C.G. (2003). Regulation of targets of mTOR (mammalian target of rapamycin) signalling by intracellular amino acid availability. Biochem J. *372*, 555-566.

Beyret, E., Liao, H.K., Yamamoto, M., Hernandez-Benitez, R., Fu, Y., Erikson, G., Reddy, P. and Izpisua Belmonte, J.C. (2019). Single-dose CRISPR-Cas9 therapy extends lifespan of mice with Hutchinson-Gilford progeria syndrome. Nat Med. *25*, 419-422.

Bianco, S., Lupianez, D.G., Chiariello, A.M., Annunziatella, C., Kraft, K., Schopflin, R., Wittler, L., Andrey, G., Vingron, M., Pombo, A., Mundlos, S. and Nicodemi, M. (2018). Polymer physics predicts the effects of structural variants on chromatin architecture. Nat Genet. *50*, 662-667.

Bikkul, M.U., Clements, C.S., Godwin, L.S., Goldberg, M.W., Kill, I.R. and Bridger, J.M. (2018). Farnesyltransferase inhibitor and rapamycin correct aberrant genome organisation and decrease DNA damage respectively, in Hutchinson-Gilford progeria syndrome fibroblasts. Biogerontology. *19*, 579-602.

Bintu, B., Mateo, L.J., Su, J.H., Sinnott-Armstrong, N.A., Parker, M., Kinrot, S., Yamaya, K., Boettiger, A.N. and Zhuang, X. (2018). Super-resolution chromatin tracing reveals domains and cooperative interactions in single cells. Science. *362*,

Birkisdottir, M.B., Jaarsma, D., Brandt, R.M.C., Barnhoorn, S., van Vliet, N., Imholz, S., van Oostrom, C.T., Nagarajah, B., Portilla Fernandez, E., Roks, A.J.M., Elgersma, Y., van Steeg, H., Ferreira, J.A., Pennings, J.L.A., Hoeijmakers, J.H.J., Vermeij, W.P. and Dolle, M.E.T. (2021). Unlike dietary restriction, rapamycin fails to extend lifespan and reduce transcription stress in progeroid DNA repair-deficient mice. Aging Cell. *20*, e13302.

Blanc, S., Schoeller, D., Kemnitz, J., Weindruch, R., Colman, R., Newton, W., Wink, K., Baum, S. and Ramsey, J. (2003). Energy expenditure of rhesus monkeys subjected to 11 years of dietary restriction. J Clin Endocrinol Metab. *88*, 16-23.

Bolster, D.R., Crozier, S.J., Kimball, S.R. and Jefferson, L.S. (2002). AMP-activated protein kinase suppresses protein synthesis in rat skeletal muscle through down-regulated mammalian target of rapamycin (mTOR) signaling. J Biol Chem. *277*, 23977-23980.

Bolzer, A., Kreth, G., Solovei, I., Koehler, D., Saracoglu, K., Fauth, C., Muller, S., Eils, R., Cremer, C., Speicher, M.R. and Cremer, T. (2005). Three-dimensional maps of all chromsomes in human male fibroblast nuclei and prometaphase rosettes PLoS Biol. *3*, 826-842.

Borroni, A.P., Emanuelli, A., Shah, P.A., Ilic, N., Apel-Sarid, L., Paolini, B., Manikoth Ayyathan, D., Koganti, P., Levy-Cohen, G. and Blank, M. (2018). Smurf2 regulates stability and the autophagic-lysosomal turnover of lamin A and its disease-associated form progerin. Aging Cell. *17*,

Boyle, S., Gilchrist, S., Bridger, J.M., Mahy, N.L., Ellis, J.A. and Bickmore, W. (2001). The spatial organization of human chromosomes within the nuclei of normal and emerin-mutant cells. Hum Mol Genet. *10*, 211-219.

Boyle, S., Rodesch, M.J., Halvensleben, H.A., Jeddeloh, J.A. and Bickmore, W.A. (2011). Fluorescence in situ hybridization with high-complexity repeat-free oligonucleotide probes generated by massively parallel synthesis. Chromosome Res. *19*, 901-909.

Branco, M.R. and Pombo, A. (2006). Intermingling of chromosome territories in interphase suggests role in translocations and transcription-dependent associations. PLoS Biol. *4*, 780-788.

Brandhorst, S., Choi, I.Y., Wei, M., *et al.* (2015). A Periodic Diet that Mimics Fasting Promotes Multi-System Regeneration, Enhanced Cognitive Performance, and Healthspan. Cell Metab. *22*, 86-99.

Buchwalter, A. and Hetzer, M.W. (2017). Nucleolar expansion and elevated protein translation in premature aging. Nat Commun. *8*, 328.

Burkewitz, K., Zhang, Y. and Mair, W.B. (2014). AMPK at the nexus of energetics and aging. Cell Metab. *20*, 10-25.

Cabelof, D.C., Yanamadala, S., Raffoul, J.J., Guo, Z.M., Soofi, A. and Heydari, A.R. (2003). Caloric restriction promotes genomic stability by induction of base excision repair and reversal of its age-related decline. DNA Repair (Amst). *2*, 295-207.

Cabreiro, F., Au, C., Leung, K.Y., Vergara-Irigaray, N., Cocheme, H.M., Noori, T., Weinkove, D., Schuster, E., Greene, N.D. and Gems, D. (2013). Metformin retards aging in *C. elegans* by altering microbial folate and methionine metabolism. Cell. *153*, 228-239.

Cai, Y., Zhang, Y., Loh, Y.P., Tng, J.Q., Lim, M.C., Cao, Z., Raju, A., Lieberman Aiden, E., Li, S., Manikandan, L., Tergaonkar, V., Tucker-Kellogg, G. and Fullwood, M.J. (2021). H3K27me3-rich genomic regions can function as silencers to repress gene expression via chromatin interactions. Nat Commun. *12*, 719.

Calabrese, E.J., Agathokleous, E., Kapoor, R., Dhawan, G., Kozumbo, W.J. and Calabrese, V. (2021a). Metformin-enhances resilience via hormesis. Ageing Res Rev. *71*, 101418.

Calabrese, E.J. and Kozumbo, W.J. (2021b). The phytoprotective agent sulforaphane prevents inflammatory degenerative diseases and age-related pathologies via Nrf2-mediated hormesis. Pharmacol Res. *163*, 105283.

Cao, K., Blair, C.D., Faddah, D.A., Kieckhaefer, J.E., Olive, M., Erdos, M.R., Nabel, E.G. and Collins, F.S. (2011a). Progerin and telomere dysfunction collaborate to trigger cellular senescence in normal human fibroblasts. J Clin Invest. *121*, 2833-2844.

Cao, K., Capell, B.C., Erdos, M.R., Djabali, K. and Collins, F.S. (2007). A lamin A protein isoform overexpressed in Hutchinson-Gilford progeria syndrome interferes with mitosis in progeria and normal cells. Proceedings of the National Academy of Sciences. *104*, 4949-4954.

Cao, K., Graziotto, J.J., Blair, C.D., Mazzulli, J.R., Erdos, M.R., Krainc, D. and Collins, F.S. (2011b). Rapamycin reverses cellular phenotypes and enhances mutant protein clearance in Hutchinson-Gilford progeria syndrome cells. Sci Transl Med. *3*, 1-11.

Capell, B.C. and Collins, F.S. (2006). Human laminopathies: nuclei gone genetically awry. Nat Rev Genet. *7*, 940-952.

Capell, B.C., Erdos, M.R., Madigan, J.P., Fiordalisi, J.J., Varga, R., Conneely, K.N., Gordon, L.B., Der, C.J., Cox, A.D. and Collins, F.S. (2005). Inhibiting farnesylation of progerin prevents the characteristic nuclear blebbing of Hutchinson-Gilford progeria syndrome. Proceedings of the National Academy of Sciences. *102*, 12879-12884.

Capell, B.C., Olive, M., Erdos, M.R., Cao, K., Faddah, D.A., Tavarez, U.L., Conneely, K.N., Qu, X., San, H., Ganesh, S.K., Chen, X., Avallone, H., Kolodgie, F.D., Virmani, R., Nabel, E.G. and Collins, F.S. (2008). A farnesyltransferase inhibitor prevents both the onset and late progression of cardiovascular disease in a progeria mouse model. Proceedings of the National Academy of Sciences. *105*, 15902-15907.

Caridi, C.P., Plessner, M., Grosse, R. and Chiolo, I. (2019). Nuclear actin filaments in DNA repair dynamics. Nat Cell Biol. *21*, 1068-1077.

Carroll, B., Maetzel, D., Maddocks, O.D., Otten, G., Ratcliff, M., Smith, G.R., Dunlop, E.A., Passos, J.F., Davies, O.R., Jaenisch, R., Tee, A.R., Sarkar, S. and Korolchuk, V.I. (2016). Control of TSC2-Rheb signaling axis by arginine regulates mTORC1 activity. eLife. *5*,

Cattoni, D.I., Cardozo Gizzi, A.M., Georgieva, M., Di Stefano, M., Valeri, A., Chamousset, D., Houbron, C., Dejardin, S., Fiche, J.B., Gonzalez, I., Chang, J.M., Sexton, T., Marti-Renom, M.A., Bantignies, F., Cavalli, G. and Nollmann, M. (2017). Single-cell absolute contact probability detection reveals chromosomes are organized by multiple low-frequency yet specific interactions. Nat Commun. *8*, 1753.

Cenni, V., Capanni, C., Columbaro, M., Ortolani, M., D'Apice, M.R., Novelli, G., Fini, M., Marmiroli, S., Scarano, E., Maraldi, N.M., Squarzoni, S., Prencipe, S. and Lattanzi, G. (2011). Autophagic degradation of farnesylated prelamin A as a therapeutic approach to lamin-linked progeria. Eur J Histochem. *55*, e36.

Chalut, K.J., Hopfler, M., Lautenschlager, F., Boyde, L., Chan, C.J., Ekpenyong, A., Martinez-Arias, A. and Guck, J. (2012). Chromatin decondensation and nuclear softening accompany Nanog downregulation in embryonic stem cells. Biophys J. *103*, 2060-2070.

Chan, J.C. and Maze, I. (2020). Nothing Is Yet Set in (Hi)stone: Novel Post-Translational Modifications Regulating Chromatin Function. Trends Biochem Sci. *45*, 829-844.

Chandra, T., Ewels, P.A., Schoenfelder, S., Furlan-Magaril, M., Wingett, S.W., Kirschner, K., Thuret, J.Y., Andrews, S., Fraser, P. and Reik, W. (2015). Global reorganization of the nuclear landscape in senescent cells. Cell Rep. *10*, 471-483.

Chantranupong, L., Scaria, S.M., Saxton, R.A., Gygi, M.P., Shen, K., Wyant, G.A., Wang, T., Harper, J.W., Gygi, S.P. and Sabatini, D.M. (2016). The CASTOR Proteins Are Arginine Sensors for the mTORC1 Pathway. Cell. *165*, 153-164.

Chaveroux, C., Jousse, C., Cherasse, Y., Maurin, A.C., Parry, L., Carraro, V., Derijard, B., Bruhat, A. and Fafournoux, P. (2009). Identification of a novel amino acid response pathway triggering ATF2 phosphorylation in mammals. Mol Cell Biol. *29*, 6515-6526.

Chen, J., Ou, Y., Li, Y., Hu, S., Shao, L. and Liu, Y. (2017). Metformin extends *C. elegans* lifespan through lysosomal pathway. eLife. *6*, 1-17.

Chen, N.Y., Kim, P., Weston, T.A., Edillo, L., Tu, Y., Fong, L.G. and Young, S.G. (2018a). Fibroblasts lacking nuclear lamins do not have nuclear blebs or protrusions but nevertheless have frequent nuclear membrane ruptures. PNAS. *115*, 10100-10105.

Chen, Y., Zhang, Y., Wang, Y., Zhang, L., Brinkman, E.K., Adam, S.A., Goldman, R., van Steensel, B., Ma, J. and Belmont, A.S. (2018b). Mapping 3D genome organization relative to nuclear compartments using TSA-Seq as a cytological ruler. J Cell Biol. *217*, 4025-4048.

Cheon Lee, B., Kaya, A., Ma, S., Kim, G., Gerashchenko, M.V., Yim, S.H., Hu, Z., Harshman, L.G. and Gladyshev, V.N. (2014). Methionine restriction extends lifespan of Drosophila melanogaster under conditions of low amino-acid status. Nat Commun. *5*, 3592.

Choi, J., Chen, J., Schreiber, S.L. and Clardy, J. (1996). Structure of the FKBP12-Rapamycin Complex Interacting with the Binding Domain of Human FRAP. Science. *273*, 239-242.

Choi, J.Y., Lai, J.K., Xiong, Z.M., Ren, M., Moorer, M.C., Stains, J.P. and Cao, K. (2018). Diminished Canonical beta-Catenin Signaling During Osteoblast Differentiation Contributes to Osteopenia in Progeria. J Bone Miner Res. *33*, 2059-2070.

Chojnowski, A., Ong, P.F., Foo, M.X.R., Liebl, D., Hor, L.P., Stewart, C.L. and Dreesen, O. (2020). Heterochromatin loss as a determinant of progerin-induced DNA damage in Hutchinson-Gilford Progeria. Aging Cell. *19*, e13108.

Chojnowski, A., Ong, P.F., Wong, E.S., Lim, J.S., Mutalif, R.A., Navasankari, R., Dutta, B., Yang, H., Liow, Y.Y., Sze, S.K., Boudier, T., Wright, G.D., Colman, A., Burke, B., Stewart, C.L. and Dreesen, O. (2015). Progerin reduces LAP2alpha-telomere association in Hutchinson-Gilford progeria. eLife. *4*,

Chuang, C.H., Carpenter, A.E., Fuchsova, B., Johnson, T., de Lanerolle, P. and Belmont, A.S. (2006). Long-range directional movement of an interphase chromosome site. Curr Biol. *16*, 825-831.

Colman, R.J., Beasley, T.M., Kemnitz, J.W., Johnson, S.C., Weindruch, R. and Anderson, R.M. (2014). Caloric restriction reduces age-related and all-cause mortality in rhesus monkeys. Nat Commun. *5*, 1-5.

Columbaro, M., Capanni, C., Mattioli, E., Novelli, G., Parnaik, V.K., Squarzoni, S., Maraldi, N.M. and Lattanzi, G. (2005). Rescue of heterochromatin organization in Hutchinson-Gilford progeria by drug treatment. Cell Mol Life Sci. *62*, 2669-2678.

Consortium, E.P., Birney, E., Stamatoyannopoulos, J.A., *et al.* (2007). Identification and analysis of functional elements in 1% of the human genome by the ENCODE pilot project. Nature. *447*, 799-816.

Cree-Green, M., Bergman, B.C., Cengiz, E., Fox, L.A., Hannon, T.S., Miller, K., Nathan, B., Pyle, L., Kahn, D., Tansey, M., Tichy, E., Tsalikian, E., Libman, I. and Nadeau, K.J. (2019). Metformin Improves Peripheral Insulin Sensitivity in Youth With Type 1 Diabetes. J Clin Endocrinol Metab. *104*, 3265-3278.

Cremer, T. and Cremer, C. (2001). Chromosome territories, nuclear architecture and gene regulation in mammalian cells. Nat Rev Genet. *2*, 292-301.

Croft, J.A., Bridger, J.M., Boyle, S., Perry, P., Teague, P. and Bickmore, W. (1999). Differences in the localization and morphology of chromosomes in the human nucleus. J Cell Biol. *145*, 1119-1131.

Csiszar, A., Labinskyy, N., Jimenez, R., Pinto, J.T., Ballabh, P., Losonczy, G., Pearson, K.J., de Cabo, R. and Ungvari, Z. (2009). Anti-oxidative and anti-inflammatory vasoprotective effects of caloric restriction in aging: role of circulating factors and SIRT1. Mech Ageing Dev. *130*, 518-527.

Csoka, A.B., English, S.B., Simkevich, C.P., Ginzinger, D.G., Butte, A.J., Schatten, G.P., Rothman, F.G. and Sedivy, J.M. (2004a). Genome-scale expression profiling of Hutchinson-Gilford progeria syndrome reveals widespread transcriptional misregulation leading to mesodermal/mesenchymal defects and accelerated atherosclerosis. Aging Cell. *3*, 235-243.

Csoka, A.B., English, S.B., Simkevich, C.P., Ginzinger, D.G., Butte, A.J., Schatten, G.P., Rothman, F.G. and Sedivy, J.M. (2004b). Genome-scale expression profiling of Hutchinson–Gilford progeria syndrome reveals widespread transcriptional misregulation leading to mesodermal/mesenchymal defects and accelerated atherosclerosis. Aging Cell. *1*, 235-243.

Cummings, N.E., Williams, E.M., Kasza, I., *et al.* (2018). Restoration of metabolic health by decreased consumption of branched-chain amino acids. J Physiol. *596*, 623-645.

Cuyas, E., Verdura, S., Llorach-Pares, L., Fernandez-Arroyo, S., Luciano-Mateo, F., Cabre, N., Stursa, J., Werner, L., Martin-Castillo, B., Viollet, B., Neuzil, J., Joven, J., Nonell-Canals, A., Sanchez-Martinez, M. and Menendez, J.A. (2018). Metformin directly targets the H3K27me3 demethylase KDM6A/UTX. Aging Cell. *17*, e12772.

Dahl, K.N., Engler, A.J., Pajerowski, J.D. and Discher, D.E. (2005). Power-law rheology of isolated nuclei with deformation mapping of nuclear substructures. Biophys J. *89*, 2855-2864.

Damodaran, K., Venkatachalapathy, S., Alisafaei, F., Radhakrishnan, I., Jokhun, D.S., Shenoy, V.B. and Shivashankar, G.V. (2018). Compressive force induces reversible chromatin condensation and cell geometry–dependent transcriptional response. Mol Biol Cell. *29*, 3039-3051.

Dao, M.C., Sokolovska, N., Brazeilles, R., *et al.* (2018). A Data Integration Multi-Omics Approach to Study Calorie Restriction-Induced Changes in Insulin Sensitivity. Front Physiol. *9*, 1958.

Darbellay, F. and Duboule, D. (2016). Topological Domains, Metagenes, and the Emergence of Pleiotropic Regulations at Hox Loci. Curr Top Dev Biol. *116*, 299-314.

Davidson, P.M., Denais, C., Bakshi, M.C. and Lammerding, J. (2014). Nuclear deformability constitutes a rate-limiting step during cell migration in 3-D environments. Cell Mol Bioeng. *7*, 293-306.

Davies, B.S.J., Barnes, R.H., Tu, Y., Ren, S., Andres, D.A., Spielmann, H.P., Lammerding, J., Wang, Y., Young, S.G. and Fong, L.G. (2010). An accumulation of non-farnesylated prelamin A causes cardiomyopathy but not progeria. Hum Mol Genet. *19*, 2682-2694.

De Sandre-Giovannoli, A., Bernard, R., Cau, P., Navarro, C., Amiel, J., Boccaccio, I., Lyonnet, S., Stewart, C.L., Munnich, A., Le Merrer, M. and Levy, N. (2003). Lamin a truncation in Hutchinson-Gilford progeria. Science. *300*, 2055.

De Sousa-Coelho, A.L., Marrero, P.F. and Haro, D. (2012). Activating transcription factor 4-dependent induction of FGF21 during amino acid deprivation. Biochem J. *443*, 165-171.

De Vos, W.H., Houben, F., Kamps, M., Malhas, A., Verheyen, F., Cox, J., Manders, E.M., Verstraeten, V.L., van Steensel, M.A., Marcelis, C.L., van den Wijngaard, A., Vaux, D.J., Ramaekers, F.C. and Broers, J.L. (2011). Repetitive disruptions of the nuclear envelope invoke temporary loss of cellular compartmentalization in laminopathies. Hum Mol Genet. *20*, 4175-4186.

de Wit, E., Vos, E.S., Holwerda, S.J., Valdes-Quezada, C., Verstegen, M.J., Teunissen, H., Splinter, E., Wijchers, P.J., Krijger, P.H. and de Laat, W. (2015). CTCF Binding Polarity Determines Chromatin Looping. Mol Cell. *60*, 676-684.

DeBusk, F. (1972). The Hutchinson-Gilford progeria syndrome. Report of 4 cases and review of the literature. J Pediatr. *80*, 697-724.

Dechat, T., Adam, S.A., Taimen, P., Shimi, T. and Goldman, R.D. (2010). Nuclear lamins. Cold Spring Harb Perspect Biol. *2*, a000547.

Dechat, T., Pfleghaar, K., Sengupta, K., Shimi, T., Shumaker, D.K., Solimando, L. and Goldman, R.D. (2008). Nuclear lamins: major factors in the structural organization and function of the nucleus and chromatin. Genes Dev. *22*, 832-853.

Dechat, T., Shimi, T., Adam, S.A., Rusinol, A.E., Andres, D.A., Spielmann, H.P., Sinensky, M.S. and Goldman, R.D. (2007). Alterations in mitosis and cell cycle progression caused by a mutant lamin A known to accelerate human aging. Proceedings of the National Academy of Sciences. *104*, 4955-4960.

Decker, M.L., Chavez, E., Vulto, I. and Lansdorp, P.M. (2009). Telomere length in Hutchinson-Gilford progeria syndrome. Mech Ageing Dev. *130*, 377-383.

Dekker, J. and Misteli, T. (2015). Long-Range Chromatin Interactions. Cold Spring Harb Perspect Biol. *7*, a019356.

Dekker, J., Rippe, K., Dekker, M. and Kleckner, N. (2002). Capturing chromosome conformation. Science. *295*, 1306-1311.

Demirovic, D., Nizard, C. and Rattan, S.I. (2015). Basal level of autophagy is increased in aging human skin fibroblasts in vitro, but not in old skin. PloS One. *10*, e0126546.

Dhillon, S. (2021). Lonafarnib: First Approval. Drugs. *81*, 283-289.

Dialynas, G., Speese, S., Budnik, V., Geyer, P.K. and Wallrath, L.L. (2010). The role of Drosophila Lamin C in muscle function and gene expression. Development. *137*, 3067-3077.

Dibble, C.C., Elis, W., Menon, S., Qin, W., Klekota, J., Asara, J.M., Finan, P.M., Kwiatkowski, D.J., Murphy, L.O. and Manning, B.D. (2012). TBC1D7 is a third subunit of the TSC1-TSC2 complex upstream of mTORC1. Mol Cell. *47*, 535-546.

Dimitrova, E., Turberfield, A.H. and Klose, R.J. (2015). Histone demethylases in chromatin biology and beyond. EMBO Rep. *16*, 1620-1639.

Dixon, J.R., Jung, I., Selvaraj, S., Shen, Y., Antosiewicz-Bourget, J.E., Lee, A.Y., Ye, Z., Kim, A., Rajagopal, N., Xie, W., Diao, Y., Liang, J., Zhao, H., Lobanenkov, V.V., Ecker, J.R., Thomson, J.A. and Ren, B. (2015). Chromatin architecture reorganization during stem cell differentiation. Nature. *518*, 331-336.

Dixon, J.R., Selvaraj, S., Yue, F., Kim, A., Li, Y., Shen, Y., Hu, M., Liu, J.S. and Ren, B. (2012). Topological domains in mammalian genomes identified by analysis of chromatin interactions. Nature. *485*, 376-380.

Duran, R.V., Oppliger, W., Robitaille, A.M., Heiserich, L., Skendaj, R., Gottlieb, E. and Hall, M.N. (2012). Glutaminolysis activates Rag-mTORC1 signaling. Mol Cell. *47*, 349-358.

Ekberg, H., Bernasconi, C., Noldeke, J., Yussim, A., Mjornstedt, L., Erken, U., Ketteler, M. and Navratil, P. (2010). Cyclosporine, tacrolimus and sirolimus retain their distinct toxicity profiles despite low doses in the Symphony study. Nephrology Dialysis Transplant. *25*, 2004-2010.

Erdel, F., Baum, M. and Rippe, K. (2015). The viscoelastic properties of chromatin and the nucleoplasm revealed by scale-dependent protein mobility. J Phys Condens Matter. *27*, 064115.

Erdos, M.R., Cabral, W.A., Tavarez, U.L., Cao, K., Gvozdenovic-Jeremic, J., Narisu, N., Zerfas, P.M., Crumley, S., Boku, Y., Hanson, G., Mourich, D.V., Kole, R., Eckhaus,

M.A., Gordon, L.B. and Collins, F.S. (2021). A targeted antisense therapeutic approach for Hutchinson-Gilford progeria syndrome. Nat Med. *27*, 536-545.

Eriksson, M., Brown, T.W., Gordon, L.B., Glynn, M.W., Singer, J., Scott, L., Erdos, M.R., Robbins, C.M., Moses, T.Y., Berglund, P., Dutra, A., Pak, E., Durkin, S., Csoka, A.B., Boehnke, M., Glover, T.W. and Collins, F.S. (2003a). Recurrent *de novo* point mutations in lamin A cause Hutchinson-Gilford progeria syndrome. Letters to Nature. *423*, 293-298.

Eriksson, M., Brown, W.T., Gordon, L.B., Glynn, M.W., Singer, J., Scott, L., Erdos, M.R., Robbins, C.M., Moses, T.Y., Berglund, P., Dutra, A., Pak, E., Durkin, S., Csoka, A.B., Boehnke, M., Glover, T.W. and Collins, F.S. (2003b). Recurrent de novo point mutations in lamin A cause Hutchinson–Gilford progeria syndrome. Letters to Nature. *423*, 293-298.

Falk, M., Feodorova, Y., Naumova, N., Imakaev, M., Lajoie, B.R., Leonhardt, H., Joffe, B., Dekker, J., Fudenberg, G., Solovei, I. and Mirny, L.A. (2019). Heterochromatin drives compartmentalization of inverted and conventional nuclei. Nature. *570*, 395-399.

Fang, J., Yang, J., Wu, X., Zhang, G., Li, T., Wang, X., Zhang, H., Wang, C.C., Liu, G.H. and Wang, L. (2018). Metformin alleviates human cellular aging by upregulating the endoplasmic reticulum glutathione peroxidase 7. Aging Cell. *17*, e12765.

Figueiredo, V.C., Markworth, J.F. and Cameron-Smith, D. (2017). Considerations on mTOR regulation at serine 2448: implications for muscle metabolism studies. Cell Mol Life Sci. *74*, 2537-2545.

Finch, J.T., Lutter, L.C., Rhodes, D., Brown, R.S., Rushton, B., Levitt, M. and Klug, A. (1977). Structure of nucleosome core particles of chromatin. Nature. *269*, 29-36.

Finlan, L.E., Sproul, D., Thomson, I., Boyle, S., Kerr, E., Perry, P., Ylstra, B., Chubb, J.R. and Bickmore, W.A. (2008). Recruitment to the nuclear periphery can alter expression of genes in human cells. PLoS Genet. *4*, 1-13.

Finn, E.H., Pegoraro, G., Brandao, H.B., Valton, A.L., Oomen, M.E., Dekker, J., Mirny, L. and Misteli, T. (2019). Extensive Heterogeneity and Intrinsic Variation in Spatial Genome Organization. Cell. *176*, 1502-1515 e1510.

Fischer, E.G. (2020). Nuclear Morphology and the Biology of Cancer Cells. Acta Cytol. *64*, 511-519.

Fong, L.D., Frost, D., Meta, M., Qiao, X., Yang, S.H., Coffinier, C. and Young, S.G. (2006). A Protein Farnesyltransferase Inhibitor Ameliorates Disease in a Mouse Model of Progeria Science. *311*, 1621-1623.

Fontana, L., Adelaiye, R.M., Rastelli, A.L., Miles, K.M., Ciamporcero, E., Longo, V.D., Nguyen, H., Vessella, R. and Pili, R. (2013). Dietary protein restriction inhibits tumor growth in human xenograft models of prostate and breast cancer. Oncotarget. *4*, 2451-2461.

Fontana, L., Mitchell, S.E., Wang, B., Tosti, V., van Vliet, T., Veronese, N., Bertozzi, B., Early, D.S., Maissan, P., Speakman, J.R. and Demaria, M. (2018). The effects of

graded caloric restriction: XII. Comparison of mouse to human impact on cellular senescence in the colon. Aging Cell. *17*, e12746.

Fontana, L., Villareal, D.T., Das, S.K., Smith, S.R., Meydani, S.N., Pittas, A.G., Klein, S., Bhapkar, M., Rochon, J., Ravussin, E., Holloszy, J.O. and Group, C.S. (2016). Effects of 2-year calorie restriction on circulating levels of IGF-1, IGF-binding proteins and cortisol in nonobese men and women: a randomized clinical trial. Aging Cell. *15*, 22-27.

Fontana, L., Weiss, E.P., Villareal, D.T., Klein, S. and Holloszy, J.O. (2008). Long-term effects of calorie or protein restriction on serum IGF-1 and IGFBP-3 concentration in humans. Aging Cell. *7*, 681-687.

Fudenberg, G., Imakaev, M., Lu, C., Goloborodko, A., Abdennur, N. and Mirny, L.A. (2016). Formation of Chromosomal Domains by Loop Extrusion. Cell Rep. *15*, 2038-2049.

Fujii, N., Uta, S., Kobayashi, M., Sato, T., Okita, N. and Higami, Y. (2019). Impact of aging and caloric restriction on fibroblast growth factor 21 signaling in rat white adipose tissue. Exp Gerontol. *118*, 55-64.

Furusawa, T., Rochman, M., Taher, L., Dimitriadis, E.K., Nagashima, K., Anderson, S. and Bustin, M. (2015). Chromatin decompaction by the nucleosomal binding protein HMGN5 impairs nuclear sturdiness. Nat Commun. *6*, 6138.

Gabriel, D., Gordon, L.B. and Djabali, K. (2016). Temsirolimus Partially Rescues the Hutchinson-Gilford Progeria Cellular Phenotype. PloS One. *11*, e0168988.

Gabriel, D., Roedl, D., Gordon, L.B. and Djabali, K. (2015). Sulforaphane enhances progerin clearance in Hutchinson–Gilford progeria fibroblast. Aging Cell. *14*, 78-91.

Gaudelli, N.M., Komor, A.C., Rees, H.A., Packer, M.S., Badran, A.H., Bryson, D.I. and Liu, D.R. (2017). Programmable base editing of A*T to G*C in genomic DNA without DNA cleavage. Nature. *551*, 464-471.

Geng, L., Liu, Z., Wang, S., Sun, S., Ma, S., Liu, X., Chan, P., Sun, L., Song, M., Zhang, W., Liu, G.H. and Qu, J. (2019a). Low-dose quercetin positively regulates mouse healthspan. Protein Cell. *10*, 770-775.

Geng, L., Liu, Z., Zhang, W., Li, W., Wu, Z., Wang, W., Ren, R., Su, Y., Wang, P., Sun, L., Ju, Z., Chan, P., Song, M., Qu, J. and Liu, G.H. (2019b). Chemical screen identifies a geroprotective role of quercetin in premature aging. Protein Cell. *10*, 417-435.

Gesson, K., Rescheneder, P., Skoruppa, M.P., von Haeseler, A., Dechat, T. and Foisner, R. (2016). A-type lamins bind both hetero- and euchromatin, the latter being regulated by lamina-associated polypeptide 2 alpha. Genome Res. *26*, 462-473.

Gillespie, Z.E., MacKay, K., Sander, M., Trost, B., Dawicki, W., Wickramarathna, A., Gordon, J., Eramian, M., Kill, I.R., Bridger, J.M., Kusalik, A., Mitchell, J.A. and Eskiw, C.H. (2015). Rapamycin reduces fibroblast proliferation without causing quiescence and induces STAT5A/B-mediated cytokine production. Nucleus. *6*, 1-16.

Gillespie, Z.E., Wang, C., Vadan, F., Yu, T.Y., Ausio, J., Kusalik, A. and Eskiw, C.H. (2019). Metformin induces the AP-1 transcription factor network in normal dermal fibroblasts. Sci Rep. *9*, 5369.

Glynn, M.W. and Glover, T.W. (2005). Incomplete processing of mutant lamin A in Hutchinson-Gilford progeria leads to nuclear abnormalities, which are reversed by farnesyltransferase inhibition. Hum Mol Genet. *14*, 2959-2969.

Goebel, T., Mausbach, S., Tuermer, A., Eltahir, H., Winter, D., Gieselmann, V. and Thelen, M. (2020). Proteaphagy in Mammalian Cells Can Function Independent of ATG5/ATG7. Mol Cell Proteomics. *19*, 1120-1131.

Goldberg, M.W., Fiserova, J., Huttenlauch, I. and Stick, R. (2008). A new model for nuclear lamina organization. Biochem Soc Trans. *36*, 1339-1343.

Goldman, R.D., Shumaker, D.K., Erdos, M.R., Eriksson, M., Goldman, A.E., Gordon, L.B., Gruenbaum, Y., Khuon, S., Mendez, M., Varga, R. and Collins, F.S. (2004). Accumulation of mutant lamin A causes progressive changes in nuclear architecture in Hutchinson-Gilford progeria syndrome. Proceedings of the National Academy of Sciences. *101*, 8963-8968.

Gonzalez-Sandoval, A., Towbin, B.D., Kalck, V., Cabianca, D.S., Gaidatzis, D., Hauer, M.H., Geng, L., Wang, L., Yang, T., Wang, X., Zhao, K. and Gasser, S.M. (2015). Perinuclear Anchoring of H3K9-Methylated Chromatin Stabilizes Induced Cell Fate in C. elegans Embryos. Cell. *163*, 1333-1347.

Gordon, C.M., Gordon, L.B., Snyder, B.D., Nazarian, A., Quinn, N., Huh, S., Giobbie-Hurder, A., Neuberg, D., Cleveland, R., Kleinman, M., Miller, D.T. and Kieran, M.W. (2011). Hutchinson-Gilford progeria is a skeletal dysplasia. J Bone Miner Res. *26*, 1670-1679.

Gordon, L.B., Harten, I.A., Patti, M.E. and Lichtenstein, A.H. (2005). Reduced adiponectin and HDL cholesterol without elevated C-reactive protein: clues to the biology of premature atherosclerosis in Hutchinson-Gilford Progeria Syndrome. J Pediatr. *146*, 336-341.

Gordon, L.B., Kleinman, M.E., Miller, D.T., *et al.* (2012). Clinical trial of farnesyltransferase inhibitor in children with Hutchinson-Gilford progeria syndrome. PNAS. *109*, 16666-16671.

Gowans, G.J. and Hardie, D.G. (2014). AMPK: a cellular energy sensor primarily regulated by AMP. Biochem Soc Trans. *42*, 71-75.

Granado, M., Amor, S., Martin-Carro, B., Guerra-Menendez, L., Tejera-Munoz, A., Gonzalez-Hedstrom, D., Rubio, C., Carrascosa, J.M. and Garcia-Villalon, A.L. (2019). Caloric restriction attenuates aging-induced cardiac insulin resistance in male Wistar rats through activation of PI3K/Akt pathway. Nutr Metab Cardiovasc Dis. *29*, 97-105.

Graziotto, J.J., Cao, K., Collins, F.S. and Krainc, D. (2012). Rapamycin activates autophagy in Hutchinson-Gilford progeria syndrome: implications for normal aging and age-dependent neurodegenerative disorders. Autophagy. *8*, 147-151.

Griveau, A., Wiel, C., Le Calve, B., Ziegler, D.V., Djebali, S., Warnier, M., Martin, N., Marvel, J., Vindrieux, D., Bergo, M.O. and Bernard, D. (2018). Targeting the phospholipase A2 receptor ameliorates premature aging phenotypes. Aging Cell. *17*, e12835.

Gruenbaum, Y. and Foisner, R. (2015). Lamins: nuclear intermediate filament proteins with fundamental functions in nuclear mechanics and genome regulation. Annu Rev Biochem. *84*, 131-164.

Guelen, L., Pagie, L., Brasset, E., Meuleman, W., Faza, M.B., Talhout, W., Eussen, B.H., de Klein, A., Wessels, L., de Laat, W. and van Steensel, B. (2008). Domain organization of human chromosomes revealed by mapping of nuclear lamina interactions. Nature. *453*, 948-951.

Guo, Y., Xu, Q., Canzio, D., *et al.* (2015). CRISPR Inversion of CTCF Sites Alters Genome Topology and Enhancer/Promoter Function. Cell. *162*, 900-910.

Gysin, S., Salt, M., Young, A. and McCormick, F. (2011). Therapeutic strategies for targeting ras proteins. Genes Cancer. *2*, 359-372.

Haithcock, E., Dayani, Y., Neufeld, E., Zahand, A.J., Feinstein, N., Mattout, A., Gruenbaum, Y. and Liu, J. (2005). Age-related changes of nuclear architecture in Caenorhabditis elegans. Proc Natl Acad Sci U S A. *102*, 16690-16695.

Halfon, M.S. (2020). Silencers, Enhancers, and the Multifunctional Regulatory Genome. Trends Genet. *36*, 149-151.

Hambly, C. and Speakman, J.R. (2005). Contribution of Different Mechanisms to Compensation for Energy Restriction in the Mouse. Obes Res. *13*, 1548-1557.

Han, S.G., Han, S.S., Toborek, M. and Hennig, B. (2012). EGCG protects endothelial cells against PCB 126-induced inflammation through inhibition of AhR and induction of Nrf2-regulated genes. Toxicol Appl Pharmacol. *261*, 181-188.

Hansen, D.V., Loktev, A.V., Ban, K.H. and Jackson, P.K. (2004). Plk1 regulates activation of the anaphase promoting complex by phosphorylating and triggering SCFbetaTrCP-dependent destruction of the APC Inhibitor Emi1. Mol Biol Cell. *15*, 5623-5634.

Hansen, K.H., Bracken, A.P., Pasini, D., Dietrich, N., Gehani, S.S., Monrad, A., Rappsilber, J., Lerdrup, M. and Helin, K. (2008). A model for transmission of the H3K27me3 epigenetic mark. Nat Cell Biol. *10*, 1291-1300.

Hara, K., Yonezawa, K., Weng, Q.P., Kozlowski, M.T., Belham, C. and Avruch, J. (1998). Amino acid sufficiency and mTOR regulate p70 S6 Kinase and eIF-4E BP1 through a common effector mechanism. J Biol Chem. *273*, 14484-14494.

Harada, T., Swift, J., Irianto, J., Shin, J.W., Spinler, K.R., Athirasala, A., Diegmiller, R., Dingal, P.C., Ivanovska, I.L. and Discher, D.E. (2014). Nuclear lamin stiffness is a barrier to 3D migration, but softness can limit survival. J Cell Biol. *204*, 669-682.

Harhouri, K., Navarro, C., Depetris, D., Mattei, M.G., Nissan, X., Cau, P., De Sandre-Giovannoli, A. and Levy, N. (2017). MG132-induced progerin clearance is mediated by autophagy activation and splicing regulation. EMBO Mol Med. *9*, 1294-1313.

Harkness, T.A.A. (2018). Activating the Anaphase Promoting Complex to Enhance Genomic Stability and Prolong Lifespan. Int J Mol Sci. *19*,

Harr, J.C., Luperchio, T.R., Wong, X., Cohen, E., Wheelan, S.J. and Reddy, K.L. (2015). Directed targeting of chromatin to the nuclear lamina is mediated by chromatin state and A-type lamins. J Cell Biol. *208*, 33-52.

Heilbronn, L.K., de Jonge, L., Frisard, M.I., DeLany, J.P., Larson-Meyer, D.E., Rood, J., Nguyen, T., Martin, C.K., Volaufova, J., Most, M.M., Greenway, F.L., Smith, S.R., Deutsch, W.A., Williamson, D.A., Ravussin, E. and Pennington, C.T. (2006). Effect of 6-month calorie restriction on biomarkers of longevity, metabolic adaptation, and oxidative stress in overweight individuals: a randomized controlled trial. JAMA. *295*, 1539-1548.

Hennekam, R.C. (2006). Hutchinson-Gilford progeria syndrome: review of the phenotype. American Journal of Medical Genetics Part A. *140*, 2603-2624.

Hernandez, L., Roux, K.J., Wong, E.S., *et al.* (2010). Functional coupling between the extracellular matrix and nuclear lamina by Wnt signaling in progeria. Dev Cell. *19*, 413-425.

Herrmann, H. and Aebi, U. (2016). Intermediate Filaments: Structure and Assembly. Cold Spring Harb Perspect Biol. *8*,

Herrmann, H., Bar, H., Kreplak, L., Strelkov, S.V. and Aebi, U. (2007). Intermediate filaments: from cell architecture to nanomechanics. Nat Rev Mol Cell Biol. *8*, 562-573.

Hnisz, D., Shrinivas, K., Young, R.A., Chakraborty, A.K. and Sharp, P.A. (2017). A Phase Separation Model for Transcriptional Control. Cell. *169*, 13-23.

Holde, K. (1995). Chromatin higher order structure: chasing a mirage? J Biol Chem. *270*, 8373-8376.

Holder, M. and Schwitzgebel, V. (2020). Early Onset Diabetes in Two Children due to Progeria, a Monogenic Disease of DNA Repair. J Clin Res Pediatr Endocrinol. *12*, 315-318.

Hon, G.C., Hawkins, R.D. and Ren, B. (2009). Predictive chromatin signatures in the mammalian genome. Hum Mol Genet. *18*, R195-201.

Horman, S., Browne, G., Krause, U., Patel, J.V., Vertommen, D., Bertrand, L., Lavoinne, A., Hue, L., Proud, C.G. and Rider, M.H. (2002). Activation of AMP-Activated Protein Kinase Leads to the Phosphorylation of Elongation Factor 2 and an Inhibition of Protein Synthesis. Curr Biol. *12*, 1419-1423.

Horvath, S. and Raj, K. (2018). DNA methylation-based biomarkers and the epigenetic clock theory of ageing. Nat Rev Genet. *19*, 371-384.

Hosseini, H., Teimouri, M., Shabani, M., Koushki, M., Babaei Khorzoughi, R., Namvarjah, F., Izadi, P. and Meshkani, R. (2020). Resveratrol alleviates non-alcoholic fatty liver disease through epigenetic modification of the Nrf2 signaling pathway. Int J Biochem Cell Biol. *119*, 105667.

Hsieh, T.S., Cattoglio, C., Slobodyanyuk, E., Hansen, A.S., Rando, O.J., Tjian, R. and Darzacq, X. (2020). Resolving the 3D Landscape of Transcription-Linked Mammalian Chromatin Folding. Mol Cell. *78*, 539-553 e538.

Husmann, D. and Gozani, O. (2019). Histone lysine methyltransferases in biology and disease. Nat Struct Mol Biol. *26*, 880-889.

Ibrahim, M.X., Sayin, V.L., Akula, M.K., Liu, M., Fong, L.G., Young, S.G. and Bergo, M.O. (2013). Targeting Isoprenylcysteine Methylation Ameliorates Disease in a Mouse Model of Progeria. Science. *340*, 1330-1333.

Ikegami, K., Egelhofer, T.A., Strome, S. and Lieb, J.D. (2010). Caenorhabditis elegans chromosome arms are anchored to the nuclear membrane via discontinuous association with LEM-2. Genome Biol. *11*, 1-20.

Ikegami, K., Secchia, S., Almakki, O., Lieb, J.D. and Moskowitz, I.P. (2020). Phosphorylated Lamin A/C in the Nuclear Interior Binds Active Enhancers Associated with Abnormal Transcription in Progeria. Dev Cell. *52*, 699-713 e611.

Il'yasova, D., Fontana, L., Bhapkar, M., Pieper, C.F., Spasojevic, I., Redman, L.M., Das, S.K., Huffman, K.M., Kraus, W.E. and Investigators, C.S. (2018). Effects of 2 years of caloric restriction on oxidative status assessed by urinary F2-isoprostanes: The CALERIE 2 randomized clinical trial. Aging Cell. *17*,

Ingle, L., Wood, T.R. and Banta, A.M. (1937). A study of longevity, growth, reproduction and heart rate in *Daphnia longispina* as influenced by limitations in quantity of food. J. Exp. Zool. *76*, 325-353.

Jewell, J.L., Kim, Y.C., Russell, R.C., Yu, F.X., Park, H.W., Plouffe, S.W., Tagliabracci, V.S. and Guan, K.L. (2015). Metabolism. Differential regulation of mTORC1 by leucine and glutamine. Science. *347*, 194-198.

Jiang, J.C., Jaruga, E., Repnevskaya, M.V. and Jazwinski, S.M. (2000). An intervention resembling caloric restriction prolongs life span and retards aging in yeast. FASEB J. *14*, 2135-2137.

Jing, Y., Wu, F., Li, D., Yang, L., Li, Q. and Li, R. (2018). Metformin improves obesity-associated inflammation by altering macrophages polarization. Mol Cell Endocrinol. *461*, 256-264.

Jost, D., Carrivain, P., Cavalli, G. and Vaillant, C. (2014). Modeling epigenome folding: formation and dynamics of topologically associated chromatin domains. Nucleic Acids Res. *42*, 9553-9561.

Jung, H.J., Coffinier, C., Choe, Y., Beigneux, A.P., Davies, B.S., Yang, S.H., Barnes, R.H., 2nd, Hong, J., Sun, T., Pleasure, S.J., Young, S.G. and Fong, L.G. (2012). Regulation of prelamin A but not lamin C by miR-9, a brain-specific microRNA. Proc Natl Acad Sci U S A. *109*, E423-431.

Kampkotter, A., Timpel, C., Zurawski, R.F., Ruhl, S., Chovolou, Y., Proksch, P. and Watjen, W. (2008). Increase of stress resistance and lifespan of Caenorhabditis elegans by quercetin. Comp Biochem Physiol B Biochem Mol Biol. *149*, 314-323.

Kannan, K. and Fridell, Y.W. (2013). Functional implications of *Drosophila* insulin-like peptides in metabolism, aging, and dietary restriction. Front Physiol. *4*, 1-8.

Karve, T.M. and Cheema, A.K. (2011). Small changes huge impact: the role of protein posttranslational modifications in cellular homeostasis and disease. J Amino Acids. *2011*, 207691.

Katiyar, A., Tocco, V.J., Li, Y., Aggarwal, V., Tamashunas, A.C., Dickinson, R.B. and Lele, T.P. (2019). Nuclear size changes caused by local motion of cell boundaries unfold the nuclear lamina and dilate chromatin and intranuclear bodies. Soft Matter. *15*, 9310-9317.

Kawakami, Y., Hambright, W.S., Takayama, K., Mu, X., Lu, A., Cummins, J.H., Matsumoto, T., Yurube, T., Kuroda, R., Kurosaka, M., Fu, F.H., Robbins, P.D., Niedernhofer, L.J. and Huard, J. (2019). Rapamycin Rescues Age-Related Changes in Muscle-Derived Stem/Progenitor Cells from Progeroid Mice. Mol Ther Methods Clin Dev. *14*, 64-76.

Kazyken, D., Magnuson, B., Bodur, C., Acosta-Jaquez, H.A., Zhang, D., Tong, X., Barnes, T.M., Steinl, G.K., Patterson, N.E., Altheim, C.H., Sharma, N., Inoki, K., Cartee, G.D., Bridges, D., Yin, L., Riddle, S.M. and Fingar, D.C. (2019). AMPK directly activates mTORC2 to promote cell survival during acute energetic stress. Sci Signal. *12*,

Ke, Z., Firsanov, D., Spencer, B., Seluanov, A. and Gorbunova, V. (2020). Short-term calorie restriction enhances DNA repair by non-homologous end joining in mice. npj Aging Mech. Dis. *6*, 9.

Khalil, A., Grant, J.L., Caddle, L.B., Atzema, E., Mills, K.D. and Arneodo, A. (2007). Chromosome territories have a highly nonspherical morphology and nonrandom positioning. Chromosome Res. *15*, 899-916.

Kilberg, M.S., Balasubramanian, M., Fu, L. and Shan, J. (2012). The transcription factor network associated with the amino acid response in mammalian cells. Adv Nutr. *3*, 295-306.

Kim, D., Paggi, J.M., Park, C., Bennett, C. and Salzberg, S.L. (2019a). Graph-based genome alignment and genotyping with HISAT2 and HISAT-genotype. Nat Biotechnol. *37*, 907-915.

Kim, D.M., Ryu, S.W. and Choi, C. (2010). Long-term treatment of farnesyltransferase inhibitor FTI-277 induces neurotoxicity of hippocampal neurons from rat embryo in a ROS-dependent manner. Biochem Biophys Res Commun. *403*, 91-96.

Kim, E.N., Lim, J.H., Kim, M.Y., Ban, T.H., Jang, I., Yoon, H.E., Park, C.W., Chang, Y.S. and Choi, B.S. (2018). Resveratrol, an Nrf2 activator, ameliorates aging-related progressive renal injury. Aging. *10*, 83-99.

Kim, H.J., Cho, J.H. and Kim, J.R. (2013). Downregulation of Polo-like kinase 1 induces cellular senescence in human primary cells through a p53-dependent pathway. J Gerontol A Biol Sci Med Sci. *68*, 1145-1156.

Kim, J. and Guan, K.L. (2019b). mTOR as a central hub of nutrient signalling and cell growth. Nat Cell Biol. *21*, 63-71.

Kind, J., Pagie, L., de Vries, S.S., Nahidiazar, L., Dey, S.S., Bienko, M., Zhan, Y., Lajoie, B., de Graaf, C.A., Amendola, M., Fudenberg, G., Imakaev, M., Mirny, L.A., Jalink, K., Dekker, J., van Oudenaarden, A. and van Steensel, B. (2015). Genome-wide maps of nuclear lamina interactions in single human cells. Cell. *163*, 134-147.

Kind, J., Pagie, L., Ortabozkoyun, H., Boyle, S., de Vries, S.S., Janssen, H., Amendola, M., Nolen, L.D., Bickmore, W.A. and van Steensel, B. (2013). Single-cell dynamics of genome-nuclear lamina interactions. Cell. *153*, 178-192.

Kind, J. and van Steensel, B. (2014). Stochastic genome-nuclear lamina interactions: modulating roles of Lamin A and BAF. Nucleus. *5*, 124-130.

Koblan, L.W., Erdos, M.R., Wilson, C., *et al.* (2021). In vivo base editing rescues Hutchinson-Gilford progeria syndrome in mice. Nature. *589*, 608-614.

Kohler, F., Bormann, F., Raddatz, G., Gutekunst, J., Corless, S., Musch, T., Lonsdorf, A.S., Erhardt, S., Lyko, F. and Rodriguez-Paredes, M. (2020). Epigenetic deregulation of lamina-associated domains in Hutchinson-Gilford progeria syndrome. Genome Med. *12*, 46.

Kohwi, M., Lupton, J.R., Lai, S.L., Miller, M.R. and Doe, C.Q. (2013). Developmentally regulated subnuclear genome reorganization restricts neural progenitor competence in Drosophila. Cell. *152*, 97-108.

Kornberg, R. (1974). Chromatin structure: a repeating unit of histones and DNA. Science. *184*, 868-871.

Krause, M., Te Riet, J. and Wolf, K. (2013). Probing the compressibility of tumor cell nuclei by combined atomic force-confocal microscopy. Phys Biol. *10*, 065002.

Kreienkamp, R., Graziano, S., Coll-Bonfill, N., Bedia-Diaz, G., Cybulla, E., Vindigni, A., Dorsett, D., Kubben, N., Batista, L.F.Z. and Gonzalo, S. (2018). A Cell-Intrinsic Interferon-like Response Links Replication Stress to Cellular Aging Caused by Progerin. Cell Rep. *22*, 2006-2015.

Krietenstein, N., Abraham, S., Venev, S.V., Abdennur, N., Gibcus, J., Hsieh, T.S., Parsi, K.M., Yang, L., Maehr, R., Mirny, L.A., Dekker, J. and Rando, O.J. (2020). Ultrastructural Details of Mammalian Chromosome Architecture. Mol Cell. *78*, 554-565 e557.

Kubben, N., Zhang, W., Wang, L., Voss, T.C., Yang, J., Qu, J., Liu, G.H. and Misteli, T. (2016). Repression of the Antioxidant NRF2 Pathway in Premature Aging. Cell. *165*, 1361-1374.

Kupper, K., Kolbl, A., Biener, D., Dittrich, S., von Hase, J., Thormeyer, T., Fiegler, H., Carter, N.P., Speicher, M.R., Cremer, T. and Cremer, M. (2007). Radial chromatin positioning is shaped by local gene density, not by gene expression. Chromosoma. *116*, 285-306.

Lakowski, B. and Hekimi, S. (1998). The genetics of caloric restriction in *Caenorhabditis elegans*. Proc. Natl. Acad. Sci USA. *95*, 13091-13096.

Lan, F. and Shi, Y. (2009). Epigenetic regulation: methylation of histone and non-histone proteins. Sci China C Life Sci. *52*, 311-322.

Lauberth, S.M., Nakayama, T., Wu, X., Ferris, A.L., Tang, Z., Hughes, S.H. and Roeder, R.G. (2013). H3K4me3 interactions with TAF3 regulate preinitiation complex assembly and selective gene activation. Cell. *152*, 1021-1036.

Le Berre, M., Aubertin, J. and Piel, M. (2012). Fine control of nuclear confinement identifies a threshold deformation leading to lamina rupture and induction of specific genes. Integr Biol (Camb). *4*, 1406-1414.

Lee, J.M., Nobumori, C., Tu, Y., Choi, C., Yang, S.H., Jung, H.J., Vickers, T.A., Rigo, F., Bennett, C.F., Young, S.G. and Fong, L.G. (2016a). Modulation of LMNA splicing as a strategy to treat prelamin A diseases. J Clin Invest. *126*, 1592-1602.

Lee, S.J., Jung, Y.S., Yoon, M.H., *et al.* (2016b). Interruption of progerin-lamin A/C binding ameliorates Hutchinson-Gilford progeria syndrome phenotype. J Clin Invest. *126*, 3879-3893.

Lee, Y.Y., Cevallos, R.C. and Jan, E. (2009). An upstream open reading frame regulates translation of GADD34 during cellular stresses that induce eIF2alpha phosphorylation. J Biol Chem. *284*, 6661-6673.

Leuba, S.H., Yang, G., Robert, C., Samori, B., van Holde, K., Zlatanova, J. and Bustamante, C. (1994). Three-dimensional structure of extended chromatin fibers as revealed by tapping-mode scanning force microscopy. Proc. Natl. Acad. Sci. USA. *91*,

Lewis, K.N., Wason, E., Edrey, Y.H., Kristan, D.M., Nevo, E. and Buffenstein, R. (2015). Regulation of Nrf2 signaling and longevity in naturally long-lived rodents. PNAS. *112*, 3722-3727.

Liao, C.Y., Anderson, S.S., Chicoine, N.H., Mayfield, J.R., Academia, E.C., Wilson, J.A., Pongkietisak, C., Thompson, M.A., Lagmay, E.P., Miller, D.M., Hsu, Y.M., McCormick, M.A., O'Leary, M.N. and Kennedy, B.K. (2016). Rapamycin Reverses Metabolic Deficits in Lamin A/C-Deficient Mice. Cell Rep. *17*, 2542-2552.

Liu, B., Ghosh, S., Yang, X., Zheng, H., Liu, X., Wang, Z., Jin, G., Zheng, B., Kennedy, B.K., Suh, Y., Kaeberlein, M., Tryggvason, K. and Zhou, Z. (2012). Resveratrol rescues SIRT1-dependent adult stem cell decline and alleviates progeroid features in laminopathy-based progeria. Cell Metab. *16*, 738-750.

Liu, B., Wang, Z., Zhang, L., Ghosh, S., Zheng, H. and Zhou, Z. (2013). Depleting the methyltransferase Suv39h1 improves DNA repair and extends lifespan in a progeria mouse model. Nat Commun. *4*, 1868.

Liu, G.H., Barkho, B.Z., Ruiz, S., Diep, D., Qu, J., Yang, S.L., Panopoulos, A.D., Suzuki, K., Kurian, L., Walsh, C., Thompson, J., Boue, S., Fung, H.L., Sancho-Martinez, I., Zhang, K., Yates, J., 3rd and Izpisua Belmonte, J.C. (2011). Recapitulation of premature ageing with iPSCs from Hutchinson-Gilford progeria syndrome. Nature. *472*, 221-225.

Liu, G.Y. and Sabatini, D.M. (2020). mTOR at the nexus of nutrition, growth, ageing and disease. Nat Rev Mol Cell Biol. *21*, 183-203.

Liu, Y., Rusinol, A., Sinensky, M., Wang, Y. and Zou, Y. (2006). DNA damage responses in progeroid syndromes arise from defective maturation of prelamin A. J Cell Sci. *119*, 4644-4649.

Liu, Y., Wang, Y., Rusinol, A.E., Sinensky, M.S., Liu, J., Shell, S.M. and Zou, Y. (2008). Involvement of xeroderma pigmentosum group A (XPA) in progeria arising from defective maturation of prelamin A. FASEB J. *22*, 603-611.

Long, X., Ortiz-Vega, S., Lin, Y. and Avruch, J. (2005). Rheb binding to mammalian target of rapamycin (mTOR) is regulated by amino acid sufficiency. J Biol Chem. *280*, 23433-23436.

Longo, V.D. and Kennedy, B.K. (2006). Sirtuins in aging and age-related disease. Cell. *126*, 257-268.

Lu, H., Jia, C., Wu, D., Jin, H., Lin, Z., Pan, J., Li, X. and Wang, W. (2021). Fibroblast growth factor 21 (FGF21) alleviates senescence, apoptosis, and extracellular matrix degradation in osteoarthritis via the SIRT1-mTOR signaling pathway. Cell Death Dis. *12*, 865.

Luger, K., Mader, A.W., Richmond, R.K., Sargent, D.F. and Richmond, T.J. (1997). Crystal structure of the nucleosome core particle at 2.8 A˚ resolution. Nature. *389*, 251-260.

Luo, Y., Mitrpant, C., Johnsen, R.D., Fabian, V.A., Fletcher, S., Mastaglia, F.L. and Wilton, S.D. (2013). Investigation of age-related changes in LMNA splicing and expression of progerin in human skeletal muscles. Int J Exp Pathol. *6*,

Lupianez, D.G., Kraft, K., Heinrich, V., *et al.* (2015). Disruptions of topological chromatin domains cause pathogenic rewiring of gene-enhancer interactions. Cell. *161*, 1012-1025.

Ma, Z., Wang, H., Cai, Y., Wang, H., Niu, K., Wu, X., Ma, H., Yang, Y., Tong, W., Liu, F., Liu, Z., Zhang, Y., Liu, R., Zhu, Z.J. and Liu, N. (2018). Epigenetic drift of H3K27me3 in aging links glycolysis to healthy longevity in Drosophila. eLife. *7*,

Maharana, S., Iyer, K.V., Jain, N., Nagarajan, M., Wang, Y. and Shivashankar, G.V. (2016). Chromosome intermingling-the physical basis of chromosome organization in differentiated cells. Nucleic Acids Res. *44*, 5148-5160.

Mair, W., Morantte, I., Rodrigues, A.P., Manning, G., Montminy, M., Shaw, R.J. and Dillin, A. (2011). Lifespan extension induced by AMPK and calcineurin is mediated by CRTC-1 and CREB. Nature. *470*, 404-408.

Makino, N. and Maeda, T. (2021). Calorie restriction delays cardiac senescence and improves cardiac function in obese diabetic rats. Mol Cell Biochem. *476*, 221-229.

Mallampalli, M.P., Huyer, G., Bendale, P., Gelb, M.H. and Michaelis, S. (2005). Inhibiting farnesylation reverses the nuclear morphology defect in a HeLa cell model for Hutchinson-Gilford progeria syndrome. Proc Natl Acad Sci U S A. *102*, 14416-14421.

Martin-Montalvo, A., Mercken, E.M., Mitchell, S.J., *et al.* (2013). Metformin improves healthspan and lifespan in mice. Nat Commun. *4*, 1-12.

Maruyama, R., Shimizu, M., Li, J., Inoue, J. and Sato, R. (2016). Fibroblast growth factor 21 induction by activating transcription factor 4 is regulated through three amino acid response elements in its promoter region. Biosci Biotechnol Biochem. *80*, 929-934.

Marzetti, E., Calvani, R., Cesari, M., Buford, T.W., Lorenzi, M., Behnke, B.J. and Leeuwenburgh, C. (2013). Mitochondrial dysfunction and sarcopenia of aging: from signaling pathways to clinical trials. Int J Biochem Cell Biol. *45*, 2288-2301.

Mattison, J.A., Colman, R.J., Beasley, T.M., Allison, D.B., Kemnitz, J.W., Roth, G.S., Ingram, D.K., Weindruch, R., de Cabo, R. and Anderson, R.M. (2017). Caloric restriction improves health and survival of rhesus monkeys. Nat Commun. *8*, 14063.

Mattison, J.A., Roth, G.S., Beasley, T.M., Tilmont, E.M., Handy, A.M., Herbert, R.L., Longo, D.L., Allison, D.B., Young, J.E., Bryant, M., Barnard, D., Ward, W.F., Qi, W., Ingram, D.K. and de Cabo, R. (2012). Impact of caloric restriction on health and survival in rhesus monkeys from the NIA study. Nature. *489*, 318-321.

Mazumder, A., Roopa, T., Basu, A., Mahadevan, L. and Shivashankar, G.V. (2008). Dynamics of chromatin decondensation reveals the structural integrity of a mechanically prestressed nucleus. Biophys J. *95*, 3028-3035.

McCay, C.M., Crowell, M.F. and Maynard, L.A. (1935). The effect of retarded growth upon the length of life span and upon the ultimate body size. J Nutr. *10*, 63-79.

McClintock, D., Ratner, D., Lokuge, M., Owens, D.M., Gordon, L.B., Collins, F.S. and Djabali, K. (2007). The mutant form of lamin A that causes Hutchinson-Gilford progeria is a biomarker of cellular aging in human skin. PloS One. *2*, e1269.

McCord, R.P., Nazario-Toole, A., Zhang, H., Chines, P.S., Zhan, Y., Erdos, M.R., Collins, F.S., Dekker, J. and Cao, K. (2013). Correlated alterations in genome organization, histone methylation, and DNA-lamin A/C interactions in Hutchinson-Gilford progeria syndrome. Genome Res. *23*, 260-269.

Meaburn, K.J., Cabuy, E., Bonne, G., Levy, N., Morris, G.E., Navelli, G., Kill, I.R. and Bridger, J.M. (2007). Primary laminopathy fibroblasts display altered genome organization and apoptosis. Aging Cell. *6*, 139-153.

Mehta, I.S., Amira, M., Harvey, A.J. and Bridger, J.M. (2010). Rapid chromosome territory relocation by nuclear motor activity in response to serum removal in primary human fibroblasts. Genome Biol. *11*, 1-17.

Mehta, I.S., Eskiw, C.H., Arican, H.D., Kill, I.R. and Bridger, J.M. (2011). Farnesyltransferase inhibitor treatment restores chromosome territory positions and active chromosome dynamics in Hutchinson-Gilford progeria syndrome cells. Genome Biol. *12*, 1-14.

Mehta, I.S., Figgitt, M., Clements, C.S., Kill, I.R. and Bridger, J.M. (2007). Alterations to nuclear architecture and genome behavior in senescent cells. Ann N Y Acad Sci. *1100*, 250-263.

Meng, D., Yang, Q., Wang, H., Melick, C.H., Navlani, R., Frank, A.R. and Jewell, J.L. (2020). Glutamine and asparagine activate mTORC1 independently of Rag GTPases. J Biol Chem. *295*, 2890-2899.

Menon, S., Dibble, C.C., Talbott, G., Hoxhaj, G., Valvezan, A.J., Takahashi, H., Cantley, L.C. and Manning, B.D. (2014). Spatial control of the TSC complex integrates insulin and nutrient regulation of mTORC1 at the lysosome. Cell. *156*, 771-785.

Mercken, E.M., Crosby, S.D., Lamming, D.W., JeBailey, L., Krzysik-Walker, S., Villareal, D.T., Capri, M., Franceschi, C., Zhang, Y., Becker, K., Sabatini, D.M., Cabo, R. and Fontana, L. (2013). Calorie restriction in humans inhibits the PI3K/AKT pathway and induces a younger transcription profile. Aging Cell. *12*, 645-651.

Merideth, M.A., Gordon, L.B., Clauss, S., *et al.* (2008). Phenotype and course of Hutchinson-Gilford progeria syndrome. New England Journal of Medicine. *358*, 592-604.

Messaoudi, I., Warner, J., Fischer, M., Park, B., Hill, B., Mattison, J., Lane, M.A., Roth, G.S., Ingram, D.K., Picker, L.J., Douek, D.C., Mori, M. and Nikolich-Zugich, J. (2006). Delay of T cell senescence by caloric restriction in aged long-lived nonhuman primates. Proc Natl Acad Sci U S A. *103*, 19448-19453.

Meuleman, W., Peric-Hupkes, D., Kind, J., Beaudry, J.B., Pagie, L., Kellis, M., Reinders, M., Wessels, L. and van Steensel, B. (2013). Constitutive nuclear lamina-genome interactions are highly conserved and associated with A/T-rich sequence. Genome Res. *23*, 270-280.

Miller, R.A., Harrison, D.E., Astle, C.M., Fernandez, E., Flurkey, K., Han, M., Javors, M.A., Li, X., Nadon, N.L., Nelson, J.F., Pletcher, S., Salmon, A.B., Sharp, Z.D., Van Roekel, S., Winkleman, L. and Strong, R. (2014). Rapamycin-mediated lifespan increase in mice is dose and sex dependent and metabolically distinct from dietary restriction. Aging Cell. *13*, 468-477.

Milon, B.C., Cheng, H., Tselebrovsky, M.V., Lavrov, S.A., Nenasheva, V.V., Mikhaleva, E.A., Shevelyov, Y.Y. and Nurminsky, D.I. (2012). Role of histone deacetylases in gene regulation at nuclear lamina. PloS One. *7*, e49692.

Min, K.J. and Tatar, M. (2006). Restriction of amino acids extends lifespan in Drosophila melanogaster. Mech Ageing Dev. *127*, 643-646.

Minard, A.Y., Tan, S.X., Yang, P., Fazakerley, D.J., Domanova, W., Parker, B.L., Humphrey, S.J., Jothi, R., Stockli, J. and James, D.E. (2016). mTORC1 Is a Major Regulatory Node in the FGF21 Signaling Network in Adipocytes. Cell Rep. *17*, 29-36.

Mirny, L.A., Imakaev, M. and Abdennur, N. (2019). Two major mechanisms of chromosome organization. Curr Opin Cell Biol. *58*, 142-152.

Misteli, T. (2020). The Self-Organizing Genome: Principles of Genome Architecture and Function. Cell. *183*, 28-45.

Mitchell, S.J., Madrigal-Matute, J., Scheibye-Knudsen, M., *et al.* (2016). Effects of Sex, Strain, and Energy Intake on Hallmarks of Aging in Mice. Cell Metab. *23*, 1093-1112.

Musich, P.R. and Zou, Y. (2009). Genomic instability and DNA damage responses in progeria arising from defective maturation of prelamin A. Aging. *1*, 28-37.

Musich, P.R. and Zou, Y. (2011). DNA-damage accumulation and replicative arrest in Hutchinson-Gilford progeria syndrome. Biochem Soc Trans. *39*, 1764-1769.

Nagano, T., Lubling, Y., Stevens, T.J., Schoenfelder, S., Yaffe, E., Dean, W., Laue, E.D., Tanay, A. and Fraser, P. (2013). Single-cell Hi-C reveals cell-to-cell variability in chromosome structure. Nature. *502*, 59-64.

Narendra, V., Rocha, P.P., An, D., Raviram, R., Skok, J.A., Mazzoni, E.O. and Reinberg, D. (2015). CTCF establishes discrete functional chromatin domains at the Hox clusters during differentiation. Science. *347*, 1017-1021.

Neff, F., Flores-Dominguez, D., Ryan, D.P., *et al.* (2013). Rapamycin extends murine lifespan but has limited effects on aging. J Clin Invest. *123*, 3272-3291.

Neubert, E., Meyer, D., Rocca, F., Gunay, G., Kwaczala-Tessmann, A., Grandke, J., Senger-Sander, S., Geisler, C., Egner, A., Schon, M.P., Erpenbeck, L. and Kruss, S. (2018). Chromatin swelling drives neutrophil extracellular trap release. Nat Commun. *9*, 3767.

Ng, S.S., Yue, W.W., Oppermann, U. and Klose, R.J. (2009). Dynamic protein methylation in chromatin biology. Cell Mol Life Sci. *66*, 407-422.

Nigg, E.A. (1992). Assembly-disassembly of the nuclear lamina. Curr Opin Cell Biol. *4*, 105-109.

Nishida, Y., Arakawa, S., Fujitani, K., Yamaguchi, H., Mizuta, T., Kanaseki, T., Komatsu, M., Otsu, K., Tsujimoto, Y. and Shimizu, S. (2009). Discovery of Atg5/Atg7-independent alternative macroautophagy. Nature. *461*, 654-658.

Nissan, X., Blondel, S., Navarro, C., Maury, Y., Denis, C., Girard, M., Martinat, C., De Sandre-Giovannoli, A., Levy, N. and Peschanski, M. (2012). Unique preservation of neural cells in Hutchinson- Gilford progeria syndrome is due to the expression of the neural-specific miR-9 microRNA. Cell Rep. *2*, 1-9.

Noll, M. (1974). Subunit structure of chromatin. Nature. *251*, 249-251.

Nora, E.P., Goloborodko, A., Valton, A.L., Gibcus, J.H., Uebersohn, A., Abdennur, N., Dekker, J., Mirny, L.A. and Bruneau, B.G. (2017). Targeted Degradation of CTCF Decouples Local Insulation of Chromosome Domains from Genomic Compartmentalization. Cell. *169*, 930-944 e922.

Novoa, I., Zhang, Y., Zeng, H., Jungreis, R., Harding, H.P. and Ron, D. (2003). Stress-induced gene expression requires programmed recovery from translational repression. EMBO J. *22*, 1180-1187.

Nuebler, J., Fudenberg, G., Imakaev, M., Abdennur, N. and Mirny, L.A. (2018). Chromatin organization by an interplay of loop extrusion and compartmental segregation. Proc Natl Acad Sci U S A. *115*, E6697-E6706.

Ocampo, A., Reddy, P., Martinez-Redondo, P., *et al.* (2016). In Vivo Amelioration of Age-Associated Hallmarks by Partial Reprogramming. Cell. *167*, 1719-1733 e1712.

Olins, A.L. and Olins, D.E. (1974). Spheroid chromatin units (v Bodies). Science. *183*, 330-332.

Olive, M., Harten, I., Mitchell, R., Beers, J., Djabali, K., Cao, K., Erdos, M.R., Blair, C., Funke, B., Smoot, L., Gerhard-Herman, M., Machan, J.T., Kutys, R., Virmani, R., Collins, F.S., Wight, T.N., Nabel, E.G. and Gordon, L.B. (2010). Cardiovascular Pathology in Hutchinson-Gilford Progeria: Correlation with the Vascular Pathology of Aging. Arterioscler Thromb Vasc Biol. *30*, 2301-2309.

Osorio, F.G., Barcena, C., Soria-Valles, C., Ramsay, A.J., de Carlos, F., Cobo, J., Fueyo, A., Freije, J.M. and Lopez-Otin, C. (2012). Nuclear lamina defects cause ATM-dependent NF-kappaB activation and link accelerated aging to a systemic inflammatory response. Genes Dev. *26*, 2311-2324.

Osorio, F.G., Navarro, C.L., Cadinanos, J., Lopez-Mejia, I.C., Quiros, P.M., Bartoli, C., Rivera, J., Tazi, J., Guzman, G., Varela, I., Depetris, D., de Carlos, F., Cobo, J., Andres, V., de Sandre-Giovannoli, A., Freije, J.M.P., Levy, N. and Lopez-Otin, C. (2011). Splicing-Directed Therapy in a New Mouse Model of Human Accelerated Aging. Sci Transl Med. *3*, 1-12.

Oudet, P., Gross-Bellard, M. and Chambon, P. (1975). Electron microscopic and biochemical evidence that chromatin structure is a repeating unit. Cell. *4*, 281-300.

Pajerowski, J.D., Dahl, K.N., Zhong, F.L., Sammak, P.J. and Discher, D.E. (2007). Physical plasticity of the nucleus in stem cell differentiation. Proc Natl Acad Sci U S A. *104*, 15619-15624.

Pan, X., Jiang, B., Wu, X., Xu, H., Cao, S., Bai, N., Li, X., Yi, F., Guo, Q., Guo, W., Song, X., Meng, F., Li, X., Liu, Y. and Cao, L. (2020). Accumulation of prelamin A induces premature aging through mTOR overactivation. FASEB J. *34*, 7905-7914.

Park, S.K. and Shin, O.S. (2017). Metformin alleviates ageing cellular phenotypes in Hutchinson-Gilford progeria syndrome dermal fibroblasts. Exp Dermatol. *26*, 889-895.

Parmar, J.J., Woringer, M. and Zimmer, C. (2019). How the Genome Folds: The Biophysics of Four-Dimensional Chromatin Organization. Annu Rev Biophys. *48*, 231-253.

Pathak, R.U., Soujanya, M. and Mishra, R.K. (2021). Deterioration of nuclear morphology and architecture: A hallmark of senescence and aging. Ageing Res Rev. *67*, 101264.

Peng, Y., Li, S., Landsman, D. and Panchenko, A.R. (2021). Histone tails as signaling antennas of chromatin. Curr Opin Struct Biol. *67*, 153-160.

Peric-Hupkes, D., Meuleman, W., Pagie, L., Bruggeman, S.W., Solovei, I., Brugman, W., Graf, S., Flicek, P., Kerkhoven, R.M., van Lohuizen, M., Reinders, M., Wessels, L. and van Steensel, B. (2010). Molecular maps of the reorganization of genome-nuclear lamina interactions during differentiation. Mol Cell. *38*, 603-613.

Pickersgill, H., Kalverda, B., de Wit, E., Talhout, W., Fornerod, M. and van Steensel, B. (2006). Characterization of the Drosophila melanogaster genome at the nuclear lamina. Nat Genet. *38*, 1005-1014.

Pietsch, K., Saul, N., Menzel, R., Sturzenbaum, S.R. and Steinberg, C.E.W. (2009). Quercetin mediated lifespan extension in *Caenorhabditis elegans* is modulated by *age-1*, *daf-2*, *sek-1* and *unc-43*. Biogerontology. *10*, 565-578.

Poleshko, A., Shah, P.P., Gupta, M., *et al.* (2017). Genome-Nuclear Lamina Interactions Regulate Cardiac Stem Cell Lineage Restriction. Cell. *171*, 573-587 e514.

Prakash, A., Gordon, L.B., Kleinman, M.E., Gurary, E.B., Massaro, J., D'Agostino, R., Sr., Kieran, M.W., Gerhard-Herman, M. and Smoot, L. (2018). Cardiac Abnormalities in Patients With Hutchinson-Gilford Progeria Syndrome. JAMA Cardiol. *3*, 326-334.

Prokocimer, M., Barkan, R. and Gruenbaum, Y. (2013). Hutchinson-Gilford progeria syndrome through the lens of transcription. Aging Cell. *12*, 533-543.

Puttaraju, M., Jackson, M., Klein, S., Shilo, A., Bennett, C.F., Gordon, L., Rigo, F. and Misteli, T. (2021). Systematic screening identifies therapeutic antisense oligonucleotides for Hutchinson-Gilford progeria syndrome. Nat Med. *27*, 526-535.

Quinodoz, S.A., Ollikainen, N., Tabak, B., *et al.* (2018). Higher-Order Inter-chromosomal Hubs Shape 3D Genome Organization in the Nucleus. Cell. *174*, 744-757 e724.

Ramazi, S. and Zahiri, J. (2021). Posttranslational modifications in proteins: resources, tools and prediction methods. Database (Oxford). *2021*,

Reddy, K.L., Zullo, J.M., Bertolino, E. and Singh, H. (2008). Transcriptional repression mediated by repositioning of genes to the nuclear lamina. Nature. *452*, 243-247.

Redman, L.M., Smith, S.R., Burton, J.H., Martin, C.K., Il'yasova, D. and Ravussin, E. (2018). Metabolic Slowing and Reduced Oxidative Damage with Sustained Caloric Restriction Support the Rate of Living and Oxidative Damage Theories of Aging. Cell Metab. *27*, 805-815 e804.

Ren, B., Wang, L., Shi, L., Jin, X., Liu, Y., Liu, R.H., Yin, F., Cadenas, E., Dai, X., Liu, Z. and Liu, X. (2021). Methionine restriction alleviates age-associated cognitive decline via fibroblast growth factor 21. Redox Biol. *41*, 101940.

Rena, G., Hardie, D.G. and Pearson, E.R. (2017). The mechanisms of action of metformin. Diabetologia. *60*, 1577-1585.

Richards, S.A., Muter, J., Ritchie, P., Lattanzi, G. and Hutchison, C.J. (2011). The accumulation of un-repairable DNA damage in laminopathy progeria fibroblasts is caused by ROS generation and is prevented by treatment with N-acetyl cysteine. Hum Mol Genet. *20*, 3997-4004.

Richardson, N.E., Konon, E.N., Schuster, H.S., *et al.* (2021). Lifelong restriction of dietary branched-chain amino acids has sex-specific benefits for frailty and lifespan in mice. Nat Aging. *1*, 73-86.

Richmond, T.J. and Davey, C.A. (2003). The structure of DNA in the nucleosome core. Nature. *423*, 145-150.

Rober, R.A., Weber, K. and Osborn, M. (1989). Differential timing of nuclear lamin A/C expression in the various organs of the mouse embryo and the young animal: a developmental study. Development. *105*, 365-378.

Robida-Stubbs, S., Glover-Cutter, K., Lamming, D.W., Mizunuma, M., Narasimhan, S.D., Neumann-Haefelin, E., Sabatini, D.M. and Blackwell, T.K. (2012). TOR signaling and rapamycin influence longevity by regulating SKN-1/Nrf and DAF-16/FoxO. Cell Metab. *15*, 713-724.

Robijns, J., Molenberghs, F., Sieprath, T., Corne, T.D., Verschuuren, M. and De Vos, W.H. (2016). In silico synchronization reveals regulators of nuclear ruptures in lamin A/C deficient model cells. Sci Rep. *6*, 30325.

Rodriguez, J., Ren, G., Day, C.R., Zhao, K., Chow, C.C. and Larson, D.R. (2019). Intrinsic Dynamics of a Human Gene Reveal the Basis of Expression Heterogeneity. Cell. *176*, 213-226 e218.

Rosengardten, Y., McKenna, T., Grochova, D. and Eriksson, M. (2011). Stem cell depletion in Hutchinson–Gilford progeria syndrome. Aging Cell. *10*, 1011-1020.

Roux, K.J. and Burke, B. (2007). Nuclear envelope defects in muscular dystrophy. Biochim Biophys Acta. *1772*, 118-127.

Ryslava, H., Doubnerova, V., Kavan, D. and Vanek, O. (2013). Effect of posttranslational modifications on enzyme function and assembly. J Proteomics. *92*, 80-109.

Saisho, Y. (2015). Metformin and Inflammation: Its Potential Beyond Glucose-lowering Effect. Endocrine, Metabolic and Immune Disorders - Drug Targets. *15*, 196-205.

Sanborn, A.L., Rao, S.S.P., Huang, S., Durand, N.C., Huntley, M.H., Jewett, A.I., Bochkov, I.D., Chinnappan, D., Cutkosky, A., Li, J., Geeting, K.P., Gnirke, A., Melnikov, A., McKenna, D., Stamenova, E.K., Lander, E.S. and Lieberman Aiden, E. (2015). Chromatin extrusion explains key features of loop and domain formation in wild-type and engineered genomes. PNAS. E6456–E6465.

Sancak, Y., Bar-Peled, L., Zoncu, R., Markhard, A.L., Nada, S. and Sabatini, D.M. (2010). Ragulator-Rag complex targets mTORC1 to the lysosomal surface and is necessary for its activation by amino acids. Cell. *141*, 290-303.

Sancak, Y., Peterson, T.R., Shaul, Y.D., Lindquist, R.A., Thoreen, C.C., Bar-Peled, L. and Sabatini, D.M. (2008). The Rag GTPases bind raptor and mediate amino acid signaling to mTORC1. Science. *320*, 1496-1501.

Sanchez-Lopez, A., Espinos-Estevez, C., Gonzalez-Gomez, C., Gonzalo, P., Andres-Manzano, M.J., Fanjul, V., Riquelme-Borja, R., Hamczyk, M.R., Macias, A., del Campo, L., Camafeita, E., Vazquez, J., Barkaway, A., ROlas, L., Nourshargh, S., Dorado, B., Benedicto, I. and Andres, V. (2021). Cardiovascular Progerin Suppression and lamin A Restoration Rescues Hutchinson-Gilford Progeria Syndrome. Circulation. *0*, 1-35.

Santiago-Fernandez, O., Osorio, F.G., Quesada, V., Rodriguez, F., Basso, S., Maeso, D., Rolas, L., Barkaway, A., Nourshargh, S., Folgueras, A.R., Freije, J.M.P. and Lopez-Otin, C. (2019). Development of a CRISPR/Cas9-based therapy for Hutchinson-Gilford progeria syndrome. Nat Med. *25*, 423-426.

Saxton, R.A., Chantranupong, L., Knockenhauer, K.E., Schwartz, T.U. and Sabatini, D.M. (2016a). Mechanism of arginine sensing by CASTOR1 upstream of mTORC1. Nature. *536*, 229-233.

Saxton, R.A., Knockenhauer, K.E., Wolfson, R.L., Chantranupong, L., Pacold, M.E., Wang, T., Schwartz, T.U. and Sabatini, D.M. (2016b). Structural basis for leucine sensing by the Sestrin2-mTORC1 pathway. Science. *351*, 53-58.

Saxton, R.A. and Sabatini, D.M. (2017). mTOR Signaling in Growth, Metabolism, and Disease. Cell. *168*, 960-976.

Scaffidi, P. and Misteli, T. (2006). Lamin A-Dependent Nuclear Defects in Human Aging. Science. *312*, 1059-1063.

Scaffidi, P. and Misteli, T. (2008). Lamin A-dependent misregulation of adult stem cells associated with accelerated ageing. Nat Cell Biol. *10*, 452.

Schneider, R., Bannister, A.J., Myers, F.A., Thorne, A.W., Crane-Robinson, C. and Kouzarides, T. (2004). Histone H3 lysine 4 methylation patterns in higher eukaryotic genes. Nat Cell Biol. *6*, 73-77.

Schreiner, S.M., Koo, P.K., Zhao, Y., Mochrie, S.G. and King, M.C. (2015). The tethering of chromatin to the nuclear envelope supports nuclear mechanics. Nat Commun. *6*, 7159.

Schwarzer, W., Abdennur, N., Goloborodko, A., Pekowska, A., Fudenberg, G., Loe-Mie, Y., Fonseca, N.A., Huber, W., Haering, C.H., Mirny, L. and Spitz, F. (2017). Two independent modes of chromatin organization revealed by cohesin removal. Nature. *551*, 51-56.

Sebestyen, E., Marullo, F., Lucini, F., Petrini, C., Bianchi, A., Valsoni, S., Olivieri, I., Antonelli, L., Gregoretti, F., Oliva, G., Ferrari, F. and Lanzuolo, C. (2020). SAMMY-seq reveals early alteration of heterochromatin and deregulation of bivalent genes in Hutchinson-Gilford Progeria Syndrome. Nat Commun. *11*, 6274.

Shah, P.P., Donahue, G., Otte, G.L., Capell, B.C., Nelson, D.M., Cao, K., Aggarwala, V., Cruickshanks, H.A., Rai, T.S., McBryan, T., Gregory, B.D., Adams, P.D. and Berger, S.L. (2013). Lamin B1 depletion in senescent cells triggers large-scale changes in gene expression and the chromatin landscape. Genes Dev. *27*, 1787-1799.

Shalev, S.A., De Sandre-Giovannoli, A., Shani, A.A. and Levy, N. (2007). An association of Hutchinson-Gilford progeria and malignancy. American Journal of Medical Genetics Part A. *143A*, 1821-1826.

Shevelyov, Y.Y., Lavrov, S.A., Mikhaylova, L.M., Nurminsky, I.D., Kulathinal, R.J., Egorova, K.S., Rozovsky, Y.M. and Nurminsky, D.I. (2009). The B-type lamin is required for somatic repression of testis-specific gene clusters. Proc Natl Acad Sci U S A. *106*, 3282-3287.

Shimamoto, Y., Tamura, S., Masumoto, H. and Maeshima, K. (2017). Nucleosome–nucleosome interactions via histone tails and linker DNA regulate nuclear rigidity. Mol Biol Cell. *28*, 1580-1589.

Shimi, T., Pfleghaar, K., Kojima, S., Pack, C.G., Solovei, I., Goldman, A.E., Adam, S.A., Shumaker, D.K., Kinjo, M., Cremer, T. and Goldman, R.D. (2008). The A- and B-type nuclear lamin networks: microdomains involved in chromatin organization and transcription. Genes Dev. *22*, 3409-3421.

Shin, S.B., Jang, H.R., Xu, R., Won, J.Y. and Yim, H. (2020). Active PLK1-driven metastasis is amplified by TGF-beta signaling that forms a positive feedback loop in non-small cell lung cancer. Oncogene. *39*, 767-785.

Shinmura, K., Tamaki, K., Sano, M., Murata, M., Yamakawa, H., Ishida, H. and Fukuda, K. (2011). Impact of long-term caloric restriction on cardiac senescence: caloric restriction ameliorates cardiac diastolic dysfunction associated with aging. J Mol Cell Cardiol. *50*, 117-127.

Shumaker, D.K., Dechat, T., Kohlmaier, A., Adam, S.A., Bozovsky, M.R., Erdos, M.R., Eriksson, M., Goldman, A.E., Khuon, S., Collins, F.S., Jenuwein, T. and Goldman, R.D. (2006). Mutant nuclear lamin A leads to progressive alterations of epigenetic

control in premature aging. Proceedings of the National Academy of Sciences. *103*, 8703-8708.

Solovei, I., Wang, A.S., Thanisch, K., Schmidt, C.S., Krebs, S., Zwerger, M., Cohen, T.V., Devys, D., Foisner, R., Peichl, L., Herrmann, H., Blum, H., Engelkamp, D., Stewart, C.L., Leonhardt, H. and Joffe, B. (2013). LBR and lamin A/C sequentially tether peripheral heterochromatin and inversely regulate differentiation. Cell. *152*, 584-598.

Song, J., Jiang, G., Zhang, J., Gui, J., Li, Z., Hao, K., Liu, L., Cheng, Z., Tong, X. and Dai, F. (2019). Metformin prolongs lifespan through remodeling the energy distribution strategy in silkworm, Bombyx mori. Aging. *11*, 240-248.

Song, J., Liu, L., Hao, K., Mao, S., Tang, Y., Tong, X. and Dai, F. (2020). Resveratrol elongates the lifespan and improves antioxidant activity in the silkworm, Bombyx mori. J Pharm Anal.

Staats, S., Wagner, A.E., Kowalewski, B., Rieck, F.T., Soukup, S.T., Kulling, S.E. and Rimbach, G. (2018). Dietary Resveratrol Does Not Affect Life Span, Body Composition, Stress Response, and Longevity-Related Gene Expression in Drosophila melanogaster. Int J Mol Sci. *19*,

Stasevich, T.J., Mueller, F., Brown, D.T. and McNally, J.G. (2010). Dissecting the binding mechanism of the linker histone in live cells: an integrated FRAP analysis. EMBO J. *29*, 1225-1234.

Stephens, A.D., Liu, P.Z., Banigan, E.J., Almassalha, L.M., Backman, V., Adam, S.A., Goldman, R.D. and Marko, J.F. (2017). Chromatin histone modifications and rigidity affect nuclear morphology independent of lamins. Mol Biol Cell. *29*, 220-233.

Stephens, A.D., Liu, P.Z., Kandula, V., Chen, H., Almassalha, L.M., Herman, C., Backman, V., O'Halloran, T., Adam, S.A., Goldman, R.D., Banigan, E.J. and Marko, J.F. (2019). Physicochemical mechanotransduction alters nuclear shape and mechanics via heterochromatin formation. Mol Biol Cell. *30*, 2320-2330.

Stewart, C.L. and Burke, B. (1987). Teratocarcinoma Stem Cells and Early Mouse Embryos Contain Only a Single Major Lamin Polypeptide Closely Resembling Lamin B. Cell. *51*, 383-392.

Stowers, R.S., Shcherbina, A., Israeli, J., Gruber, J.J., Chang, J., Nam, S., Rabiee, A., Teruel, M.N., Snyder, M.P., Kundaje, A. and Chaudhuri, O. (2019). Matrix stiffness induces a tumorigenic phenotype in mammary epithelium through changes in chromatin accessibility. Nat Biomed Eng. *3*, 1009-1019.

Stracka, D., Jozefczuk, S., Rudroff, F., Sauer, U. and Hall, M.N. (2014). Nitrogen source activates TOR (target of rapamycin) complex 1 via glutamine and independently of Gtr/Rag proteins. J Biol Chem. *289*, 25010-25020.

Strandgren, C., Nasser, H.A., McKenna, T., Koskela, A., Tuukkanen, J., Ohlsson, C., Rozell, B. and Eriksson, M. (2015). Transgene silencing of the Hutchinson-Gilford progeria syndrome mutation results in a reversible bone phenotype, whereas resveratrol treatment does not show overall beneficial effects. FASEB J. *29*, 3193-3205.

Stuurman, N., Heins, S. and Aebi, U. (1998). Nuclear Lamins: Their Structure, Assembly, and Interactions. J Struct Biol. *122*, 42-66.

Sun, H.B., Shen, J. and Yokota, H. (2000). Size-Dependent Positioning of Human Chromosomes in Interphase Nuclei. Biophys J. *79*, 184-190.

Sun, X.J., Man, N., Tan, Y., Nimer, S.D. and Wang, L. (2015). The Role of Histone Acetyltransferases in Normal and Malignant Hematopoiesis. Front Oncol. *5*, 108.

Takenaka, A., Oki, N., Takahashi, S. and Noguchi, T. (2000a). Dietary Restriction of Single Essential Amino Acids Reduces Plasma Insulin-Like Growth Factor-I (IGF-I) but Does Not Affect Plasma IGF-Binding Protein-1 in Rats. ASN. *130*, 2910-2914.

Takenaka, A., Oki, N., Takahashi, S. and Noguchi, T. (2000b). Dietary Restriction of Single Essential Amino Acids Reduces Plasma Insulin-Like Growth Factor-I (IGF-I) but Does Not Affect Plasma IGF-Binding Protein-1 in Rats. American Society for Nutritional Sciences. *130*, 2910-2914.

Tamiello, C., Kamps, M.A., van den Wijngaard, A., Verstraeten, V.L., Baaijens, F.P., Broers, J.L. and Bouten, C.C. (2013). Soft substrates normalize nuclear morphology and prevent nuclear rupture in fibroblasts from a laminopathy patient with compound heterozygous LMNA mutations. Nucleus. *4*, 61-73.

Tang, G., Guo, J., Zhu, Y., Huang, Z., Liu, T., Cai, J., Yu, L. and Wang, Z. (2018). Metformin inhibits ovarian cancer via decreasing H3K27 trimethylation. Int J Oncol. *52*, 1899-1911.

Tang, X., Keenan, M.M., Wu, J., Lin, C.A., Dubois, L., Thompson, J.W., Freedland, S.J., Murphy, S.K. and Chi, J.T. (2015). Comprehensive profiling of amino acid response uncovers unique methionine-deprived response dependent on intact creatine biosynthesis. PLoS Genet. *11*, e1005158.

Tavares-Cadete, F., Norouzi, D., Dekker, B., Liu, Y. and Dekker, J. (2020). Multi-contact 3C reveals that the human genome during interphase is largely not entangled. Nat Struct Mol Biol. *27*, 1105-1114.

Tominaga, K. and Suzuki, H.I. (2019). TGF-beta Signaling in Cellular Senescence and Aging-Related Pathology. Int J Mol Sci. *20*,

Towbin, B.D., Gonzalez-Aguilera, C., Sack, R., Gaidatzis, D., Kalck, V., Meister, P., Askjaer, P. and Gasser, S.M. (2012). Step-wise methylation of histone H3K9 positions heterochromatin at the nuclear periphery. Cell. *150*, 934-947.

Trojer, P. and Reinberg, D. (2007). Facultative heterochromatin: is there a distinctive molecular signature? Mol Cell. *28*, 1-13.

Ulianov, S.V., Doronin, S.A., Khrameeva, E.E., Kos, P.I., Luzhin, A.V., Starikov, S.S., Galitsyna, A.A., Nenasheva, V.V., Ilyin, A.A., Flyamer, I.M., Mikhaleva, E.A., Logacheva, M.D., Gelfand, M.S., Chertovich, A.V., Gavrilov, A.A., Razin, S.V. and Shevelyov, Y.Y. (2019). Nuclear lamina integrity is required for proper spatial organization of chromatin in Drosophila. Nat Commun. *10*, 1176.

Ullrich, N.J. and Gordon, L.B. (2015). Hutchinson-Gilford progeria syndrome. Handb Clin Neurol. *132*, 249-264.

Um, J.H., Kim, S.J., Kim, D.W., Ha, M.Y., Jang, J.H., Kim, D.W., Chung, B.S., Kang, C.D. and Kim, S.H. (2003). Tissue-specific changes of DNA repair protein Ku and mtHSP70 in aging rats and their retardation by caloric restriction. Mech Ageing Dev. *124*, 967-975.

Ustinova, M., Silamikelis, I., Kalnina, I., Ansone, L., Rovite, V., Elbere, I., Radovica-Spalvina, I., Fridmanis, D., Aladyeva, J., Konrade, I., Pirags, V. and Klovins, J. (2019). Metformin strongly affects transcriptome of peripheral blood cells in healthy individuals. PloS One. *14*, e0224835.

Valenzano, D.R., Terzibasi, E., Genade, T., Cattaneo, A., Domenici, L. and Cellerino, A. (2006). Resveratrol prolongs lifespan and retards the onset of age-related markers in a short-lived vertebrate. Curr Biol. *16*, 296-300.

van Bemmel, J.G., Pagie, L., Braunschweig, U., Brugman, W., Meuleman, W., Kerkhoven, R.M. and van Steensel, B. (2010). The insulator protein SU(HW) fine-tunes nuclear lamina interactions of the Drosophila genome. PloS One. *5*, e15013.

Van der Laan, S. and Maiorano, D. (2014). Post-translational modifications in embryonic cell cycle. Cell Cycle. *13*, 1364-1365.

VanGenderen, C., Harkness, T.A.A. and Arnason, T.G. (2020). The role of Anaphase Promoting Complex activation, inhibition and substrates in cancer development and progression. Aging. *12*, 15818-15855.

Varela, I., Pereira, S., Ugalde, A.P., Navarro, C.L., Suarez, M.F., Cau, P., Cadinanos, J., Osorio, F.G., Foray, N., Cobo, J., de Carlos, F., Levy, N., Freije, J.M. and Lopez-Otin, C. (2008). Combined treatment with statins and aminobisphosphonates extends longevity in a mouse model of human premature aging. Nat Med. *14*, 767-772.

Vargas, J.D., Hatch, E.M., Anderson, D.J. and Hetzer, M.W. (2012). Transient nuclear envelope rupturing during interphase in human cancer cells. Nucleus. *3*, 88-100.

Vermeij, W.P., Dollé, M.E.T., Reiling, E., *et al.* (2016). Restricted diet delays accelerated ageing and genomic stress in DNA-repair-deficient mice. Nature. *537*, 427-431.

Vermunt, M.W., Zhang, D. and Blobel, G.A. (2019). The interdependence of gene-regulatory elements and the 3D genome. J Cell Biol. *218*, 12-26.

Voigt, P., Tee, W.W. and Reinberg, D. (2013). A double take on bivalent promoters. Genes Dev. *27*, 1318-1338.

Walaszczyk, A., Dookun, E., Redgrave, R., Tual-Chalot, S., Victorelli, S., Spyridopoulos, I., Owens, A., Arthur, H.M., Passos, J.F. and Richardson, G.D. (2019). Pharmacological clearance of senescent cells improves survival and recovery in aged mice following acute myocardial infarction. Aging Cell. *18*, e12945.

Wang, C. and Eskiw, C.H. (2019). Cytoprotective effects of Avenathramide C against oxidative and inflammatory stress in normal human dermal fibroblasts. Sci Rep. *9*, 2932.

Wang, C., Wheeler, C.T., Alberico, T., Sun, X., Seeberger, J., Laslo, M., Spangler, E., Kern, B., de Cabo, R. and Zou, S. (2013). The effect of resveratrol on lifespan depends on both gender and dietary nutrient composition in Drosophila melanogaster. Age. *35*, 69-81.

Wang, D., Liu, S. and Xu, S. (2020). Identification of hub genes, key pathways, and therapeutic agents in Hutchinson-Gilford Progeria syndrome using bioinformatics analysis. Medicine (Baltimore). *99*, e19022.

Wang, P., Dreger, M., Madrazo, E., Williams, C.J., Samaniego, R., Hodson, N.W., Monroy, F., Baena, E., Sanchez-Mateos, P., Hurlstone, A. and Redondo-Munoz, J. (2018a). WDR5 modulates cell motility and morphology and controls nuclear changes induced by a 3D environment. Proc Natl Acad Sci U S A. *115*, 8581-8586.

Wang, W., Cai, G. and Chen, X. (2018b). Dietary restriction delays the secretion of senescence associated secretory phenotype by reducing DNA damage response in the process of renal aging. Exp Gerontol. *107*, 4-10.

Wang, Y., Ostlund, C. and Worman, H.J. (2010). Blocking protein farnesylation improves nuclear shape abnormalities in keratinocytes of mice expressing the prelamin A variant in Hutchinson-Gilford progeria syndrome. Nucleus. *1*, 432-439.

Warnsmann, V., Hainbuch, S. and Osiewacz, H.D. (2018). Quercetin-Induced Lifespan Extension in Podospora anserina Requires Methylation of the Flavonoid by the O-Methyltransferase PaMTH1. Front Genet. *9*, 160.

Weber, K., Plessmann, U. and Traub, P. (1989). Maturation of nuclear lamin A involves a specific carboxy-terminal trimming, which removes the polyisoprenylation site from the precursor; implications for the structure of the nuclear lamina. FEB. *257*, 411-414.

Weeks, S.C. (2020). Effects of dietary restriction on lifespan, growth, and reproduction of the clam shrimp Eulimnadia texana. Hydrobiologia. *847*, 3067-3076.

Weindruch, R., Walford, R.L., Fligiel, S. and Guthrie, C. (1986). The Retardation of Aging in Mice by Dietary Restriction: Longevity, Cancer, Immunity and Lifetime Energy Intake. J Nutr. *116*, 641-654.

Wilkinson, J.E., Burmeister, L., Brooks, S.V., Chan, C.C., Friedline, S., Harrison, D.E., Hejtmancik, J.F., Nadon, N., Strong, R., Wood, L.K., Woodward, M.A. and Miller, R.A. (2012). Rapamycin slows aging in mice. Aging Cell. *11*, 675-682.

Williamson, I., Kane, L., Devenney, P.S., Flyamer, I.M., Anderson, E., Kilanowski, F., Hill, R.E., Bickmore, W.A. and Lettice, L.A. (2019). Developmentally regulated Shh expression is robust to TAD perturbations. Development. *146*,

Winter-Vann, A.M. and Casey, P.J. (2005). Post-prenylation-processing enzymes as new targets in oncogenesis. Nat Rev. *5*, 405-412.

Wolfson, R.L., Chantranupong, L., Saxton, R.A., Shen, K., Scaria, S.M., Cantor, J.R. and Sabatini, D.M. (2016). Sestrin2 is a leucine sensor for the mTORC1 pathway. Science. *351*, 43-48.

Woodcock, C.L., Grigoryev, S.A., Horowitz, R.A. and Whitaker, N. (1993). A chromatin folding model that incorporates linker variability generates fibers resembling the native structures. Proc. Natl. Acad. Sci. USA. *90*, 9021-9025.

Wu, F. and Yao, J. (2017). Identifying Novel Transcriptional and Epigenetic Features of Nuclear Lamina-associated Genes. Sci Rep. *7*, 100.

Wu, Q., Schapira, M., Arrowsmith, C.H. and Barsyte-Lovejoy, D. (2021). Protein arginine methylation: from enigmatic functions to therapeutic targeting. Nat Rev Drug Discov. *20*, 509-530.

Xia, Y., Ivanovska, I.L., Zhu, K., Smith, L., Irianto, J., Pfeifer, C.R., Alvey, C.M., Ji, J., Liu, D., Cho, S., Bennett, R.R., Liu, A.J., Greenberg, R.A. and Discher, D.E. (2018). Nuclear rupture at sites of high curvature compromises retention of DNA repair factors. J Cell Biol. *217*, 3796-3808.

Xiao, F., Yu, J., Guo, Y., Deng, J., Li, K., Du, Y., Chen, S., Zhu, J., Sheng, H. and Guo, F. (2014). Effects of individual branched-chain amino acids deprivation on insulin sensitivity and glucose metabolism in mice. Metabolism. *63*, 841-850.

Xie, W.J., Meng, L., Liu, S., Zhang, L., Cai, X. and Gao, Y.Q. (2017). Structural Modeling of Chromatin Integrates Genome Features and Reveals Chromosome Folding Principle. Sci Rep. *7*, 2818.

Yang, S.H., Bergo, M.O., Toth, J.I., Qiao, X., Hu, Y., Sandoval, S., Meta, M., Bendale, P., Gelb, M.H., Young, S.G. and Fong, L.G. (2005). Blocking protein farnesyltransferase improves nuclear blebbing in mouse fibroblasts with a targeted Hutchinson-Gilford progeria syndrome mutation. Proceedings of the National Academy of Sciences. *102*, 10291-10296.

Yang, S.H., Qiao, X., Fong, L.G. and Young, S.G. (2008). Treatment with a Farnesyltransferase Inhibitor Improves Survival in Mice with a Hutchinson-Gilford Progeria Syndrome Mutation. Biochim Biophys Acta. *1281*, 36-39.

Yang, X., Kord-Varkaneh, H., Talaei, S., Clark, C.C.T., Zanghelini, F., Tan, S.C., Zarezadeh, M., Mousavi, S.M., Rahmani, J. and Zhang, Y. (2020). The influence of metformin on IGF-1 levels in humans: A systematic review and meta-analysis. Pharmacol Res. *151*, 104588.

Zehfus, L.R., Gillespie, Z.E., Almendariz-Palacios, C., Low, N.H. and Eskiw, C.H. (2021). Haskap Berry Phenolic Subclasses Differentially Impact Cellular Stress Sensing in Primary and Immortalized Dermal Fibroblasts. Cells. *10*,

Zhang, J. and Liu, F. (2014). Tissue-specific insulin signaling in the regulation of metabolism and aging. IUBMB Life. *66*, 485-495.

Zhang, Y., Xie, Y., Berglund, E.D., Coate, K.C., He, T.T., Katafuchi, T., Xiao, G., Potthoff, M.J., Wei, W., Wan, Y., Yu, R.T., Evans, R.M., Kliewer, S.A. and Mangelsdorf, D.J. (2012). The starvation hormone, fibroblast growth factor-21, extends lifespan in mice. eLife. *1*, e00065.

Zheng, X., Hu, J., Yue, S., Kristiani, L., Kim, M., Sauria, M., Taylor, J., Kim, Y. and Zheng, Y. (2018). Lamins Organize the Global Three-Dimensional Genome from the Nuclear Periphery. Mol Cell. *71*, 802-815 e807.

Zullo, J.M., Demarco, I.A., Pique-Regi, R., Gaffney, D.J., Epstein, C.B., Spooner, C.J., Luperchio, T.R., Bernstein, B.E., Pritchard, J.K., Reddy, K.L. and Singh, H. (2012). DNA sequence-dependent compartmentalization and silencing of chromatin at the nuclear lamina. Cell. *149*, 1474-1487.